The effect of Retinol Binding Protein on the Proteome of muscle cells.

Pamela A. Young BSc.

Biology Department

NUI MAYNOOTH

Ollscoil na hÉireann Má Nuad

Thesis submitted for the degree of Doctor of Philosophy

National University of Ireland Maynooth

October 2013

Head of the department: Prof. Paul Moynagh

Supervisor: Prof. John Findlay

Table of Contents

Page

Declaration……..**i**

Acknowledgements……..**ii**

Abstract……..**iii**

List of Figures……..**iv**

List of Tables……..**x**

List of Abbreviations……..**xi**

Chapter 1 Introduction

1.1 Vitamin A regulation and transport....1

1.1.1 The Vitamin A transport protein, retinol binding protein 2

1.1.2 The Structure of RBP....2

1.1.3 RBP and its interaction with Transthyretin....4

1.1.4 Delivery of ROH into the cell 5

1.1.5 Interaction of RBP with STRA6 and TTR....6

1.1.6 The internal acceptor for ROH, CRBP....7

1.1.7 The function of CRBP....7

1.1.8 Cellular Retinoic Acid Binding Protein 9

1.2 STRA6 mediated ROH transport 10

1.2.1 The dynamics of ROH transport across the cell membrane....10

1.2.2 ROH efflux via STRA6....11

1.2.3 The physiological relevance of ROH efflux via STRA6....12

1.2.4 The influence of other retinoids on STRA6 activity 13

1.3 The RBP Receptor; STRA6 14
1.3.1 Discovery of the RBP receptor 14
1.3.2 Identification of the RBP Receptor, STRA6 15
1.3.3 STRA6 and embryonic development 15
1.3.4 Matthew Wood Syndrome 17
1.3.5 STRA6 knockout studies 20
1.3.6 STRA6 topology 21
1.3.7 Extracellular loop 3 23
1.3.8 Intracellular loop 3 24
1.3.9 C-Terminal region 25
1.4 The biological activity of retinoids 26
1.4.1 Diverse functions of retinol metabolites 26
1.4.2 The retinoic acid receptor 28
1.4.3 The retinoid X receptor 29
1.4.4 Regulation of retinoid signalling 30
1.5 Type II diabetes, a new epidemic 32
1.5.1 RBP, a biomarker for insulin resistance 33
1.5.2 Physiological relevance 34
1.5.3 The molecular mechanism of RBP induced insulin resistance 36
1.5.4 Cytokines and insulin resistance 37
1.5.5 The role of TNFα in insulin resistance 37
1.5.6 STRA6 and the JAK/STAT pathway 38
1.6 Project aims 40

Chapter 2 Materials and Methods

2.1 Tissue culture 42

2.1.1 General tissue culture reagents 42

2.1.2 C2C12 cell line maintenance and storage 42

2.1.3 HEK293T STRA6 stable cell line maintenance and storage 43

2.1.4 HEPG2 cell line maintenance and storage 43

2.1.5 BMDM cell line maintenance and storage 44

2.1.6 C2C12 RTC15 treatment 44

2.1.7 C2C12 RBP treatment 44

2.1.8 C2C12 insulin treatment 44

2.2 Sample preparation 45

2.2.1 Cell lysis 45

2.2.2 Cell membrane isolation 45

2.2.3 BCA protein assay 46

2.2.4 PIERCE protein assay 46

2.3 Two dimensional electrophoresis 47

2.3.1 Sample preparation for the RBP proteomic study 47

2.3.2 Sample preparation for the RTC15 proteomic study 47

2.3.3 Strip rehydration 48

2.3.4 Isoelectric focusing 48

2.3.5 Gel casting 49

2.3.6 Equilibration of IPG strip 49

2.3.7 2nd dimension electrophoresis 50

2.4 Gel visualisation 52

2.4.1 ProQ Diamond staining 52
2.4.2 Sypro Ruby staining 52
2.4.3 Silver staining 53
2.4.4 Image acquisition 53
2.5 Image analysis 54
2.6 Spot excision and mass spectrometry 55
2.6.1 Spot excision 55
2.6.2 Gel destaining 55
2.6.3 In-gel digestion 55
2.6.4 LC/MS/MS 56
2.6.5 Protein identification 56
2.7 One dimensional electrophoresis and Western blotting 57
2.7.1 SDS-PAGE 57
2.7.2 Coomassie brilliant blue staining 58
2.7.3 Silver staining 58
2.7.4 Semi-dry electro blotting 58
2.7.5 Western blotting 59
2.7.6 Stripping and re-probing PVDF membranes 59
2.8 Molecular Biology 60
2.8.1 PCR 60
2.8.2 Agarose gel electrophoresis of DNA 61
2.8.3 Restriction digestion 62
2.8.4 Ligation 62
2.8.5 Transformation of competent *E. coli* 62

2.8.6 Miniprep and subsequent analysis....63
2.8.7 Midiprep culture of plasmid....63
2.8.8 Preparation of glycerol stocks....63
2.9 Protein expression and purification....64
2.9.1 Expression of RBP in *Pichia pastoris*....64
2.9.2 Expression and purification of recombinant CRBP....65
2.9.3 Cleavage of recombinant CRBP....66
2.9.4 General protocol for C-Terminus expression and purification....67
2.9.5 Cleavage of recombinant C-Terminus using TEV protease....68
2.9.6 Strep-tactin purification of STRA6 from a stable cell line....69
2.9.7 Immunoprecipitation of proteins of interest....70
2.9.8 Co-immunoprecipitation of proteins of interest....70
2.10 Structural and functional assays....71
2.10.1 Size exclusion chromatography....71
2.10.2 Circular dichroism....73
2.10.3 Chemical crosslinking....73
Chapter 3 Proteomic investigation of the molecular effects of holo-RBP on a mouse muscle cell line
3.1 Introduction....75
3.2 Method....78
3.3 Results....79
3.3.1 Identification of changes in the proteome in response to holo-RBP....86
3.3.2 Analysis of changes in the proteome of the cytosolic fraction....87
3.3.2.1 Analysis of decreased expression of LAT-2....87

3.3.2.2 Analysis of decreased expression of OAT 87

3.3.2.3 Analysis of decreased expression of PP1β 88

3.3.3 Analysis of changes in the proteome of the cytosolic fraction 88

3.3.3.1 Analysis of decreased expression of IMMT 88

3.3.3.2 Analysis of decreased phosphorylation of PP2A subunit A 89

3.3.3.3 Analysis of increased expression of PDIA3 91

3.3.3.4 Analysis of increased expression of vimentin 91

3.3.3.5 Analysis of increased phosphorylation of SCaMC-1 92

3.3.3.6 Analysis of decreased expression of DCAF12 93

3.3.3.7 Analysis of decreased phosphorylation of CMYA5 94

3.3.3.8 Analysis of increased expression of lamin B1 94

3.3.4 Analysis of the effect of RBP on the PP1β signalling pathway 96

3.3.4.1 The effect of decreased PP1β expression on glycogen synthase and glycogen phosphorylase 98

3.3.4.2 Time course analysis of PP1β expression, glycogen phosphorylase expression and glycogen synthase phosphorylation 99

3.3.4.3 Assessment of ROH dependence in the PP1β signalling pathway 100

3.3.4.4 Assessment of the effect of holo-RBP on STRA6 deficient cells 102

3.3.5 The PP2A trimeric complex 104

3.3.5.1 Regulation of the PP2A dimer complex by phosphorylation 105

3.3.5.2 Mass spectrometry analysis of the PP2A holoenzyme 105

3.3.6 The B56 delta regulatory subunit of PP2A 107

3.3.6.1 Assessment of B56δ expression in response to holo-RBP treatment 110

3.3.6.2 Analysis of GSK3β phosphorylation in response to holo-RBP treatment 112

3.4 Summary of proteomic analysis of holo-RBP stimulated C2C12 muscle cells 114

Chapter 4 Proteomic profiling of a muscle cell line treated with a novel therapeutic for Type II Diabetes

4.1 Introduction 120

4.1.1 Novel small molecules for the treatment of insulin resistance 121

4.1.2 *In vivo* study of novel compounds developed to interrupt RBP-TTR complex formation 121

4.1.3 Independent action of retinoid derivatives on glucose uptake 123

4.1.4 Proteomics as a tool to decipher molecular mechanism of action 124

4.1.5 Direct assessment of the mechanism of action of RTC-15 124

4.2 Method 125

4.3 Results 126

4.3.1 Identification of common trends in proteome changes 136

4.3.2 Analysis of changes in the proteome affecting metabolism 137

4.3.2.1 Analysis of increased expression of isovaleryl co-A dehydrogenase 138

4.3.2.2 Analysis of increased expression of delta(3,5)-delta(2,4)-dienoyl-CoA isomerase 140

4.3.2.3 Analysis of decreased expression of PDH protein x component 141

4.3.2.4 Analysis of increased expression of ribonuclease/angiogenesis inhibitor-1 142

4.3.2.5 Analysis of increased phosphorylation of δ-aminolevulinic acid dehydratase 142

4.3.2.6 Analysis of increased expression of triose phosphate isomerase 144

4.3.2.7 Analysis of increased expression of ATP synthase subunit α 144

4.3.2.8 Analysis of decreased expression of ciapin-1 145
4.3.3 Analysis of changes in the proteome affecting integral structural proteins 146
4.3.3.1 Analysis of increased expression of pre-lamin A/C 146
4.3.3.2 Analysis of decreased expression of vimentin 147
4.3.3.3 Analysis of increased expression of PANDA_012419 147
4.3.3.4 Analysis of increased phosphorylation of calponin-3 148
4.3.3.5 Analysis of increased expression of PDZ and LIM domain protein 1 148
4.3.4 Analysis of changes in the proteome affecting protein biosynthesis.....149
4.3.4.1 Analysis of increased expression of hnRNP H2, EfTu and EfTs.....149
4.3.4.2 Analysis of increased phosphorylation of eIF-6.....149
4.3.4.3 Analysis of increased expression of protein LSM12 homolog 149
4.3.5 Analysis of changes in the proteome affecting calcium binding proteins.....150
4.3.5.1 Analysis of increased expression of annexin A2.....150
4.3.5.2 Analysis of increased expression of calumenin 151
4.3.5.3 Analysis of decreased phosphorylation of RCN-1 152
4.3.5.4 Analysis of decreased phosphorylation of alpha-actinin.....155
4.3.5.5 Analysis of increased expression of swiprosin-1 155
4.3.6 Analysis of changes in the proteome affecting protein degradation 156
4.3.6.1 Analysis of increased expression of MHR23A 156
4.3.6.2 Analysis of increased expression of cathepsin Z and cathepsin B 156
4.3.7 Analysis of changes in the proteome affecting other cellular processes 157
4.3.7.1 Analysis of increased expression of ZPR1.....157
4.3.7.2 Analysis of decreased expression of STRAP 158

4.4 Conclusions of proteomic profiling of the effect of RTC-15 on C2C12 cells 159

Chapter 5 Structural and functional characterisation of the C-Terminus of STRA6

5.1 Introduction 164

5.1.1 STRA6 topology 164

5.1.2 Inter-species conservation of the C-terminal region 165

5.1.3 The function of the C-term 166

5.1.4 Fusion tags to aid protein expression and purification 166

5.2 Materials and methods 168

5.2.1 Molecular cloning 169

5.2.2 Insertion of MBP into pET-30a 170

5.2.3 Sequence verification of MBP in pET-30a 171

5.2.4 Completion of the MBP-C-term expression plasmid 172

5.2.5 Sequence verification of the C-terminus region of STRA6 in pET-30a 173

5.2.6 TEV MBP-C-term plasmid 173

5.2.7 Expression of the MBP C-term fusion protein 175

5.2.8 Protein purification 175

5.2.9 TEV cleavage of the MBP-C-term fusion protein 177

5.2.10 Detection of protein expression 177

5.3 Results 178

5.3.1 Expression of MBP-C-term in BL21 *E. coli* cells 178

5.3.2 Size Exclusion Chromatography 179

5.3.3 SEC of MBP-C-term 182

5.3.4 SEC of MBP-FLAG 183

5.3.5 Optimisation of MBP-FLAG SEC 184
5.3.6 Optimisation of MBP-C-term SEC 186
5.3.7 Further optimisation of MBP-C-term SEC 187
5.3.8 Detergent solubilisation of MBP-C-term 189
5.3.9 Characterisation of cleaved C-term 191
5.3.10 SEC of purified and cleaved C-term 192
5.3.11 Long-term stability of mono-disperse protein 193
5.3.12 Optimisation of C-term stability at room temperature 193
5.3.13 Secondary structure analysis of purified mono-disperse C-term 196
5.3.14 Calculation of structural content of recombinant proteins 199
5.3.15 Modelling the predicted structure of the C-terminus of STRA6 200
5.3.16 Functional analysis of purified, soluble C-term 203
5.3.17 Chemical crosslinking of potential protein interactions 204
5.4 Summary of the structural and functional analysis of the C-terminus of STRA6 207

Chapter 6 Discussion

6.1 Summary of glycogen enzyme alterations in response to holo-RBP 210
6.1.1 The potential long-term consequences of PP1β downregulation 211
6.1.2 The physiological impact of decreased abundance of glycogen phosphorylase 211
6.1.3 Elevated glycogen synthase phosphorylation and its impact on glycogen storage 213
6.2 Summary of the proteomic analysis of the effect of RTC-15 on C2C12 cells 215

6.3 Characterisation of the C-terminal domain of STRA6.....216

6.4 Future work.....217

6.4.1 Investigation of the effect of holo-RBP on the proteome of muscle cells.....217

6.4.2 Investigation of the effect of RTC-15 on the proteome of muscle cells.....218

6.4.3 Characterisation of the C-terminus of STRA6.....219

Chapter 7 Bibliography.....220

Declaration

I hereby declare that the contents of this thesis are entirely my own work and that it has not been previously submitted as an exercise for a degree to this or any other university. The work and information of others have been acknowledged and cited in the text.

Signed: Date:

Acknowledgements

Firstly I would like to thank my supervisor Prof. John Findlay for the opportunity to complete this PhD, along with his constant and much appreciated guidance. I would also like to thank Science Foundation Ireland for the funding for my project. Taking the plunge and starting a PhD in Maynooth was a scary decision, but one I will never regret. I have learned so much in the last four years here and met so many great people. To all members of the Membrane Protein Lab past and present thank you for your support, copious amounts of cake and wise words. This thesis could not have been possible without you guys. Special thanks to Gemma, Darren and Conor for all their advice and putting up with my many annoying questions over the last four years. A very special thank you to my parents for supporting my decision to venture back into academia. Not everyone would be so understanding and I truly appreciate that. To my sister, Leanne, you've been a shoulder, a cleaning lady, a cook and friend thank you so much for putting up with me for the last year. Andrew, you were a constant source of entertainment and distraction, thank you. To all my close and dear friends, thank you so much for listening to my whining about lab work, I can't promise you that's over! Last but by no means least, I'd like to thank my comrade in arms, Enda. You've helped me at my lowest points and I hope I helped you through yours. Thank you for all your advice and support. Here's to no more late night pizza in the staff room and every weekend off.

Abstract

Vitamin A is essential for normal embryonic development and vision. Retinol binding protein (RBP) and its receptor, STRA6, are vital for the maintenance of intracellular stores of vitamin A. Recently, elevated serum RBP concentration has been implicated as a contributing factor to the development of insulin resistance and type II diabetes. However, conflicting opinions exist as to how increased RBP levels can cause insulin resistance. Some suggest it is as a result of the activation of macrophages in adipose tissue and the secretion of cytokines. Others suggest it is as a result of RBP induced STRA6 phosphorylation, and the activation of the JAK/STAT signalling pathway. Regardless of the mechanism, reducing circulating levels of RBP may be a novel strategy for the treatment of type II diabetes. Several small molecules have been designed to promote renal clearance of RBP, thus lowering serum levels. In order to consolidate the theories surrounding RBP induced insulin resistance, a proteomic study was devised to determine the direct effect of RBP on muscle cells, since the muscle is the main target of insulin induced glucose uptake. Results suggest that RBP may be affecting the enzymes involved in glucose storage and glycogen catabolism. Artificial methods aimed at reducing serum RBP levels may act by preventing RBP induced glycogen disruption. In a related study, it was noted that small molecules aimed at reducing circulating RBP levels had a direct effect on muscle cells to stimulate glucose uptake. This phenomenon occurred independently of the predicted mechanism of action. A second proteomic study was conducted to determine the direct mechanism of action of the compounds in muscle cells. The molecules appear to stimulate the influx of glucose by reducing the ATP yield from oxidative phosphorylation and enhancing the utilisation of alternate energy stores.

The C-terminal region of STRA6 appears to be a large SH2 motif-containing intracellular segment which may be capable of forming an independently folding domain. As such it may represent the site of interaction with other proteins in the system. Therefore, it was cloned, expressed and characterised. The secondary structure of the domain was shown to be largely α-helical and a model was constructed. Possible functional roles for this region were investigated.

List of Figures

Chapter 1: Introduction

Figure 1.1 The chemical structure of ROH....1

Figure 1.2 The crystal structure of Retinol Binding Protein....3

Figure 1.3 Crystal structure of TTR coupled to holo-RBP....4

Figure 1.4 The transport of ROH through the cell membrane....5

Figure 1.5 Structure of CRBP with ROH bound....8

Figure 1.6 Tissue distribution of retinoid handling receptors....16

Figure 1.7 Locations in the STRA6 sequence where genetic mutations have been observed18

Figure 1.8 Topology model of STRA6 as revealed by epitope tagging....22

Figure 1.9 Cross-species sequence alignment of the putative RBP-binding domain of STRA6 as identified by random large scale mutagenesis....23

Figure 1.10 The metabolic processing of retinoids....27

Figure 1.11 Metabolic pathway of retinol and subsequent transcriptional activation....31

Figure 1.12 Recruitment of SOCS3 to Y960 of the insulin receptor inhibits IRS-1 association....38

Figure 1.13 Activation of STRA6 leads to increased SOCS3 expression and inhibition of the insulin receptor....39

Chapter 2: Methods

Figure 2.1 2D electrophoresis schematic....51

Figure 2.2 Diagram of distribution of molecular weight markers used for SDS-PAGE....57

Figure 2.3 Diagram of distribution of markers used for DNA electrophoresis....61

Chapter 3: Proteomic investigation of the molecular effects of holo-RBP on a mouse muscle cell line

Figure 3.1 Identified spots from C2C12 cytosolic fraction generated from cells treated with 75µg/mL holo-RBP 80

Figure 3.2 Identified spots from C2C12 membrane fraction generated from cells treated with 75µg/mL holo-RBP 81

Figure 3.3 Phosphorylation changes observed in C2C12 muscle cells treated with 75µg/ml holo-RBP 83

Figure 3.4 Changes in protein abundance observed in C2C12 muscle cells treated with 75µg/ml holo-RBP 84

Figure 3.5 Sequence alignment of peptide fragments from LAT-2 and chicken lysozyme 86

Figure 3.6 Analysis of expression levels of PP1β 88

Figure 3.7 Analysis of phosphorylation levels of PP2A subunit A 90

Figure 3.8 Prediction of potential phosphorylation sites in the sequence of the A subunit of PP2A 90

Figure 3.9 Analysis of expression levels of vimentin 91

Figure 3.10 Prediction of potential phosphorylation sites in the sequence of SCaMC-1 92

Figure 3.11 Analysis of phosphorylation levels of SCaMC-1 93

Figure 3.12 Analysis of expression levels of lamin B1 95

Figure 3.13 Regulation of glycogen metabolism by PP1β 97

Figure 3.14 The effect of holo-RBP treatment on glycogen synthase phosphorylation levels and glycogen phosphorylase expression levels 98

Figure 3.15 Time course analysis of the effect of holo-RBP treatment on PP1β expression, glycogen phosphorylase expression and glycogen synthase phosphorylation levels 99
Figure 3.16 The effect of apo-RBP and ROH treatment on PP1β, glycogen phosphorylase and glycogen synthase 101
Figure 3.17 Expression of STRA6 in C2C12, BMDM and HEPG2 cell membranes 102
Figure 3.18 The effect of holo-RBP treatment on PP1β, glycogen phosphorylase and glycogen synthase in STRA6 deficient cells 103
Figure 3.19 The trimeric structure of PP2A 104
Figure 3.20 The Wnt/β-catenin signalling pathway 107
Figure 3.21 Proposed pathway involving PP2A activation and increased glycogen synthase phosphorylation 109
Figure 3.22 Time course analysis of the effect of holo-RBP treatment on B56δ expression 111
Figure 3.23 Time course analysis of the effect of holo-RBP treatment on B56δ expression using early timepoints 111
Figure 3.24 Time course analysis of the effect of holo-RBP treatment on GSK3β serine 9 phosphorylation levels 113
Figure 3.25 Time course analysis of the effect of holo-RBP treatment on GSK3β serine 9 phosphorylation levels using early timepoints 113
Figure 3.26 Model of the negative feedback mechanism involved in the regulation of c-Myc abundance 117

Chapter 4: Proteomic profiling of a muscle cell line treated with a novel therapeutic for Type II Diabetes

Figure 4.1 The effect of RTC-1 on glucose and insulin tolerance in high fat diet fed mice 122

Figure 4.2 The effect of insulin, RTC-1 and RTC-15 on glucose uptake in C2C12 cells 123

Figure 4.3 Identified protein changes from C2C12 cell lysate treated with 10µM RTC-15 127

Figure 4.4 Phosphorylation changes observed in C2C12 muscle cells treated with 10µM RTC-15 130

Figure 4.5 Changes in protein abundance observed in C2C12 muscle cells treated with 10µM RTC-15 131

Figure 4.6 Distribution of common trends among proteins showing changes in response to RTC-15 136

Figure 4.7 Representation of oxidative phosphorylation and the protein complexes involved 138

Figure 4.8 The citric acid cycle 139

Figure 4.9 Analysis of expression levels of IVD 140

Figure 4.10 Analysis of expression levels of ECH1 141

Figure 4.11 The haem biosynthetic pathway 143

Figure 4.12 Prediction of potential phosphorylation sites in the sequence of ALAD 143

Figure 4.13 Analysis of expression levels of TPI 144

Figure 4.14 Analysis of expression levels of Pre-lamin A/C 146

Figure 4.15 Analysis of expression levels of vimentin 147

Figure 4.16 Analysis of expression levels of annexin A2 151

Figure 4.17 Analysis of expression levels of calumenin 152

Figure 4.18 Analysis of phosphorylation levels of RCN-1 153

Figure 4.19 Sequence alignment of human and mouse RCN-1 154

Figure 4.20 Analysis of expression levels of ZPR1 158

Chapter 5: Structural and functional characterisation of the C-Terminus of STRA6

Figure 5.1 Sequence alignment of the C-terminal region of STRA6 across *Mus musculus*, *Bos taurus*, *Rattus norvegicus* and *Homo sapiens* species 165

Figure 5.2 Topology model of human STRA6 generated using PredictProtein 168

Figure 5.3 Expression plasmid pET-30a 169

Figure 5.4 Validation of the MBP sequence in the pET30a expression plasmid 171

Figure 5.5 Cloning region of the pET-30a expression plasmid 172

Figure 5.6 Validation of the presence of the sequence of the C-terminal domain of STRA6 in the pET30a expression plasmid**.** 173

Figure 5.7 Validation of the insertion of the TEV protease cleavage sequence in the pET30a expression plasmid 174

Figure 5.8 Expression and purification of MBP-C-term 178

Figure 5.9 Molecular weight standards utilised to calibrate the Superose 6 column 180

Figure 5.10 Molecular weight standards utilised to calibrate the Superdex 200 column 181

Figure 5.11 Elution profile of MBP-CT 182

Figure 5.12 Elution profile of MBP-FLAG 183

Figure 5.13 Optimisation of the MBP-FLAG elution profile 185

Figure 5.14 Elution profile of MBP-CT in the presence of 100mM KCl 186

Figure 5.15 Optimisation of the MBP-CT elution profile via the use of chaotropic

agents 188
Figure 5.16 Amylose affinity chromatography of MBP-CT previously denatured with 8M urea and re-folded by dialysis 189
Figure 5.17 Elution profile of MBP-C-term in the presence of detergent 190
Figure 5.18 Optimisation of removal of the MBP-FLAG tag by the addition of TEV protease 191
Figure 5.19 Elution profile of MBP-C-term and cleaved C-term in the presence of 2mM DDM 192
Figure 5.20 Long term stability of MBP-C-term and cleaved C-term when incubated at room temperature 194
Figure 5.21 Optimisation of room temperature stability of cleaved C-term, using varying pH 195
Figure 5.22 Representative plot of structural motifs depicted by CD 196
Figure 5.23 Purity of protein samples utilised for CD analysis 197
Figure 5.24 High voltage tension spectra of buffer used with recombinant proteins analysed by CD 198
Figure 5.25 CD spectra of MBP, MBP-C-term and cleaved C-term 198
Figure 5.26 iTasser structural homology comparison 201
Figure 5.27 3D model of the C-terminus of STRA6 202
Figure 5.28 Binding assay to determine the interaction of MBP-C-term with CRBP 203
Figure 5.29 Chemical crosslinking of C-term with CRBP 205
Figure 5.30 Chemical crosslinking of C-term with full length STRA6 206

List of Tables

Chapter 1: Introduction

Table 1.1 Summary of the location of point mutations found in STRA6 to date and the effect on membrane expression, RBP binding and ROH transport 19

Table 1.2 The effect of medical interventions on circulating RBP levels 35

Chapter 2: Methods

Table 2.1 Molecular weight standards used to define elution position of defined molecular weight using SEC 72

Chapter 3: Proteomic investigation of the molecular effects of holo-RBP on a mouse muscle cell line

Table 3.1 Proteins identified by mass spectrometry showing changes in phosphorylation or abundance in response to 75 µg/ml holo-RBP 82

Table 3.2 Function of proteins identified by MS showing changes in response to holo-RBP 85

Table 3.3 Components of the PP2A complex identified from PP2A subunit A immunoprecipitation 106

Chapter 4: Proteomic profiling of a muscle cell line treated with a novel therapeutic for Type II Diabetes

Table 4.1 Proteins identified by mass spectrometry showing changes in phosphorylation or abundance in response to RTC-15 treatment 128

Table 4.2 Function of proteins identified by MS showing changes in response to RTC-15 134

Chapter 5: Structural and functional characterisation of the C-Terminus of STRA6

Table 5.1 Fractional structural content of purified and analysed recombinant proteins ..199

List of Abbreviations

2D	Two dimensional
ALAD	Delta-aminolevulinic acid dehydratase
AKAP	A kinase anchoring protein
APC	Adenomatosis polyposis coli
AMPK	AMP-activated protein kinase
ATRA	All trans retinoic acid
B-ME	β-mercaptoethanol
BMDM	Bone marrow derived macrophage
BSA	Bovine serum albumin
CD	Circular dichroism
CK1	Casein kinase 1
CMYA5	Cardiomyopathy-associated protein 5
CRBP	Cellular retinol binding protein
CRABP	Cellular retinoic acid binding protein
CT	C-terminal domain of STRA6
DCAF12	DDB1- and CUL4-associated factor 12
DDM	n-Dodecyl β-D-Maltopyranoside
D-GAP	D-glyceraldehyde-3-phosphate
DHAP	Dihydroxyacetone phosphate
DMEM	Dulbecco's modified eagle medium
DMSO	Dimethylsulphoxide
DTT	Dithiothreitol
EC3	Extracellular loop 3 of STRA6
ECL	Enhanced chemiluminescent
eNOS	Endothelial nitric oxygen synthase
ECH1	Delta(3,5)-delta(2,4)-dienoyl-CoA isomerase
EFTs	Elongation factor Ts
EfTu	Elongation factor Tu
eIF-6	Eukaryotic translation initiation factor 6

ER	Endoplasmic reticulum
ETC	Electron transport chain
FABP	Fatty acid binding protein
FBS	Fetal bovine serum
FXR	Farnesoid X receptor
GFP	Green fluorescent protein
G-HCl	Guanidine hydrochloride
GSK3β	Glycogen synthase kinase 3 β
GST	Glutathione S transferase
HAT	Histone acetyltransferase
HDAC	Histone deacetylase
HEK	Human embryonic kidney
HFD	High fat diet
hnRNP	Heterogeneous nuclear ribonucleoprotein H2
IEF	Isoelectric focusing
IC3	Intracellular loop 3 of STRA6
IL-6	Interleukin-6
IMMT	Mitochondrial inner membrane protein isoform 1
IPTG	Isopropyl β-D-1-thiogalactopyranoside
IRS-1	Insulin receptor substrate-1
IVD	Isovaleryl co-A dehydrogenase
JAK2	Janus kinase 2
JNK	c-Jun N-terminal kinase
KRB	Krebs Ringer buffer
LAT-2	Lysozyme homolog AT-2
LDAO	N,N-Dimethyldodecylamine N-oxide
LRAT	Lecithin retinol acyltransferase
LXR	Liver X receptor
MBP	Maltose binding protein
MCP-1	Monocyte chemoattractant protein-1
MINOS	Mitochondrial inner membrane organising system

MS	Mass spectrometry
MUP	Mouse urinary protein
NCoA	Nuclear receptor co-activator
NCoR	Nuclear receptor co-repressor
OAT	Ornithine aminotransferase
OD	Optical density
PBS	Phosphate buffered saline
PCR	Polymerase chain reaction
PDH	Pyruvate dehydrogenase
PDIA3	Protein disulphide-isomerase A3
Pdlim1	PDZ and LIM domain protein 1
PI3K	Phosphatidylinositide 3 kinase
PICOT	Protein kinase C θ interacting cousin of thioredoxin
PKA	Protein kinase A
PKC	Protein kinase C
PP1β	Protein phosphatase 1 β
PP2A	Protein phosphatase 2A
PPAR	Peroxisome proliferator-activated receptor
PVDF	Polyvinylidenedifluoride
RA	Retinoic acid
RAR	Retinoic acid receptor
RARE	Retinoic acid response element
RALDH	Retinaldehyde dehydrogenase
RCN-1	Reticulocalbin-1
Rnh1	Ribonuclease/angiogenesis inhibitor-1
RoDHI	Retinol dehydrogenase I
RE	Retinyl ester
RBP	Retinol binding protein
RPE	Retinal pigment epithelium
ROH	Retinol
ROS	Reactive oxygen species

RyR1	Ryanodine receptor 1
RXR	Retinoid x receptor
SDAD	Sulfo-NHS-SS-diazerine
SDS	Sodium Dodecyl Sulphate
SDS-PAGE	Sodium Dodecyl Sulphate Polyacrylamide Gel Electrophoresis
SEC	Size exclusion chromatography
SERCA	Sarco/endoplasmic reticulum Ca^{2+} ATPase
SH2	Src homology 2 domain
SMN	Smooth muscle neuron
SMRT	Silencing mediator of retinoic acid
SnRNP	Small nuclear ribonucleoproteins
SnRNA	Small nuclear ribonucleic acid
SOCS3	Suppressor of cytokine signalling 3
SR	Sarcoplasmic reticulum
SRC-1	Steroid receptor co-activator-1
STAT5	Signal transducer and activator of transcription 5
STRA6	Stimulated by retinoic acid gene 6
STRAP	Ser/Thr kinase receptor associated protein
TB	Terrific broth
TBS	Tris buffered saline
TIF2	Transcriptional intermediary factor 2
TLR-4	Toll like receptor-4
TNFα	Tumour necrosis factor α
TPI	Triose phosphate isomerase
TR	Thyroid hormone receptor
TTR	Transthyretin
VDR	Vitamin D receptor
WHO	World health organisation
WT	Wild type
ZPR1	Zinc finger protein-1

Chapter 1

Introduction

1.1 Vitamin A regulation and transport:

Vitamin A or retinol (ROH) is a fat soluble vitamin. Fig 1.1 depicts the chemical structure of ROH. It contains a β-ionone ring which is characteristic of retinoid molecules and a polyunsaturated side chain (Pitt, 1965). It is a highly hydrophobic molecule and can be toxic in large amounts. Plants and some bacteria have the ability to synthesise ROH. However, animals must obtain it from the diet. Foods such as carrots, sweet potato, liver and dark leafy greens are rich in ROH. ROH is an essential dietary requirement and is vitally important for vision and gene transcription. It is absorbed in the small intestine, from there it is stored in the liver. Indeed, the ingestion of fresh liver was once used by the ancient Egyptians as a cure for night blindness. It was not until thousands of years later that the active ingredient was identified as ROH. Retinol based therapies are used for a number of illnesses such as cancer, acne and visual defects. However, in excess, retinoids can be harmful and the regulation and transport of these toxic agents must be tightly controlled. Deregulation of retinoids can lead to diseases as diverse as cancer, visual disorders, teratogenicity and neurological disorders.

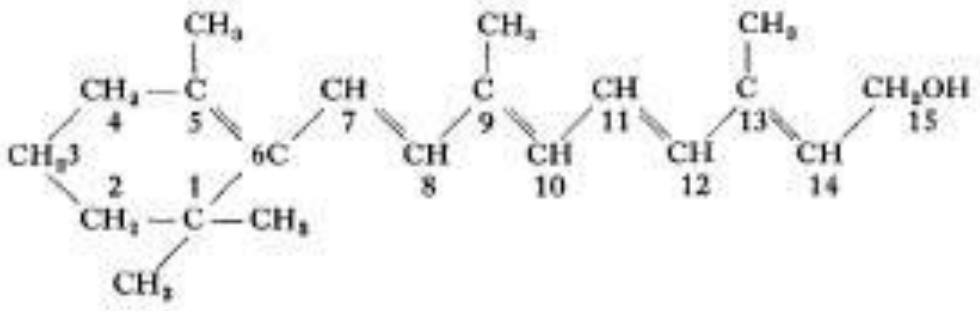

Fig. 1.1 The chemical structure of ROH.

Representation of the chemical structure of ROH (Pitt, 1965). The structure of ROH is based on a β-ionone ring and a polyunsaturated side chain.

1.1.1 The vitamin A transport protein, Retinol Binding Protein:

Retinol Binding Protein (RBP) is responsible for the transport of ROH throughout the body. The liver is one of its main expression sites. RBP binds ROH in the liver to form holo-RBP. As ROH is hydrophobic in nature, binding to RBP facilitates its movement through the aqueous environment of the bloodstream. ROH distribution throughout the body is tightly regulated, suggesting the importance of its use and disposal. It is a strong reducing agent and can cause toxicity in high amounts. RBP is necessary for its safe and efficient transport. RBP belongs to a family of proteins known as lipocalins. Lipocalins are involved in the transport of a diverse range of hydrophobic molecules such as vitamins and steroid hormones.

1.1.2 The structure of RBP:

RBP is part of the lipocalin family of proteins, which transport small hydrophobic molecules such as steroids and retinoids. It contains a single binding site for ROH (Newcomer et al., 1984). The crystal structure of RBP revealed that it contains a coiled N-terminus, an eight stranded β-barrel, an α-helix and a C-terminal coil (Fig 1.2) (Newcomer et al., 1984). The β-barrel acts as the binding pocket for ROH. ROH enters through 3 important loops of the structure which guard the entrance to the binding pocket (Zanotti et al., 1993). The three loop regions consist of residues 33 to 36, 64 to 68 and 92 to 98 and demonstrate a conformational change when ROH binds (Zanotti et al., 1993). The β-ionone ring of ROH lies near the bottom of the pocket with the isoprene tail lying towards the opening. This may be important for trafficking of ROH across the cell membrane.

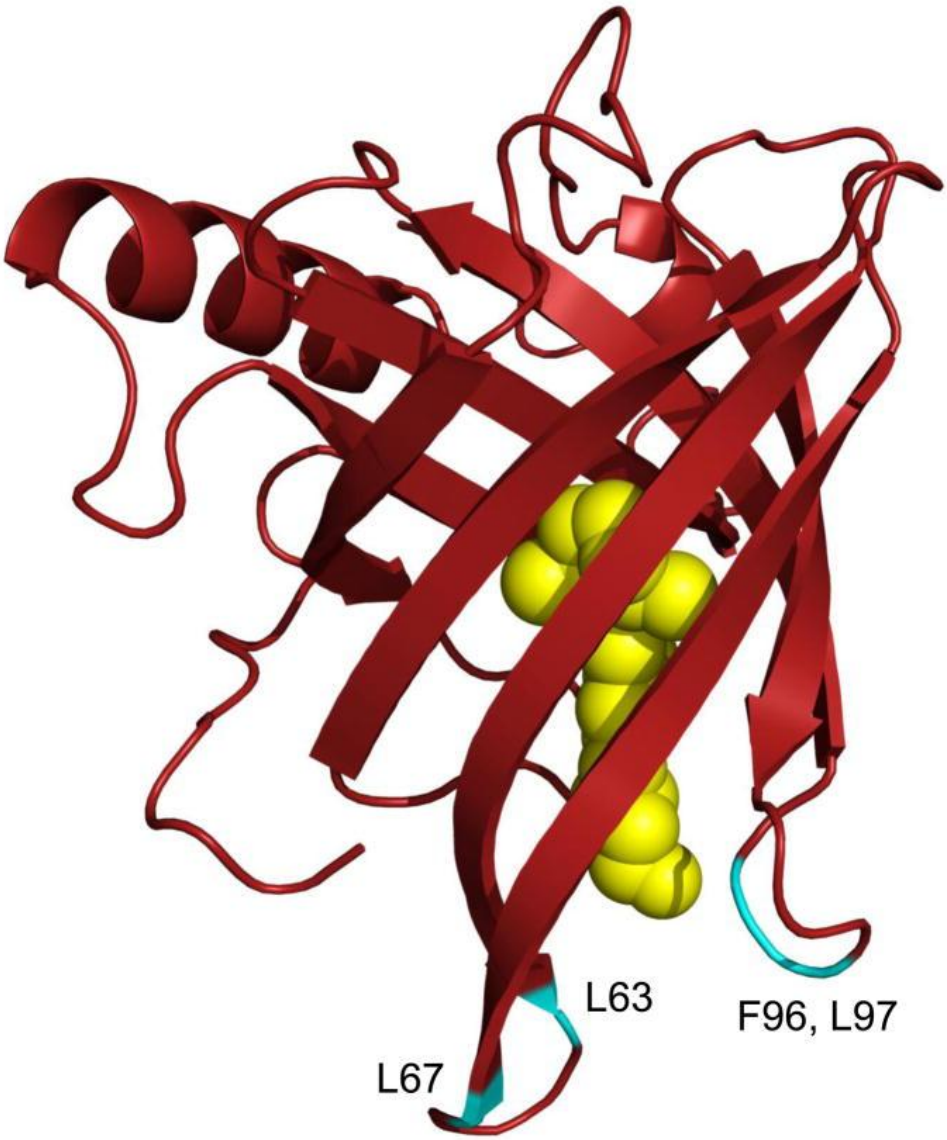

Fig. 1.2 The crystal structure of retinol binding protein.

RBP is shown in red with ROH shown in yellow. ROH is orientated with the β-ionone ring inserted in the binding pocket and the isoprene tail pointing outwards (Berry and Noy, 2012).

1.1.3 RBP and its interaction with Transthyretin:

RBP circulates through the bloodstream bound to Transthyretin (TTR). When holo-RBP is generated in the liver a conformational change occurs allowing it to interact stably with TTR. This initiates the release of the complex into the serum. TTR itself is a homotetrameric structure with four potential binding sites for RBP (Fig 1.3) (Hyung et al., 2010). Due to an excess of TTR in the serum, generally only one RBP molecule binds per TTR homotetramer (Goodman, 1984). RBP alone has a molecular weight of 21kDa, when bound to TTR the complex has a molecular weight of 76kDa. The increased mass of the complex allows it to pass through the glomerulus unfiltered, thus preventing excretion of holo-RBP in the urine. TTR only has affinity for holo-RBP and not the ROH un-bound version (apo-RBP), (Heller and Horwitz, 1973). The TTR-RBP complex then travels through the bloodstream delivering ROH to target tissues.

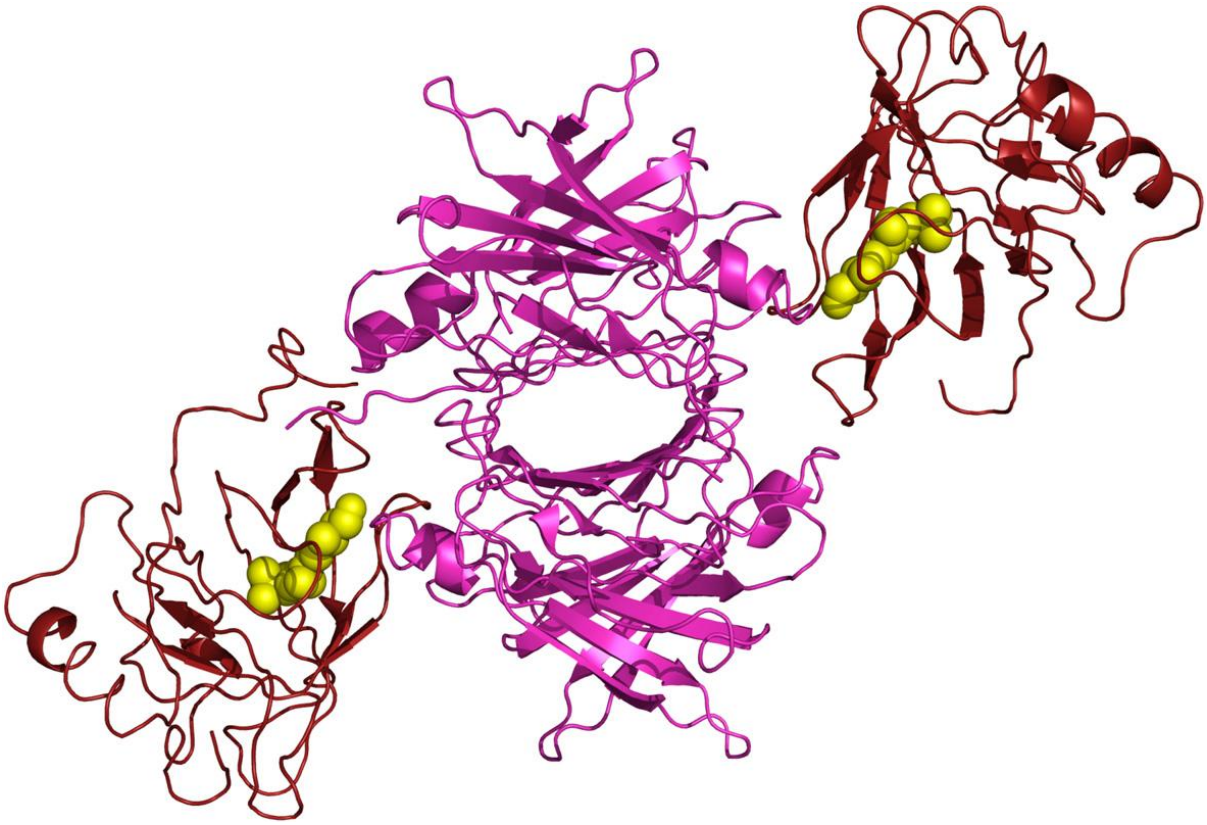

Fig. 1.3 Crystal structure of TTR coupled to holo-RBP.

Holo-RBP is shown in red and TTR shown in purple. The TTR homotetramer can bind two molecules of holo-RBP but usually only binds one (Berry et al., 2011).

1.1.4 Delivery of ROH into the cell:

ROH is transported across the cell membrane via a receptor called Stimulated by Retinoic Acid 6 or STRA6 (Kawaguchi et al., 2007). STRA6 competes with TTR for the same region on the RBP molecule. Therefore, in order for the TTR-RBP complex to dissociate, STRA6 must have a higher affinity than TTR for RBP binding. Indeed this is the case, the affinity of TTR for RBP is in the micro molar range (Malpeli et al., 1996) and the affinity of STRA6 for RBP is in the nanomolar range (Kawaguchi et al., 2007). As TTR does not rebind apo-RBP, RBP is then small enough to be excreted by the kidney. ROH is subsequently free to traverse the membrane to its intracellular acceptor molecule, cellular retinol binding protein (CRBP) (Fig. 1.4).

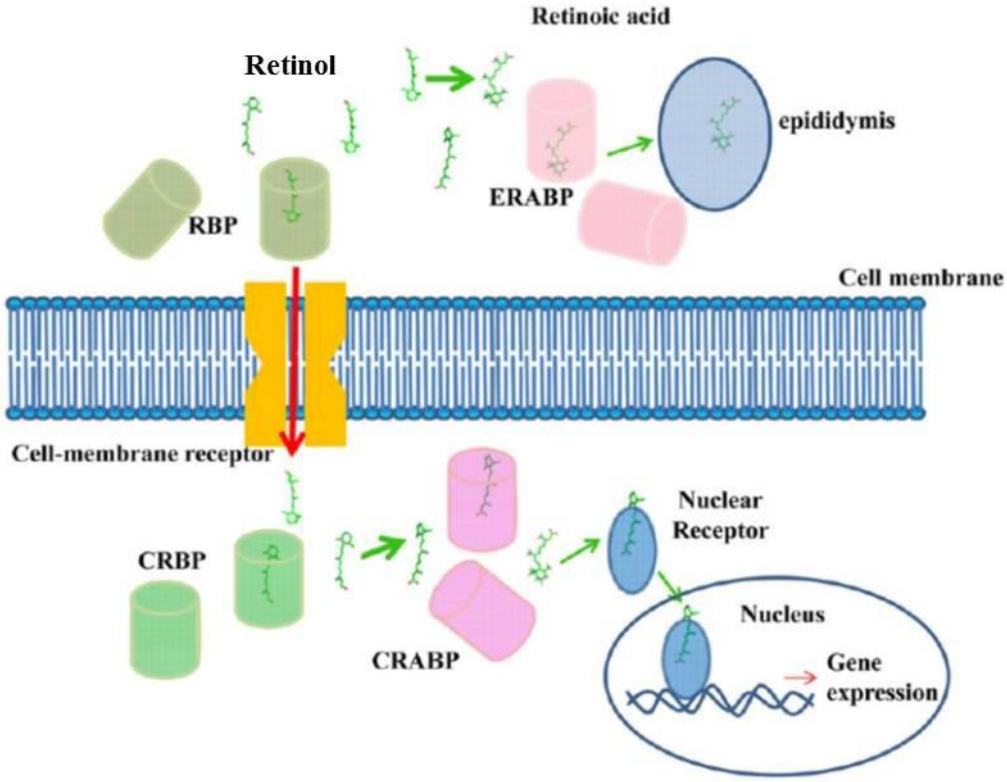

Fig. 1.4 The transport of ROH through the cell membrane.

Holo-RBP binds to the cell membrane receptor (STRA6) and ROH traverses the membrane to bind to intracellular CRBP. Once inside the cell ROH is metabolised and induces gene expression (Zhang et al., 2012).

1.1.5 Interaction of RBP with STRA6 and TTR:

RBP has three potential areas of interaction with STRA6. The carboxy domain of RBP is altered when RBP is excreted in the urine. RBP extracted from the urine differs from serum RBP in that it appears to undergo cleavage after excretion through the kidney, resulting in removal of the final four residues of the sequence (Rask et al., 1980). Urinary RBP was shown to have a much lower affinity for TTR. The C-terminal region of RBP may act to stabilise the structure of the protein and its interaction with ROH. A mutagenesis study carried out by Sundaram et al demonstrated that altering the loop regions between the β strands of RBP, around the ROH exit site, can greatly affect both TTR and STRA6 binding (Sivaprasadarao and Findlay, 1994). Mutation of residue L35, located in the loop region connecting β strands A and B, showed a marked decrease in TTR binding but not STRA6 binding. Mutation of residues L63 and L64 in the loop region connecting β strands C and D showed a significant decrease in TTR binding and completely abolished the ability of RBP to bind to STRA6. In addition, deletion of the loop region connecting β strands E and F completely removed the ability of RBP to bind to TTR but RBP still had some affinity for STRA6. Crystallographic studies of RBP complexed with TTR confirmed that RBP binds to TTR at the ROH exit site (Naylor and Newcomer, 1999). The crystal structure also confirmed that the C-terminus of RBP is involved in TTR binding, specifically the terminal leucine residues, Leu 182 and Leu 183. RBP and TTR both contribute 21 amino acids to the interaction site. The majority of the residues contributed by RBP are located on the loop region connecting β strands E and F, as predicted by mutagenic analysis. Therefore, TTR and STRA6 must bind to RBP around the exit site for ROH but with different affinity for some of the loop regions. Redondo et al went on to further demonstrate that the loop region between β strands C and D (CD loop) was enough to confer binding affinity of RBP to STRA6 (Redondo et al., 2008). A unique chimera of a mouse lipocalin, mouse urinary protein (MUP) fused with the CD loop of RBP, was used to demonstrate that this protein could bind to STRA6. MUP is a protein that binds to pheromones excreted in male mouse urine and has no natural affinity for STRA6. MUP with the CD loop replacing residues 59-68 of the native protein, bound to HEK cell membranes that express STRA6

and showed a higher affinity when its natural ligand 3-isobutyl-2-methoxypyrazine (IBMP) was present (Redondo et al., 2008).

1.1.6 The internal acceptor for ROH, CRBP:

Once inside the cell, ROH binds to its acceptor molecule CRBP. The two most prominent isoforms of CRBP are CRBP I and CRBP II. They share 56% sequence identity and both proteins are highly conserved across species. CRBP II is predominantly expressed in the intestinal mucosa and is involved in the uptake of ROH from dietary sources (Napoli, 2000). CRBP has a very specific affinity for ROH, with a Kd of 0.1 nM. RBP and CRBP share a very similar tertiary structure, CRBP contains 10 β-strands as opposed to 8 in RBP (Fig 1.5). Similar to RBP, the β-strands form a binding pocket for ROH. However, ROH has the opposite orientation in the binding pocket of CRBP compared to RBP (Fig 1.4). The β-ionone ring lies at the outside of the binding pocket with the isoprene tail lying in the inside face of the β-barrel (Franzoni et al., 2002). This would suggest that ROH simply slips out of the binding pocket located in RBP, through STRA6, directly into the binding pocket of CRBP (Fig.1.3) but this is likely to be a simplistic view. Once ROH enters the cell it is quickly converted to retinyl ester (RE) by lecithin retinol acyltransferase (LRAT) for storage. Indeed, LRAT may even be a specific component of the ROH transport process (Kawaguchi et al., 2011).

1.1.7 The function of CRBP:

CRBP is integral for the controlled utilisation and storage of ROH inside the cell. Holo-CRBP acts as a substrate for esterification and hydrolysing enzymes, such as LRAT. However, LRAT can convert ROH to RE in the absence of CRBP. CRBP I knockout mice present a perfectly normal phenotype when fed a vitamin A supplemented diet. However, there is very rapid turnover of ROH. When the knockout mice were fed a vitamin A deficient diet RE stores became fully depleted compared to wild type (WT) which never became depleted (Ghyselinck et al., 1999). Conversely, apo-CRBP has a strong inhibitory action on LRAT, preventing ROH storage when there is ROH deficiency. Apo-CRBP can also stimulate the hydrolysis of RE to supply free ROH for metabolism by activating the enzyme retinyl ester hydrolase (Napoli, 1999). This would suggest that CRBP plays a crucial role in

maintaining RE stores and ensuring that the cell has a constant supply of ROH. In the intracellular environment an equilibrium of ROH levels exists which is tightly controlled by both the holo and apo versions of CRBP. This would suggest a structural change of some sort is allowing CRBP to regulate ROH metabolic enzymes in very different ways.

Fig. 1.5 Structure of CRBP I with ROH bound.

The solved crystal structure of CRBP with retinol bound (shown in grey). The β-ionone ring of retinol lies at the outside of the binding pocket with the isoprene tail lying in the inside face of the β-barrel (Franzoni et al., 2002)

1.1.8 Cellular Retinoic Acid Binding Protein:

Outside of the eye, the functionally active form of ROH is predominantly retinoic acid (RA). RA is produced in a bi-phasic reaction. ROH is first oxidised to form the intermediary substrate, retinal by retinol dehydrogenase I (RoDHI). Retinal is then converted to RA by retinal dehydrogenase (RALDH). RA is sequestered by cellular retinoic acid binding protein (CRABP) which then allows its interaction with the target molecule, the retinoic acid receptor (RAR). There are two isoforms of CRABP, CRABP I and CRABP II which share 72% sequence identity in humans. They are extremely well conserved across species, highlighting their evolutionary significance in retinoid processing. They differ in their tissue distribution with CRABP II mainly confined to the skin and CRABP I being ubiquitously expressed (Li and Norris, 1996).

Both CRABP I and CRABP II bind all-trans-retinoic acid with high affinity. The exact molecular function of CRABP is still under debate. Like CRBP, CRABP acts to protect the cell from free retinoid. CRABP is also thought to play a role in directing RA to its target destination. This was highlighted in a study that demonstrated that in cells overexpressing CRABP, differentiation induced by RA was reduced rather than increased, CRABP could be acting to mop up "excess" RA in the cell. In addition, the cellular expression of both CRABP I and CRABP II is under the direct control of RA, suggesting that in times of excess, increased CRABP levels are stimulated to control the distribution of RA (Donovan et al., 1995). Holo-CRABP also acts as a substrate for RA metabolising enzymes. CRABP has been shown to bind several metabolites of RA. Indeed, increased expression of CRABP led to elevated intracellular levels of known RA metabolites (Donovan et al., 1995). Knockout studies of both CRABP I and CRABP II reveal physiologically normal phenotypes with postaxial forelimb polydactyly being the only abnormality. This demonstrates that other retinoid binding proteins such as fatty acid binding protein (FABP) could be compensating for CRABP absence (Theodosiou et al., 2010).

1.2 STRA6 mediated ROH transport:

It is as yet unknown how STRA6 transports ROH across the cell membrane. Only structural studies will truly reveal how this biological process is occurring. Historically, it was thought that upon binding to its receptor, RBP is internalized (Matarese and Lodish, 1993). However, evidence from Heller et al showed that ^{125} I-RBP could be displaced from its receptor by unlabelled RBP. If endocytosis occurred upon RBP binding, unlabelled RBP could not dissociate labelled RBP from its receptor (Heller, 1975). Thus, RBP is not taken up into the cell via endocytosis. In addition, Sivaprasadarao and Findlay (19988b) demonstrated uptake of ROH without uptake of RBP. They also observed that excess amounts of TTR can inhibit holo-RBP binding to the receptor (Sivaprasadarao and Findlay, 1988a). ROH alone must simply traverse the membrane via its receptor, STRA6.

1.2.1 The dynamics of ROH transport across the cell membrane:

STRA6 does not utilise traditional uptake mechanisms such as active transport or endocytosis. Kawaguchi et al and Sundaram et al suggest that STRA6 functions as an enzyme to catalyse the release of ROH from holo-RBP to intracellular partners (Kawaguchi et al., 2011; Sundaram et al., 1998). Sundaram and colleagues demonstrated that ROH transport through the cell membrane is coupled to an intracellular storage protein. Placental membranes stimulated the release of [^{3}H] ROH from RBP to apo-CRBP, an effect that was abrogated when membranes were denatured (Sundaram et al., 1998). Interestingly, it was found that by increasing expression of the ROH storage proteins CRBP-I and LRAT, both independently, ROH influx into the cell was greatly enhanced (Kawaguchi et al., 2011). CRBP-I displayed saturation kinetics possibly due to lack of availability of the apo-form of the protein, which could also be further evidence that CRBP-I tightly controls the levels of ROH in the cell. LRAT did not display saturation, this may be due to the production of retinyl esters by LRAT. LRAT could not be saturated with ROH in this experimental system as it simply converts ROH into its storage form and is free to bind more substrate.

LRAT specifically enhanced the transport of ROH and not other retinoid molecules such as retinylamine and RA. It appears other retinoids were not the correct substrate for the transportation to

occur. Other retinoid handling proteins were also shown to enhance retinoid uptake into the cell. The enzyme retinol dehydrogenase when overexpressed, led to an increase in STRA6 mediated ROH influx into the cell (Kawaguchi et al., 2011). STRA6 can also transport RA across the cell membrane. CRABP-I when overexpressed was shown to increase RA uptake from RBP loaded with RA (Kawaguchi et al., 2011). As the transport of retinoids is highly reliant on intracellular storage proteins it is possible that these proteins couple directly to STRA6. Potential interaction sites could be the large C-terminal tail and intracellular loop regions.

1.2.2 ROH efflux via STRA6:

Interestingly, in cells solely overexpressing STRA6, saturation for ROH influx into the cell was observed. In addition, free ROH was found to inhibit STRA6 catalysed ROH release from RBP (Kawaguchi et al., 2011). This inhibitory effect was ameliorated by the addition of LRAT or CRBP-I. Once there is a storage protein present for ROH only then will more ROH enter the cell. In 1988, Sivaprasadarao and Findlay (1988b) demonstrated that apo-RBP can reverse the uptake of ROH via membrane vesicles. Kawaguchi et al also observed that following ROH influx into the cell, the addition of apo-RBP to STRA6 led to an efflux of retinol from the intracellular environment to extracellular apo-RBP (Kawaguchi et al., 2012). It seems that STRA6 can also catalyse the re-loading of ROH back onto RBP. This would explain why saturation was observed in STRA6 overexpressing cells. Without increased intracellular recipients for ROH, ROH was simply re-loaded back to the apo form of RBP. In addition, free ROH was found to inhibit further retinol release. Therefore, a negative feedback inhibition occurs, as ROH is released it can negatively impact the release of more ROH from holo-RBP. In cells overexpressing LRAT and STRA6 little efflux of ROH to apo-RBP was observed, presumably due to storage of ROH as retinyl esters. However, in cells overexpressing CRBP-I and STRA6 near complete efflux of previously created ROH stores to apo-RBP was observed (Kawaguchi et al., 2012). Holo-RBP was shown to inhibit the STRA6 catalysed efflux of ROH onto apo-RBP, presumably due to the higher affinity of STRA6 for holo-RBP.

In normal human serum, holo-RBP is found in vast excess compared to the apo version of the protein. Kawaguchi et al demonstrated that cells overexpressing STRA6 and CRBP-I or LRAT do not cause ROH efflux when incubated with human serum. However, when STRA6 and CRBP-I cells were pre-loaded with [^{3}H] ROH an exchange was observed between extracellular cold ROH and intracellular [^{3}H] ROH. This effect was not observed in cells overexpressing LRAT presumably because ROH had already been converted to RE. This phenomenon could be happening as a mechanism to maintain fresh ROH stores, as over time ROH may oxidise. In conclusion, ROH efflux depends on the ratio of holo-RBP versus apo-RBP in the serum and expression levels of CRBP-I and LRAT. Interestingly, it seems that CRBP-I and LRAT are not necessary for STRA6 to be active but they are necessary for the retention and utilisation of ROH.

1.2.3 The physiological relevance of ROH efflux via STRA6:

Kawaguchi et al propose that STRA6 can cause ROH efflux from its intracellular storage partners to apo-RBP (Kawaguchi et al., 2012). When apo-RBP is in vast excess of holo-RBP, ROH can be "re-loaded" to apo-RBP from CRBP-I via STRA6. In normal human serum holo-RBP makes up 90% of the total RBP levels with 10% apo-RBP (Mills et al., 2008). Therefore, the ability of STRA6 to cause ROH efflux out of the cell may not bear any physiological relevance in a normal setting. However, in obese patients serum apo-RBP levels were found to be two fold higher than in lean subjects (Mills et al., 2008). Interestingly, Quadro et al showed that extra-hepatically expressed RBP was able to prevent visual defects which would normally arise in RBP knockout animals (Quadro et al., 2002). In addition, the same group demonstrated that extra-hepatic RBP could not mobilise hepatic ROH stores (Quadro et al., 2004). Thus extra-hepatic RBP must mobilise stores of ROH from other tissues via STRA6.

ROH re-loading onto apo-RBP may be a unique mechanism to allow re-distribution of ROH from ROH sufficient tissues to tissues which are ROH depleted. This may have a profound physiological relevance. A recent publication by Muenzner et al detailed how apo-RBP can cause ROH efflux from adipocytes in a STRA6 dependant manner (Muenzner et al., 2013). The biologically active ROH

derivative, retinoic acid (RA) has a known inhibitory effect on adipocyte differentiation via activation of retinoic acid receptor α (RARα) responsive genes (Kamei et al., 1994). Treatment of pre-adipocytes with apo-RBP led to re-partitioning of ROH into the extracellular milieu causing a subsequent decrease in RARα mediated gene expression. This effect was concomitant with increased adipogenesis. As detailed in section 1.5.1 RBP was identified as a secretory signal produced by adipose tissue leading to increased insulin resistance (Yang et al., 2005). It is unknown at present how much apo-RBP present in the serum is excreted by adipose tissue. The exact ratio of apo-RBP versus holo-RBP excreted by adipose tissue may be an interesting aspect of retinoid homeostasis in fat tissue. RBP produced in mature adipocytes may be having a paracrine effect on neighbouring pre-adipocytes to promote increased adipogenesis.

1.2.4 The influence of other retinoids on STRA6 activity:

Following on from the observation that free ROH can inhibit further ROH release (Kawaguchi et al., 2011), Kawaguchi et al observed that several retinoids can inhibit the ability of STRA6 to load ROH onto apo-RBP, most notably fenretinide (a synthetic derivative of retinoic acid), all trans retinal, all trans retinoic acid and 13-cis retinoic acid (Kawaguchi et al., 2013). The same retinoids also increased STRA6 catalysed ROH release from holo-RBP. The effect of retinoids on STRA6 activity appears to be isomer specific with the 9-cis isomers being much less effective than all-trans isomers. The ability of certain retinoids to inhibit ROH loading onto RBP is partially due to the transfer of the retinoid to RBP by STRA6 in place of ROH. Therefore, STRA6 can recognise and bind to other retinoids apart from ROH. This interaction is highly specific as 9-cis isomers do not show the same properties as the all-trans isomers, thus STRA6 will only recognise a certain structural conformation of retinoids.

In the experiments described above, the retinoids were interacting with STRA6 in an extracellular manner. In a physiological setting this may not occur frequently, as the retinoids are produced as products of enzymatic reactions intracellularly. Where it does bear physiological relevance is in the treatment of certain disorders. Several retinoids are utilised for treatments such as acne, cancer and visual defects. Fenretinide has traditionally been used as an anti-cancer therapeutic particularly in the

treatment of breast cancer. The exact mechanism of action has yet to be identified but fenretinide has been shown to induce apoptosis rather than cell differentiation (Lazzeroni et al., 2011). STRA6 is known to be up-regulated in several types of cancer. Fenretinide could be functioning by interrupting STRA6 interaction with its native ligand, ROH. Fenretinide was shown to increase ROH release from holo-RBP and prevent ROH loading back to apo-RBP, therefore the net effect would be an increase in intracellular ROH leading to activation of RAR target genes.

1.3 The RBP receptor; STRA6:

It was originally believed that ROH simply partitioned through the cell membrane, due to its hydrophobic nature (Noy and Xu, 1990). As ROH is highly toxic in large amounts, a more practical view developed that there exists a controlled delivery system for ROH intracellular transport.

1.3.1 Discovery of the RBP-Receptor:

The first account of RBP binding to a specific membrane protein appeared in 1975 (Heller, 1975). Heller et al found that ^{125} I-RBP specifically bound to some unknown protein present in pigment epithelial cells. This interaction was displaced by unlabelled RBP, and ^{125} I-RBP could not be displaced by TTR, showing that it was a specific, high affinity interaction. Sivaprasadarao and Findlay (1988a) further demonstrated that a protein present in the cell membrane could bind to holo-RBP and initiate ROH transport through the cell membrane. RBP was observed to bind to a protein present in membrane vesicles generated from placental brush border cells and this protein greatly enhanced [^{3}H] ROH transport to its acceptor protein, CRBP (Sundaram et al., 1998). This was further evidence that there was a specific protein present in the membrane responsible for the uptake of ROH. In addition, it showed that the developing foetus was able to absorb ROH from maternal stores via a receptor located in the placental membrane.

1.3.2 Identification of the RBP Receptor, STRA6:

The interaction of RBP with STRA6 is transient in nature. This is due to the decreased affinity of STRA6 for apo-RBP compared to holo-RBP. This transient interaction made identification of the RBP receptor extremely difficult. In 2007, Kawaguchi et al employed a novel crosslinking technique to stabilise the interaction of RBP with its receptor. Subsequent affinity purification of RBP and mass spectrometry analysis of co-purified protein, revealed the receptor to be STRA6. Cells transfected with this novel receptor were found to have a much higher affinity for RBP binding and dramatically increased ROH uptake (Kawaguchi et al., 2007). STRA6 was originally identified as a gene which was upregulated in embryonic carcinoma P19 cells treated with retinoic acid (RA) (Bouillet et al., 1997). It is unlike any other protein in the human genome. In addition to RA stimulation, STRA6 expression is also induced via the wnt-1 signalling pathway (Szeto et al., 2001). Activation of the wnt-1 pathway inhibits the degradation of the signalling molecule, β-catenin, thus enabling it to travel to the nucleus and induce expression of wnt-1 responsive genes. Szeto et al also demonstrated that cells overexpressing wnt-1 showed a concomitant increase in STRA6 mRNA. The induction of STRA6 expression was augmented by the addition of al-trans retinoic acid (ATRA). In addition, STRA6 expression was completely blocked with the addition of a pan-RAR antagonist, which implies that STRA6 expression is dependent on RAR activity. Wnt-1 signalling synergistically augments STRA6 expression via crosstalk between β-catenin and RAR, through some as yet unknown mechanism.

1.3.3 STRA6 and embryonic development:

STRA6 is expressed in most tissues throughout the body (Fig.1.6), especially in blood organ barriers like the blood brain barrier and the retinal pigment epithelium. This allows for the efficient uptake of ROH from holo-RBP present in the bloodstream. STRA6 is transiently expressed in many tissues during development. A study conducted by Chazaud et al utilised *in situ* hybridisation to trace the expression pattern of STRA6 in developing mouse embryos (Chazaud et al., 1996). The study showed that STRA6 is heavily expressed in the limb bud outgrowth, distally from the origin of the limb and in regions of rapid differentiation. This correlates strongly with the finding that RA induces extension of

the limb bud (Summerbell, 1983). STRA6 is highly expressed in the labyrinthine region of the placenta, which is the zone of exchange between the maternal and fetal bloods (Bouillet et al., 1997), reinforcing the importance of the vitamin for normal embryonic development.

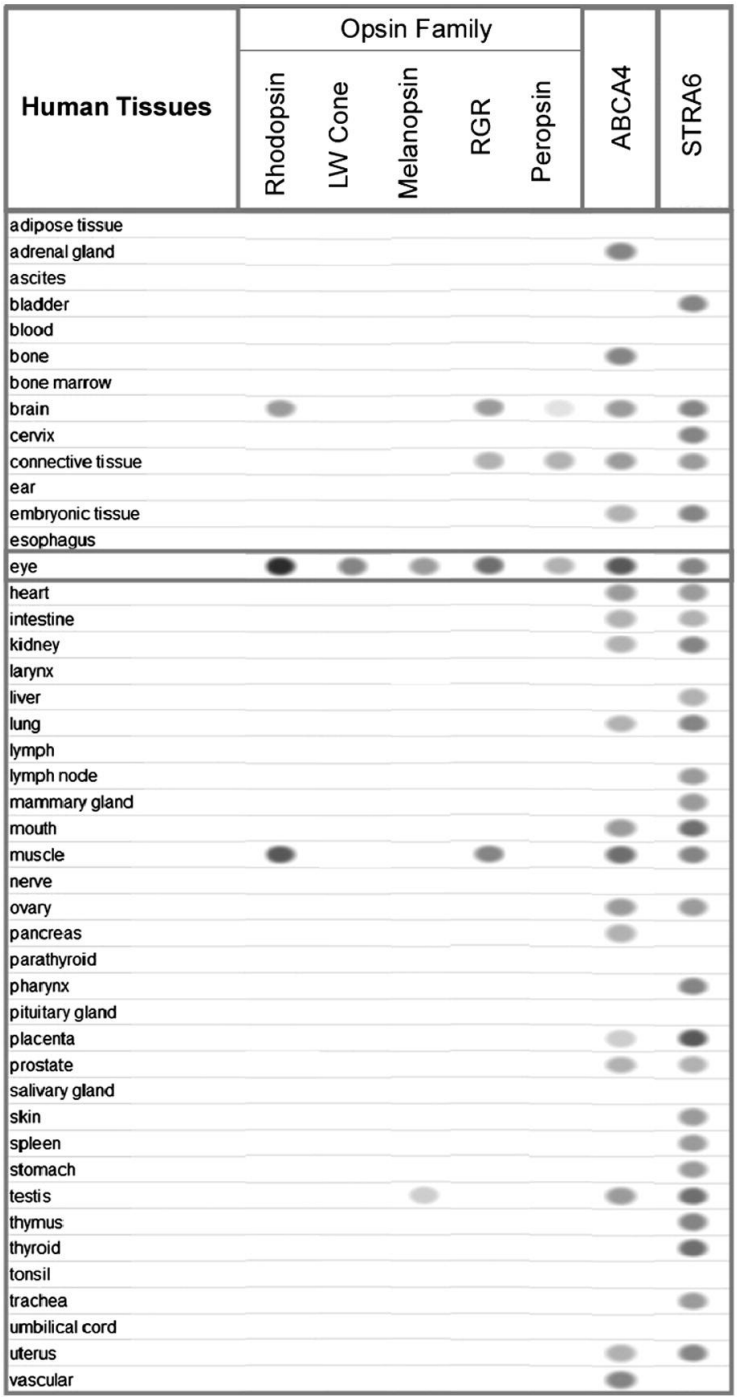

Fig. 1.6 Tissue distribution of retinoid handling receptors.

Table representing the expression levels of STRA6 in various tissues, as assessed by expressed sequence tag (EST) counts recorded by NCBI's EST Profile Viewer. Intensity of the oval represents relative abundance of STRA6 mRNA. Absence of an oval represents undetectable expression levels (Sun, 2012).

1.3.4 Matthew Wood Syndrome:

The importance of STRA6 to human development is clearly evident from studies on specific human mutations. Genetic polymorphisms give us a clear insight as to what role a protein has *in vivo*. Known genetic mutations in STRA6 range from single point mutations, to missense or frame shift mutations which result in truncated translated protein (Fig 1.7). They are extremely deleterious, often embryos do not reach full gestation and if they do, they are severely compromised. Abnormalities include microphthalmia or anophthalmia, congenital heart and lung defects as well as mental retardation. The collective phenotype is now known as the underlying genetic cause of Matthew Wood Syndrome. This is a congenital disorder which displays the characteristic abnormalities associated with STRA6 mutations (Golzio et al., 2007).

The detection of STRA6 mutations in cases of anophthalmia is becoming increasingly common. When a cohort of random cases of anophthalmia were screened approximately 4% of those cases were due to mutations located in the STRA6 gene (White et al., 2008). Patients with these particular mutations did not display any other phenotype apart from anophthalmia, thus some STRA6 mutations may be more severe than others. Genetic mutations highlight how essential STRA6 is for normal ocular development. Mutations mostly arise in the intracellular loops 1 and 3, the extracellular loop 3 and the C-terminal region of STRA6 (Pasutto et al., 2007). Table 1.1 summarises known genetic point mutations, their location and how they affect STRA6 expression, RBP binding and ROH transport.

Kawaguchi et al conducted large scale mutagenic analysis of STRA6 (Kawaguchi et al., 2008a). The known genetic mutations yielded varying results. Most mutations led to retention of STRA6 in the endoplasmic reticulum (ER). This of course would cause a decrease in availability of the receptor at the cell membrane and subsequent decrease in RBP binding and ROH transport. The T321P genetic mutation appears not to affect STRA6 transport to the membrane. However, this mutation was identified alongside mutation P90L, suggesting that it is the dominant negative of the two (Kawaguchi et al., 2008a). Mutations that arise in the human population appear to affect trafficking of the receptor during development. This would lead to a decrease in ROH influx into the cell which is vital during

embryonic development. Interestingly, missense mutations are often associated with a more severe phenotype than truncation mutations and there is vast phenotypic variability among patients and across known mutations (Ng et al., 2013). In contrast, genetic mutations in RBP exhibit a much milder phenotype in comparison to STRA6. This may suggest that STRA6 has other functions in addition to its ROH transport function.

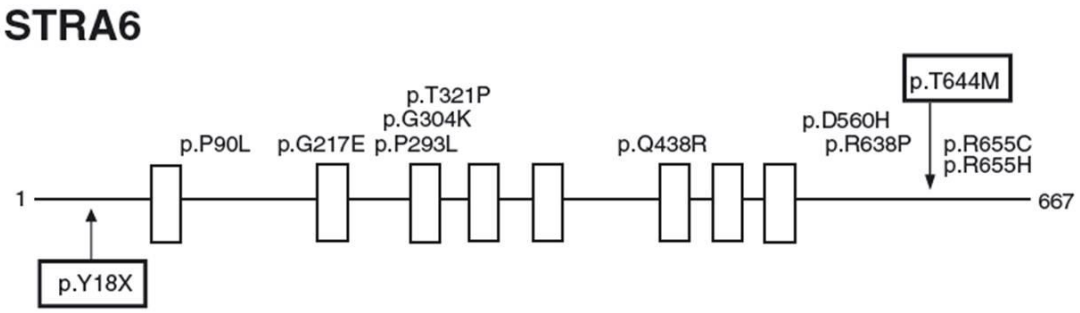

Fig 1.7 Locations in the STRA6 protein sequence where genetic mutations have been observed.

Representation of the location of all known genetic mutations found in STRA6. Vertical boxes denote transmembrane regions in the protein sequence from amino acid 1 to 667. Point mutations are positioned at the approximate location in the STRA6 sequence (Ng et al., 2013).

Mutation	Location	Membrane Localisation	RBP Binding	ROH Transport
P90L	IC-1	None, localised in ER	Greatly Reduced	Reduced
G217E	TM5	Unknown	Unknown	Unknown
P293L	IC-3	None, localised in ER	Greatly Reduced	Reduced
G304K	TM7	None, localised in ER	Greatly Reduced	Reduced
T321P	EC-3	Expressed at the cell membrane	Not affected	Not affected
Q438R	TM8	Unknown	Unknown	Unknown
D560H	C-Term	Unknown	Unknown	Unknown
R638P	C-Term	Unknown	Unknown	Unknown
T644M	C-Term	None, localised in ER	Greatly Reduced	Reduced
R655C	C-Term	None, localised in ER	Greatly Reduced	Reduced

Table 1.1 Summary of the location of point mutations found in STRA6 to date and the effect on membrane localisation, RBP binding and ROH transport.

Table summarising the known genetic mutations that occur in the STRA6 gene and their impact on receptor expression, RBP binding and ROH transport. Intracellular loop (IC), extracellular loop (EC), transmembrane region (TM). Data was compiled from (Casey et al., 2011; Chassaing et al., 2012; Kawaguchi et al., 2008a; Ng et al., 2013; White et al., 2008).

1.3.5 STRA6 knockout studies:

Although human genetic mutations in STRA6 are extremely deleterious, murine knockout models of the receptor are viable and give us some insight into the functioning of the receptor. Deletion of the orthologous STRA6 gene in mice produced very mild phenotypic abnormalities (Ruiz et al., 2012). This was surprising considering the severity of malformations in the human counterpart. The only abnormalities observed were localised to the eye region, in particular the retinal pigment epithelium (RPE). A slight reduction in eye diameter was observed in STRA6 null mice compared to wild type (WT). The inner and outer segments of the retina were thinner in diameter in the STRA6 null mice and densely packed cell masses were observed in the vitreous humour of the knockout. Visual responsiveness to light was significantly diminished in the knockout, but not fully abolished, suggesting that there may be some sort of compensatory mechanism for ROH uptake. This was reflected in the level of ROH metabolites present in the RPE, where significant levels of retinyl esters were present along with other ROH metabolites necessary for vision, such as ATRA and 11-cis-retinal. This would suggest that ROH was entering the cell and being actively metabolised via a STRA6 independent mechanism. Considering the fatal defects observed in humans carrying even a single point mutation in the STRA6 gene, the same compensatory mechanism may not be present in humans.

Interestingly, STRA6 knockdown in a zebrafish model demonstrated much more severe morphological defects compared to the murine model (Isken et al., 2008). Microphthalmia was observed along with malformed body axis, heart edema and cardiac malformations, phenotypic characteristics similar to the Matthew-Wood Syndrome. One would assume that defects caused by STRA6 deficiency occur as a result of decreased ROH uptake. However, Isken et al observed normal RA production in some tissues, even excess RA in some areas of the STRA6 knockdown model. Therefore, STRA6 deficiency did not result in decreased RA production, but excess RA production. Isken and colleagues propose that the malformations observed with STRA6 deficiency occur as a result of uncontrolled ROH uptake. They demonstrated that reduction of RBP expression in the developing larvae prevented the malformations caused by STRA6 knockdown (Isken et al., 2008).

Some malformations were still apparent with reduced RBP levels, but not as severe when RBP levels were normal (Isken et al., 2008). Reduction of RBP expression blocked mobilisation of yolk vitamin A stores. This suggests that uncontrolled utilisation of ROH stores is responsible for genetic mutations caused by STRA6 knockdown.

Interestingly, RBP knockout models develop a normal phenotype and human deletion mutations have been observed with no medical complications, when a vitamin A rich diet is maintained. STRA6 mutations may be more severe compared to RBP abnormalities, due to uncontrolled utilisation of ROH. This may explain the discrepancy between the RBP deficient model and the STRA6 deficient model.

1.3.6 STRA6 topology:

STRA6 is 667 amino acids long and has a molecular weight of 72 kDa. Computational analysis to reveal the folding of a protein in the cell membrane can be a valuable tool to gain insights into its structure and function. Topology modelling of STRA6 has yielded conflicting results about the exact number of transmembrane regions, with some groups suggesting anywhere between eight and twelve transmembrane segments. Topology modelling software may predict varying transmembrane structures but extensive experimental analysis suggests a 9 transmembrane topology (Kawaguchi et al., 2008b). Kawaguchi et al inserted a Myc epitope tag into putative extra and intracellular regions of the receptor. Subsequent analysis of accessibility of an anti-Myc antibody to each of the mutated regions revealed the topology of STRA6 (Fig 1.8). Along with 9 transmembrane (TM) regions the receptor contains several interesting putative domains. The N-terminal region appears to be extracellular leaving the large C-terminal region intracellular. Other domains of interest include a large third extracellular loop, connecting TM 6 and 7 and two large intracellular loop regions, connecting TM 5 and 6 and TM 7 and 8, respectively.

STRA6 Constructs	Live Cell Staining	Permeabilized Cell Staining	Retinol Uptake Activity [%±SD of WT]	Surface Expression Quantitation [%±SD of M10]	RBP Binding Activity [%±SD of WT]	Category
M1	+	+	86.43±5.97	35.33±2.88	41.67±2.87	1
M2	-	+	55.07±2.00	0.17±0.29	57.87±1.97	3
M3	+	+	59.40±7.96	23.67±3.22	56.00±7.00	1
M4	-	+	55.68±2.59	0.43±0.59	24.32±5.94	3
M5	+	+	56.21±4.85	41.33±4.04	15.66±1.32	2
M6	-	+	70.25±2.58	0.13±0.35	99.31±14.00	3
M7	-	+	0.39±1.08	0.40±0.53	8.47±4.48	4
M8	-	+	0.00±0.624	0.77±1.08	8.53±4.01	4
M9	-	+	97.90±6.44	0.23±0.25	96.51±10.16	3
M10	+	+	47.15±4.96	100±8.43	14.43±0.90	2
M11	-	+	49.59±3.56	0.43±0.49	70.75±4.28	3
M12	-	+	0.00±1.87	0.73±1.02	8.08±4.24	4
M13	-	+	80.76±2.27	0.33±0.58	96.51±4.53	3
M14	-	+	108.41±3.19	0.27±0.29	119.00±4.58	3

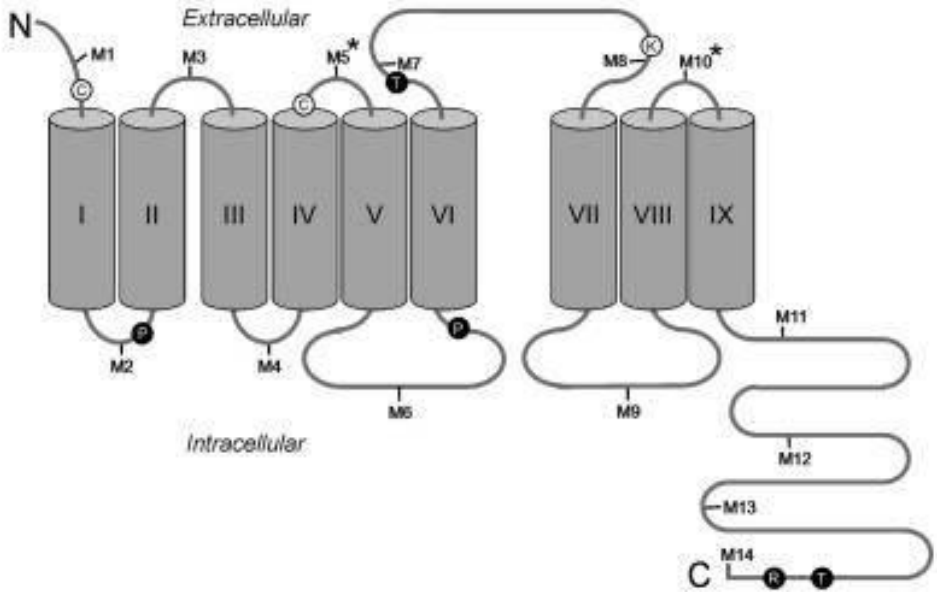

Fig 1.8 Topology model of STRA6 as revealed by epitope tagging.

Epitope tagging experiments have revealed potential extra and intracellular regions of STRA6. Each of the locations where the Myc epitope tag was inserted is denoted by M and depicted on the topology model of STRA6. A positive sign with live cell staining revealed that anti-Myc antibody was able to gain access to the respective inserted Myc epitope without cell permeabilization, thus revealing this location to be extracellular (Kawaguchi et al., 2008b).

1.3.7 Extracellular loop 3:

The large third extracellular loop region (EC3) between TM 6 and TM7 consists of 44 amino acids. Large scale mutagenesis suggests an essential binding site for RBP located in this region. (Kawaguchi et al., 2008a). When residues Y336, G340 and G342 of the bovine sequence of STRA6 were mutated individually, RBP binding and subsequent ROH transport, were significantly reduced. All 3 mutated versions of the protein were expressed at the cell membrane and were readily available to RBP. The three residues implicated in RBP binding are highly conserved among species and they correlate to residues Y335, G339 and G341 in the human sequence (Fig 1.9). Interestingly, leucine 336 in the human sequence is replaced with a methionine residue in the monkey sequence. Inclusion of methionine at this site would significantly shift the relative position of the critical tyrosine residue in relation to the other putative RBP binding sites. This could indicate that some of the 3 residues are more important for the interaction to occur between STRA6 and RBP than others. When the three critical residues were mutated respectively, ROH uptake was significantly impaired. However, mutation of bovine STRA6 at residue 342 was not as detrimental on uptake activity (Kawaguchi et al., 2008a). In addition, RBP binding was completely abolished when residues Y336 and G342 were replaced, but some affinity still remained when residue G340 was mutated (Kawaguchi et al., 2008a). As elucidated by Redondo et al the binding site of RBP for STRA6 is the CD loop region (Redondo et al., 2008). These three key residues may be directly interacting with the CD loop of RBP. It is unknown as yet whether interaction of RBP with these three residues is enough to stimulate ROH release from RBP.

```
BOVINE          ITTDVSYLLAGFGIVLSEDRQE
RAT             ITTDVSYLLAGFGIVLSEDRQE
MOUSE           INTDVSYLLAGFGIVLSEDRQE
HUMAN           VTTDVSYLLAGFGIVLSEDKQE
MONKEY          VTTDVSYMLAGFGIVLSEDKQE
```

Fig 1.9 Cross-species sequence alignment of the putative RBP-binding domain of STRA6 as identified by random large scale mutagenesis.

Y336, G340 and G342 along with other residues in this region of the bovine sequence of STRA6, are highly conserved across species. Mutations in any three of these residues (shown in yellow) result in loss of RBP-binding and consequently, loss of vitamin A uptake activity (Kawaguchi et al., 2008a). Alignment performed using ClustalW 2.1.

1.3.8 Intracellular loop 3:

STRA6 also possesses a large third intracellular loop (IC3) between TM 5 and 6, consisting of approximately 73 amino acids. Mutations in this region resulted in a marked decrease in ROH transport (Kawaguchi et al., 2008a). As it is not accessible to RBP binding it may be a potential binding site for the intracellular storage partners for ROH, such as CRBP or LRAT, which are essential for ROH transport. Berry et al observed that a fusion protein generated from residues 235-293 of STRA6, conjugated to green fluorescent protein (GFP) was capable of binding CRBP (Berry et al., 2012). The complex that formed was dissociated with increasing amounts of ROH, showing that STRA6 has a decreased affinity for holo-CRBP. It is as yet undetermined if this domain alone is enough to stimulate ROH transport across the cell membrane. Specific mutation of leucine 255 to alanine in the IC3 loop resulted in loss of CRBP binding (Berry et al., 2012). Mutation of full length STRA6 at L255 resulted in below basal levels of ROH uptake. Therefore, this residue appears to be critical for ROH transport and CRBP binding.

As discussed in section 1.3.9, Berry et al have demonstrated that STRA6 is phosphorylated at the C-terminal region (Berry et al., 2012). They propose that phosphorylation of the C-terminus is necessary to allow CRBP recruitment to IC3. IC3 was shown to directly bind to CRBP with leucine 255 being a critical residue involved in the interaction. Previously, this group demonstrated that phosphorylation of STRA6 is transient with peak phosphorylation at 30 minutes. Treatment of cells overexpressing STRA6, with holo-RBP resulted in increased recruitment of CRBP to STRA6 with a peak interaction at 30 minutes. ROH transport occurs instantaneously and therefore it is unlikely that it would be dependent on a phosphorylation event which peaks at 30 minutes.

1.3.9 C-terminal region:

The C-terminus of STRA6 may also be an important domain for protein interactions and possibly signalling events. It is a large domain, containing approximately 170 amino acids, based on topology modelling. Berry et al have suggested that residue T644 located in the C-terminal domain of STRA6 is phosphorylated upon holo-RBP treatment (Berry et al., 2011). This residue is a known genetic mutation site and is a putative src homology 2 (SH2) domain (Pasutto et al., 2007). Mutation of residues Y643 and T644, respectively, abolished phosphorylation of STRA6. In this study, mutated STRA6 was still found to be expressed at the cell membrane. However, in another mutagenesis study, it was observed that when T644 is mutated, cell surface expression is lost (Kawaguchi et al., 2008a). Lack of expression at the cell surface could be a possible reason why the receptor was not phosphorylated. Nevertheless, STRA6 does appear to be phosphorylated upon holo-RBP treatment and in a transient manner. Peak phosphorylation was observed 30 minutes after holo-RBP treatment (Berry et al., 2011). SH2 domains are known binding sites for the JAK/STAT signalling proteins. Increased phosphorylation of the signalling partner proteins Janus Kinase 2 (JAK2) and Signal Transducer and Activator of Transcription 5 (STAT5) was also observed in response to holo-RBP treatment (Berry et al., 2012). The SH2 domain at residue T644 in the C-terminal region of STRA6 appears to be the binding site for JAK2. Decreased expression of JAK2 results in decreased phosphorylation of STRA6, suggesting that JAK2 is in fact responsible for STRA6 phosphorylation (Berry et al., 2012). Mutation of the STRA6 phosphorylation site to alanine resulted in loss of CRBP binding to STRA6. Berry et al do not claim that CRBP binds directly to the C-terminus of STRA6, rather that phosphorylation of the C-terminus results in increased accessibility to the CRBP binding site located in IC3. Mutation of residue 644 to the phosphomimetic residue glutamic acid resulted in increased CRBP binding to STRA6 (Berry et al., 2012). They also claim that increased expression of CRBP results in increased signalling via the JAK/STAT pathway by some as yet unknown mechanism. All this evidence suggests that the C-terminus of STRA6 is an essential ligand binding and signalling domain. Structural studies of this region are crucial to facilitate our understanding of the unique aspects of STRA6 mediated ROH transport and downstream signalling events.

1.4 The biological activity of retinoids:

Retinoids are very important signalling molecules and they activate a very diverse and complex signalling cascade.

1.4.1 Diverse functions of retinol metabolites:

Once ROH enters the cell, it is either stored as retinyl esters via LRAT or oxidised to form retinal also known as retinaldehyde via a family of alcohol dehydrogenases (Fig 1.10) (Theodosiou et al., 2010). Retinaldehyde is the precursor for one of the most biologically active retinoids, RA. Retinaldehyde is irreversibly oxidised to RA via the enzyme RALDH. RA and its stereoisomers ATRA, 9-cis RA and 13-cis RA are responsible for a diverse array of biological activities. Retinoids signal via the ligand activated transcription factors, Retinoic Acid Receptors (RAR) and Retinoid X Receptors (RXR). Both of these receptors have 3 isotypes, denoted α, β and γ. Each isotype exhibits different splice variants resulting in numerous isoforms of the receptor (Chambon, 1996).

ATRA and its isomers 9-cis retinoic acid and 13-cis retinoic acid activate RAR. Metabolites of ATRA have also been shown to be biologically active via RAR with varying specificities for each isotype (Idres et al., 2002). Retinoids are extremely important for normal embryonic growth. Expression of a group of genes known as HOX genes are under the control of RA and promote anteroposterior development (Theodosiou et al., 2010). Increased expression of STRA6 in limb buds further highlights the importance of retinoid activity in normal limb formation (Chazaud et al., 1996). RA signalling can induce expression of many proteins involved in ROH transport and handling, most notably CRBP and even STRA6 itself (Rochette-Egly and Germain, 2009). RA can also induce expression of enzymes responsible for retinoid degradation such as members of the cytochrome P450 family e.g. CYP26 (Theodosiou et al., 2010).

ROH is also vitally important for vision. The earliest indicator of vitamin A deficiency is night-blindness. In humans 11-cis retinal is the retinol chromophore utilised by opsin proteins for photoreception in the retina. Once consumed it is isomerised to all trans-retinal. It must be quickly regenerated to 11-cis retinal to allow for constant photoreception. The isomerisation reaction is

mediated by the retinoid isomerase, RPE65 (Palczewski, 2012). Retinoids are also required for normal reproduction. Spermatogenesis is highly reliant on RA. Knockout animals for the various RAR isoforms are often sterile (Clagett-Dame and Knutson, 2011). Retinoid involvement in the female reproductive system is highly dependent on the stage of the reproductive cycle. If ROH deficiency occurs before fertilisation often conception will not occur.

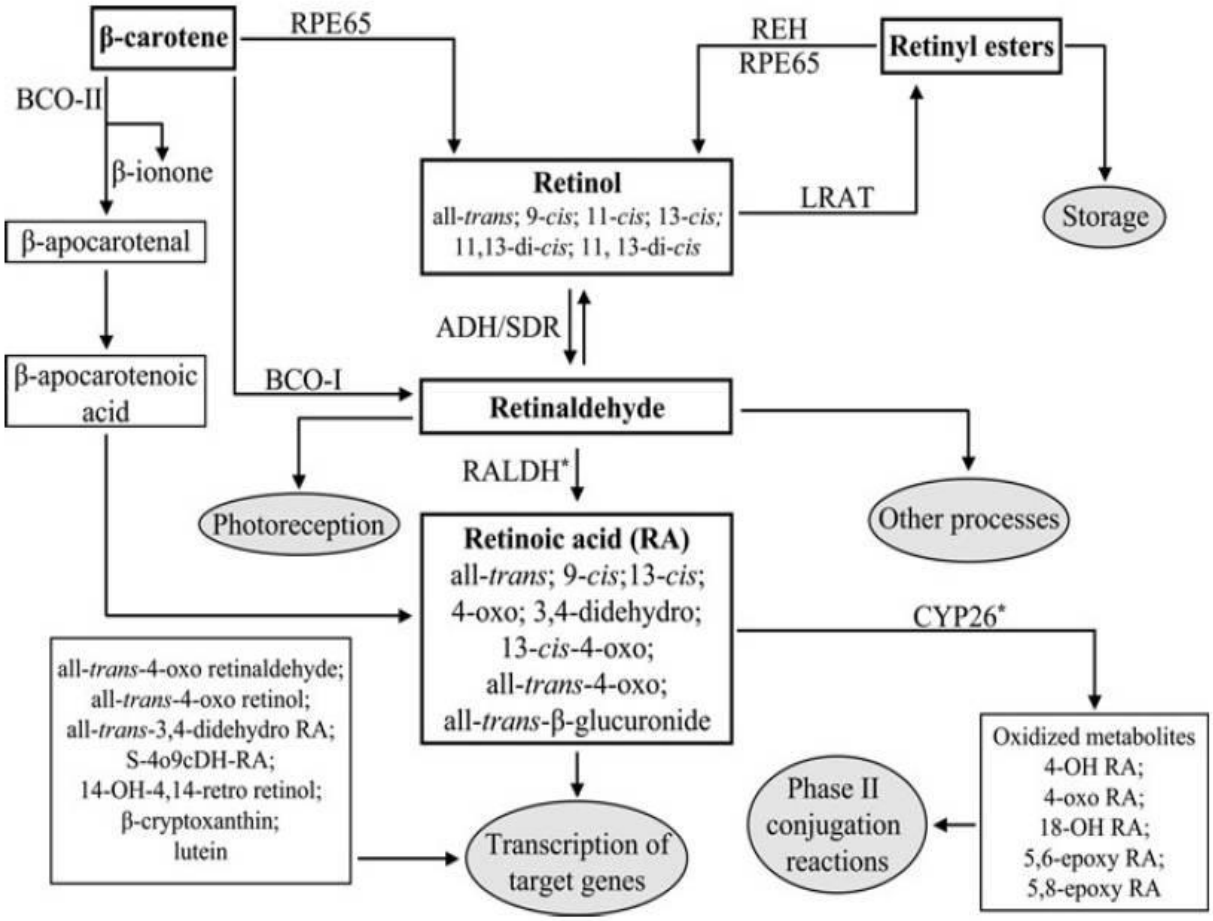

Fig 1.10 The metabolic processing of retinoids.

Representative diagram of retinoid metabolic processing in the cell. Retinoids are denoted by the closed boxes and the physiological processes affected are denoted by the grey circles (Theodosiou et al., 2010).

1.4.2 The retinoic acid receptors:

Fig 1.9 shows the diversity of the metabolic processing of retinol. RA and its metabolites are the predominant retinoids involved in transcription activation. Retinoids signal via the ligand activated transcription factors RAR and RXR (Chambon, 1996). As mentioned previously, many isoforms exist of the two receptors and to add to the complexity, RARs can form homodimers, or heterodimers with RXR. RXR has also been shown to form heterodimers with steroid hormone receptors, such as the thyroid hormone receptor, peroxisome proliferator activated receptor (PPAR) and the vitamin D receptor. Given the many isoforms of the RAR and RXR receptors, and their ability to form complexes, the potential combinations are vast and vary greatly with cell type. This may explain the pleiotropic effects of retinoid signalling during development.

RAR and RXR bind to specific promoter regions called Retinoic Acid Response Elements (RARE). RAREs can be found as direct repeats of the RARE sequence separated by 2 nucleotides (DR2) or most commonly as direct repeats of the RARE sequence separated by 5 nucleotides (DR5) before the gene of interest. When RXR is activated by its natural ligand, it binds a DNA sequence known as DR1. The CRBP gene itself has a DR2 RARE sequence in its promoter region (Rochette-Egly and Germain, 2009). This would suggest a positive feedback loop, i.e. when ROH enters the cell it is metabolised and triggers an RAR response, increasing levels of CRBP to mop up any excess ROH. Both RAR and RXR exhibit a DNA binding domain which forms a similar zinc finger motif. They also both contain a ligand binding domain which varies greatly in specificity for the activating ligand or retinoid.

RARs play a crucial role in embryonic development particularly in organogenesis and limb formation. This specific role has been highlighted through several knockout studies of the various subtypes of RAR (Mark et al., 2006). Knockout of some subtypes of RAR results in a phenotype similar to embryos lacking RALDH. This demonstrates the dependence of RA signalling on RARs.

1.4.3 The retinoid X receptor:

RXR is activated by 9-cis retinoic acid and traditionally thought to only function as a partner for other nuclear receptors. There are 3 subtypes RXR α, β and γ with RXRα being the most active. They display different tissue expression patterns. The RXRα isotype is largely expressed in the kidney, spleen, liver, visceral tissues, epidermis and placenta. The RXRβ isotype is ubiquitously expressed and the RXRγ isotype is mostly found in the muscle and brain (Szanto et al., 2004). RXRα is particularly important in myocardial development. Knockout mouse embryos displayed severe congenital heart defects along with ocular defects. Whereas RXRβ and γ knockout mice displayed no morphogenic effects only sterility in reproducing adult males lacking the RXRβ isotype (Mark et al., 2006). The exact ligand for RXR is still under debate. 9-cis RA has been shown to bind in vitro but has yet to be detected *in vivo*. RXR is known to be activated by fatty acids, namely phytanic acid, docosahexaenoic acid and lithocholic acid (Dawson and Xia, 2012). It can form heterodimers with many nuclear receptors such as PPAR, RAR, vitamin D receptor (VDR), thyroid hormone receptor (TR), liver x receptor (LXR) and farnesoid x receptor (FXR), having a diverse physiological function ranging from cell differentiation, apoptosis, metabolism and embryonic development (Szanto et al., 2004). Much debate surrounds the exact role of RXR in these heterodimeric complexes. It is now thought that RXR is not just a silent partner in gene regulation but can have a direct affect along with the other nuclear receptor in the complex. The heterodimeric binding partners of RXR can be classed as permissive, non-permissive or conditionally permissive to RXR transcriptional activity. Non-permissive receptors include TR and VDR, permissive receptors include PPAR, LXR and FXR, with conditionally permissive receptors being the RAR. When a heterodimer partner is said to be non-permissive, the RXR receptor is said to be subordinate to the other nuclear receptor, thus RXR activation by its own ligand would not enhance the transcriptional activity of the complex. When the heterodimer partner is permissive it means that transcription is activated by agonist binding to either partner or to both. In the case of conditionally permissive receptors, activation of the complex occurs as a result of agonist binding to the RAR but once active, allows activation of RXR (Dawson and Xia, 2012).

1.4.4 Regulation of retinoid signalling:

Transcription via RAR and RXR is tightly regulated through interacting partner proteins known as co-repressors and co-activators (Fig 1.11). In the absence of a ligand, RARs can repress gene activation by binding to exposed RARE sequences in chromatin. RAR binds to a RARE and recruits co-repressors such as nuclear receptor co-repressor (NCoR) and silencing mediator for RAR and TR (SMRT) to form a large molecular weight complex which impedes gene activation (Rochette-Egly and Germain, 2009). NCoR and SMRT bind to histone deacetylases (HDAC) to condense the chromatin structure. Once the active ligand or retinoid binds to the RAR, it initiates a conformational change causing the co-repressor complex to dissociate, allowing co-activators to bind and chromatin unravelling to occur. Co-repressors bind to un-liganded RAR or RXR using specific domains with the consensus sequence LxxxIxxxI/L. Co-activators bind to RAR or RXR using specific domains with the consensus sequence LxxLL (Szanto et al., 2004). Co-activator proteins were originally identified as 160kDa proteins that interacted with nuclear receptors in a ligand-dependent manner. Known human co-activators include nuclear receptor co-activator-1 (NcoA1) also known as steroid receptor co-activator 1 (SRC-1), and nuclear receptor co-activator-2 (NcoA2) also known as transcriptional intermediary factor 2 (TIF2). They bind to the activated RAR or RXR and initiate complex formation to recruit histone acetyltransferases (HAT) to de-condense the chromatin structure (Torchia et al., 1998). This allows transcriptional complexes access to target genes and transcription to occur.

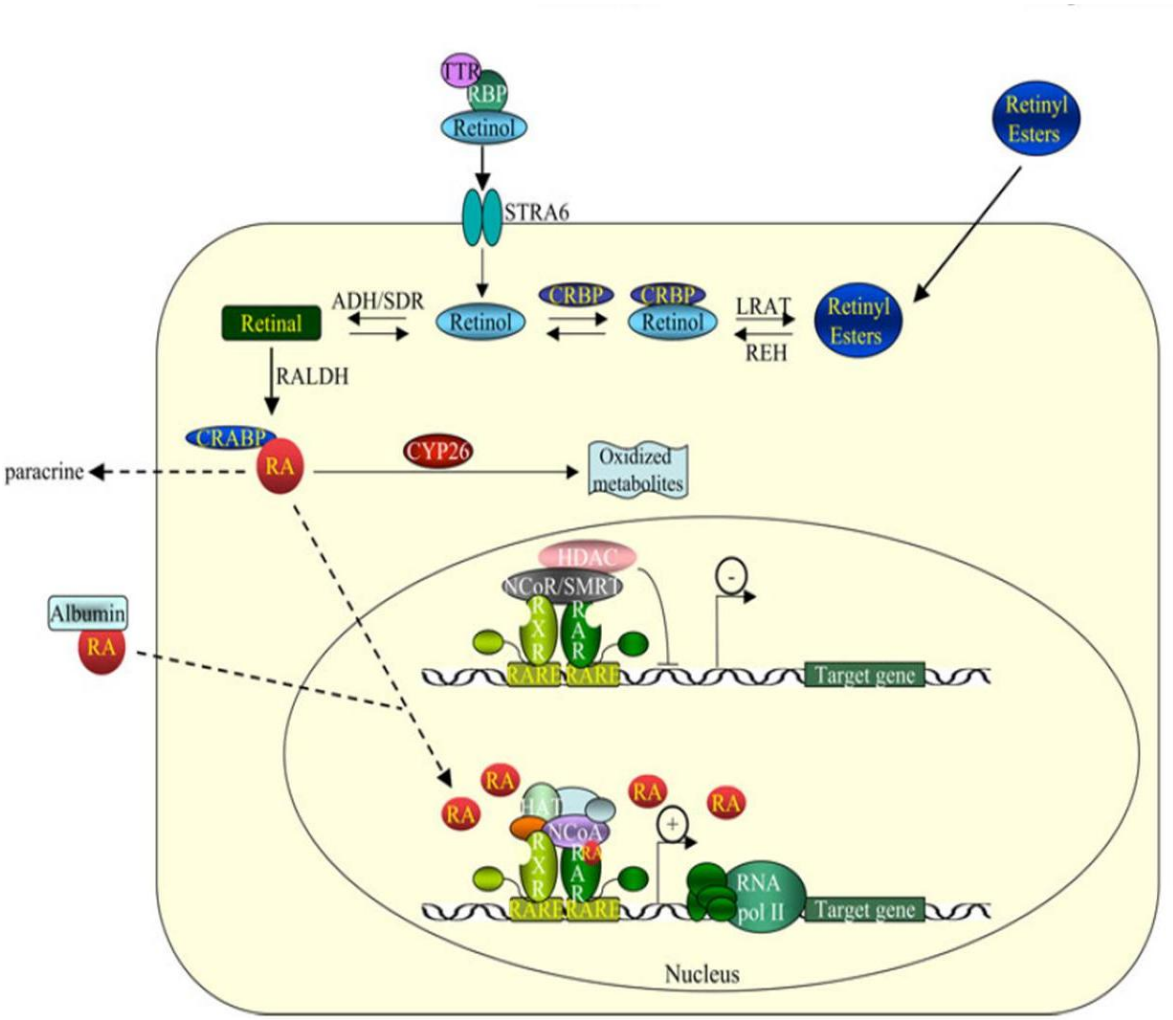

Fig 1.11 Metabolic Pathway of Retinol and Subsequent transcriptional activation.

ROH enters the cell via STRA6 where it is either converted to retinyl esters via LRAT for storage or oxidised via RALDH to form RA. RA then travels to the nucleus to activate gene transcription via RAR and RXR (Theodosiou et al., 2010).

1.5 Type II diabetes, a new epidemic:

Type II diabetes is one of the fastest growing epidemics of the western world. The prevalence has also risen rapidly in developing countries like China and India, leading to an enormous financial burden on health care systems on a global scale. In addition, the percentage of adolescents diagnosed with insulin resistance is rising rapidly. The world health organisation (WHO) predicts that diabetes will be the 7th leading cause of death in 2030, with 439 million people suffering from the disease. Obesity, in particular excess visceral fat tissue, along with a more sedentary lifestyle is the predominant cause of this worldwide epidemic. Indeed, visceral fat adiposity is a defined risk factor for insulin resistance and type II diabetes in its own right (Chen et al., 2012).

Overt type II diabetes is caused by a systemic insulin resistant state. Following ingestion of food, cells fail to respond to insulin secreted by the pancreas and as a result serum glucose levels rise to progressively higher levels. To combat this, the pancreas strives to produce more insulin, eventually leading to dysfunction of the pancreatic β islet cells (Kahn et al., 2006). Before the onset of type II diabetes there exists a condition which in many cases can remain undiagnosed, where the body is becoming increasingly insulin resistant. Insulin resistance is defined as a diminished responsiveness of the signalling pathway to its activating molecule, insulin. The most effective therapy for insulin resistance is a dramatic change in lifestyle, increasing physical activity and adopting a healthier diet. Many theories abound as to what metabolic effect excess fat mass is having on glucose tolerance. Many groups suggest it is as a result of an immune response. Other groups report that it is a result of increased circulating fatty acids. Several studies have demonstrated that excess fat mass leads to the secretion of numerous signals or adipokines, most notably non-esterified fatty acids. Several inflammatory cytokines have also been shown to be increased, such as tumour necrosis factor α (TNFα) and interleukin-6 (IL-6) (Kahn et al., 2006). Adipose tissue is now widely regarded as an endocrine organ in its own right. Due to the wide range of theories as to the root molecular factor behind the disorder, one can only conclude that it is a multifactorial disease.

1.5.1 RBP, a biomarker for insulin resistance:

In 2005, RBP was identified as a potential contributing factor to the development of insulin resistance. A study conducted by Yang et al revealed that elevated levels of serum RBP can lead to insulin resistance (Yang et al., 2005). Obesity is the leading cause of type II diabetes, particularly excess visceral adipose tissue. An adipose tissue specific GLUT4 knockout mouse was used to study what adipokines are secreted in response to insulin resistance. GLUT4 is the main membrane transporter for glucose. Mice in which GLUT4 was selectively knocked out in adipose tissue exhibit an insulin resistant phenotype, due to decreased uptake of glucose. Amongst a plethora of other proteins secreted from adipose tissue, serum RBP was shown to be increased (Yang et al., 2005). The liver is the primary site for RBP secretion with adipose tissue being the second largest contributor to serum RBP levels (Tsutsumi et al., 1992). Serum RBP was identified to be elevated 2.5 fold in GLUT4 knockout mice compared to WT (Yang et al., 2005).

The direct effect of RBP on glucose tolerance and insulin sensitivity was subsequently investigated. Mice injected with human RBP showed marked insulin resistance over time, when compared to controls (Yang et al., 2005). Conversely, RBP knockout mice exhibit increased insulin sensitivity. Pharmacological methods aimed at reducing circulating RBP levels can also improve insulin sensitivity. Fenretinide, a synthetic retinoid, was found to improve glucose tolerance in obese, insulin resistant mice (Yang et al., 2005). Fenretinide actively reduces circulating RBP levels by inhibiting the interaction of RBP and TTR, thus enabling RBP to be filtered by the kidneys and excreted. Fenretinide was initially developed to treat cancer and acts by inducing apoptosis in rapidly dividing cells, by an unknown mechanism (Fontana and Rishi, 2002). As it is an anti-cancer therapeutic it would not be suitable for the long term treatment of insulin resistance. RBP is therefore a potential drug target for the treatment of insulin resistance and type 2 diabetes.

1.5.2 Physiological relevance:

When the findings of the seminal paper by Yang et al in 2005 were translated to human subjects with type II diabetes, the results were in agreement. Epidemiology studies have shown that obese patients with type II diabetes display elevated levels of serum RBP (Graham et al., 2006). Even in lean subjects with a genetic predisposition to type II diabetes, serum RBP levels were found to be elevated. In non-obese subjects elevated serum RBP levels were concomitant with decreased GLUT4 expression in adipose tissue, as seen with the GLUT4 adipose selective knockout mouse. There has been some discrepancy in epidemiology studies investigating levels of serum RBP in diabetic patients. Some groups report a positive correlation with increased serum RBP levels and increased insulin resistance; others show no correlation at all. Graham et al suggest that the reason behind the conflicting results is the methodology used. Quantitative Western blot appears to be the most accurate method to assess levels of circulating RBP levels between subjects (Graham et al., 2007).

Exercise is the first line of treatment for insulin resistance in obese diabetic patients. RBP levels were analysed in the serum of diabetic subjects following periods of increased physical activity. Improved glucose tolerance correlated positively with a reduction in serum RBP levels (Graham et al., 2006). Table 1.2 depicts the effect of medical intervention for type II diabetes on serum RBP levels. Most treatments associated with weight loss also correlate positively with decreased RBP levels. This would most likely be due to a decrease in adipose tissue and associated secretion of this adipokine. Monitoring of serum RBP levels may become a non-invasive method to assess the onset of insulin resistance and monitor its improvement.

The question remains whether elevated RBP levels are also associated with increased ROH levels. TTR will only bind to holo-RBP, and as RBP would be filtered from the blood without TTR one would presume that if serum RBP levels are elevated ROH is also present. In obese subjects serum apo-RBP levels were found to be two fold higher than non-obese subjects (Mills et al., 2008). The ratio of RBP to ROH was found to be lower in obese patients. This is thought to be due to increased levels of circulating apo-RBP which could dilute down the proportion of RBP with ROH bound.

Medical interventions	Plasma RBP_4 levels	Comments
Insulin	↑	Insufficient data
Thiazolidinediones	↓	Mainly in patients with T2DM
Metformin	↔	Insufficient data
Sulfonylureas	↑	Insufficient data
Exenatide	↓	Insufficient data
Acarbose	↓	Insufficient data
Diet	↓	Well established. Negative energy balance is possibly more important than body weight per se
Exercise	↓	Resistance exercise is possibly more effective in reducing circulating RBP_4, than aerobic exercise
Orlistat	↓	Unknown if there is an impact of orlistat on circulating RBP_4 independently from the applied diet
Sibutramine	↓	Unknown if there is an impact of sibutramine on circulating RBP_4 independently from the applied diet
Rimonabant	↓	The decrease in circulating RBP_4 is possibly due to the rimonabant-induced reduction in production of RBP_4 by adipose tissue
Bariatric Surgery	↓	Well established. Negative energy balance is possibly more important than body weight per se
Statins	↓ or ↔	Conflicting data
Fibrates	Early ↑ and late ↓	The metabolic action of fibrates reduces circulating RBP_4. The fenofibrate-induced change in renal function increases circulating RBP_4
Cholestyramine	↓	Insufficient data
Ezetimibe	↔	Insufficient data

T1DM: Type 1 Diabetes Mellitus; T2DM: Type 2 Diabetes Mellitus; RBP_4: Retinol binding protein 4
Symbols: ↑: Increase; ↓: Decrease; ↔: No change

Table 1.2 The effect of medical interventions on circulating RBP levels.

Table representing the relative effect of medical treatment for type II diabetes on circulating RBP levels (Christou et al., 2012).

1.5.3 The molecular mechanisms of RBP induced insulin resistance:

Much debate surrounds the exact mechanism by which RBP can contribute to insulin resistance. Recent studies by Norseen et al have shown that increased RBP may lead to an immune response (Norseen et al., 2012). Elevated levels of RBP in white adipose tissue led to an increase in the mitogenic signals IL-6, TNF-α and Monocyte Chemoattractant Protein-1 (MCP-1). The cytokines were produced by a direct effect of RBP on macrophages present in adipose tissue, not by stimulating the adipocytes. The researchers suggest that elevated cytokine levels produced by macrophages in response to RBP have a detrimental effect on insulin signalling in adjacent adipocytes.

Interestingly, it was found that apo-RBP had a greater effect in stimulating cytokine production than holo-RBP. STRA6 was not found to be expressed in the macrophages used in this study. Therefore, the immune response elicited by RBP acts via a STRA6 independent mechanism. Analysed together these results would suggest a retinoid independent mechanism of action. In order to determine what secretory pathway was activated to promote cytokine production, inhibitors of known cytokine production pathways were used. Specific inhibition of the c-Jun N-Terminal Kinase (JNK) pathway caused a marked reduction in cytokine levels. The study went on to show that when Toll Like Receptor 4 (TLR4) knockout macrophages were stimulated with RBP, significantly lower amounts of cytokines were secreted. However, the effect was not totally abrogated, suggesting that other pathways may be involved. In addition, the 3T3L1 adipocytes used in this study endogenously express TLR4 (Song et al., 2006) but did not themselves exhibit TLR4 activation with direct RBP treatment. RBP may be acting by an as yet undiscovered mechanism to cause cytokine production.

1.5.4 Cytokines and insulin resistance:

The interruption of insulin signalling by immune response cytokines has been well documented (see below). Large numbers of macrophages can be found in visceral adipose tissue. Weisberg et al found that in obese rodents 40% of cells present in visceral adipose tissue were macrophages compared to 10% in lean rodents (Weisberg et al., 2003). The macrophages in this region are active and secrete pro-inflammatory cytokines such as TNFα, IL-6 and IL-1β. These cytokines have been shown to impact indirectly on the insulin signalling pathway by activation of the JNK pathway (Patel et al., 2013).

1.5.5 Role of TNFα in insulin resistance:

TNFα is one of the most prominent pro-inflammatory cytokines. Stimulation of the tumour necrosis factor receptor by TNFα leads to activation of the JNK signalling pathway. TNFα has been shown to cause an interruption of insulin signalling at an early point in the pathway. Complete TNFα inhibition of insulin receptor substrate-1 (IRS-1) activation occurs after several hours which would suggest that it is not a direct inhibition but one reliant on a change in the proteomic profile of the cell. TNFα is thought to inhibit insulin signalling by two proposed mechanisms, firstly by causing an increase in IRS-1 phosphorylation at serine 307 and secondly by inducing Suppressor of Cytokine Signalling 3 (SOCS3) expression. Serine 307 phosphorylation of IRS-1 blocks tyrosine phosphorylation of IRS-1 using an unknown mechanism (Aguirre et al., 2000). It is thought that JNK is the kinase responsible for phosphorylation of IRS-1 at Serine 307. Tyrosine phosphorylation of IRS-1 is vital for the downstream propagation of the insulin signal as it generates SH2 sites necessary for PI3 Kinase to bind (Copps and White, 2012).

TNFα may also be inducing insulin resistance by increasing SOCS3 expression. SOCS3 can bind to the insulin receptor specifically at tyrosine 960 (Ueki et al., 2004). This residue is vital for IRS-1 recruitment to the insulin receptor. Thus, by binding to the insulin receptor SOCS3 blocks the association of these two proteins (Fig 1.12). Inhibition of the insulin signalling pathway at this level leads to a decrease in glucose uptake into the cell.

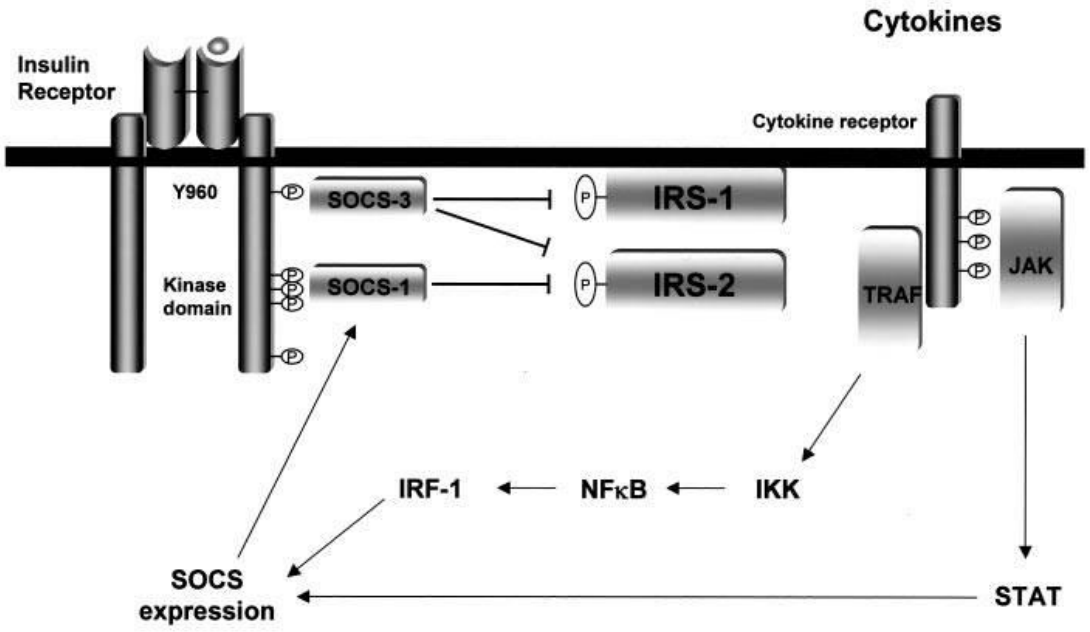

Fig. 1.12 Recruitment of SOCS3 to Y960 of the insulin receptor inhibits IRS-1 association.

Proposed model of how cytokine production can act to inhibit insulin receptor activation by increased SOCS3 expression (Ueki et al., 2004).

1.5.6 STRA6 and the JAK/STAT pathway:

Another group has suggested that RBP is functioning as a signalling molecule to cause a disruption in the cell's insulin response. The genetic mutation site of STRA6, T644M, is a putative SH2 domain. Berry and Noy (2012) investigated whether this site was phosphorylated and indeed, when cells overexpressing STRA6 were stimulated with holo-RBP, they saw a marked increase in STRA6 tyrosine phosphorylation. Holo-RBP was shown to induce phosphorylation of STRA6 in a time dependent manner, with maximal phosphorylation at 30 minutes. Apo-RBP and ROH alone did not induce phosphorylation. SH2 domains are typically associated with the JAK/STAT signalling pathway. Holo-RBP was shown to cause an increase in STAT5 phosphorylation, and this phosphorylation was linked to JAK2. JAK2 was found to associate directly with STRA6 (Berry and Noy, 2012). Berry and Noy suggest that association of JAK2 with STRA6 leads to JAK2 phosphorylation and subsequent activation of STAT5 (Fig 1.13). STAT5 is a known transcription

factor. Using a luciferase reporter assay Berry et al observed that a number of genes regulated by STAT5 were increased in expression following holo-RBP treatment. One gene in particular that was found to be up-regulated in expression was SOCS3. As described previously, SOCS3 has been shown to directly bind to the insulin receptor and inhibit downstream insulin signalling (Ueki et al., 2004).

In a separate study, Muenzner et al demonstrated that overexpression of RBP specifically in the liver led to increased serum holo-RBP levels (Muenzner et al., 2013). When they examined gene expression in adipose tissue, they saw increased expression of several RARα responsive genes such as CRBPI and CYP26A1 but no increase in SOCS3 expression or TNFα expression (Muenzner et al., 2013). In addition, they did not observe an increase in STAT5 phosphorylation in response to apo-RBP, holo-RBP or ROH alone in pre-adipocytes overexpressing STRA6. This work is in direct conflict with that described by Berry and Noy. The cause behind this discrepancy is unknown.

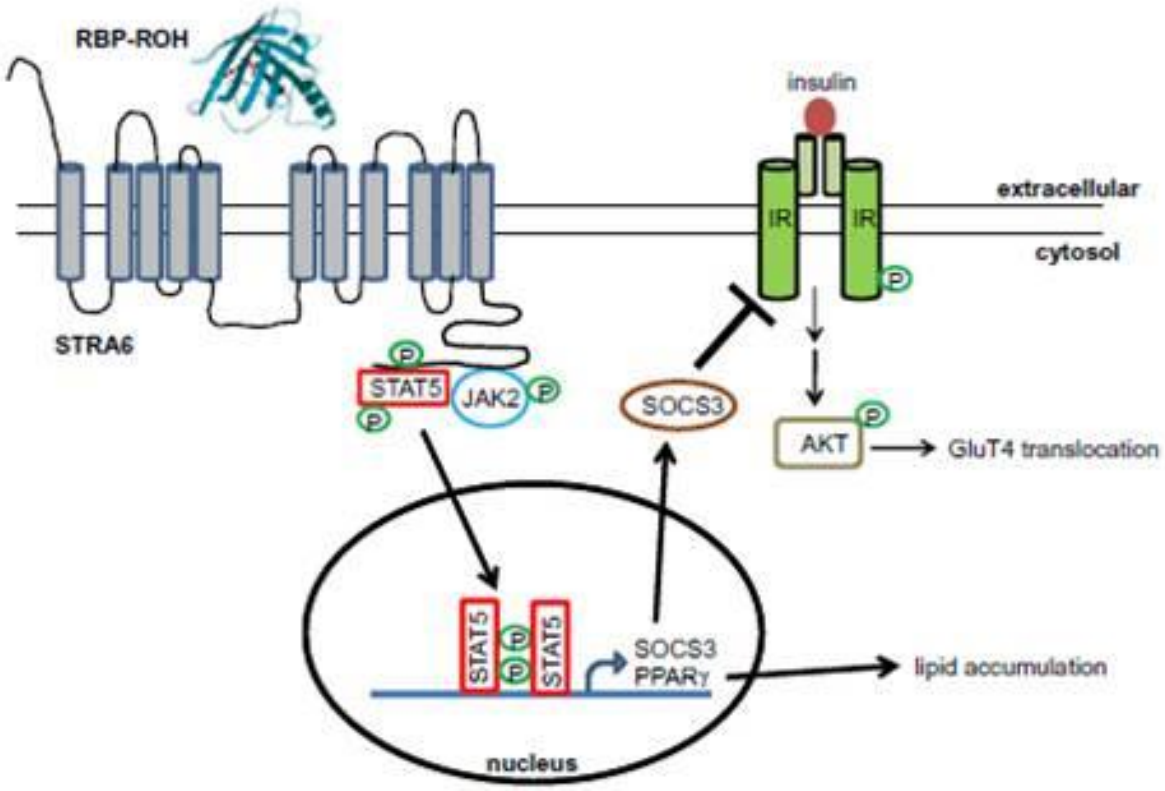

Fig. 1.13 Activation of STRA6 leads to increased SOCS3 expression and inhibition of the insulin receptor.

Proposed model of holo-RBP activation of the JAK/STAT signalling pathway via STRA6 (Berry et al., 2011).

1.6 Project Aims:

It has been widely reported that, in patients with type II diabetes, elevated serum RBP levels correlate positively with insulin resistance. Reduction of serum RBP levels can have a beneficial effect on glucose tolerance. Conflicting theories surround the exact mechanism by which increased RBP levels can cause insulin resistance.

The aim of this investigation is to use proteomic technologies and techniques to investigate the effect of elevated RBP levels on muscle cells. Information gained from studying alterations in the proteome due to RBP treatment could reveal the molecular mechanism by which insulin resistance occurs in this tissue.

In conjunction with this study, the effect of a successful novel therapeutic for type II diabetes on muscle cells was investigated. This small molecule prevents the association of TTR and RBP and in theory should cause an increase in RBP excretion in the urine. When cells were stimulated directly with the drug an increase in glucose uptake was observed. This effect was independent of the predicted mechanism of action. In order to reveal the mechanism of action when added directly to muscle cells, a proteomic study was conducted. Proteomic profiling of a small molecule for the treatment of type II diabetes may reveal a novel effect on cell homeostasis and uncover any potentially toxic effects of the drug.

Another aspect of this study was to analyse the structure and function of the C-terminal region of STRA6. The C-terminus is a large intracellular, potentially independently-folding domain which could be of functional significance. Evaluation of the structural characteristics of the C-terminus could reveal the domain's secondary and quaternary structure. In addition, studies with potential binding partners such as CRBP could uncover novel interaction sites. A recombinant version of the domain was produced in *E. coli* and purified to a high standard. The protein was then used to investigate its secondary structure and any potential functional characteristics.

Chapter 2

Materials and Methods

2.1 Tissue Culture:

All cell lines were maintained in a sterile environment at 37°C with 5% CO_2.

2.1.1 General Tissue Culture Reagents:

Fetal bovine serum (FBS) was purchased from either Sigma or Thermo Scientific and heat inactivated at 56°C for 30 minutes. Horse serum and Dulbeccos phosphate buffered saline (DPBS) was supplied by Gibco. Horse serum was also heat inactivated at 56°C for 30 minutes. High glucose Dulbecco's Modified Eagles Medium (DMEM) was obtained from Thermo scientific or Sigma. Trypsin-EDTA solution was supplied by Thermo Scientific. L-glutamine, and penicillin/streptomycin were supplied by Sigma. L-glutamine was used at a final concentration of 2mM. Penicillin/Streptomycin was used at 100U/mL Penicillin and 100µg/mL streptomycin.

2.1.2 C2C12 cell line maintenance and storage:

C2C12 cells were purchased from Sigma (91031101). Cells were routinely maintained in high glucose DMEM 4500 mg/ml Glucose, 2mM L-Glutamine, 10% FBS, 1% Pen/Strep (complete media). Cells were thawed at 37°C and washed in 10mL complete media, to remove the cryo-preservative DMSO, then re-suspended in complete media and cultured in a T75 flask at 37°C with 5% CO_2. When 80% confluent, cells were detached from the flask using trypsin-EDTA, 0.25% (v/v), 3mL for 5 minutes. Protease action was inhibited using 8mL complete media. Cells were then re-seeded at $1x10^5$ cells per flask until 80% confluent. C2C12 cells were then either passaged once more or differentiated into myotubes with high glucose DMEM 4500 mg/ml glucose, 2mM L-glutamine, 2% horse serum, 1% Pen/Strep for 3 days. Storage of C2C12 cells was carried out by freezing $2x10^6$ cells in 1mL complete media with 10% DMSO at -80°C overnight. Cells were then placed in liquid nitrogen for long term storage.

2.1.3 HEK293T STRA6 stable cell line maintenance and storage:

HEK293T cells, transfected with either N-Terminally tagged or C-Terminally tagged STRA6 were kindly donated by Dr. Conor Breen as a frozen culture. Storage of stable cells was carried out by freezing $3x10^6$ cells in 1mL complete media with 10% DMSO at -80^{o}C overnight. Cells were then placed in liquid nitrogen for long term storage. They were thawed at 37^{o}C and washed in 10mL complete media, to remove the cryo-preservative DMSO, then re-suspended in complete media and cultured in a T75 flask at 37^{o}C with 5% CO_2 overnight. Media was then replaced with complete media containing 100µg/mL hygromycin (Invitrogen) and 15µg/mL blasticidin (Merck).When approximately 80% confluent, cells were detached from the flask using Trypsin-EDTA, 3mL for 5 minutes. Protease action was then inhibited using 8mL complete media. Cells were then re-seeded by diluting 1:7.5 in 15mL complete media. STRA6 expression was induced at 70% confluency by replacing media with complete media containing 1 µg/mL tetracyclin (Sigma).

2.1.4 HEPG2 cell line maintenance and storage:

HEPG2 cells were obtained from ATTC (77400). Cells were routinely maintained in high glucose DMEM 4500 mg/ml glucose, 2mM L-glutamine, 10% FBS, 1% Pen/Strep. Storage of HEPG2 cells was carried out by freezing $2x10^6$ cells in 1mL complete media with 10% DMSO at -80^{o}C overnight. Cells were then placed in liquid nitrogen for long term storage. They were thawed at 37^{o}C and washed in 10mL complete media, to remove the cryo-preservative DMSO, then re-suspended in complete media and cultured in a T25 flask at 37^{o}C with 5% CO_2. When approximately 80% confluent, cells were detached from the flask using Trypsin-EDTA, 3mL for 5 minutes. Protease action was then inhibited using 8mL complete media. Cells were re-seeded by diluting 1:5 in 15mL complete media.

2.1.5 BMDM cell line maintenance and storage:

Bone marrow derived macrophages (BMDM) were kindly donated as a live culture courtesy Prof. Paul Moynagh. Cells were routinely maintained in high glucose DMEM 4500 mg/ml glucose, 2mM L-Glutamine, 10% FBS, 1% Pen/Strep. When approximately 80% confluent, cells were detached from the flask using a cell scraper. Cells were then re-seeded at $1x10^6$ in a T175 flask. Storage of BMDM cells was carried out by freezing $2x10^6$ cells in 1mL complete media with 10% DMSO at -80^{o}C overnight. Cells were then placed in liquid nitrogen for long term storage.

2.1.6 C2C12 RTC15 Treatment:

Differentiated C2C12 cells were washed once with 10 ml DPBS at 37^{o}C. Cells were then incubated for 16 hours with 10µM RTC15 in complete media with 2% horse serum. Control cells were incubated with an equal volume of the vehicle, DMSO, in complete media with 2% horse serum.

2.1.7 C2C12 RBP Treatment:

Differentiated C2C12 cells were serum starved for 7 hours using complete media with 0.1% horse serum, then washed with DPBS warmed to 37^{o}C. RBP was pre-incubated with ROH in equimolar concentrations at 37^{o}C for ten minutes. Cells were then incubated with 75µg/ml holo-RBP in complete media with 0.1% horse serum for 16 hours. Control cells were incubated with an equal volume of the vehicle, PBS in complete media with 0.1% horse serum.

2.1.8 C2C12 insulin treatment:

Differentiated C2C12 cells were washed once with pre-warmed DPBS. 9.5mg/ml insulin supplied by Sigma (I9278) was diluted 1:172 in sterile Krebs Ringer buffer (KRB) with 5mM glucose to give 55µg/ml insulin. KRB was composed of 136mM NaCl, 20mM HEPES, 4.7mM KCl, 1mM $MgSO_4$, 1mM $CaCl_2$, 4.05mM Na_2HPO_4, 0.95mM NaH_2PO_4, pH 7.4. 55µg/ml insulin was diluted 1:100 in KRB with 5mM glucose to give 0.5µg/ml insulin. Cells were incubated with 0.5µg/ml insulin in KRB with 5mM glucose for 1 hour at 37^{o}C, and then washed with 1mL of KRB without glucose.

2.2 Sample Preparation:

2.2.1 Cell lysis:

For co-immunoprecipitation experiments, cells were lysed in HEPES lysis buffer 50mM HEPES (pH7.5), 150mM NaCl, 10mM Na_2HPO_4, 50mM NaF, 1mM EDTA, 1.5mM $MgCl_2$, 2mM Na_3VO_4, 1mM $Na_4P_2O_7$, 1X protease inhibitor cocktail (Sigma S8380), 10% glycerol, 10µg/ml aprotonin and 1% Triton x-100. Cells were re-suspended in HEPES lysis buffer and incubated at 4^oC for 1 hour with rotation. Lysates were spun at 13,000 RCF for 5 minutes at 4^oC. The insoluble pellet was discarded and the soluble supernatant was retained for further analysis.

For Western blotting cells were lysed in RIPA buffer 50mM Tris-HCL (pH 7.4), 150mM NaCl, 1% Triton x-100, 0.1% SDS, 0.5% sodium deoxycholate, 1X protease inhibitor cocktail, 1mM EDTA, 50mM NaF, 2mM Na_3VO_4, 1mM $Na_4P_2O_7$.

2.2.2 Cell membrane isolation:

Attached cells were washed 3 times with ice cold PBS, then detached using a cell scraper in 10mL PBS. Cells were then pelleted at 500 RCF for 10 minutes at 4^oC. The supernatant was discarded and the cells resuspended in 2mL hypotonic buffer (10mM HEPES (pH 7.9), 1.5mM $MgCl_2$, 10mM KCl, 0.5mM DTT, 1X protease inhibitor cocktail, 50mM NaF, 2mM Na_3VO_4, 1mM $Na_4P_2O_7$). Cells were sonicated for 1 minute on ice. The lysate was spun at 3,000 RCF for 15 minutes at 4^oC, to remove cell debris. The supernatant was then transferred to an Optiseal Polyallomer tube (Beckman 362185). The tube was filled to the brim with hypotonic buffer (fill volume 5mL) and centrifuged at 100,000 RCF for 1 hour at 4^oC in a NVT90 rotor using the Optima L-100 XP Ultracentrifuge (Beckman Coulter). The supernatant was removed and membrane pellets were resuspended in 50µl MES buffer (25mM MES, 150mM M NaCl, 1% Triton X-100, pH6.5). To aid solubilisation membranes were sonicated on ice for 10 seconds.

2.2.3 BCA protein assay:

A standard protein curve was prepared using bovine serum albumin (BSA) at 0, 50, 100, 200, 400, 600, 800, 1000, 1250, 1500, 1750 and 2000 µg/ml. Samples were diluted as required and 10µl used for the assay in duplicate. 10µl of each standard or sample was used in duplicate in a 96 well plate. Copper sulphate was diluted 1:50 into biochinchinoic acid. 200µl of the copper sulphate and biochinoic acid mix was added to each well. The plate was incubated at 37^{o}C for 30 minutes. The plate was then analysed using a BIO-TEK EL800 plate reader at 562nm. Protein concentration of the samples was deduced from the standard curve.

2.2.4 Pierce protein assay:

A standard protein curve was prepared using BSA at 0, 50, 100, 200, 400, 600, 800, 1000, 1250, 1500, 1750 and 2000 µg/ml. Samples were diluted as required and 10µl used for the assay in duplicate. 10µl of each standard or sample was used in duplicate in a 96 well plate along with 150µl Pierce Protein Assay reagent (PN22660). The plate was incubated at room temperature for 5 minutes. The plate was then analysed using a BIO-TEK EL800 plate reader at 630nm. Protein concentration of the samples was deduced from the standard curve.

2.3 Two Dimensional Electrophoresis:

2.3.1 Sample preparation for the RBP proteomic study:

C2C12 cells were treated overnight with holo-RBP as described in section 2.17. Cells were subsequently lysed and separated into the cytosolic and membrane fractions as described in section 2.2.2. The membrane pellet was resuspended in MES buffer with 1% Triton X-100 (v/v) and centrifuged at 10,000 RCF for 5 minutes at 4^{o}C. The pellet was discarded and the protein concentration of the supernatant was analysed using the BCA assay. 1mg of protein was used per electrophoresis strip (Bio-Rad) and made up to 600µl in 2D sample buffer (7M urea, 2M thiourea, 100mM DTT, 4% (w/v) CHAPS, 1% (v/v) Trion X-100, 0.06% (v/v) ampholytes pH4-7, 0.06% (v/v) bromophenol blue). Samples were left to solubilise at room temperature for 6 hours. The cytosolic fraction from the membrane preparation was retained for each sample. Protein was precipitated using 3 times the volume of ice-cold acetone at -20^{o}C for 2 hours. The reaction was centrifuged at 13,000 RCF for 10 minutes at 4^{o}C and the pellet retained. Residual acetone was removed by air-drying. The protein pellet was resuspended in MES buffer with 1% Triton X-100 (v/v). Resuspended cytosolic proteins were spun at 10,000 RCF for 5 minutes at 4^{o}C. The pellet was discarded and the protein concentration of the supernatant was analysed using the BCA assay.1mg of protein was used per strip and made up to 600µl in 2D sample buffer. Samples were left to solubilise at room temperature for 6 hours.

2.3.2 Sample preparation for the RTC15 proteomic study:

C2C12 cells were treated with 10µM RTC15 overnight as described in section 2.16. Briefly, cells were lysed in 2D sample buffer and left to solubilise for 6 hours at room temperature. Cell lysate was centrifuged at 13,000 RCF for 5 minutes. The supernatant was retained and assessed for protein concentration using the Pierce protein assay. 500µg of protein was used per electrophoresis strip and the sample was made up to 500µl in 2D sample buffer.

2.3.3 Strip rehydration:

IPG strips were obtained from Biorad (163-2044), pH gradient 4-7. Samples were prepared as per sections 2.3.1 and 2.3.2. The protein sample was pipetted along a single well in a rehydration tray. The plastic backing was removed from the IPG strip and the strip was placed gel side down onto the sample. The strip was left to rehydrate for one hour then overlaid with mineral oil. Strips were rehydrated overnight by passive rehydration.

2.3.4 Isoelectric focusing:

Isoelectric focusing (IEF) allows the separation of proteins based on the pI of the protein. When current is applied to the protein sample, individual proteins will migrate to the pH at which the charge of the protein is neutral (Fig. 2.1). For the RBP proteomics study IEF was performed using an Ettan IPGphor 3 supplied by GE. For the RTC15 proteomics study IEF was performed using the PROTEAN IEF cell supplied by Biorad. The same protocol was used for both studies. Electrode wicks were dampened with distilled H_2O and any excess water blotted off. When using the GE system the strips were placed gel side up in the correct orientation and the electrode wicks placed on the ends of the gel respectively. When using the Biorad system the electrode wicks were placed onto the electrode and the gel strip placed gel side down onto the wicks. For both systems the strips were completely covered with mineral oil. When using the GE system the electrodes were carefully placed onto the ends of the strip in the correct orientation. For both systems the lid was then placed on top and the following IEF protocol initiated.

Step 1. Hold at 250V for 4 hours

Step 2. Gradient to 10,000 V 2 and half hours

Step 3. Hold at 10,000 V for 60,000 volt hours

Step 4. Hold at 500V for 24 hours to store

2.3.5 Gel casting:

Acrylamide gels for SDS-Page were prepared the night before to allow polymerisation of the gel overnight. Acrylamide was present at 10% for all proteomic studies. The gel composition was as follows; 10% acrylamide, 0.38M Tris-HCl pH 8.8, 0.1% SDS (V/V), APS 0.05% (V/V), TEMED 0.04%, Rhinohide 1.67% (V/V). 100mL was prepared for each gel with an excess of 100mL. Once gels were poured, each gel was overlaid with 50:50 water saturated butanol and allowed to set at room temperature. When set, gels were overlaid with 1X SDS running buffer to store.

2.3.6 Equilibration of IPG strip:

Following IEF, strips were drained of excess mineral oil and transferred to a clean IEF tray for equilibration to allow SDS to bind for 2^{nd} dimension electrophoresis. Strips were first saturated with reducing equilibration buffer (6M urea, 0.05M Tris-HCL pH 8.8, 2% SDS, 20% glycerol, 2% DTT). Strips were incubated with reducing equilibration buffer for 15 minutes at room temperature. After 15 minutes the buffer was replaced with equilibration buffer containing iodoactemide to prevent re-oxidation of cysteine residues and formation of disulphide bonds (6M urea, 0.05M Tris-HCL pH 8.8, 2% SDS, 20% glycerol, 2.5% iodoacetamide). Strips were incubated for a further 15 minutes at room temperature.

2.3.7 2nd dimension electrophoresis:

The second dimension of 2D electrophoresis allows for the separation of proteins based on molecular weight (Fig. 2.1). IPG strips were removed from the final equilibration buffer and washed in 1X SDS running buffer. Strips were placed on top of the gel with the plastic backing along the back glass plate. A molecular weight marker was added to a piece of blotting paper and positioned alongside the anode side of the IPG strip. The strips were then overlaid with 0.5 % agarose sealing solution (0.5% agarose (w/v), 0.002% bromophenol blue (w/v) prepared in 1X SDS electrophoresis buffer). The agarose gel was allowed to set at room temperature for 20 minutes. For the RBP proteomics study, gels were electrophoresed using the Ettan DALT twelve system. For the RTC15 proteomics study, the gels were electrophoresed using the Biorad PROTEAN plus Dodeca Cell system. For both studies gels were run at 200V constant for approximately 6 hours in 1X SDS electrophoresis buffer (25mM tris-base, 192mM glycine, 1% SDS (w/v)). The gels were then carefully removed from the glass plates and transferred to fixing reagent (40% ethanol (v/v), 10% acetic acid (v/v)) for 30 minutes. Gels were immersed in fresh fixing solution and left overnight at room temperature with constant shaking.

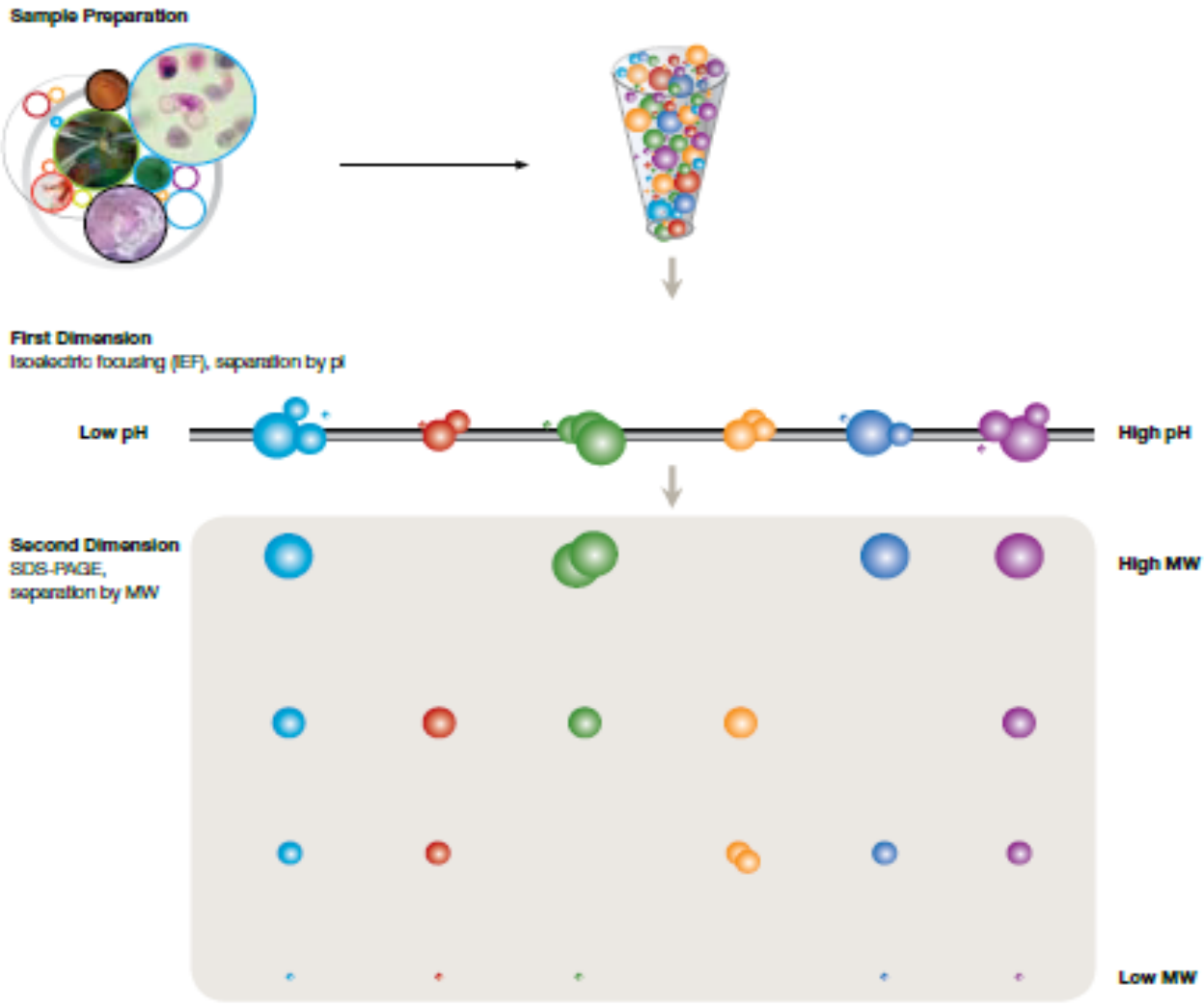

Fig 2.1 2D electrophoresis schematic.

Protein samples are resolved first by isoelectric focusing using the pI of the protein and secondly by SDS-Page using the molecular weight of the protein. Taken from the 2D guide supplied by Bio-Rad.

2.4 Gel visualisation:

Changes in protein phosphorylation were analysed using ProQ Diamond phospho stain supplied by Invitrogen (P-33300). Changes in total protein expression levels were analysed using Sypro Ruby stain supplied by Bio-Rad (170-3125). Gels used to excise spots for mass spectrometry analysis were stained with silver stain compatible with mass spectrometry, using a kit supplied by Thermo Scientific, (24600).

2.4.1 ProQ Diamond staining:

Following overnight fixation, gels were washed 3 times with milliq (MQ) H_2O for 10 minutes, then immersed in 250mL ProQ diamond stain diluted 1:3. Stain can be diluted without compromising staining efficiency (Agrawal and Thelen, 2005). Gels were incubated in the dark with ProQ diamond as per manufacturer's instruction for 90 minutes and destained in 50mM sodium acetate pH 4, 20% acetonitrile (v/v) for 30 minutes, 3 times. Before imaging gels were washed twice in MQ water for 5 minutes each.

2.4.2 Sypro Ruby staining:

Following ProQ diamond staining, gels were washed in MQ water 3 times for 10 minutes. Then incubated with 250mL Sypro Ruby stain in the dark overnight, then washed with destaining solution (10% ethanol (v/v) and 7% acetic acid (v/v)) for 30 minutes, twice. Gels were washed twice with MQ water for 5 minutes.

2.4.3 Silver staining:

The spot pattern was visualised using a silver staining kit supplied by Thermo Scientific (24600) subsequent to ProQ diamond and Sypro Ruby staining. All steps were carried out as per manufacturer's instructions. Briefly, gels were incubated with sensitising solution for 1 minute (1 part sensitiser solution with 500 parts MQ water), washed twice with MQ water for 1 minute and then incubated with silver stain enhancer solution for 5 minutes (1 part silver stain enhancer with 100 parts silver stain). Gels were washed twice with MQ water for 20 seconds and then incubated with developer solution (1 part silver stain enhancer with 100 parts silver stain developer), for 3 minutes, followed by stop solution (5% (v/v) acetic acid), for 10 minutes. Gels were finally washed in MQ water for ten minutes.

2.4.4 Image acquisition:

Gel images used for the RBP proteomics study were scanned using the Typhoon Trio Variable Mode Imager supplied by GE. Gel images used for the RTC15 proteomics study were scanned using the BioRad molecular imager FX. ProQ diamond images were acquired at excitation 532nm and emission 560nm using the Typhoon scanner. ProQ diamond images were acquired at excitation 532nm and emission 555nm using the Molecular Imager FX. Sypro Ruby images were acquired at excitation 532nm and emission 610nm using the Typhoon scanner. Sypro Ruby images were acquired using the Molecular Imager FX were scanned using the pre-set Sypro Ruby settings outlined by the software.

2.5 Image analysis:

All images were analysed using Progenesis SameSpots software. For each study both ProQ Diamond and Sypro Ruby stained images were matched to a Sypro Ruby stained "reference gel" (manually chosen as the most representative from the general experiment). The spot pattern for each gel was aligned to the reference gel for subsequent spot analysis. Spot alignment was conducted automatically by the software with subsequent manual manipulation to remove artefacts and misaligned areas. The original gel images were then categorised into replicate groups so that the software could recognise a group of gels separately from one another and allow statistical analysis between the groups. In the case of these experiments, analysis was conducted between a control group and a treatment group for both phosphorylation and expression changes. The software automatically normalised spot quantity values in each gel by dividing the raw quantity of each spot by the total quantity of all the spots in the respective gel. One-way analysis of variance (ANOVA) was conducted between treatment groups. Only spots showing a >1 fold change with a p-value <0.005 were included for further investigation.

2.6 Spot excision and mass spectrometry:

2.6.1 Spot excision:

Protein spots selected for mass spectrometry analysis were excised from a silver stained gel manually using a cut pipette tip and transferred to a 0.5µl Eppendorf tube.

2.6.2 Gel destaining:

Silver stained gel pieces were destained using the silver stain mass spectrometry kit supplied by Thermo Scientific (24600), according to the manufacturer's instructions. Briefly, gel plugs were destained with 200µl destaining solution for 15 minutes (74µl of silver destain reagent A, 245µl of silver destain reagent B and 4mL MQ water). The gel pieces were destained again for 15 minutes with 200µl of destaining solution, the destaining solution was removed and gel pieces were incubated with 200µl wash solution (25mM ammonium bicarbonate, 50% (v/v) acetonitrile), 3 times for ten minutes.

2.6.3 In-gel digestion:

Once gel pieces were destained protein digestion was carried out as per Shevchenko et al (Shevchenko et al., 2006). Briefly trypsin digestion solution was prepared using 20µg sequencing grade trypsin supplied by Promega (V511C). 20µg trypsin was resuspended in 1.5mL 10mM ammonium bicarbonate containing 10% (v/v) acetonitrile. 50µl of trypsin solution was incubated with each gel piece on ice for 2 hours. The digestion solution was increased on any gel pieces that were not saturated with solution. 10µl of 10mM ammonium bicarbonate, 10% acetonitrile solution was layered on top of the gel pieces to prevent drying out. The gel pieces were then incubated at 37^{o}C overnight. Protein was then extracted from the gel plugs using 100µl extraction buffer (1:2 (v/v) 5% Formic acid/acetonitrile). Samples were incubated at 37^{o}C for 15 minutes with shaking. The solution containing extracted peptides was then removed from each sample and placed in a fresh Eppendorf tube. Samples were vacuum dried using an Eppendorf concentrator 5301and stored at -20^{o}C until mass spec analysis.

2.6.4 LC/MS/MS:

All peptide identifications were carried out using the Ion Trap 6340 LC/MS/MS system supplied by Agilent. Digested samples were resuspended in 20µl 0.1% (v/v) trifluroacetic acid (TFA) in MQ water. Samples were then filtered using spin filters supplied by Fisher (MPA-150-020W). 5µl of trypsin digest was loaded onto a C18 chip (G4240-62006) supplied by Agilent at a rate of 0.6µl/min in 0.1% formic acid (FA). The mobile phases were aqueous solutions of 0.1% (v/v) FA and an acetonitrile solution of 0.1% (v/v) FA. A 10 minute gradient was carried out to increase the acetonitrile concentration to 100% linearly. Charged ions were generated using an electrospray ionisation source. Spray voltage was set to 2000V.

2.6.5 Protein identification:

All peptides were submitted to the Mascot search engine (Matrix Science, London, UK; http://www.matrixscience.com) to identify proteins and searched against the NCBI and Swiss-Prot databases. The enzyme used was selected as trypsin and up to 2 missed cleavages were allowed. Peptide mass tolerance was set at ±2 for precursor ions and a tolerance of ±1 for fragment ions. Variable modifications allowed for were carboxymethyl (C) and oxidation (M). Taxonomy was selected as mammalia. When using the NCBI database, individual ion scores >54 indicate protein identity or extensive homology. Only peptides matched with an ion score above 54 were accepted as significant. When using the Swiss-Prot, database individual ion scores >40 indicate protein identity or extensive homology. Only peptides matched with a score >40 were accepted as significant.

2.7 One dimensional electrophoresis and Western blotting:

2.7.1 SDS-PAGE:

Proteins were separated by molecular weight using SDS Polyacrylamide Gel Electrophoresis (SDS-PAGE). Before electrophoresis samples were denatured in Laemmli sample buffer. 5X Laemmli buffer was prepared with 300mM Tris-HCl, 50% (v/v) glycerol, 10% (w/v) SDS, 0.02% (w/v) Bromophenol Blue, 10% (v/v) β-mercaptoethanol, pH 6.8. Samples were heated to 75^{o}C for 5 minutes and electrophoresed through an acrylamide gel at 100 volts for approximately 2 hours. The running buffer was composed of 0.1% (w/v) SDS, 25mM Tris-Base and 192mM glycine, pH 8.3. A prepared protein ladder supplied by Thermo Scientific (SM1811) was used to assess the molecular weight of electrophoresed proteins (Fig 2.2).

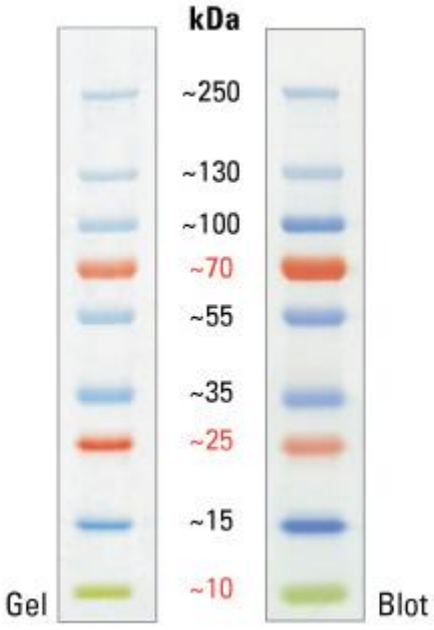

Fig. 2.2 Diagram of distribution of molecular weight markers used for SDS-PAGE.

Distribution of the molecular weight standards present in the Thermo Scientific PageRuler Plus Prestained Protein Ladder when analysed by SDS-PAGE. Image taken from www.thermoscientificbio.com.

2.7.2 Coomassie brilliant blue staining:

SDS-PAGE gels were stained with Coomassie blue using Coomassie Brilliant Blue G250 powder supplied by Ams Biotechnology (17524). Gels were stained according to manufacturer's instructions. Briefly gels were fixed in 40% (v/v) ethanol, 10% (v/v) acetic acid for 15 minutes with shaking, twice. Gels were then immersed in a 1:1 mix of staining solution I (0.2% (w/v) Brilliant Blue G250, 90% (v/v) ethanol) and staining solution II (20% (v/v) acetic acid) and left overnight. Gels were destained for 5 minutes in fixing solution. Gels were then immersed in destaining solution (20% (v/v) ethanol, 10% (v/v) acetic acid) until completely destained, then washed in distilled H_2O before imaging.

2.7.3 Silver staining:

Silver staining was performed using the silver staining kit supplied by Thermo Scientific (24600). Gels were stained as described in section 2.4.3.

2.7.4 Semi-dry electro blotting:

Following SDS-PAGE, identification of proteins of interest was carried out by Western blotting. Proteins were transferred from SDS-PAGE gels onto a polyvinylidene fluoride (PVDF) membrane in transfer buffer (10mM CAPS, pH 11, 10% (v/v) methanol) for 2 hours 10 minutes at a constant 140mA, using a semi-dry transfer unit.

2.7.5 Western blotting:

Membranes were blocked in either 10% (w/v) non-fat dried milk prepared in PBS-T (10mM NaH_2PO_4, 0.14 M NaCl, 3mM KCL, 0.05% (v/v) Tween-20, pH 7.4), or 5% (w/v) BSA in TBS-T (150mM NaCl, 3mM KCl, 25mM Tris-Base, 0.05% (v/v) Tween-20, pH 7.4) for 1 hour at room temperature. Membranes were washed once with PBS-T or TBS-T for 5 minutes at room temperature. Primary antibody was incubated with the membrane in a 5mL volume of PBS-T or TBS-T at the appropriate dilution overnight at 4^oC or for 2 hours at room temperature. If secondary antibody was required, it was used at a 1:5000 dilution in either 5mL PBS-T or TBS-T for 1 hour at room temperature. Membranes were washed 4 times for 5 minutes in either PBS-T or TBS-T. Blots were developed by incubating with enhanced chemiluminescent (ECL) substrate supplied by Roche (11500694001) for 2 minutes. Signal was detected by exposure with X-ray film supplied by Santa Cruz (SC-201697).

2.7.6 Stripping and re-probing PVDF membranes:

In order to visualise different proteins on the same PVDF membrane, the initial primary antibody used must be removed. PVDF membranes were stripped of antibody using 5mL of Restore Western Blot Stripping Buffer (21059) supplied by Thermo Scientific and incubated with rotation for 5 minutes at room temperature. Residual stripping solution was removed by washing 3 times for 5 minutes with either PBS-T or TBS-T. In order to ascertain complete removal of antibody used for initial detection, membranes were incubated with ECL and developed as described in 2.7.7, above. Where no signal was detected, complete removal of the enzyme conjugate could be assumed. Successfully stripped membranes were then re-blocked with either 10% (w/v) non-fat dried milk prepared in PBS-T or 5% (w/v) BSA in TBS-T for a minimum of 30 minutes at room temperature. Successfully stripped membranes were then probed with alternative antibodies.

2.8 Molecular Biology:

Cloning of various genes of interest was performed using the polymerase chain reaction (PCR). PCR reactions were conducted using a G-Storm thermo cycler.

2.8.1 PCR:

DNA template at a concentration of 10ng was used to amplify the sequence of interest. Forward and reverse primers were used at final concentration of 0.4µM. 1X Pfu reaction buffer, was combined with 200µM dNTPs and 1µl Pfu Hotstart Polymerase supplied by Stratagene (600322) and made up to 50µl with RNA and DNA free water. An initial heat step of 95^{o}C for 5 minutes was used to initialize the enzyme for PCR. The PCR reaction was typically cycled using the following parameters for 30 cycles.

1. Denaturing 95^{o}C for 30 seconds.
2. Annealing 5^{o}C lower than the average Tm of the forward and reverse primers for 45 seconds
3. Elongation 72^{o}C for 1 minute per kilo base pair

A final elongation step at 72^{o}C for 5 minutes was used to ensure any single stranded DNA was fully extended. PCR reactions were then stored at 4^{o}C until use.

2.8.2 Agarose gel electrophoresis of DNA:

DNA was analysed using a 0.8% agarose gel with SYBR Safe DNA gel stain supplied by Invitrogen (S33102). 0.4 g agarose was heated to dissolve in 50mL 1X TAE buffer (40mM Tris-acetate, 1mM EDTA, pH 8.4). The solution was cooled and 5µL of SYBR Safe added. Gels were poured and allowed to set at room temperature. DNA loading dye supplied by Thermo Scientific (R0631) was used at a 1:6 dilution with the DNA sample. Gels were electrophoresed at 100 volts constant and visualised using a UV light source. GeneRuler 1kb DNA ladder supplied by Thermo Scientific (SM0313) was used to assess the size of electrophoresed DNA (Fig.2.3). When DNA was required for downstream reactions the DNA product of desired size was excised from the gel using UV illumination. DNA was then extracted from the gel, using a DNA extraction kit supplied by Qiagen (28704) according to the manufacturer's instructions.

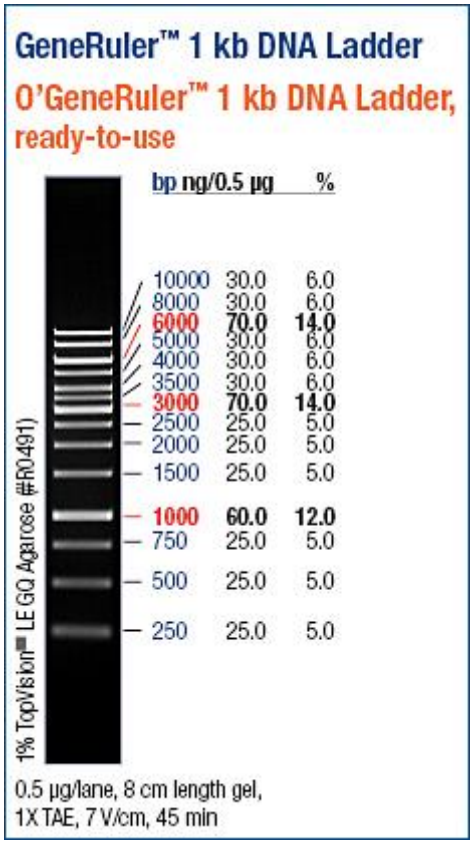

Fig. 2.3 Diagram of distribution of markers used for DNA electrophoresis.

Distribution of the DNA standards present in the Thermo Scientific GeneRuler 1kb DNA Ladder when analysed by DNA agarose electrophoresis. Image taken from www.thermoscientificbio.com.

2.8.3 Restriction digestion:

Destination plasmid and PCR product were digested with desired enzymes. Where possible a double digestion of the DNA of interest was performed, using a buffer compatible with both restriction enzymes. If the enzymes were not compatible in the same buffer, each digest was carried out consecutively. 1µg of destination plasmid and total PCR product were digested using 1 µl of each enzyme. Enzymes were used at a final concentration of 0.1U/µl, in 1X reaction buffer with 100ng/ml BSA. The digestion reaction was incubated overnight at 37^{o}C. Total digested plasmid and PCR product were electrophoresed using a 0.4% agarose gel with SYBR Safe as the DNA visualisation agent. Bands were excised and purified as described previously. Total DNA was combined for plasmid and PCR product respectively. DNA concentration was assessed using the Nanodrop 2000 supplied by Thermo Scientific by reading the absorbance at 260nm.

2.8.4 Ligation:

Digested destination plasmid was combined with digested insert in a 1:1 ratio. 100ng of plasmid and 100ng of insert were combined in 1X T4 DNA ligase buffer. 1µl of T4 DNA Ligase supplied by New England Biolabs (M0202S) was added to the ligation reaction at a final concentration of 20U/µl. Plasmid and insert were incubated at 16^{o}C overnight in a thermocycler.

2.8.5 Transformation of competent *E. coli*:

Either TOP10 *E. coli* cells supplied by Invitrogen (C4040-03) or XL-Blue *E. coli* cells supplied by Stratagene (200249) were used to propagate all ligation reactions as per manufacturer's instructions. 5µl of the total ligation reaction was added to 50µl of competent cells and incubated on ice for 30 minutes. Cells were then incubated at 42^{o}C for 30 seconds. Cells were placed on ice and 250µl of pre-warmed SOC media was added (5% tryptone (w/v), 0.5% yeast extract (w/v), 10mM NaCl, 2.5mM KCl, 10mM $MgCl_2$, 10mM $MgSO_4$, 20mM glucose). Cells were incubated at 37^{o}C for 1 hour with shaking, then plated on LB agar plates (1% tryptone (w/v), 0.5% yeast extract (w/v), 1% NaCl (w/v), 1% agar (w/v), pH 7) with 50µg/ml of appropriate antibiotic for selection and left at 37^{o}C overnight.

2.8.6 Miniprep and subsequent analysis:

Colonies that grew on selection agar plates were transferred into 3mL LB media (1% tryptone (w/v), 0.5% yeast extract (w/v), 1% NaCl (w/v), pH 7). Colonies were incubated in media overnight at 37^{o}C. 2mL of each respective culture was spun at 6800 RCF for 2 minutes. DNA was then extracted from the bacteria using the plasmid purification kit supplied by Thermo Scientific (K0503) as per manufacturer's instructions. 10µl of purified plasmid was then digested as described previously, using the appropriate restriction enzyme to assess the presence of the desired insert.

2.8.7 Midiprep culture of plasmid:

Plasmids were propagated in 50mL LB media with 50µg/ml of required selection antibiotic. Media was inoculated with either 100µL of miniprep culture or if culturing from a glycerol stock a scraping was taken of the stock using a 200µl pipette tip placed into the culture. Cultures were grown at 37^{o}C for 48 hours. Plasmid was then purified using the S.N.A.P. Midiprep kit supplied by Invitrogen (K1910-01), as per manufacturer's instructions. DNA was eluted using 750µL sterile MQ water. DNA concentration was assessed by reading absorbance at 260nm. DNA was then stored at -20^{o}C.

2.8.8 Preparation of glycerol stocks:

For long term storage of plasmids, liquid cultures of *E. coli* transformed with the plasmid of interest were frozen at -80^{o}C. Briefly, 150µl of a 50ml culture of desired *E. coli* was combined with 850µl of sterile glycerol and mixed thoroughly. Cells were then stored at -80^{o}C.

2.9 Protein expression and purification:

2.9.1 Expression of RBP in *Pichia pastoris*:

Recombinant RBP was routinely expressed using a *Pichia pastoris* yeast strain stably transfected with a pPICZα plasmid containing the DNA sequence encoding RBP (Wysocka-Kapcinska et al., 2010). Transformed *Pichia pastoris* were streaked onto a YPD agar plate (1% (w/v) yeast extract, 2% (w/v) peptone, 2% (w/v) dextran, 1% (w/v) agar) with 100µg/ml Zeocin and incubated at 30^{o}C for 3 days. 1 Litre of YP media (1% (w/v) yeast extract, 2% (w/v) peptone, 10% (v/v) PBS) with 2% (v/v) glycerol) was inoculated with yeast colonies from the YPD plate. Yeast was cultured overnight at 30^{o}C with constant shaking (200-250rpm). The 1L culture was pelleted in 250mL aliquots, separately at 7000rpm using a Sorvall RC5C Plus ultracentrifuge, rotor SLA-3000, at room temperature for 10 minutes. Supernatant was discarded and each pellet was resuspended in 1L of YP media with 1% (v/v) methanol to induce expression. Cultures were incubated at 30^{o}C for 3 days. 1% (v/v) methanol was replenished every 24 hours. Cultures were spun at 7000rpm 4^{o}C for 10 minutes. As RBP is excreted into the media the cell pellet was discarded and the media filtered on ice to remove any contaminants. Recombinant RBP was purified using 3mL washed Ni-NTA resin (30410) supplied by Qiagen. Ni-NTA was incubated with the culture media at 4^{o}C overnight with constant agitation. Resin was collected and washed with PBS at room temperature. RBP was eluted from the resin using PBS with 250mM imidazole. Collected eluate was dialysed in PBS overnight at 4^{o}C to remove the imidazole. Aliquots were placed at -20^{o}C for long term storage.

2.9.2 Expression and purification of recombinant CRBP:

Recombinant CRBP was expressed using a BL21 *E. coli* strain stably transformed with a pGEX-4T-3 plasmid containing the DNA sequence for CRBP coupled to a glutathione S-transferase tag. Glycerol stocks were streaked onto a LB agar plate and incubated at 37^{o}C overnight. Single colonies were transferred into 100mL of LB media and incubated overnight at 37^{o}C with shaking (200-250 rpm). Starter cultures were then diluted 1:100 into fresh LB media. BL21 cells were allowed to reach an optical density (OD) of 0.6 when measured at 600nm. After the desired OD was achieved, expression of recombinant protein was induced by addition of 0.1mM isopropyl-β-D-1-thiogalactopyranoside (IPTG). Cultures were allowed to grow for a further 4 hours with constant shaking (200-250 rpm). Cells were harvested by centrifugation at 8,000 RCF for 10 minutes at 4^{o}C. The supernatant was discarded and the cells re-suspended in ice-cold PBS supplemented with protease inhibitors supplied by Sigma (S8830). Suspended cells were sonicated on ice for 1 minute with 1 minute intervals until the lysate cleared. To aid protein solubilisation Triton X-100 was added at 1% (v/v) to the lysate and incubated at 4^{o}C for 30 minutes with constant rotation. Lysozyme was then added to the lysate (0.5mg/ml) for 30 minutes at 37^{o}C with constant agitation. DNAse I (2U/ml) was added to remove viscosity caused by DNA, and lysate incubated for a further 30 minutes at 37^{o}C. Soluble protein was isolated by centrifugation of lysates at 10,000 RCF for 20 minutes at 4^{o}C. The soluble supernatant fraction was then added to an appropriate volume of washed Glutathione Sepharose 4 supplied by GE (17-0756-01) and incubated overnight at 4^{o}C with gentle agitation. Resin was then collected by gravity flow using 5mL disposable columns supplied by Thermo Scientific (29922). Collected resin was washed with ten bed volumes of ice-cold PBS and protein eluted with 50mM Tris-HCl, 10mM reduced glutathione, pH 8.0. Eluate was assessed for protein concentration using absorbance at 280nm and aliquots stored at -20^{o}C.

2.9.3 Cleavage of recombinant CRBP:

When CRBP was required for binding assays in its native form, it was necessary to remove the GST fusion tag. Cleavage was carried out with the protein bound to the resin. Following column packing of the resin with CRBP bound, as described in section 2.9.2, the Sepharose was washed with ten bed volumes of ice-cold PBS. Thrombin was added to the resin at 80U/ml in 1 bed volume of PBS. Cleavage was allowed to occur at room temperature overnight with constant agitation. The flow-through from the column, containing cleaved CRBP was then added to washed Benzamidine Sepharose 6B resin (17-5123-10) supplied by GE for 1 hour at 4^{o}C with gentle agitation to remove the protease. The flow through from the benzamidine Sepharose, containing purified cleaved CRBP was then applied to washed Glutathione Sepharose to remove any residual GST. Flow through from the resin was collected and protein concentration assessed by absorbance at 280nm and aliquots stored at -20^{o}C.

2.9.4 General protocol for C-Terminus expression and purification:

A recombinant version of the C-Terminus of STRA6 was expressed and purified as a fusion protein with a maltose binding protein (MBP) epitope tag for the purposes of structural and functional studies. The general protocol was finalised as follows. BL21 competent cells supplied by Invitrogen (44-0048), a strain optimised for protein expression, were transformed with a pET30a plasmid containing the DNA sequence encoding for the C-Terminus of STRA6 with a MBP fusion tag. Glycerol stocks were prepared as described in section 2.7.7. Glycerol stocks were streaked onto a LB agar plate containing kanamycin at 50µg/ml and incubated at 37^{o}C overnight. Single colonies were transferred into 10mL of terrific broth (TB) media (1.2% (w/v) tryptone, 2.4% (w/v) yeast, 0.4% (v/v) glycerol, 17mM KH_2PO_4, 72mM K_2HPO_4, pH 7.0) with 50µg/ml of kanamycin and incubated overnight at 37^{o}C with shaking (200-250 rpm). Starter cultures were then diluted 1:100 into 400mL of TB media with 50µg/ml kanamycin. BL21 cells were allowed to reach an OD of 0.6 when measured at 600nm. After the desired OD was achieved, expression of recombinant protein was induced by addition of 0.1mM IPTG. Cultures were left at room temperature overnight with constant shaking (200-250 rpm). The cultures were centrifuged at 4,000 RCF for 15 minutes using a Sorvall RC5C Plus ultracentrifuge with rotor SLA-3000 at 4^{o}C. Cells were washed in 300mM NaCl, 50mM Na_2HPO_4, pH 7.5 and re-centrifuged at 4,000 RCF for 15 minutes at 4^{o}C. Cells were lysed in lysis buffer (300mM NaCl, 50mM Na_2HPO_4, 100mM KCl, 1% (w/v) n-Dodecyl β-D-maltopyranoside (DDM), 10mM β-mercaptoethanol, 1X protease inhibitor cocktail, 1mM PMSF, 1mg/ml lysozyme, pH 7.5) for 1 hour at 4^{o}C with constant rotation. Lysates were sonicated on ice for 3 minutes using a Bandelin Sonopuls probe sonicator. Soluble protein was separated from insoluble by high speed centrifugation. Lysates were spun at 12,000 RCF at 4^{o}C using the SS-34 rotor for 20 minutes. The supernatant was retained and added to 2mL of washed Ni-NTA resin supplied by Qiagen (30410), for every 400mL of original culture. Protein was allowed to bind to the resin at 4^{o}C for 90 minutes with constant rotation. Resin was then collected by gravity flow using 5mL disposable columns. Collected resin was washed with ten bed volumes of ice-cold wash buffer (300mM NaCl, 50mM Na_2HPO_4, 100mM KCl, 0.5% (w/v) DDM, 10mM β-mercaptoethanol, pH 7.5). Bound protein was eluted with 3 bed volumes of elution

buffer (20 % glycerol, 300mM NaCl, 20mM Tris-HCl , 100mM KCl, 0.5%(w/v) DDM, 10mM β-mercaptoethanol, 250mM imidazole pH 7.5).

In order to prepare >95% pure protein a second affinity chromatography step was carried out. Amylose affinity chromatography was performed following Ni-NTA purification to prevent contamination of expressed MBP-C-Term fusion protein with native *E. coli* MBP. Protein previously purified using Ni-NTA resin was applied to 2mL washed amylose resin supplied by New England Biolabs (E8021S). Protein was allowed to bind to the resin at 4^{o}C for 90 minutes with constant rotation. Resin was then collected by gravity flow using 5mL disposable columns. Collected resin was washed with ten bed volumes of ice-cold wash buffer (300mM NaCl, 20mM Tris-HCl, 100mM KCl, 0.5% (w/v) DDM, 10mM β-mercaptoethanol, pH 7.5). Bound protein was eluted with 3 bed volumes of elution buffer (20 % glycerol, 300mM NaCl, 20mM Tris-HCl , 100mM KCl, 0.5%(w/v) DDM, 10mM β-mercaptoethanol, 10mM maltose, pH 6.5). Protein concentration was assessed by measuring absorbance at 280nm. Eluted protein was then stored at -20^{o}C.

2.9.5 Cleavage of recombinant C-Terminus using TEV protease:

The concentration of purified recombinant MBP-C-Term was assessed by absorbance at 280nm. The fusion protein contains a TEV protease site to allow the removal of the MBP epitope tag. 1µl of halo-TEV protease supplied by Promega (G6601) was used per 100µg of purified MBP-C-Term. The cleavage reaction was then incubated with rotation at room temperature for 16 hours. Cleaved C-terminus was then purified away from the cleavage reaction by Ni-NTA affinity chromatography. Briefly, the cleavage reaction was incubated with 0.5mL of washed Ni-NTA per 1mg of cleaved protein at 4^{o}C for 1 hour with rotation. Resin was then collected by gravity flow in a 5mL disposable column. The resin was washed with 3 column volumes of ice cold wash buffer (300mM NaCl, 50mM Na_2HPO_4, 100mM KCl, 0.5% (w/v) DDM, 10mM β-mercaptoethanol, pH 7.5). C-Term was eluted in 3 resin bed volumes of elution buffer (20% glycerol (v/v) 300mM NaCl, 100mM KCl, 20mM Tris-HCl, 2mM DDM, 250mM imidazole, pH 6.5). Purified protein was then either dialysed overnight to remove the imidazole or concentrated for size exclusion chromatography analysis.

2.9.6 Strep-tactin purification of STRA6 from a stable cell line:

Stable HEK293 cells induced to express STRA6-HA were lysed in HNG lysis buffer (50mM HEPES, 150mM NaCl, 5% (v/v) glycerol, 1% DDM, 5µg/µl avidin,10mM NaF, 1.5mM Na_3VO_4, 1mM $Na_4P_2O_7$, 1X Protease inhibitor cocktail). Cells were incubated with lysis buffer for 1 hour at 4^oC with rotation. Lysates were spun at 13,000 RCF for 5 minutes at 4^oC. The insoluble pellet was discarded and the soluble supernatant was incubated with 200µl of washed Strep-Tactin resin supplied by Qiagen (30002). Lysates were incubated with the resin for 1 hour at 4^oC with rotation. The lysates were then spun at 2,000 RCF for 2 minutes at 4^oC and the supernatant removed. The resin was washed twice with HNG wash buffer (50mM HEPES, 150mM NaCl, 5% (v/v) glycerol, 0.5% (w/v) DDM, pH 7.4). Protein was eluted from the resin with HNG elution buffer (50mM HEPES, 150mM NaCl, 5% (v/v) glycerol, 0.5% (w/v) DDM, 10mM biotin, pH 7.4).

2.9.7 Immunoprecipitation of proteins of interest:

Cells expressing the desired protein of interest were lysed using RIPA buffer (50mM Tris-HCL, pH 7.4, 1% (v/v) Triton X-100, 0.1% (w/v) SDS, 150mM NaCl, 0.5% (w/v) sodium deoxycholate, 1mM EDTA, 10mM NaF, 1.5mM Na_3VO_4, 1mM $Na_4P_2O_7$, 1X Protease inhibitor cocktail) at 4^oC for 1 hour with rotation. Cell lysate was centrifuged at 10,000 RCF for 5 minutes at 4^oC. The supernatant was then incubated overnight with the desired antibody at 4^oC with constant rotation. Cell lysates were incubated with 100µl washed protein-G agarose supplied by Sigma (P7700) for 4 hours at 4^oC with constant rotation. The immunoprecipiation reaction was then centrifuged at 2,000 RCF for 2 minutes at 4^oC. Supernatant was removed and the agarose was washed twice by centrifugation with 20mM Na_2HPO_4, 150mM NaCl, pH 7.5 at 4^oC. Protein was eluted from the resin either by incubation with 2X Laemmli sample buffer at 95^oC for 5 minutes or by incubation with 10mM glycine pH 3.

2.9.8 Co-immunoprecipitation of proteins of interest:

Cells expressing the desired protein of interest were lysed using HEPES lysis buffer (50mM HEPES, pH 7.5, 1% (v/v) Triton X-100, 150mM NaCl, 1.5mM MgCl2, 1mM EGTA, 10mM NaF, 1.5mM Na_3VO_4, 1mM $Na_4P_2O_7$, 1X Protease inhibitor cocktail 10% (v/v) glycerol, 100µg/mL aprotonin) at 4^oC for 1 hour with rotation. Cell lysate was centrifuged at 10,000 RCF for 5 minutes at 4^oC. The supernatant was then incubated overnight with the desired antibody at 4^oC with constant rotation. Cell lysates were incubated with 100µl washed protein-g agarose for 4 hours at 4^oC with constant rotation. The immunoprecipiation reaction was then centrifuged at 2,000 RCF for 2 minutes at 4^oC. Supernatant was removed and the agarose was washed twice by centrifugation with 20mM Na_2HPO_4, 150mM NaCl, pH 7.5 at 4^oC. Protein was eluted from the resin either by incubation with 2X Laemmli sample buffer at 95^oC for 5 minutes or by incubation with 10mM glycine pH 3.

2.10 Structural and functional assays:

Several techniques were employed to gain some insight into the structural and functional characteristics of purified recombinant proteins.

2.10.1 Size exclusion chromatography:

In order to determine the molecular mass of purified recombinant proteins, size exclusion chromatography (SEC) was employed. Purified proteins were analysed using either a Superose 6 10/300 column (17-5172-01) or a Superdex 200 10/300 GL column (17-5175-01) supplied by GE coupled to an AKTA purifier system (Amersham Biosciences), courtesy of Prof. Sean Doyle, Biotechnology Lab, NUI Maynooth. The Superose 6 column is composed of crosslinked agarose. The Superose 200 10/300 is composed of crosslinked agarose and dextran. The column was first flushed with two column volumes (48mL) of MQ water to remove the ethanol storage buffer. The column was then equilibrated with two column volumes (48mL) of the same buffer the sample was prepared in. On first use of a new column the void volume was assessed by running blue dextran as a large molecular weight calibrant. The void volume is defined as the volume of eluent used to elute a large molecular weight protein such as blue dextran. For each column the void volume was defined as 7mL. Concentrated protein samples were injected onto the column at a flow rate of 0.2ml/min. Once the void volume of the column had been evacuated every 0.5mL fraction was collected in a clean Eppendorf tube for further analysis. Absorbance at 280nm was recorded in order to determine when protein was eluting from the column. In order to determine the exact molecular weight of the protein of interest, defined molecular weight calibrants were used. Molecular weight markers supplied by Sigma were used at a concentration of 1mg/ml. Molecular marker features are defined in table 2.1.

Protein Marker	**Catalogue Number**	**Molecular Mass**	**Elution position Superose 6**	**Elution Position Superdex 200**
Apoferritin	A3660	443 kDa	14mL	10mL
β-Amylase	A8781	200 kDa	15mL	11mL
Alcohol dehydrogenase	A8656	150 kDa	15.5mL	13mL
Bovine Serum Albumin	A8531	66 kDa	16.5mL	13.5mL
Cytochrome C	C7150	12.4 kDa	18.5mL	17mL
Blue dextran	D4772	2,000 kDa	7mL	7mL

Table 2.1 Molecular weight standards used to define elution position of defined molecular weight using SEC.

Molecular weight standards were prepared in the mobile phase used to analyse the proteins of interest. Following resuspension in the mobile phase, samples were centrifuged at 10,000 RCF for 5 minutes to remove particulates. Standards were applied to the column and eluted protein analysed by measuring absorbance at 280nm per mL of mobile phase eluted.

2.10.2 Circular dichroism:

Circular dichroism (CD) analysis was conducted using the Chiroscan spectropolarimeter supplied by AppliedPhotophysics. Samples were purified to approximately 95% purity, ascertained by gel electrophoresis and Coomassie staining as described in sections 2.7.1 and 2.7.2. Samples were diluted to 0.2mg/ml in the respective buffer and analysed compared to that buffer in a quartz cuvette, width 1mm. Samples were scanned every 1nm from 280nm to 180nm at 20^{o}C. Two spectra scans were acquired and data points averaged across the two scans. Data was acquired in millidegrees (mθ) and converted to mean residue ellipticity utilising the following formula (Greenfield, 2006) where mean residue weight represents (molecular weight (Da) / number of amino acids – 1).

$$\text{mean residue ellipticity} = \frac{\text{mθ x mean residue weight}}{\text{path length (mm) x concentration (mg/ml)}}$$

Mean residue ellipticity was then plotted against wavelength. Fractional structural content was analysed using the online server DichroWeb. The analysis was conducted using the CONTIN algorithm with the structural reference database SMP180 (Abdul-Gader et al., 2011).

2.10.3 Chemical crosslinking:

In order to demonstrate protein-protein interactions where the interaction may be highly unstable a chemical crosslinker was utilised to covalently bind two proteins together in complex formation. The putative proteins involved in an interaction were incubated at equimolar concentrations at room temperature for 30 minutes with constant rotation. The photo-activated chemical crosslinker sulfo-NHS-SS-diazerine (SDAD) supplied by Thermo Scientific (26175) was then added to a final concentration of 1mM to the reaction. SDAD was allowed to bind to amine residues for 2 hours on ice. The reaction was quenched by the addition of 100mM Tris, pH 8 and incubated on ice for 15 minutes. SDAD was then photo-activated on ice for 5 minutes using a UV light source at 365nm to covalently link any peptides in close proximity. Crosslinked proteins were then incubated with Laemmli sample buffer either with or without 10% (v/v) β-mercaptoethanol and analysed by SDS-PAGE and Western blotting as described in sections 2.7.1, 2.7.4 and 2.7.5.

Chapter 3

Proteomic investigation of the molecular effects of holo-RBP on a mouse muscle cell line.

3.1 Introduction:

RBP is now widely regarded as a novel biomarker for the development of insulin resistance and type II diabetes. Excess visceral fat may lead to an increase in RBP secretion into the bloodstream. Even in lean patients with type II diabetes, elevated serum levels of RBP were observed (Graham et al., 2006). In 2005, Yang et al associated increased serum RBP levels with the development of insulin resistance (Yang et al., 2005). The synthetic retinoid, fenretinide, induced RBP excretion into the urine from the bloodstream and this led to an improvement in glucose tolerance. Several theories exist as to what the exact molecular mechanism is behind RBP stimulated insulin resistance.

Berry et al suggest that excess serum holo-RBP leads to activation of the JAK/STAT signalling pathway via STRA6 phosphorylation (Berry et al., 2011). JAK2 appears to co-purify with STRA6 and is responsible for phosphorylation of the receptor (Berry et al., 2012). Subsequent activation of STRA6 and JAK2 association leads to STAT5 recruitment and phosphorylation. Activation of STAT5 by phosphorylation results in the transcription of several target genes, but in particular it was demonstrated to cause an increase in SOCS3 mRNA (Berry et al., 2011). SOCS3 is a known inhibitor of the insulin signalling pathway, and can directly bind to and inhibit the insulin receptor (Ueki et al., 2004).

Norseen et al suggest that excess RBP levels are having an indirect effect on adipocytes, by causing cytokine excretion from peripheral macrophages (Norseen et al., 2012). Macrophages treated with holo or apo-RBP displayed increased secretion of TNF-α, IL-6, and MCP-1. Therefore, it appears to be a retinol independent reaction. In addition, the macrophages used in this study are thought not express STRA6, thus RBP could not promote cytokine production via activation of this membrane protein. The cytokines elevated in response to RBP are known to cause inhibition of the insulin signalling pathway (Patel et al., 2013).

The theories that surround RBP-induced insulin resistance are in disagreement about the involvement of STRA6. One group suggests insulin resistance occurs as a result of direct stimulation of STRA6 whereas another suggests it is not involved at all. In addition, Norseen et al demonstrated that apo-

RBP was just as effective at inducing insulin resistance as holo-RBP, whereas Berry and colleagues declare that only holo-RBP is capable of inducing insulin resistance. Both groups directly stimulated 3T3-L1 adipocytes with holo-RBP (Berry et al., 2011; Norseen et al., 2012). Berry et al observed impaired signalling in the insulin pathway. Norseen and colleagues observed that insulin signalling is only impaired in adipocytes when co-cultured with macrophages (Norseen et al., 2012). In an separate study, Muenzner et al did not observe an increase in SOCS3 expression, in response to elevated levels of holo-RBP (Muenzner et al., 2013). The same 3T3-L1 adipocyte cell line was utilised and stimulated directly with holo-RBP. No increase in phosphorylation of STAT5 was observed and no alteration of SOCS3 mRNA, even in cells over-expressing STRA6.

Muscle tissue is the main site for insulin stimulated glucose uptake in the body. If glucose uptake is impaired in this tissue for a prolonged period, plasma glucose levels can reach high enough levels to cause damage to other areas of the body, such as the eyes and kidney. The study conducted by Norseen et al did not assess the effect of increased RBP levels and subsequent cytokine production on muscle cell signalling (Norseen et al., 2012). In a previous publication by the same group, they observed that elevated serum RBP levels in whole animal studies resulted in impaired insulin signalling in muscle tissue (Yang et al., 2005). No change was observed in insulin receptor phosphorylation. However, phosphatidylinositide 3 kinase (PI3K) activity was reduced as was IRS-1 phosphorylation at tyrosine 612. Phosphorylation of this residue in IRS-1 provides the docking site for PI3K. Berry and colleagues also observed that insulin signalling was impaired in muscle tissue of mice treated with elevated levels of RBP (Berry et al., 2011). However, they observed a reduction in phosphorylation of the insulin receptor which would correlate with their theory that SOCS3 was having an inhibitory action on this protein.

We are still a long way from understanding the precise molecular mechanisms involved in RBP mediated insulin resistance. A global, unbiased view of the proteome of muscle cells treated with holo-RBP may provide a definitive answer as to what cellular pathways are affected.

Aims and Objectives:

In order to determine the molecular mechanism of RBP induced insulin resistance, a proteomic study was devised to identify proteins in muscle cells affected by increased RBP levels. Skeletal muscle is regarded as the main site for insulin-induced glucose uptake. The investigation asked whether holo-RBP has a direct effect on signalling pathways in the mouse muscle cell line, C2C12. Normal plasma RBP levels are approximately 25µg/ml, elevated levels in obese patients can vary greatly but on average are approximately 70µg/ml (Graham et al., 2006). Therefore, 75µg/ml holo-RBP was used to simulate elevated serum RBP levels. Overnight stimulation with holo-RBP was chosen to represent long-term exposure.

2D-electrophoresis in conjunction with mass spectrometry was utilised as a method to identify changes in the proteome of cells treated with holo-RBP. Cells used in this study were lysed and the membrane and cytosolic fractions isolated and analysed separately. This was performed to enrich the membrane fraction and to possibly observe protein recruitment to the membrane. A number of protein changes were identified and subjected to secondary validation and further analysis.

3.2 Method:

The mouse muscle cell line, C2C12, was cultured and differentiated into myotubes as described in section 2.1.2. Cells were treated with 75μg/ml holo-RBP for 16 hours, with PBS used as an appropriate control. Cells were harvested and the whole cell lysate was separated into membrane and cytosolic fractions (sections 2.2.2 and 2.3.1). The membrane and cytosolic fractions were used for proteomic analysis (section 2.3.2 through to 2.3.7). 2D gels were first visualised using the phospho-protein stain Pro-Q Diamond to assess changes in the phospho-proteome of the cell, (section 2.4.1). Gels were subsequently visualised for total protein levels using the sypro ruby fluorescent stain (section 2.4.2). Three technical replicates were performed for each sample and samples were produced in triplicate. Therefore, 9 gels were run for each treatment group for the cytosolic and membrane fraction, equalling 36 gels in total. Changes in the proteome of the cell were identified using Progenesis SameSpots software. Only proteins showing a greater than 1.1 fold change with a statistical significance of <0.05 were chosen for identification by mass spectrometry (MS). A 2D gel was then selected as a reference gel and stained using silver stain (section 2.4.3). Proteins showing altered phosphorylation or expression were excised and trypsin digested. MS analysis was subsequently conducted on digested protein spots (section 2.6). Once proteins were identified by peptide matching software, a number of the most interesting proteins were selected for secondary validation using SDS-PAGE and Western blotting.

3.3 Results:

Several proteins were identified that showed changes in either phosphorylation or expression levels in response to overnight treatment with 75µg/ml holo-RBP. Fig 3.1 depicts a representative gel of the cytosolic fraction isolated from cells treated with holo-RBP overnight, with proteins showing changes in expression circled and numbered. Fig 3.2 depicts a representative gel of the membrane fraction isolated from cells treated with holo-RBP overnight, with proteins showing changes in phosphorylation or expression circled and numbered.

Selected protein spots were trypsin digested and peptides identified by mass spectrometry (MS)-Table 3.1. Peptides were identified using the NCBI protein database and only proteins matched with a score >54 were chosen as significant protein identifications. Fig. 3.3 represents individual phosphorylation changes observed in the proteins identified by MS. Fig. 3.4 represents individual expression changes observed in the proteins identified by MS. The function of each protein was identified using the NCBI and UniProt databases, summarised in Table 3.2.

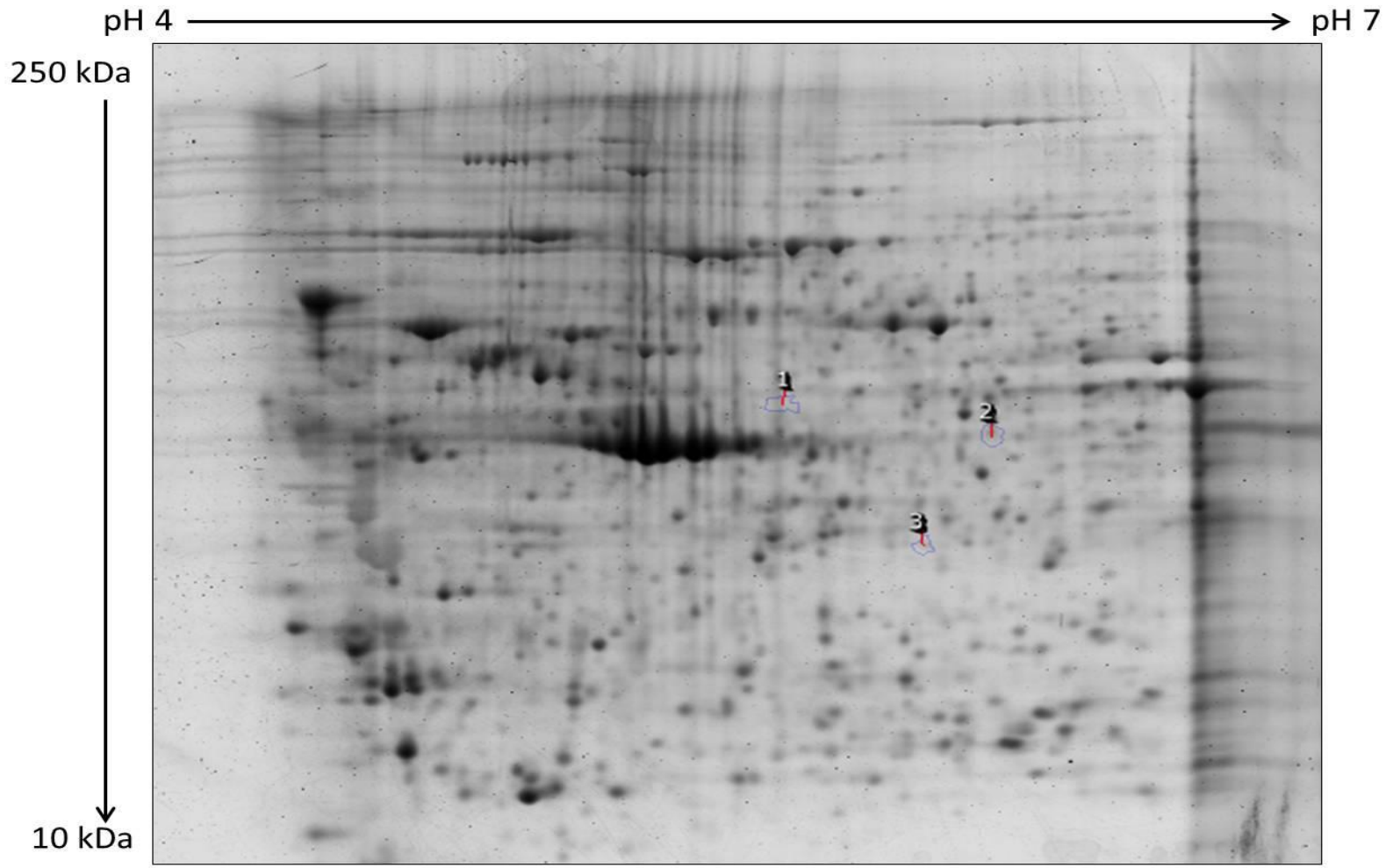

Fig 3.1 Identified spots from C2C12 cytosolic fraction generated from cells treated with 75µg/mL holo-RBP.

Representative Sypro ruby image of C2C12 cytosolic fraction generated from cells treated with 75µg/ml holo-RBP, resolved by 2D electrophoresis. Spots circled and numbered represent proteins showing a statistically significant change in expression.

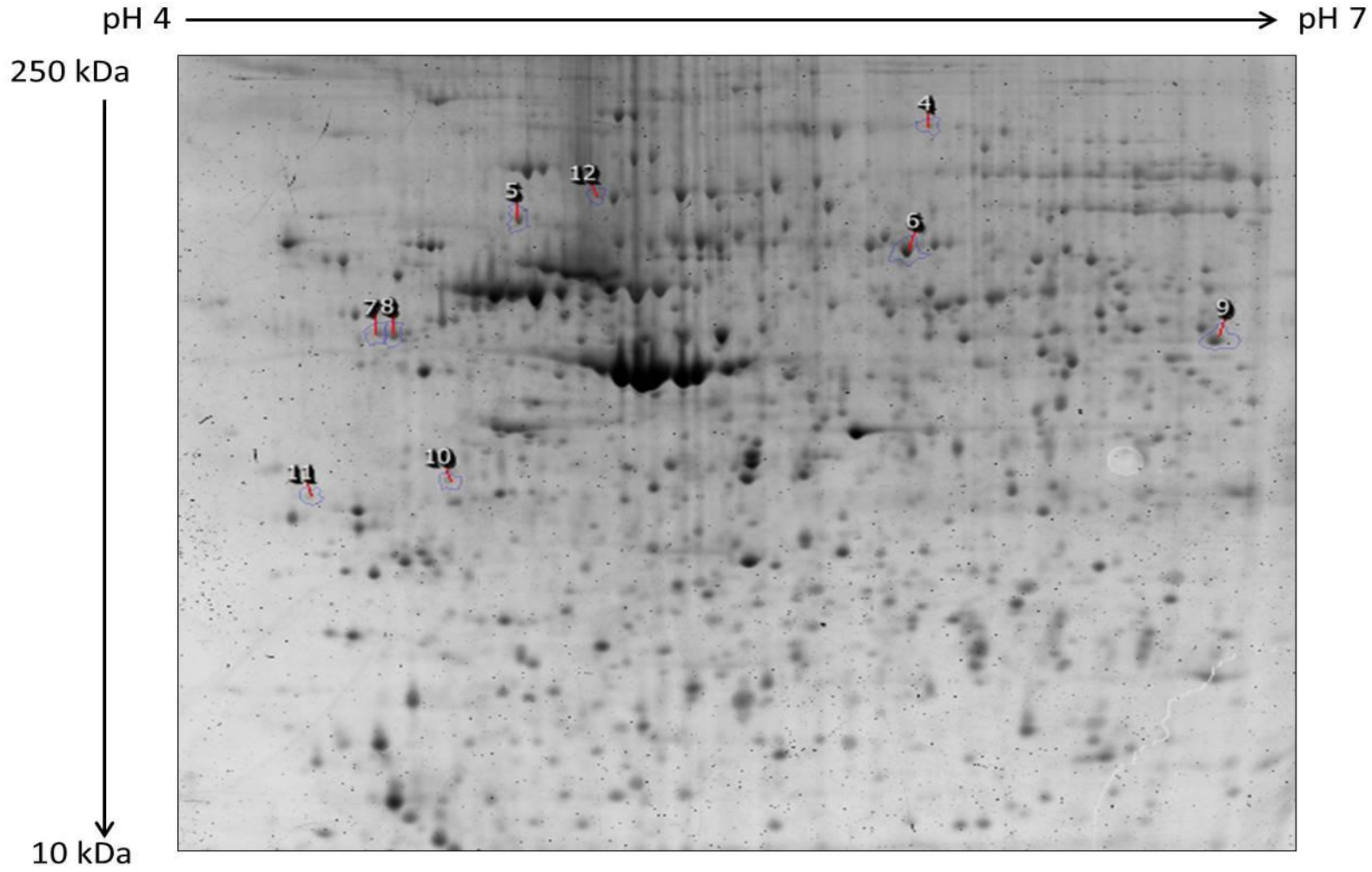

Fig 3.2 Identified spots from C2C12 membrane fraction generated from cells treated with 75µg/mL holo-RBP.

Representative Sypro ruby image of C2C12 membrane fraction generated from cells treated with 75µg/ml holo-RBP, resolved by 2D electrophoresis. Spots circled and numbered represent proteins showing a statistically significant change in phosphorylation or expression.

Spot No.	Protein Identified	Accession No.	Fold Change	Change	Score	Peptides Matched	Cov (%)	MW
1	Lysozyme homolog AT-2	gi|539969	1.3	Down	153	6	100	31.62
2	Ornithine aminotransferase	gi|8393866	1.3	Down	105	1	4	48.32
3	Protein Phosphatase1β	gi|148705446	1.5	Down	304	6	23	35.29
4	Mitochondrial Inner Membrane Protein	gi|70608131	1.2	Down	485	9	18	83.85
5	*Protein Phosphatase 2A	gi|122921194	1.2	Down	642	18	30	64.38
6	Protein disulfide-isomerase A3	gi|112293264	1.4	Up	914	25	48	56.64
7	Vimentin	gi|2078001	1.4	Up	494	14	25	51.53
8	Vimentin	gi|2078001	1.4	Up	558	18	29	51.53
9	*SCaMC-1	gi|27369998	1.6	Up	248	6	14	52.87
10	DDB1- and CUL4-associated factor 12	gi|22218619	1.3	Down	31	1	2	50.49
11	*Cardiomyopathy-associated protein 5	gi|308912513	1.4	Down	59	3	0	45.05
12	Lamin B1	gi|15126742	1.8	Up	415	10	15	66.37

Table 3.1 Proteins identified by mass spectrometry showing changes in phosphorylation or abundance in response to 75 µg/ml holo-RBP.

All proteins were identified using the NCBI protein database and demonstrated a score >54, indicating significant protein identification. Proteins denoted with * represent proteins showing a change in phosphorylation.

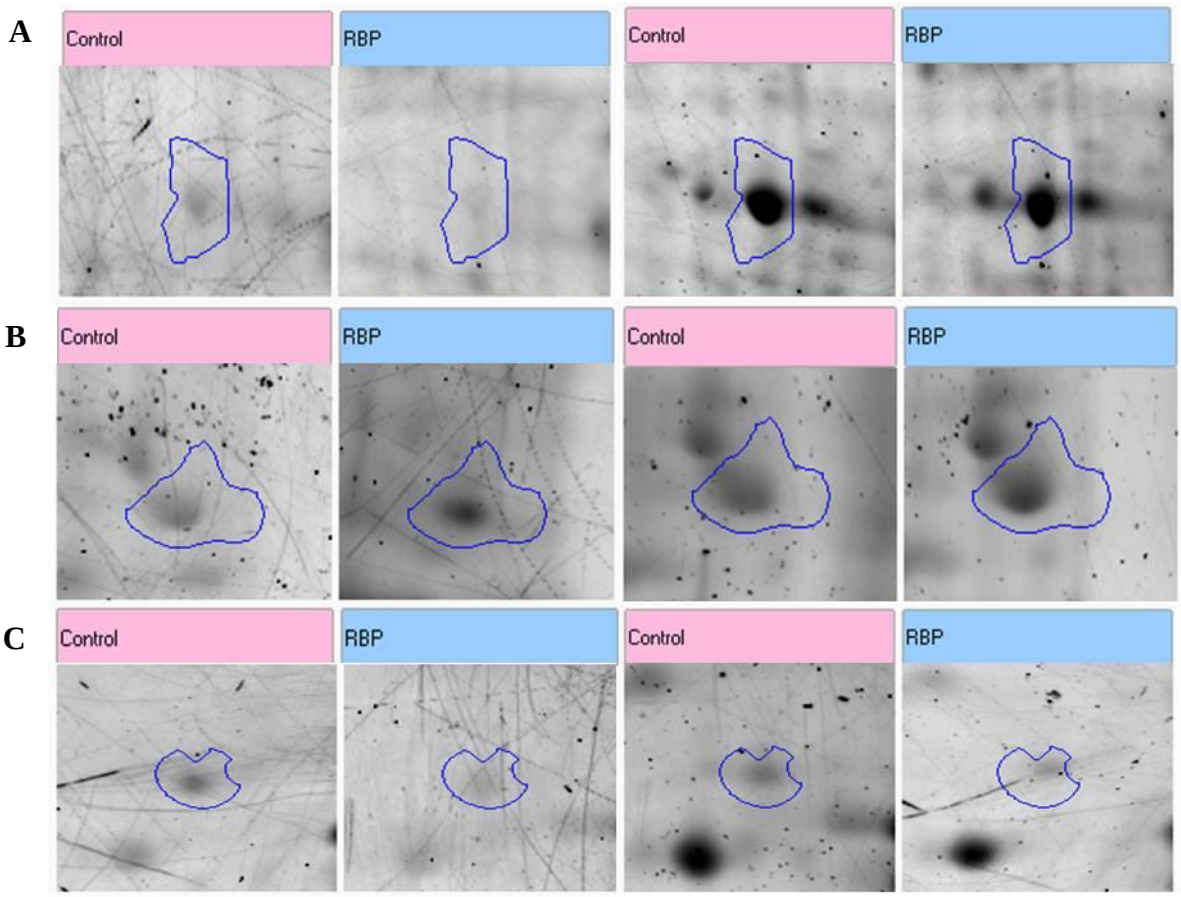

Fig 3.3 Phosphorylation changes observed in C2C12 muscle cells treated with 75µg/ml holo-RBP.

Single spot analysis of statistically significant phosphorylation changes in C2C12 cells treated with 75µg/ml holo-RBP versus control. ProQ Diamond stained images are shown on the left and Sypro Ruby stained images are shown on the right. The following proteins are represented **A**. Protein Phosphatase 2A subunit A **B**. SCaMc-1 **C**. Cardiomyopathy associated protein 5.

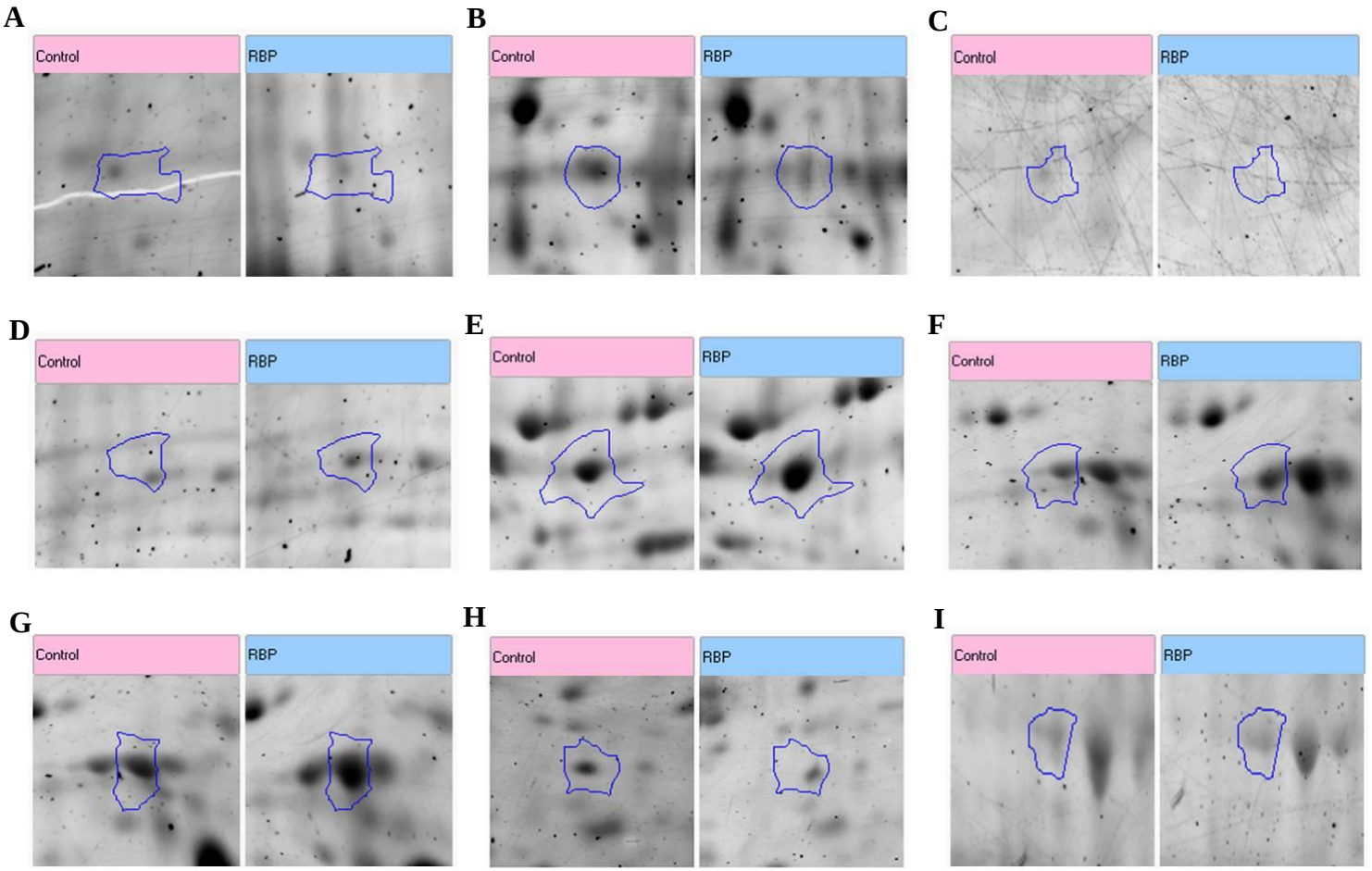

Fig 3.4 Changes in protein abundance observed in C2C12 muscle cells treated with 75µg/ml holo-RBP.

Single spot analysis of statistically significant changes in protein abundance in C2C12 cells treated with 75µg/ml holo-RBP versus control. Each panel depicts a sypro ruby stained control sample and RBP treated sample. The following proteins are represented **A**. Lysozyme Homologue AT-2 **B**. Ornithine Aminotransferase **C**. Protein Phosphatase 1β **D**. Mitochondrial Inner Membrane Protein **E**. Protein Disulphide Isomerase A 3 **F**. Vimentin **G**. Vimentin **H**. DDB1- and CUL4-associated factor 12 **I**. Lamin B1

Spot No.	Protein Identified	Function
1	Lysozyme homolog AT-2	Homologue of the bacteriolytic enzyme lysozyme.
2	Ornithine aminotransferase	Ornithine aminotransferase catalyses the transfer of the δ amino group of ornithine to 2-oxoglutereate.
3	Serine/threonine-protein phosphatase PP1-beta, catalytic subunit (PP1β)	PP1β is involved in the regulation of glycogen synthesis and metabolism.
4	Mitochondrial Inner Membrane Protein 1	Mitochondrial inner membrane chaperone that helps import and insert transmembrane proteins into the mitochondrial membrane.
5	*Protein Phosphatase 2A subunit A	PP2A subunit A (PR65) serves as a scaffolding molecule to form the complete PP2A complex.
6	Protein disulphide-isomerase A3	Protein disulphide-isomerase A3 catalyses the re-arrangement of disulphide bonds in proteins.
7	Vimentin	Vimentin is an intermediate filament involved in cell migration and adhesion. It may also be involved in vesicle trafficking to the cell membrane.
8	Vimentin	Vimentin is an intermediate filament involved in cell migration and adhesion. It may also be involved in vesicle trafficking to the cell membrane.
9	*SCaMC-1	ScaMC-1 is a solute carrier that may shuttle metabolites, nucleotides and co-factors through the membrane of the mitochondria.
10	DDB1- and CUL4-associated factor 12	DDB1- and CUL4-associated factor 12 may function as a substrate receptor for the ubiquitin-protein ligase complex.
11	*Cardiomyopathy-associated protein 5 (Cmya5)	Cmya5 is involved in compartmentalisation of protein kinase A (PKA).
12	Lamin B1	Lamin B1 is a structural component of the nuclear lamina. It belongs to the intermediate filament family.

Table 3.2 Function of proteins identified by MS showing changes in response to holo-RBP.

Proteins denoted with * represent proteins showing a change in phosphorylation. The function of each protein identified was compiled using the UniProt and NCBI protein databases.

3.3.1 Identification of changes in the proteome in response to holo-RBP:

A number of changes in the proteome of the cell were observed in the cytosolic and membrane fraction of C2C12 cells treated with 75µg/ml holo-RBP overnight. More changes would have been expected in protein abundance, as cell stimulation with holo-RBP would in theory prompt the delivery of ROH into the cell. As cells were harvested after 16 hours incubation with holo-RBP, any changes in the proteome due to increased ROH may have been missed. In addition, the cell lysate was separated into membrane and cytosolic fractions across three replicate samples with three technical replicate gels per sample. Therefore, due to the high stringency of technical and experimental replicates some protein changes may not have been statistically significant and remained unidentified. Of the proteins that were identified 5 were chosen for secondary validation.

3.3.2 Analysis of changes in the proteome of the cytosolic fraction:

Three proteins demonstrated altered expression levels in the cytosolic fraction of C2C12 cells treated with holo-RBP, lysozyme homolog AT-2 (LAT-2), ornithine aminotransferase (OAT) and protein phosphatase 1β (PP1β).

3.3.2.1 Analysis of decreased expression of LAT-2:

LAT-2 expression was decreased 1.3-fold in response to holo-RBP. BLAST analysis revealed that it is a member of the lysozyme family. The peptide fragment used to confer protein identity in this study, shares considerable sequence similarity with chicken lysozyme (Fig 3.5).

```
LAT-2           FESNFNTQATNRNTDGSTDYGILQINSR 28
Lysozyme        FESNFNTQATNRNTDGSTDYGILQINSR 28
                ****************************
```

Fig 3.5 Sequence alignment of peptide fragments from LAT-2 and chicken lysozyme.

Sequence similarity between peptide fragments from LAT-2 and chicken lysozyme. Sequence alignment performed using ClustalW 2.1.

Lysozyme has a bactericidal action by binding to peptidoglycan in the bacterial cell wall (Chipman and Sharon, 1969). Hydrolysis of the β-glycosidic bonds present in peptidoglycan results in destabilisation of the structure of the cell wall and subsequent cell lysis. A study conducted by Yoon et al showed that lysozyme levels are increased in times of RA deprivation (Yoon et al., 1999). When cells were deprived of RA in the media, lysozyme secretion increased (Yoon et al., 1999). However, this was not associated with an increase in mRNA transcripts of the protein, but it is thought to be associated with a decrease in lysozyme metabolism. Thus, stimulation of cells with holo-RBP would lead to increased intracellular levels of RA, which may be having an oppressive effect on LAT-2 protein levels. Decreased levels of LAT-2 in response to holo-RBP may occur as a result of RA stimulated lysozyme degradation by some unknown mechanism.

3.3.2.2 Analysis of decreased expression of OAT:

OAT is involved in the inter-conversion of proline and ornithine. Ornithine is an essential intermediate in the production of the amino acid, arginine. In hepatic tissues, OAT is involved in urea production. In non-hepatic tissues, OAT is involved in the metabolism of arginine to form proline, an essential component of collagen (Dekaney, 2000). A study conducted by Dekaney et al determined that exposure of intestinal epithelial cells to RA resulted in increased expression of OAT (Dekaney et al., 2008). This is the opposite expression profile observed with exposure of muscle cells to holo-RBP. The expression profile of OAT in muscle in response to RA has not been studied. However, OAT transcription may be controlled differently in various tissues. Shull and colleagues observed that OAT mRNA was reduced in the liver of mice fed a vitamin A deficient diet (Shull et al., 1995). When mRNA levels were analysed in the kidney, no effect was observed on OAT transcription levels. Therefore, RA may elicit a cell type specific effect on the control of OAT transcription.

3.3.2.3 Analysis of decreased expression of PP1β:

PP1β is a serine/threonine phosphatase that is involved in the regulation of the enzymes that control glycogen metabolism (Cohen, 2002). PP1β expression was reduced 1.5-fold in response to holo-RBP treatment. Secondary validation by Western blotting did reveal a significant decrease in expression following holo-RBP treatment (Fig 3.6). It is not known how transcription of this phosphatase is regulated. Expression is thought to occur constitutively and the translated protein is subsequently regulated by binding to various targeting subunits, which control its subcellular distribution and activity (Cohen, 2002).

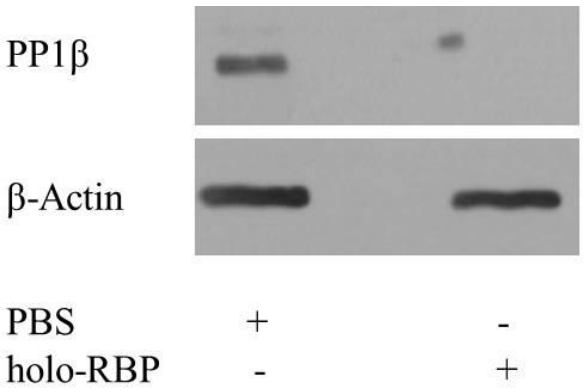

Fig 3.6 Analysis of expression levels of PP1β.

Representative Western blot depicting expression levels of PP1β in response to PBS or 75µg/ml holo-RBP overnight. Serum starved C2C12 cells were treated with PBS or 75µg/ml holo-RBP overnight. Cells were harvested and lysed in RIPA buffer. Protein concentration was assessed using the PIERCE protein assay and 30µg/ml protein was used per sample. Cell lysate was electrophoresed using a 10% SDS-PAGE gel and protein was subsequently transferred to PVDF membrane. Western blotting analysis was conducted using anti-PP1β specific antibody and β-Actin as a loading control. All analysis was conducted in triplicate.

3.3.3 Analysis of changes in the proteome of the membrane fraction:

Several proteins were altered in the membrane fraction of C2C12 cells treated with holo-RBP. These include mitochondrial inner membrane protein isoform 1 (IMMT), protein phosphatase 2A (PP2A) subunit A, Protein disulphide-isomerase A3 (PDIA3), vimentin, SCaMc-1, DDB1- and CUL4-associated factor 12 (DCAF12), cardiomyopathy-associated protein 5 (CMYA5) and lamin B1.

3.3.3.1 Analysis of decreased expression of IMMT:

IMMT is associated with the inner mitochondrial membrane. It is involved in the maintenance of cristae in the membrane (Zerbes et al., 2012b). IMMT is also known as mitofilin and it exists in the mitochondrial membrane as a central component of a mitochondrial inner membrane organising system (MINOS) complex. The MINOS complex functions as a scaffold structure in the membrane and may also be involved in protein biosynthesis (Zerbes et al., 2012a). Mitofilin demonstrated a 1.2-fold decrease in expression in response to holo-RBP treatment. It is unknown what direct effect holo-RBP would have on mitofilin expression.

3.3.3.2 Analysis of decreased phosphorylation of PP2A subunit A:

PP2A is a ubiquitously expressed serine/threonine protein phosphatase. It functions mainly as a trimeric structure composed of a scaffolding A subunit, a regulatory B subunit and a catalytic C subunit (Lechward et al., 2001). The B subunit determines the phosphatase activity of the enzyme. The A subunit acts as a scaffold for the rest of the complex, it can also be denoted PR65 and exists in two isoforms α and β. The α isoform of the A subunit of PP2A displayed a 1.2-fold decrease in phosphorylation in response to holo-RBP treatment. As no phospho-specific antibodies were commercially available for the A subunit of PP2A, the subunit was first purified by immunoprecipitation from C2C12 cells treated with holo-RBP or PBS, using a PP2A A subunit, α isoform specific antibody. Purified protein was then analysed by Western blotting using general anti-phospho amino acid antibodies. Fig 3.7 depicts the secondary validation of PP2A A subunit phosphorylation levels in response to holo-RBP treatment. Only the anti-phospho-serine antibody was reactive with the A subunit of PP2A.

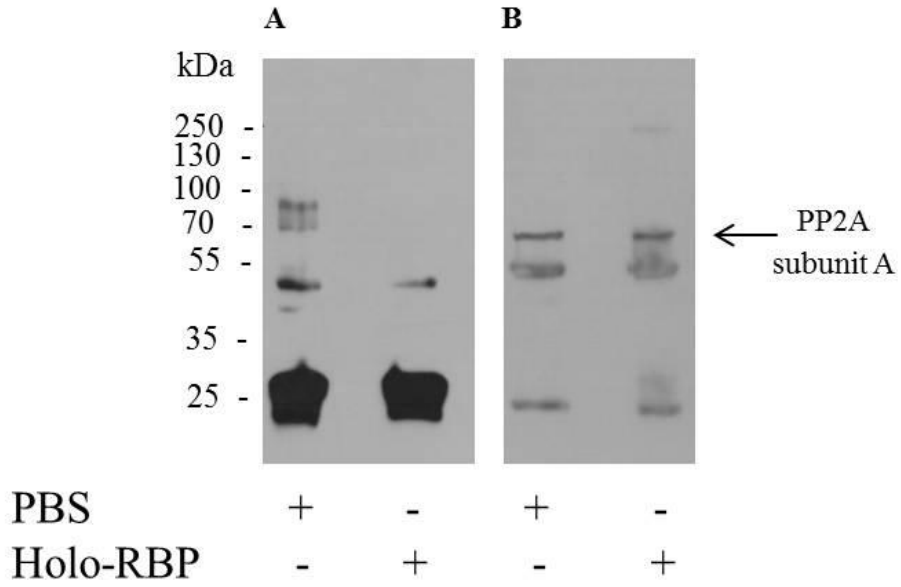

Fig 3.7 Analysis of phosphorylation levels of PP2A subunit A.

Representative Western blot depicting phosphorylation levels of PP2A A subunit in response to PBS or 75µg/ml holo-RBP overnight. All analysis was conducted in triplicate. C2C12 cells were treated with PBS or 75µg/ml holo-RBP for 16 hours. Cells were harvested and lysed in HEPES lysis buffer. Cell lysate was then incubated with anti-PP2A subunit A, α isoform antibody overnight. Immunoprecipitated protein was purified using protein G agarose beads. Purified protein was then electrophoresed using a 10% SDS-PAGE gel and protein was subsequently transferred to PVDF membrane. **A**. Western blot representing total protein immunoblotted with anti-phospho-serine antibody. The A subunit of PP2A is approximately 64 kDa. The bands present at 55 kDa and 25 kDa respectively, represent the heavy and light chain of the PP2A subunit A antibody used in the immunoprecipitation reaction. **B**.Western blot representing total levels of PP2A subunit A using anti-PP2A subunit A α isoform antibody.

There is no known serine phosphorylation site in the A subunit of PP2A. Analysis of the murine amino acid sequence using the phosphorylation prediction server PhosphoSitePlus, predicted several potential serine phosphorylation sites at residue 9, 36, 335, 343, 401, 403 and 554 (Fig 3.8).

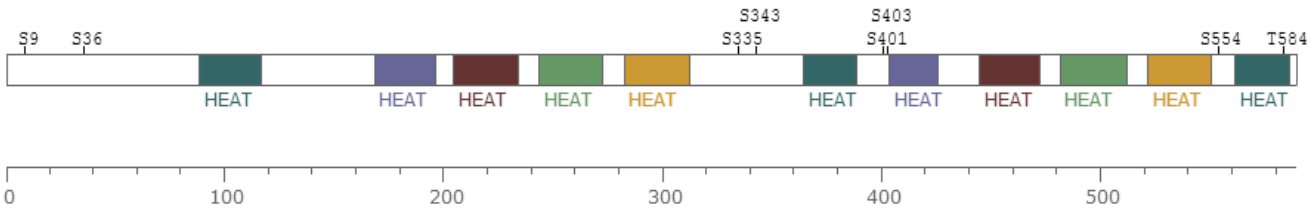

Fig 3.8 Prediction of potential phosphorylation sites in the sequence of the A subunit of PP2A.

Diagram depicting the potential phosphorylation sites of the A subunit of PP2A. Image generated using the phosphorylation site prediction software, PhosphoSitePlus.

3.3.3.3 Analysis of increased expression of PDIA3:

PDIA3 is expressed in the endoplasmic reticulum (ER) (Lee, 1987). It is an isomerase which catalyses the rearrangement of disulphide bonds. A 1.4-fold increase in expression was observed in response to holo-RBP treatment. PDIA3 is a common protein which appears upregulated in several proteomic studies and is thought to be a response to cellular stress. It is also known as 58kDa glucose-regulated protein, as it was upregulated in response to glucose starvation (Lee, 1987). PDIA3 has also been observed to increase in expression following viral infection and dopamine treatment (Dukes et al., 2008; Mazzarella et al., 1994). Upregulation of enzymes involved in protein folding is a cellular defence mechanism to protect the cell from stress damage. Increased PDIA3 expression in response to holo-RBP could be occurring as a result of cellular stress, due to increased intracellular ROH levels.

3.3.3.4 Analysis of increased expression of vimentin:

Vimentin is a member of the intermediate filament family. It is thought to be involved in cell motility and has a scaffolding function in the cell (Ivaska et al., 2007). Fig 3.9 depicts the expression level of vimentin in response to PBS or holo-RBP treatment. Secondary validation by Western blotting did not reveal a significant increase in expression following holo-RBP treatment.

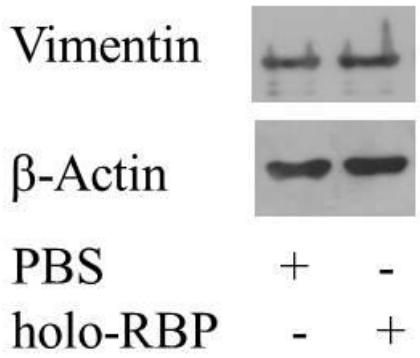

Fig 3.9 Analysis of expression levels of vimentin.

Representative Western blot depicting expression levels of vimentin in response to PBS or 75µg/ml holo-RBP overnight. Serum starved C2C12 cells were treated with PBS or 75µg/ml holo-RBP overnight. Cells were harvested and lysed in RIPA buffer. Protein concentration was assessed using the PIERCE protein assay and 30µg/ml protein was used per sample. Cell lysate was electrophoresed using a 10% SDS-PAGE gel and protein was subsequently transferred to PVDF membrane. Western blotting analysis was conducted using anti-vimentin specific antibody and β-Actin as a loading control. All analysis was conducted in triplicate.

3.3.3.5 Analysis of increased phosphorylation of SCaMC-1:

SCaMc-1 is a small calcium dependent solute carrier which shuttles proteins across the inner mitochondrial membrane (del Arco and Satrústegui, 2004). SCaMc-1 displayed a 1.6-fold increase in phosphorylation in response to holo-RBP stimulation. It has no known phosphorylation site. Analysis of the murine amino acid sequence using the phosphorylation prediction server PhosphoSitePlus, predicted potential phosphorylation sites at S208, S229, Y322, Y326 and Y355 respectively (Fig 3.10).

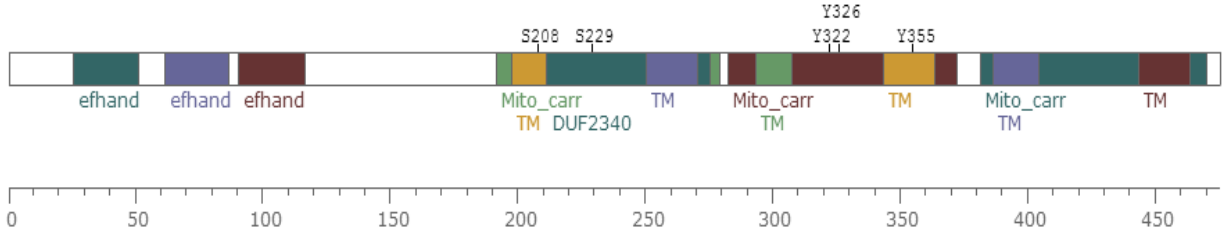

Fig 3.10 Prediction of potential phosphorylation sites in the sequence of SCaMC-1.

Diagram depicting the potential phosphorylation sites of SCaMC-1. Image generated using the phosphorylation site prediction software, PhosphoSitePlus.

As no phospho-specific antibodies were commercially available for SCaMC-1, the protein was first immunoprecipitated using SCaMC-1 specific antibody then analysed by SDS-PAGE and Western blotting using general phospho-amino acid antibodies. SCaMC-1 only demonstrated reactivity with the anti-phospho-serine antibody. Fig 3.11 depicts the secondary validation of SCaMC-1 phosphorylation. SCaMC-1 did not display any significant alteration in phosphorylation levels in response to holo-RBP treatment when analysed directly. As this protein has a molecular weight of 53 kDa, it ran at a similar position to the heavy chain of the antibody used in the immunoprecipitation reaction. This made secondary validation of the phosphorylation levels of this protein extremely difficult as the fluorescence overlapped significantly from the heavy chain band.

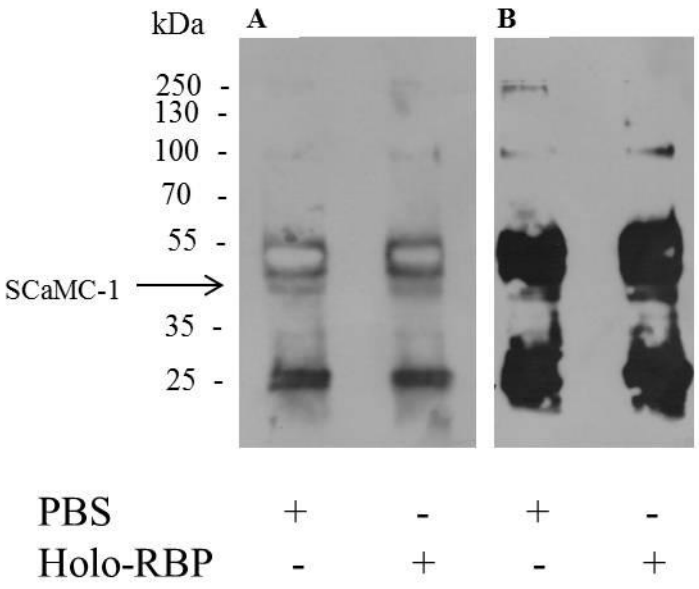

Fig 3.11 Analysis of phosphorylation levels of SCaMC-1.

Representative Western blot depicting phosphorylation levels of SCaMC-1 in response to PBS or 75µg/ml holo-RBP overnight. All analysis was conducted in triplicate. C2C12 cells were treated with PBS or 75µg/ml holo-RBP for 16 hours. Cells were harvested and lysed in RIPA buffer. Cell lysate was then incubated with anti-SCaMC-1 antibody overnight. Immunoprecipitated protein was purified using protein G agarose beads. Purified protein was then electrophoresed using a 10% SDS-PAGE gel and protein was subsequently transferred to PVDF membrane. **A**. Western blot representing total protein immunoblotted with anti-phospho-serine antibody. SCaMC-1 is a 53 kDa protein. The bands present at 55 kDa and 25 kDa, represent the heavy and light chain of the SCaMC-1 antibody used in the immunoprecipitation reaction. **B**.Western blot representing total levels of SCaMC-1 using anti-SCaMC-1 antibody.

3.3.3.6 Analysis of decreased expression of DCAF12:

DCAF12 is a binding partner of the CUL4-DDB1 E3 ubiquitin ligase complex (Jin et al., 2006). The CUL4-DDB1 complex adds ubiquitin groups onto proteins targeted for proteasomal degradation. DCAF12 binds to the complex via the DDB1 subunit. The functional significance of this interaction is unknown but it is thought to enhance substrate binding to the complex. DCAF12 contains a WD40 domain which is known to aid protein complex formation. DCAF12 demonstrated a 1.3-fold decrease in expression in response to holo-RBP treatment. Very little is known about the regulation of DCAF12 expression and what effect holo-RBP stimulation would have.

3.3.3.7 Analysis of decreased phosphorylation of CMYA5:

CMYA5 is also known as myospryn. It acts as an anchoring protein for cAMP-protein kinase A (PKA) (Reynolds et al., 2007). PKA is a ubiquitous kinase and specificity is achieved by spatial regulation conferred by regulatory complexes known as A kinase anchoring proteins (AKAP). CMYA5 is a known AKAP and is thought to anchor PKA to α-actinin at the costamere in skeletal muscle (Reynolds et al., 2007). The costamere is involved in binding the sarcomere to the cell membrane. PKA was demonstrated to phosphorylate CMYA5 in vitro (Reynolds et al., 2007). A 1.4-fold decrease in phosphorylation of CMYA5 was observed in response to holo-RBP stimulation. A study conducted by Streb et al revealed that ATRA treatment regulated the AKAP protein, AKAP12, which shares significant sequence identity to CMY5A (Reynolds et al., 2007; Streb et al., 2011). ROH influx into the cell may also regulate CMY5A in a similar manner to AKAP12, resulting in altered regulation of this protein. It is unknown how phosphorylation regulates CMY5A and what downstream affect it may have.

3.3.3.8 Analysis of increased expression of lamin B1:

Lamin B1 is an intermediate filament protein of the inner nuclear lamina. It is thought to maintain the structure of the nucleus (Vergnes et al., 2004). A proteomic study conducted by Baron et al demonstrated that lamin B1 expression was upregulated in response to RA and some of its metabolites (Baron et al., 2005). Fig 3.12 depicts the expression level of lamin B1 in response to PBS or holo-RBP treatment. 2D analysis predicted a 1.8-fold increase in laminB1. Following secondary validation by Western blotting, no significant change in expression levels of lamin B1 was observed in response to holo-RBP treatment when analysed directly.

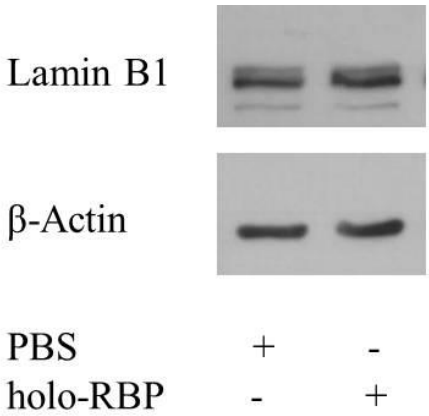

Fig 3.12 Analysis of expression levels of lamin B1.

Representative Western blot depicting expression levels of lamin B1 in response to PBS or 75µg/ml holo-RBP overnight. Serum starved C2C12 cells were treated with PBS or 75µg/ml holo-RBP overnight. Cells were harvested and lysed in RIPA buffer. Protein concentration was assessed using the PIERCE protein assay and 30µg/ml protein was used per sample. Cell lysate was electrophoresed using a 10% SDS-PAGE gel and protein was subsequently transferred to PVDF membrane. Western blotting analysis was conducted using anti-lamin B1 specific antibody and β-Actin as a loading control. All analysis was conducted in triplicate.

3.3.4 Analysis of the effect of RBP on the PP1β signalling pathway:

In skeletal muscle, one of the functions of PP1β is to regulate the rate-limiting enzymes of glycogen metabolism, glycogen synthase and glycogen phosphorylase (Ceulemans and Bollen, 2004). Fig 3.13 depicts the involvement of PP1β in glycogen metabolism. Insulin stimulates the cell to increase intracellular glucose levels via activation of the insulin signalling pathway and subsequent GLUT4 translocation to the cell membrane. As glucose enters the cell it is phosphorylated to glucose-6-phosphate and converted to glycogen as an energy store, by glycogen synthase. Glycogen synthase is only in its active form when it is not phosphorylated. Its phosphorylation is mediated by glycogen synthase kinase 3β (GSK3β). Upon insulin stimulation of the cell, Akt is activated and causes GSK3β inactivation. This removes the inhibitory kinase preventing glycogen synthesis. However, glycogen synthase must be de-phosphorylated. PP1β is the phosphatase responsible for the de-phosphorylation of glycogen synthase and its subsequent activation. Glycogen synthesis occurs in the cell in times of glucose abundance. Therefore, when glycogen synthesis is occurring, glycogen utilisation is not required. Glycogen phosphorylase is the enzyme responsible for glycogenolysis. In its active state, it is phosphorylated. Therefore, it is inactivated by de-phosphorylation and PP1β is the phosphatase responsible for its deactivation (Brady and Saltiel, 2001). Through de-phosphorylation events, PP1β helps to control the homeostasis of glycogen levels in the cell.

Very little is known about how PP1β expression is regulated. PP1β activity is tightly regulated by several targeting subunits which direct the phosphatase to particular cellular compartments. The G_m regulatory subunit is responsible for targeting the phosphatase to glycogen granules (Cohen, 2002). Insulin is thought to regulate PP1β by increasing its concentration in areas of glycogen storage via phosphorylation of the regulatory subunits of PP1β (Saltiel and Kahn, 2001). A 1.2-fold decrease in abundance of the catalytic subunit of PP1β was observed in response to holo-RBP treatment. This could occur via two mechanisms, firstly, by decreased expression of the protein or secondly, by increased degradation of the protein. By whichever mechanism, decreased levels of PP1β may have downstream consequences on glycogen metabolism.

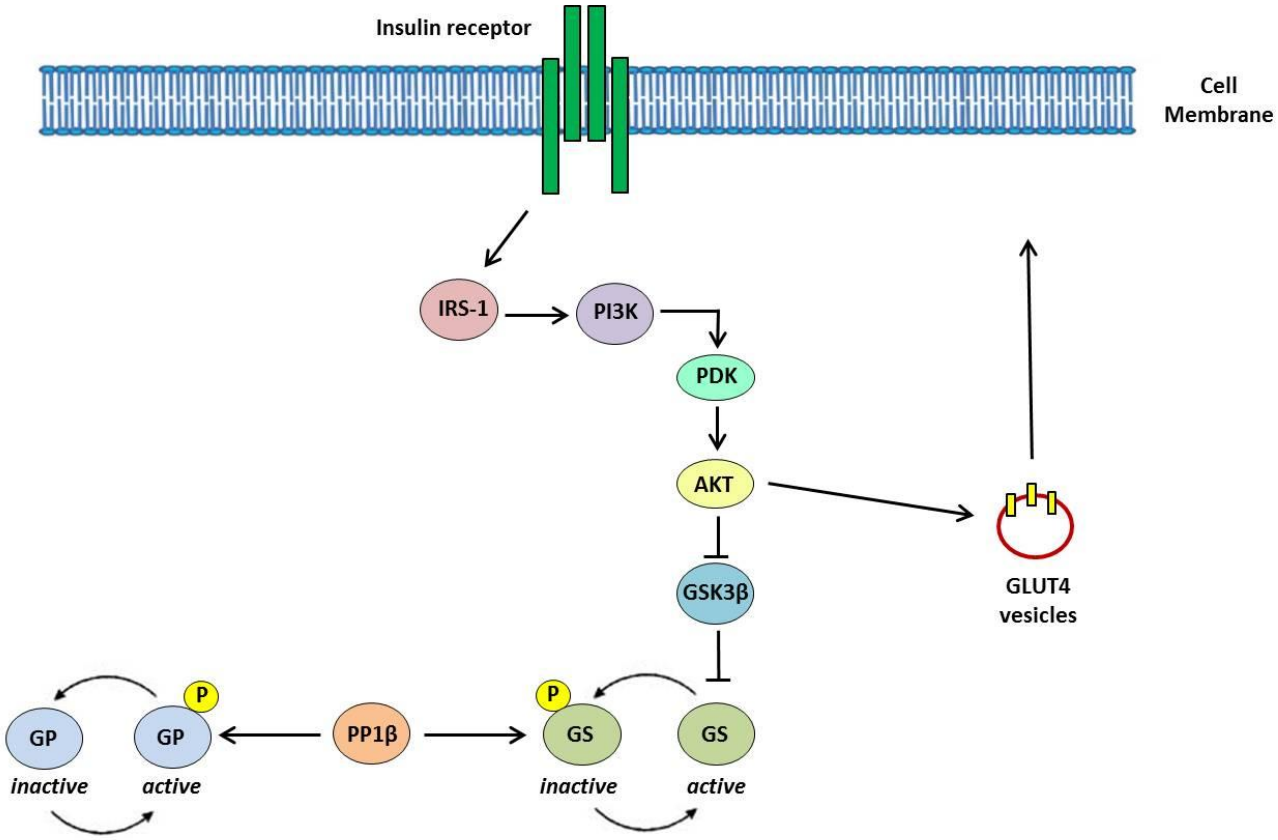

Fig 3.13 Regulation of glycogen metabolism by PP1β.

Diagram depicting the involvement of PP1β in glycogen metabolism. When the insulin receptor is activated by its native ligand, insulin, it prompts the activation of the insulin signalling pathway. Subsequent activation of Akt results in the translocation of GLUT4 vesicles to the cell membrane and glucose transport into the cell. Concomitantly Akt also deactivates GSK3β, preventing GSK3β mediated inhibition of glycogen synthase (GS). When GS is phosphorylated, it is in an inactive state. PP1β is the phosphatase responsible for the de-phosphorylation of GS, resulting in its activation. GS is then free to convert the glucose entering the cell into glycogen stores. When glycogen production is occurring glycogenolysis should not occur. Glycogen phosphorylase (GP) is the enzyme responsible for glycogen utilisation. When GP is phosphorylated it is in an active state, PP1β is the phosphatase responsible for the de-phosphorylation of GP, resulting in its inhibition. Therefore, net glycogen production occurs.

3.3.4.1 The effect of decreased PP1β expression on glycogen synthase and glycogen phosphorylase:

C2C12 muscle cells stimulated with holo-RBP overnight demonstrated decreased PP1β expression. As a result of this event, one would expect a downstream effect on the proteins regulated by PP1β. PP1β regulates the de-phosphorylation of both glycogen synthase and glycogen phosphorylase. Therefore, a net increase in phosphorylation of both of these proteins would be expected. As predicted glycogen synthase phosphorylation levels appear to be increased with holo-RBP treatment overnight (Fig 3.14). As no phospho-specific antibodies were commercially available for glycogen phosphorylase it was necessary to immunoprecipitate the protein first and then assess phosphorylation levels using general phospho amino acid antibodies. Immunoprecipitated protein was analysed by Western blotting. After several failed attempts to purify glycogen phosphorylase from holo-RBP treated cells, total glycogen phosphorylase levels were assessed in whole cell lysate by Western blotting (Fig 3.14). Following holo-RBP treatment overnight, there appears to be a decrease in total glycogen phosphorylase expression.

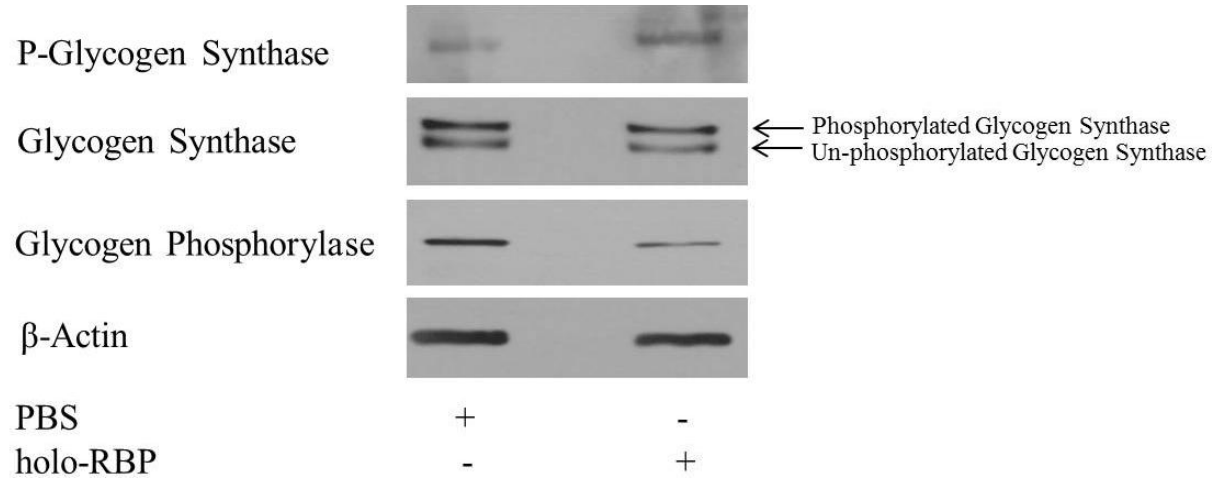

Fig. 3.14 The effect of holo-RBP treatment on glycogen synthase phosphorylation levels and glycogen phosphorylase expression levels.

Serum starved C2C12 cells were incubated with either PBS or 75µg/ml holo-RBP for 16 hours. Cells were collected and lysed in RIPA buffer. Protein concentration was assessed using the PIERCE protein assay and 30µg of each sample was electrophoresed using a 10% acrylamide SDS gel. Protein was transferred to PVDF membrane. Phospho-glycogen synthase, glycogen synthase, glycogen phosphorylase and β-Actin levels were assessed by Western blotting. β-Actin levels were used as a loading control. All experiments were conducted in triplicate. A double band appears when blotting total glycogen synthase. The upper band corresponds to the phosphorylated version of the protein and the lower band corresponds to unphosphorylated protein (Jensen et al., 2006).

3.3.4.2 Time course analysis of PP1β expression, glycogen phosphorylase expression and glycogen synthase phosphorylation:

Overnight treatment of C2C12 cells with holo-RBP resulted in increased phosphorylation of glycogen synthase and decreased expression of glycogen phosphorylase. As a decrease in glycogen phosphorylase expression was unexpected, it was necessary to determine which event was occurring first, decreased PP1β expression or decreased glycogen phosphorylase expression. C2C12 cells were treated with holo-RBP for 0, 6, 8, 10, 12, 14 and 16 hours and protein expression and/or phosphorylation levels assessed by Western blotting (Fig 3.15). PP1β expression appears to decrease after 12 hours incubation with holo-RBP. Glycogen phosphorylase expression levels drop subsequent to PP1β levels, at 14 hours. Interestingly, glycogen synthase phosphorylation increases prior to PP1β downregulation, as early as 8 hours. Maximal phosphorylation appears at 12 hours which correlates with the decrease of the phosphatase, PP1β at 12 hours. However, as phosphorylation increases before a decline in PP1β is evident there may be another contributing factor, such as increased GSK3β activity, leading to this event.

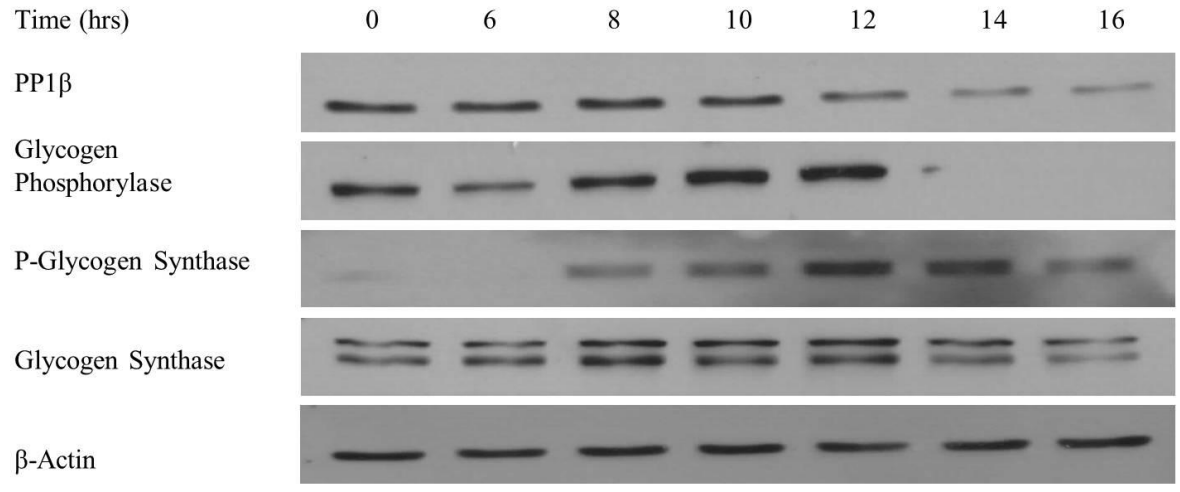

Fig 3.15 Time course analysis of the effect of holo-RBP treatment on PP1β expression, glycogen phosphorylase expression and glycogen synthase phosphorylation levels.

C2C12 muscle cells were treated with 75μg/ml holo-RBP for 0, 6, 8, 10, 12, 14 and 16 hours. Cells were collected at each time point and lysed in RIPA buffer. Protein concentration was assessed using the PIERCE protein assay and 30μg of each sample was electrophoresed using a 10% acrylamide SDS-PAGE gel. Protein was subsequently transferred to PVDF membrane. PP1β, glycogen phosphorylase, phospho-glycogen synthase, glycogen synthase and β-Actin levels were assessed by Western blotting. β-Actin levels were used as a loading control.

3.3.4.3 Assessment of ROH dependence in the PP1β signalling pathway:

Several changes in protein expression and phosphorylation have been observed as a result of holo-RBP stimulation overnight. Alterations in the proteome of the cell could be occurring as a result of ROH influx into the cell or as a result of RBP interaction with a cell surface protein. In order to determine whether RBP alone or ROH alone was responsible for changes in the proteome, C2C12 cells were treated with either 75µg/ml apo-RBP or 3.45µM ROH for 16 hours. Neither apo-RBP nor ROH alone initiated changes in expression of glycogen phosphorylase or PP1β (Fig 3.16). In addition, no change in glycogen synthase phosphorylation was observed with either apo-RBP or ROH treatment alone. Therefore, only holo-RBP treatment elicits a change in the proteins involved in glycogen metabolism of the muscle cell.

Changes in protein expression may still be reliant on ROH, as holo-RBP would allow the influx of ROH into the cell via STRA6. In addition, apo-RBP has been shown to cause ROH efflux out of the cell (Kawaguchi et al., 2012). This could mean that ROH influx is necessary for these changes to occur. The lack of protein changes with apo-RBP treatment suggests that holo-RBP may interact with a cell surface receptor to initiate proteome alterations. Therefore, the receptor may have a lower affinity for the apo version of RBP and that may be why no alterations in protein phosphorylation or expression occurred. ROH alone may still enter the cell as it is a highly hydrophobic molecule. Specific interaction of holo-RBP with STRA6 may be essential to initiate a signalling pathway which results in the alteration in several enzymes involved in glycogen regulation.

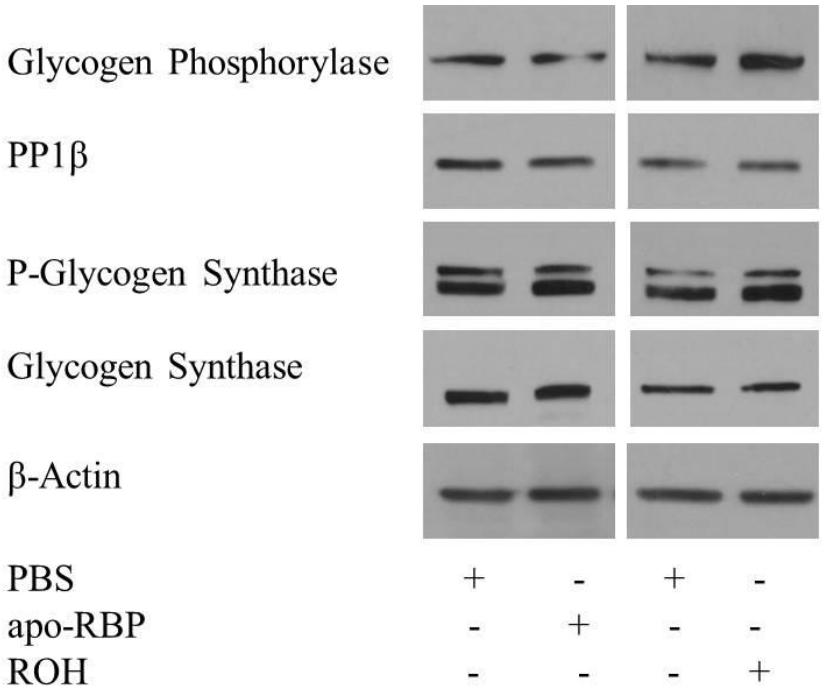

Fig. 3.16 The effect of apo-RBP and ROH treatment on PP1β, glycogen phosphorylase and glycogen synthase.

Serum starved C2C12 cells were incubated with PBS, 75µg/ml apo-RBP or 3.45µM ROH for 16 hours. Cells were collected and lysed in RIPA buffer. Protein concentration was assessed using the PIERCE protein assay and 30µg of each sample was electrophoresed using a 10% acrylamide SDS gel. Protein was subsequently transferred to PVDF membrane. Glycogen phosphorylase, PP1β, phospho-glycogen synthase, glycogen synthase, and β-Actin levels were assessed by Western blotting. β-Actin levels were used as a loading control. All experiments were conducted in triplicate.

3.3.4.4 Assessment of the effect of holo-RBP on STRA6 deficient cells:

The cell surface receptor for RBP is STRA6 (Kawaguchi et al., 2007). It has a higher affinity for the holo version of RBP and binding of holo-RBP to STRA6 results in ROH influx into the cell (Sivaprasadarao and Findlay, 1988b). ROH influx may be a mechanism by which alterations in the glycogen metabolising enzymes occur or it could also occur via some unknown signalling pathway initiated by STRA6. In order to determine the significance of STRA6 in holo-RBP-induced protein changes, cell lines were chosen which are believed not to express STRA6. Norseen et al demonstrated by PCR that primary or cultured macrophages derived from mice or humans do not express STRA6 (Norseen et al., 2012). In addition to macrophages, the liver is thought not to express the receptor (Bouillet et al., 1997). A murine immortalised bone marrow derived macrophage (BMDM) cell line and human hepatic HEPG2 cells were utilised to determine the effect of holo-RBP on STRA6 deficient cells. Firstly, membranes isolated from each cell line were assessed for the presence of STRA6 using a polyclonal antibody raised against the receptor, with C2C12 cells as a positive control (Fig 3.17).

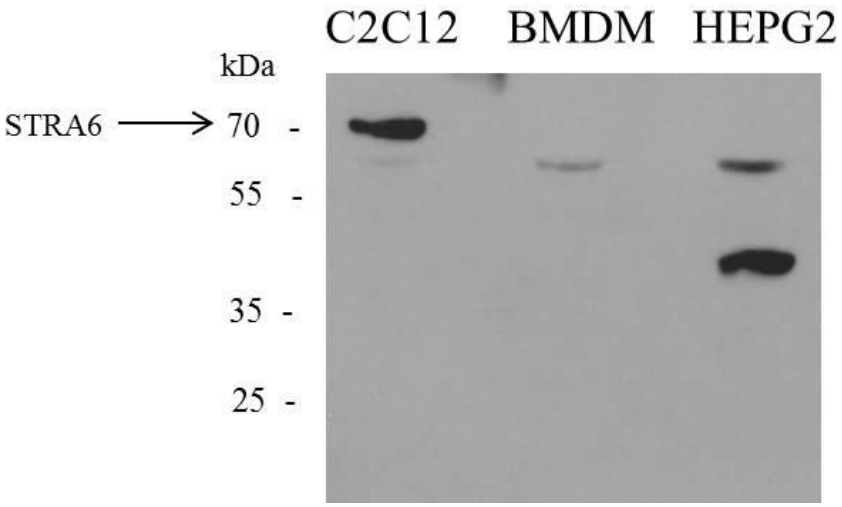

Fig. 3.17 Expression of STRA6 in C2C12, BMDM and HEPG2 cell membranes.

Cell membranes were isolated from C2C12, BMDM and HEPG2 cells. Membranes were resuspended in the presence of 1% Triton X-100 and protein quantity assessed using the PIERCE protein assay. 100µg of each membrane suspension was electrophoresed using a 10% acrylamide SDS gel. Protein was subsequently transferred to PVDF membrane. Total STRA6 expression levels were assessed by Western blotting using a polyclonal STRA6 antibody. STRA6 is a 72kDa molecular weight protein and appears in C2C12 cell membranes.

As demonstrated in Fig 3.17 STRA6 was only present in C2C12 cell membranes. The effect of holo-RBP on PP1β and glycogen phosphorylase expression levels and glycogen synthase phosphorylation levels in STRA6 deficient cell lines was assessed by Western blotting (Fig 3.18). BMDM and HEPG2 cells do not appear to be susceptible to the same changes in protein expression and phosphorylation observed in C2C12 cells. This indicates that STRA6 may be a key mediator in RBP-induced changes in glycogen regulating enzymes. STRA6 may simply be necessary to mediate ROH influx or it may initiate a unique signalling mechanism which terminates in the alteration of glycogen metabolism.

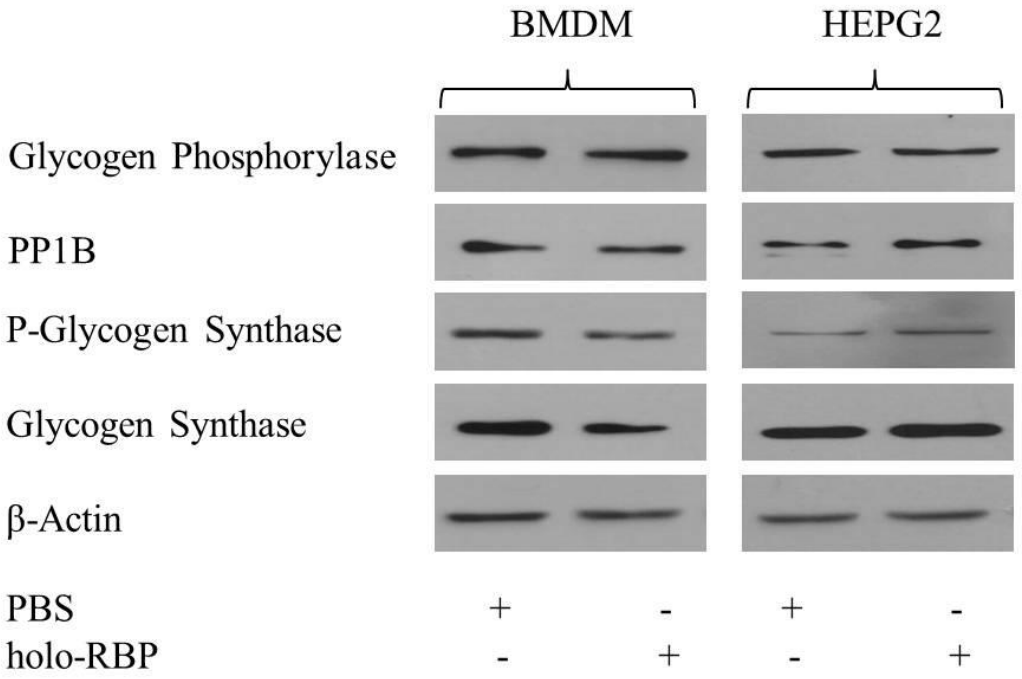

Fig. 3.18 The effect of holo-RBP treatment on PP1β, glycogen phosphorylase and glycogen synthase in STRA6 deficient cells.

Serum starved BMDM and HEPG2 cells were incubated with either PBS or 75μg/ml holo-RBP for 16 hours. Cells were collected and lysed in RIPA buffer. Protein concentration was assessed using the PIERCE protein assay and 30μg of each sample was electrophoresed using a 10% acrylamide SDS gel. Protein was subsequently transferred to PVDF membrane. Glycogen phosphorylase, PP1β, phospho-glycogen synthase, glycogen synthase, and β-Actin levels were assessed by Western blotting. β-Actin levels were used as a loading control. All experiments were conducted in triplicate. Comparative result to Fig. 3.14.

3.3.5 The PP2A trimeric complex:

PP2A is a common cellular phosphatase. It is a trimeric structure composed of a scaffolding A subunit, a regulatory B subunit and a catalytic C subunit (Fig 3.19). The A and C subunits are found bound to each other at all times in the cell. They form the core dimer to which the regulatory, B subunit binds (Lechward et al., 2001). Association of the regulatory B subunit allows the generation of functional holoenzyme and this event confers the specificity of the complete phosphatase complex. There are 4 main classes of B subunit, the B family (also known as B55), of which there are 3 isoforms, the B' family (also known as B56), which has 5 isoforms, the B" family, with 3 isoforms and the striatin family (also known as B"') which has 3 isoforms (Lechward et al., 2001). The B subunits are expressed differentially during development and in specific tissues which adds another dimension to PP2A regulation. The B subunit can often direct the phosphatase to specific compartments of the cell and therefore, dictates the function of the enzyme.

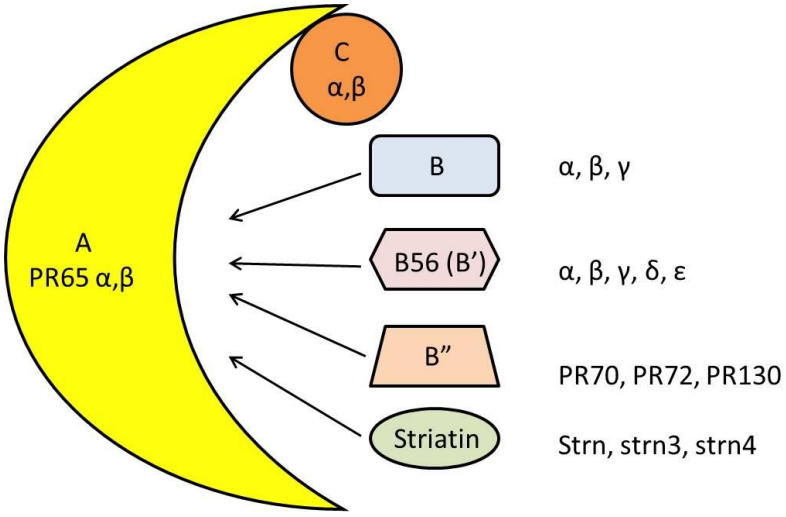

Fig 3.19 The trimeric structure of PP2A

PP2A is composed of three subunits. The A and C subunits exist pre-coupled in the cytosol and exhibit 2 isoforms each. The regulatory B subunit confers specificity of the enzyme and can have several isoforms with distinct functions (Seshacharyulu et al., 2013).

3.3.5.1 Regulation of the PP2A dimer complex by phosphorylation:

In the present study, the scaffolding A subunit of PP2A was observed to have decreased levels of serine phosphorylation in response to holo-RBP treatment. Phosphorylation of this subunit has not been extensively studied. The C subunit is known to be phosphorylated at tyrosine 307 and this leads to decreased binding affinity for the B subunit (Brautigan, 1995). In a study conducted by Guo and Damuni (1993), it was noted that an autophosphorylation-activated protein kinase caused an increase in ^{32}P incorporation into the C subunit of PP2A and this resulted in marked inhibition of the enzyme. Some incorporation of ^{32}P was also observed in the A subunit but at unknown residues, this may also contribute to inhibition of the enzyme but it has never been studied. Phosphorylation of residues in the dimer complex could result in steric hindrance, preventing B subunit association. Serine phosphorylation of the A subunit of PP2A is a novel observation and may also have a similar function to phosphorylation of the C subunit. Thus, a decrease in phosphorylation of this subunit may allow increased association of the B subunit, generating increased levels of functional holoenzyme.

3.3.5.2 Mass spectrometry analysis of the PP2A holoenzyme:

In order to assign a function to the PP2A complex altered with holo-RBP treatment, the A subunit was immunoprecipitated from C2C12 cells using the same antibody used to validate the phosphorylation change. Purified protein was fractionated by SDS-PAGE and visualised using silver staining as described in section 2.7.1 and 2.4.3. All protein bands were excised and trypsin digested as described in sections 2.6.2 and 2.6.3. Digested peptides were identified by MS analysis. Table 3.3 depicts the proteins identified relevant to PP2A complex identification. The only B subunit found to co-immunoprecipitate with the scaffolding A subunit was B56, in particular the δ isoform.

Protein Identified	Accession No.	Score	Peptides Matched	Cov (%)	MW	PI
Serine/threonine-protein phosphatase 2A 65 kDa regulatory subunit A alpha isoform	gi|8394027	222	5	13	65.28	5.00
Protein phosphatase 2A B56 delta subunit	gi|33285883	214	5	14	69.08	7.99

Table 3.3 Components of the PP2A complex identified from PP2A subunit A immunoprecipitation.

Summary of PP2A subunit proteins isolated from C2C12 cells using anti-PP2A subunit A α isoform antibody. All proteins were identified using the NCBI protein database and demonstrated a score >54 indicating significant protein identification.

3.3.6 The B56 delta regulatory subunit of PP2A:

MS analysis revealed that the PP2A subunit A α isoform forms a complex with the B56δ regulatory subunit in C2C12 muscle cells. PP2A with this specific B subunit bound is involved in the wnt signalling pathway. Wnt is responsible for the regulation of β-catenin-induced gene transcription (Fig 3.20). When the receptor for wnt, frizzled, is inactive, β-catenin remains bound to a degradation complex in the cytosol (Kim et al., 2013a). This complex is composed of adenomatosis polyposis coli (APC), axin, casein kinase 1 (CK1) and GSK3β and mediates the phosphorylation of β-catenin. Once phosphorylated, β-catenin is destined for degradation via the proteasome. When wnt stimulates the frizzled receptor, the degradation complex dissociates and β-catenin is free to translocate to the nucleus and initiate gene transcription (Kim et al., 2013a).

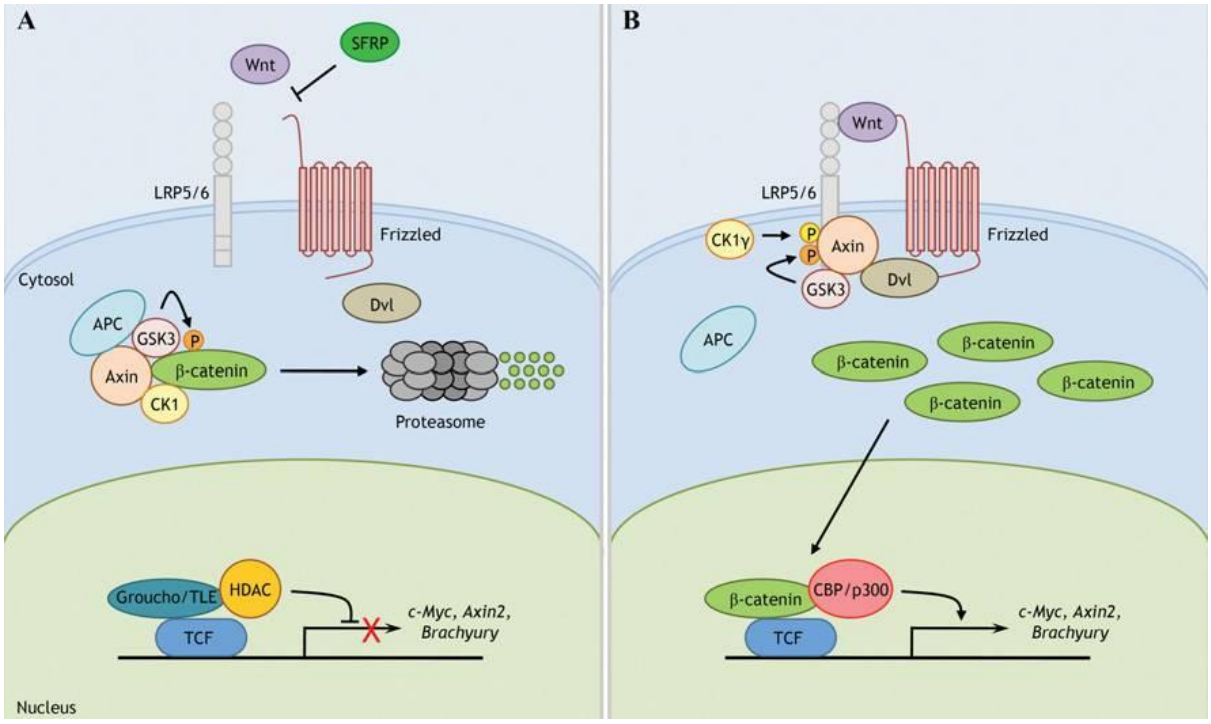

Fig 3.20 The Wnt/β-Catenin signalling pathway.

A. In the absence of wnt, β-Catenin is sequestered in the cytosol by a degradation complex composed of APC, Axin, GSK3β and CK1. This complex mediates the phosphorylation of β-Catenin and targets it for proteasomal degradation. Therefore, β-Catenin controlled transcription does not occur. **B**. Upon wnt binding at the cell surface the β-Catenin degradation complex dissociates. β-Catenin then translocates to the nucleus and initiates transcription of target genes (Kim et al., 2013a).

In 1999, Seeling et al demonstrated that the B56 regulatory subunits of PP2A are negative regulators of the wnt signalling pathway (Seeling et al., 1999). All of the isoforms of the B56 subunit were found to positively regulate the degradation complex, thus increasing β-catenin degradation. The addition of the PP2A inhibitor, okadaic acid, resulted in increased levels of β-catenin. In addition, co-expression of GSK3β and B56 resulted in increased degradation of β-catenin. These results suggest that the degradation complex is positively regulated by PP2A-B56. B56δ has been shown to interact with several proteins in the degradation complex, in particular APC and GSK3β (Liu and Eisenman, 2012; Seeling et al., 1999).

B56δ is known to positively regulate GSK3β (Liu and Eisenman, 2012). GSK3β is also a component of the insulin signalling pathway and is responsible for the inhibition of glycogen synthase as discussed in section 4.3.4. GSK3β is regulated by several enzymes some of which include Akt and PKA. These kinases phosphorylate GSK3β at serine 9, resulting in its inhibition. Phosphorylation at this residue results in the generation of a pseudosubstrate which blocks the catalytic domain of the enzyme. When the insulin signalling pathway is activated, Akt phosphorylates GSK3β on serine 9, leading to its inactivation and subsequent downstream activation of glycogen synthase. The PP2A, B56δ complex is the phosphatase responsible for de-phosphorylating GSK3β at serine 9 and thus rendering it more active (Liu and Eisenman, 2012). As a result of holo-RBP treatment an increase in glycogen synthase phosphorylation was observed before the onset of PP1β downregulation, this could be an indicator that GSK3β was more active. Increased PP2A activity may provide the link between holo-RBP treatment and increased glycogen synthase phosphorylation (Fig 3.21).

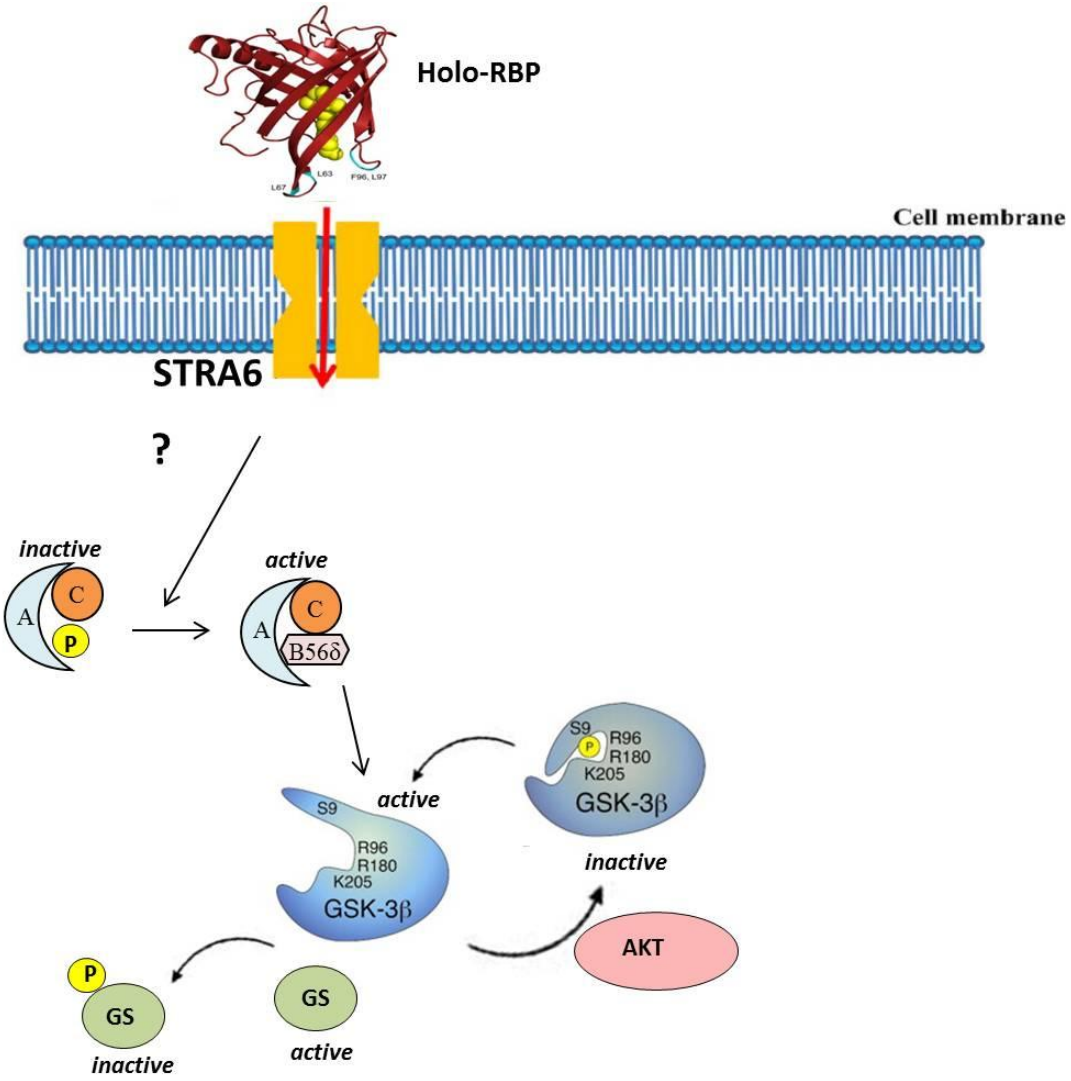

Fig 3.21 Proposed pathway involving PP2A activation and increased glycogen synthase phosphorylation.

Diagram depicting the potential involvement of PP2A in the activation of GSK3β and subsequent glycogen synthase inhibition. Activation of STRA6 by holo-RBP stimulation appears to cause a decrease in PP2A phosphorylation, via an as yet unknown mechanism. This may lead to an increase in association of the B56δ subunit, forming active holo-enzyme. Akt deactivates GSK3β by phosphorylation at serine 9, preventing GSK3β mediated inhibition of glycogen synthase (GS). PP2A is known to dephosphorylate GSK3β at serine 9. Thus, increased PP2A activity could cause elevated levels of active GSK3β. Increased GSK3β activity would cause increased phosphorylation of GS and inhibition of this important enzyme.

3.3.6.1 Assessment of B56δ expression in response to holo-RBP treatment:

Interestingly, RA has been shown to cause an increase in B56δ expression (McCright et al., 1996). Differentiation of a neuroblastoma cell line, IMR-32, into neurone like cells with RA led to an increase in mRNA levels of all isoforms of B56 but in particular B56β and B56δ. In addition, Park et al found that PP2A may also mediate the effects of ATRA on nitric oxide (NO) production (Park et al., 2013). Decreased NO levels are observed following ATRA treatment via inhibition of endothelial nitric oxide synthase (eNOS). When eNOS is phosphorylated at serine 1179 it is active. PP2A is a known phosphatase of eNOS and de-phosphorylation leads to its inactivation. ATRA treatment resulted in increased PP2A activity and decreased eNOS serine 1179 phosphorylation. This effect was mediated through increased expression of B56α. B56δ expression was unaltered in this study.

Induction of B56δ expression could be a means by which holo-RBP is eliciting an effect on glycogen synthase phosphorylation levels. B56δ expression was analysed in C2C12 cells treated with holo-RBP for 0, 6, 8, 10, 10, 12, 14 and 16 hours (Fig 3.22). As demonstrated in Fig 3.22 no increase in B56δ expression was observed with holo-RBP treatment, in fact a marked decrease in total expression levels was observed from 10 hours onwards. In order to determine if B56δ expression was increased at an earlier time point, a second time course analysis was conducted. B56δ expression was assessed in C2C12 cells treated with holo-RBP for 0, 1, 2, 3 and 4 hours (Fig 3.23). No effect on B56δ abundance was observed with holo-RBP treatment for shorter time intervals. It appears that holo-RBP treatment does not result in elevated expression levels of the B56δ subunit of PP2A. However, a decrease in PP2A A subunit phosphorylation was observed and as discussed in section 3.3.5.1, this could still indicate that the complex was more active.

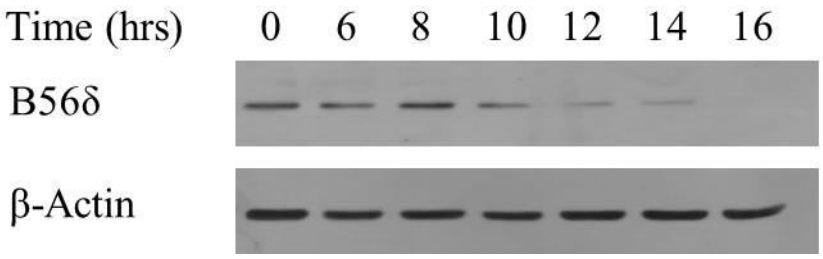

Fig 3.22 Time course analysis of the effect of holo-RBP treatment on B56δ expression.

C2C12 muscle cells were treated with 75µg/ml holo-RBP for 0, 6, 8, 10, 12, 14 and 16 hours. Cells were collected at each time point and lysed in RIPA buffer. Protein concentration was assessed using the PIERCE protein assay and 30µg of each sample was electrophoresed using a 10% acrylamide SDS-PAGE gel. Protein was subsequently transferred to PVDF membrane. B56δ and β-Actin levels were assessed by Western blotting. β-Actin levels were used as a loading control.

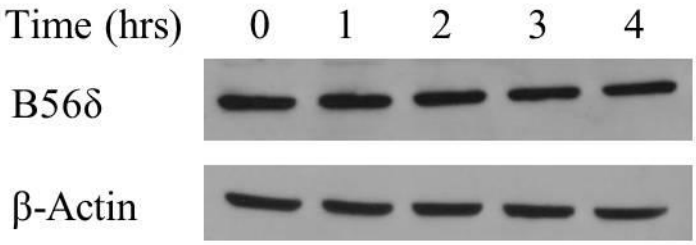

Fig 3.23 Time course analysis of the effect of holo-RBP treatment on B56δ expression using early time points.

C2C12 muscle cells were treated with 75µg/ml holo-RBP for 0, 1, 2, 3 and 4 hours. Cells were collected at each time point and lysed in RIPA buffer. Protein concentration was assessed using the PIERCE protein assay and 30µg of each sample was electrophoresed using a 10% acrylamide SDS-PAGE gel. Protein was subsequently transferred to PVDF membrane. B56δ and β-Actin levels were assessed by Western blotting. β-Actin levels were used as a loading control.

3.3.6.2 Analysis of GSK3β phosphorylation in response to holo-RBP treatment:

If the PP2A holoenzyme was more active, one would expect to see a decrease in phosphorylation of GSK3β at serine 9. Therefore, the level of GSK3β serine 9 phosphorylation was assessed to determine if this enzyme was activated in response to holo-RBP treatment.

GSK3β serine 9 phosphorylation was assessed in C2C12 cells treated with holo-RBP for 0, 6, 8, 10, 10, 12, 14 and 16 hours (Fig 3.23). Serine 9 phosphorylation levels appear to drop slightly at 6 hours which could be an indication that PP2A is more active. Following 6 hours treatment, phosphorylation levels appear to remain constant. As observed in section 3.3.4.2 glycogen synthase phosphorylation was maximal at 12 hours so this may not be associated with increased GSK3β activity.

In order to determine if GSK3β phosphorylation was decreased at an earlier time point, a second time course analysis was conducted. GSK3β phosphorylation was analysed in C2C12 cells treated with holo-RBP for 0, 1, 2, 3 and 4 hours (Fig 3.24). No decrease in phosphorylation levels was observed, which is indicative that GSK3β may not be more active.

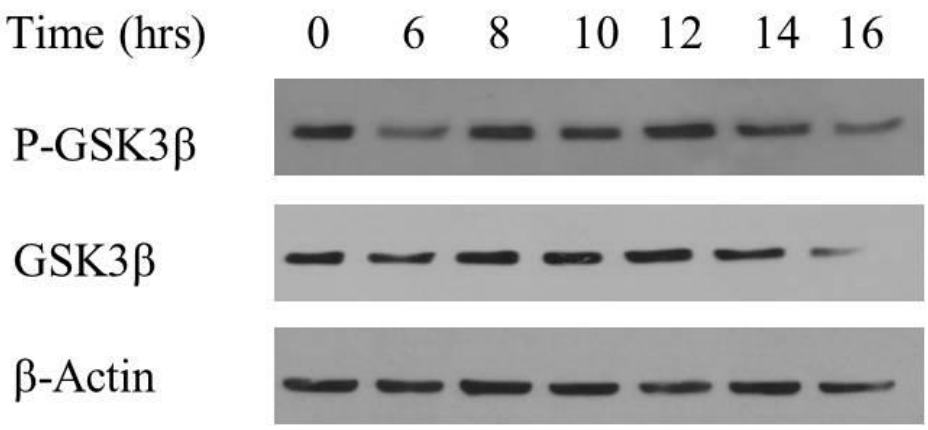

Fig 3.24 Time course analysis of the effect of holo-RBP treatment on GSK3β serine 9 phosphorylation levels.

C2C12 muscle cells were treated with 75µg/ml holo-RBP for 0, 6, 8, 10, 12, 14 and 16 hours. Cells were collected at each time point and lysed in RIPA buffer. Protein concentration was assessed using the PIERCE protein assay and 30µg of each sample was electrophoresed using a 10% acrylamide SDS-PAGE gel. Protein was subsequently transferred to PVDF membrane. GSK3β serine 9 phosphorylation levels, GSK3β total expression and β-Actin expression were assessed by Western blotting. β-Actin levels were used as a loading control.

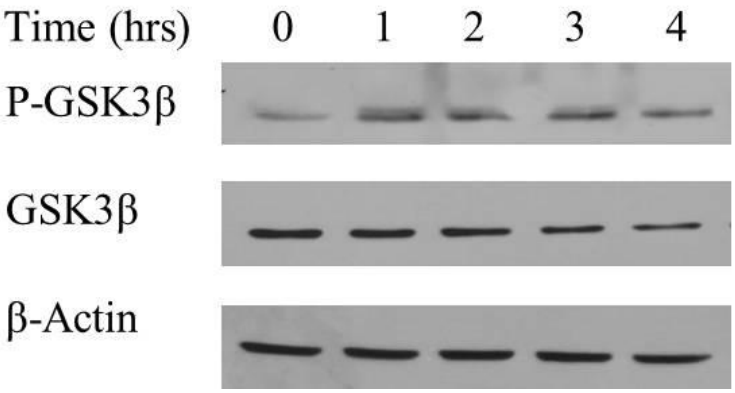

Fig 3.25 Time course analysis of the effect of holo-RBP treatment on GSK3β serine 9 phosphorylation using early time points.

C2C12 muscle cells were treated with 75µg/ml holo-RBP for 0, 1, 2, 3 and 4 hours. Cells were collected at each time point and lysed in RIPA buffer. Protein concentration was assessed using the PIERCE protein assay and 30µg of each sample was electrophoresed using a 10% acrylamide SDS-PAGE gel. Protein was subsequently transferred to PVDF membrane. GSK3β serine 9 phosphorylation levels, GSK3β total expression and β-Actin expression were assessed by Western blotting. β-Actin levels were used as a loading control.

3.4 Summary of proteomic analysis of holo-RBP stimulated C2C12 muscle cells:

Several proteins in the mouse muscle cell line, C2C12, appeared altered in response to holo-RBP treatment overnight. Some of the alterations in the proteome may occur as a result of increased ROH influx into the cell. LAT-2, OAT, PDIA3 and CMYA5 may be altered as a result of elevated metabolites produced from ROH.

LAT-2 abundance is known to decrease as a result of increased metabolism initiated by RA (Yoon et al., 1999). OAT was observed to be elevated in intestinal epithelial cells in response to RA treatment (Dekaney et al., 2008). The opposite expression profile was observed in C2C12 muscle cells, this may be due to a cell type specific effect of RA on OAT transcription (Shull et al., 1995). PDIA3 expression seems to be elevated in times of cellular stress (Dukes et al., 2008; Lee, 1987; Mazzarella et al., 1994). Influx of ROH into the cell may lead to some cellular stress and this may be the cause of increased PDIA3 expression. CMYA5 shares significant sequence similarity to AKAP12 and is a known regulator of protein kinase A (Reynolds et al., 2007). AKAP12, was demonstrated to be regulated by ATRA treatment and has a RARE sequence in the promoter region of its gene (Streb et al., 2011). Clearly retinoids play a role in regulating AKAP12 and CMYA5 could be controlled in a similar manner. No alteration in expression level was observed with 2D analysis. However, altered phosphorylation of CMYA5 may still occur in a retinoid dependent manner by some unknown mechanism.

Alterations in the structural proteins vimentin and lamin B1 were not validated by secondary methods. This discrepancy may be as a result of variances in the 2D electrophoresis and Western blotting techniques utilised in this study. Increased abundance of vimentin and lamin B1 was observed in the membrane fraction of muscle cells when analysed by 2D electrophoresis, but this may not be as a result of increased translation of protein. Western blotting was conducted on whole cell lysate. This was necessary to determine if holo-RBP treatment led to induced expression of these proteins. Holo-RBP may have no direct effect on expression levels but it may alter the subcellular distribution of the proteins, which requires further study.

A number of proteins involved in glycogen regulation were affected by holo-RBP treatment. Decreased expression of PP1β occurs after 12 hours holo-RBP treatment. This may occur as a result of decreased transcription of the gene or as a result of increased degradation. Decreased levels of the phosphatase PP1β would be expected to have a downstream effect on the enzymes glycogen synthase and glycogen phosphorylase. As expected glycogen synthase phosphorylation was elevated in response to holo-RBP but this event may slightly precede PP1β downregulation. Maximal glycogen synthase phosphorylation levels occurred at 12 hours which is the time point of the apparent onset of PP1β downregulation. Therefore, PP1β decline may be the underlying causative agent for increased glycogen synthase phosphorylation, but there may be other contributing factors.

Unexpectedly, glycogen phosphorylase expression declined following PP1β downregulation. As described previously, an increase in glycogen synthase phosphorylation was also observed. As glycogen synthase is rendered less active by phosphorylation one would expect the net production of glycogen to decline. Glycogen synthase diminished activity appears to precede a reduction in glycogen phosphorylase expression. Decreased levels of glycogen in the cell may have an inhibitory action on glycogen phosphorylase expression (Wang et al., 2013). Knockout studies of the glycolytic enzyme glucokinase, revealed decreased levels of glycogen in the liver. Following long-term glycogen depletion, glycogen phosphorylase mRNA levels declined (Wang et al., 2013). Conversely, elevated levels of glycogen can cause upregulation of glycogen phosphorylase. Transgenic mice overexpressing glycogen synthase in skeletal muscle, displayed elevated levels of glycogen stores (Manchester et al., 1996). Concomitantly upregulation of glycogen phosphorylase in skeletal muscle was observed. Assessment of glycogen levels in the cell in response to holo-RBP stimulation is necessary to determine if this could be an explanation for reduced glycogen phosphorylase expression.

Interestingly, when the observed changes in glycogen regulating enzymes were assessed in cells treated with apo-RBP or ROH alone, no alteration in phosphorylation or expression levels occurred. This is indicative that holo-RBP is the active molecule, but at least some of the changes may be dependent on ROH influx into the cell, as this would be increased with holo-RBP treatment compared

to ROH alone. It also indicates that a cell surface receptor may be necessary for the proteomic changes to occur. STRA6 has a higher affinity for holo-RBP compared to apo-RBP, which may explain why apo-RBP did not elicit the same changes as the retinol bound version. Cell lines that are not believed to express STRA6 were stimulated with holo-RBP and expression of PP1β and glycogen phosphorylase was analysed along with glycogen synthase phosphorylation levels. No alteration in this cohort of proteins was observed in STRA6 deficient cell lines. One can conclude from this analysis that interaction of holo-RBP with STRA6 is necessary for the inhibition of several proteins involved in glycogen regulation via a mechanism that requires further elucidation.

RBP treatment resulted in decreased serine phosphorylation of the A subunit of PP2A. A decrease in phosphorylation of this subunit of the phosphatase results in increased activity of the enzyme (Guo and Damuni, 1993). It is unknown how RBP may be causing a decrease in PP2A phosphorylation as the kinase or phosphatase involved has not been characterised. In order to determine the function of PP2A in the muscle cell, the holoenzyme was immunoprecipitated and the regulatory B subunit identified. The B56δ subunit was found to associate with the A subunit of PP2A. PP2A in complex with B56δ is known to regulate GSK3β (Seeling et al., 1999) and could be the link between holo-RBP treatment and altered glycogen synthase phosphorylation levels. The expression of the B56 subunit family is known to be regulated by RA (McCright et al., 1996). B56δ expression levels were assessed in response to holo-RBP treatment. However, no significant increase in expression was identified. In fact, a definite decline in expression was observed, which was unexpected and needs further investigation.

A study conducted by Liu and Eisenman (2012) demonstrated that a negative feedback loop exists in B56 expression. Prolonged c-Myc activity resulted in a marked decrease in B56δ expression. Interestingly, increased GSK3β activity results in the phosphorylation and subsequent degradation of c-Myc. Therefore, there exists a negative feedback mechanism whereby excess active c-Myc can stimulate its own degradation via the proteasome (Fig 3.25). Increased c-Myc activity causes the up-regulation of B56δ, this leads to increased activation of GSK3β and ultimately increased c-Myc proteosomal degradation. Therefore, with prolonged activation of PP2A-B56δ as a result of decreased

phosphorylation levels, GSK3β activity may be increased. This would in theory result in c-Myc degradation and could account for the decrease in B56δ expression observed in this study. Identification of reduced B56δ expression as a result of holo-RBP stimulation could itself be an indication that the PP2A holoenzyme is more active.

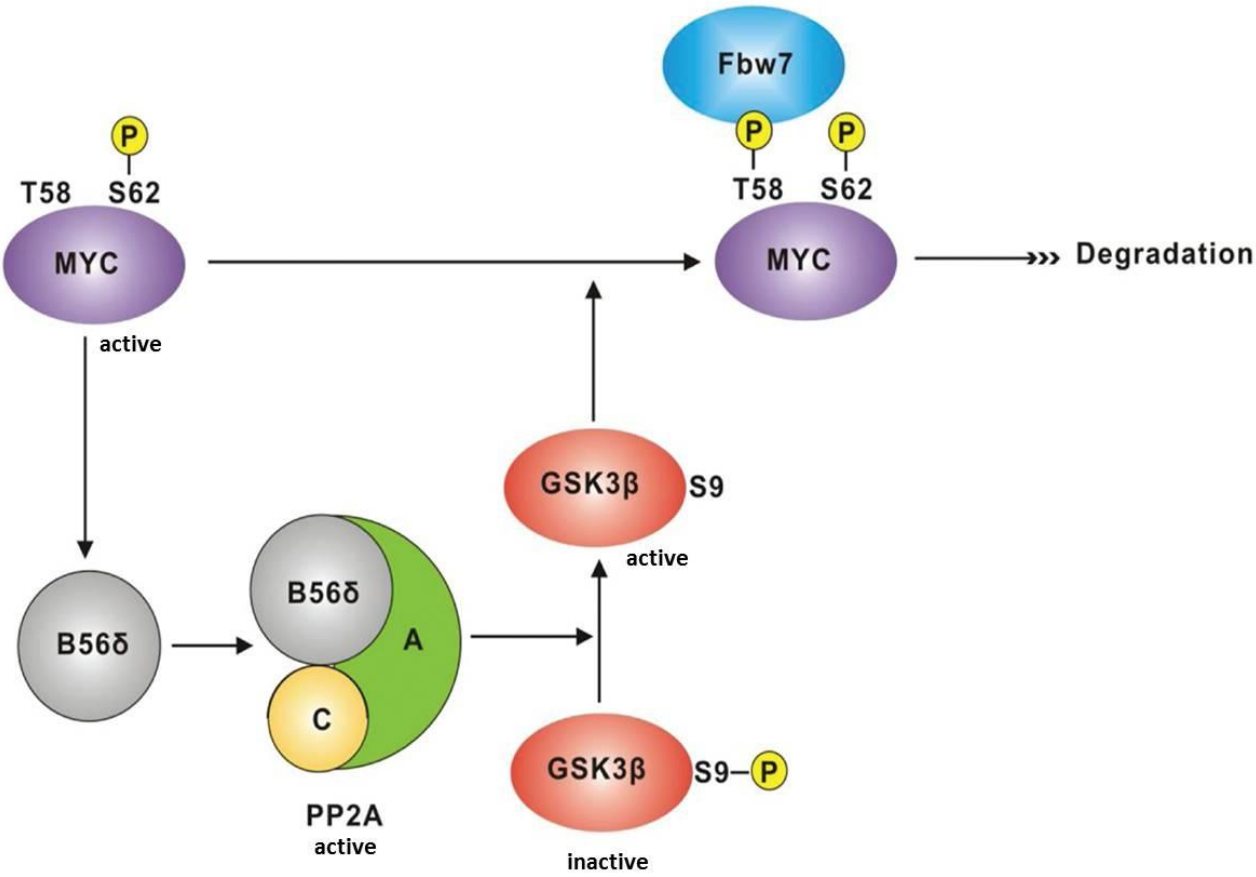

Fig 3.26 Model of the negative feedback mechanism involved in the regulation of c-Myc abundance.

C-Myc controls its own abundance via a negative feedback loop involving B56δ expression and GSK3β activity. When c-Myc is activated it causes increased expression of B56δ. This allows association of this subunit with the PP2A phosphatase complex, resulting in active holoenzyme. PP2A can then mediate the activation of GSK3β by removing the inhibitory phosphorylation at serine 9. Active GSK3β then phosphorylates c-Myc which ultimately results in its degradation by the proteasome. Image taken from (Liu and Eisenman, 2012).

Although no elevation of B56δ expression was observed with holo-RBP treatment, a decrease in phosphorylation of the PP2A enzyme may still have an impact on the holoenzyme's activity. PP2A in complex with B56δ is a known regulatory phosphatase for GSK3β, specifically by the removal of phosphate from serine 9. Therefore, GSK3β serine 9 phosphorylation levels were assessed. A slight decrease in phosphorylation was observed at 6 hours which may be indicative of increased activity which correlates with the onset of glycogen synthase phosphorylation prior to PP1β downregulation.

A combination of events may have a dramatic effect on the glycogen metabolic pathway of muscle cells. This effect occurs as a result of STRA6 and holo-RBP interaction, solely through ROH influx via STRA6 together with some unknown signalling pathway. Therefore, further study is required to determine how holo-RBP causes some of the alterations in the proteome observed in this study.

Chapter 4

Proteomic profiling of a muscle cell line treated with a novel therapeutic for Type II Diabetes

4.1 Introduction:

In 2005, Yang and colleagues demonstrated that increased serum RBP levels can contribute to insulin resistance (Yang et al., 2005). Pharmacological methods aimed at reducing circulating RBP levels were shown to improve insulin sensitivity (Yang et al., 2005). Fenretinide, a synthetic retinoid, was found to improve glucose and insulin tolerance in obese, insulin resistant mice. Fenretinide actively reduces circulating RBP levels by inhibiting the interaction of RBP and TTR, thus enabling RBP to be filtered by the kidneys and excreted. As it has already been FDA approved for use as an anti-cancer therapeutic, it quickly entered clinical trials and is currently in a randomized trial, due to finish in 2015, to assess the effect of fenretinide administration to obese subjects (Preitner et al., 2009). In order to pre-empt extended exposure to the drug, Preitner et al conducted a long term study on high fat diet (HFD) fed mice which resulted in a marked decrease in fat mass accumulation in a preventative and intervention regime (Preitner et al., 2009). In both cases, insulin resistance was improved significantly with fenretinide treatment. Preitner et al also administered the drug to RBP knockout mice maintained on a HFD. Interestingly, fenretinide also prevented diet induced adiposity in these mice suggesting that this effect was independent of lowered levels of RBP. This correlates with the observation that RBP knockout control mice in this study showed no change in adiposity.

Mcilroy et al showed that direct treatment of 3T3-L1 adipocytes with fenretinide resulted in the prevention of differentiation to mature adipocytes (Mcilroy et al., 2013). In addition, fenretinide prevented lipid accumulation in previously matured adipocytes. Direct RA treatment can also prevent maturation of adipocytes (Kamei et al., 1994). Several RA responsive genes were found to be upregulated, notably CRBP1, RARβ and CYP26A1 by fenretinide, suggesting that fenretinide acts in a similar manner to RA in prevention of adipocyte differentiation.

4.1.1 Novel small molecules for the treatment of insulin resistance:

As discussed in chapter 3, the exact molecular mechanism for RBP-induced insulin resistance is still under debate. It may be due to an effect on macrophages located in close proximity to adipocytes in visceral fat, or to activation of the JAK/STAT pathway in muscle cells, or to disruptions in glycogen homeostasis. Regardless of the mechanism of action, a strategy aimed at reducing serum RBP levels may be a direct method to prevent RBP-induced insulin resistance. A number of compounds have been developed as retinoid alternatives in the hope of mimicking the inhibitory effect of fenretinide (Campos-Sandoval et al., 2011). Several of these compounds were shown to bind to RBP, inhibit RBP-TTR interaction and interrupt RBP-STRA6 interaction.

4.1.2 *In vivo* study of novel compounds developed to interrupt RBP-TTR complex formation:

Following on from the study conducted by Campos-Sandoval and colleagues, an in-silico screening study was conducted by Dr. Gemma Kinsella (this laboratory) using compounds in commercial databases. Compounds which bound to RBP and inhibited the RBP-TTR and RBP-STRA6 interactions were used in animal trials to assess efficacy in both the prevention of insulin resistance and the rescue of insulin resistance in obese mice. Compounds that performed well in these trials were subsequently subjected to structure-activity relationship (SAR) analysis. One of these derivatives, RTC-1, resulted in dramatic improvement in glucose and insulin tolerance tests (Fig 4.1). In a 32 week intervention study mice were fed a HFD for 16 weeks and a subset of mice was subsequently treated with RTC-1 and HFD for a further 16 weeks. Glucose tolerance and insulin tolerance were then assessed compared to mice fed a normal chow diet and mice maintained on a HFD. Mice treated with RTC-1 demonstrated dramatically improved glucose clearance from the serum and improved responsiveness to insulin treatment. Results obtained for mice treated with RTC-1 were comparable to controls fed a normal chow diet. In addition, it was observed that RTC-1 elicited much reduced fat mass accumulation compared to HFD fed mice alone.

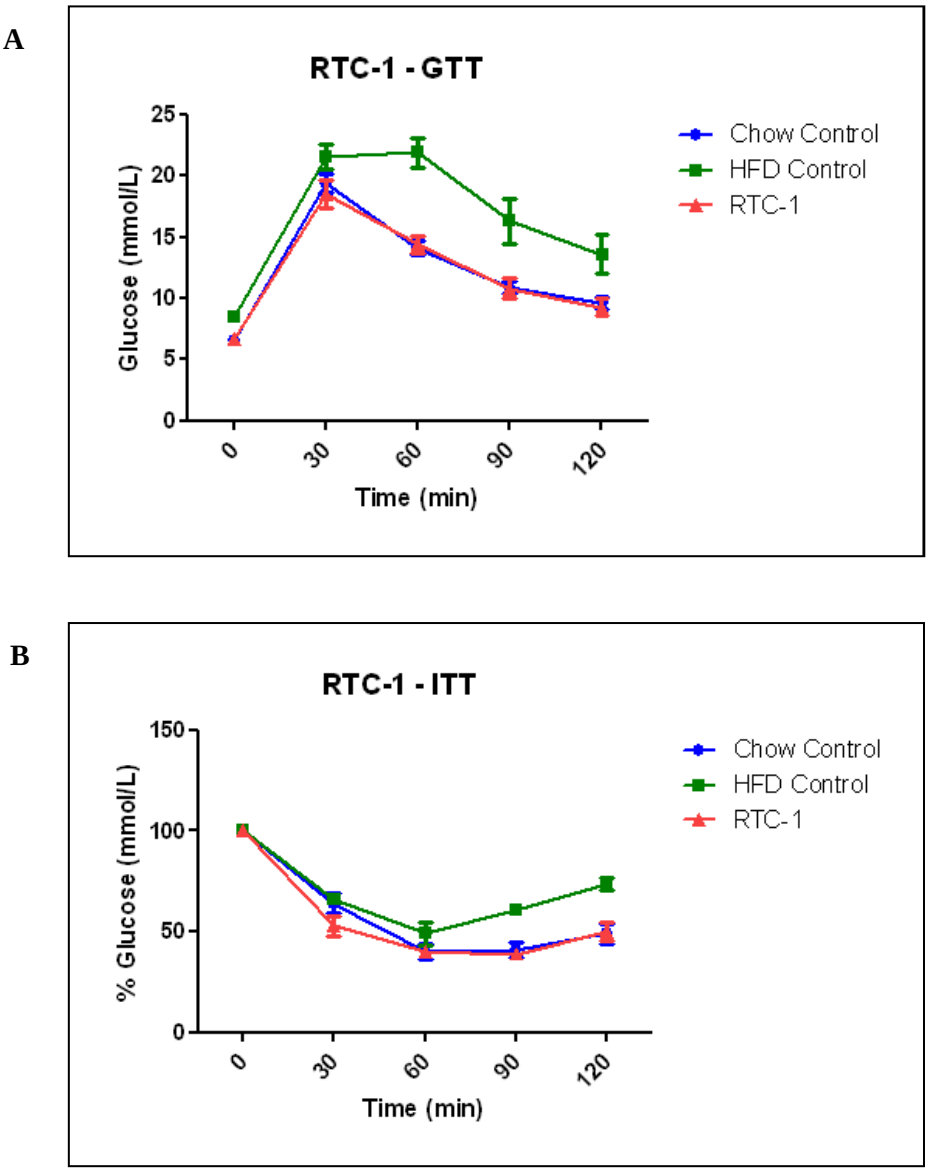

Fig 4.1. The effect of RTC-1 on glucose and insulin tolerance in high fat diet fed mice.

Mice fed a high fat diet (HFD) for 16 weeks were subsequently treated with RTC-1 for a further 16 weeks and assessed for glucose tolerance and insulin tolerance. **A**. Mice fed either normal chow, HFD, HFD with RTC-1 were injected with a bolus of glucose, serum glucose clearance was subsequently monitored for 2 hours. **B**. Mice fed either normal chow, HFD, HFD with RTC-1 were injected with a bolus of insulin and serum glucose levels monitored for 2 hours. Images kindly provided by Dr. Darren Martin.

4.1.3 Independent action of retinoid derivatives on glucose uptake:

Due to the dramatic effect of the compounds on insulin resistance and the reduction of fat mass accumulation in whole animal studies, it was thought that there may be an additional mechanism of action of the drugs. Thus, the compounds were directly tested in a glucose uptake assay using differentiated C2C12 mouse myotubes. RTC-1 out-performed insulin in inducing glucose uptake (unpublished results, Dr. Darren Martin). A derivative of RTC-1, RTC-15, was even more superior to RTC-1 in this respect (Fig 4.2). The effect of the compounds is independent of inhibition of the RBP-TTR complex, as this would not have a physiological effect in a cell culture assay.

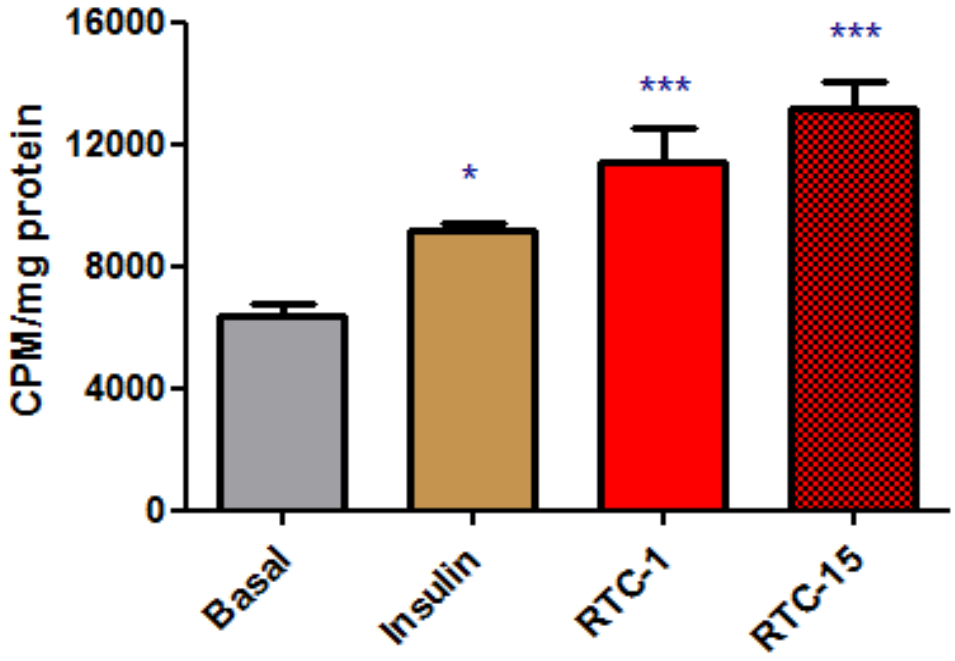

Fig 4.2. The effect of insulin, RTC-1 and RTC-15 on glucose uptake in C2C12 cells.

Differentiated C2C12 mouse muscle cells were treated with 10µM RTC-1 and 10µM RTC-15 overnight. Control cells were untreated or treated with insulin alone. Glucose uptake was then assessed by measuring levels of intracellular [^{3}H] deoxyglucose. All treatments showed a significant increase in glucose uptake. RTC-1 and RTC-15 both induced glucose uptake in the absence of insulin. Image kindly provided by Dr. Darren Martin.

4.1.4 Proteomics as a tool to decipher molecular mechanism of action:

Proteomics has been used to help decipher the exact molecular mechanisms of diseases and therapies. To decipher a potentially novel mechanism of action, for the compounds discussed above, a 2D electrophoresis experiment was devised to assess changes in the proteome in response to direct drug treatment.

4.1.5 Direct assessment of the mechanism of action of RTC-15:

As the mice fed a HFD with RTC-1 had reduced fat mass compared to HFD fed mice, it was postulated that the mice may be more metabolically active. One common cause of increased metabolic activity is un-coupling of the electron transport chain (ETC) of the mitochondrial membrane. In a separate study conducted in the laboratory, Dr. Conor Breen assessed the effect of the RTC-1 derivatives on complex 1 function in isolated mitochondria. Complex I is involved in the first step of the ETC and the production of NAD from NADH to generate a proton gradient. Dr. Breen observed that the compounds directly inhibited complex I activity, resulting in a decrease in oxygen consumption by mitochondria.

In a separate study conducted by Siobhan Leonard in conjunction with the proposed proteomic study, the AMP-activated protein kinase (AMPK) pathway was investigated as a potential mechanism of action of the compounds. AMPK acts as an energy sensor in the cell. When ATP levels are low, or AMP levels high, the AMP to ATP ratio increases and more AMP binds to AMPK. This stimulates phosphorylation of AMPK activating the kinase and ultimately resulting in translocation of the glucose transporter, GLUT4, to the cell membrane (Carling, 2007). RTC-15 was demonstrated to cause an increase in AMPK phosphorylation. Inhibition of complex I would result in increased cellular levels of AMP due to increased activity of adenylate kinase which catalyses the conversion of 2 ADP molecules to AMP plus ATP. Thus, AMPK is activated causing GLUT4 translocation to the cell membrane in an insulin-independent mechanism. This could be the mechanism by which RTC-15 is having a direct effect on glucose uptake in a cell culture system.

Aims and Objectives:

As a result of these observations on the action of RTC-1 and RTC-15, the following proteomic study was devised to identify the global effect of this set of compounds. As RTC-15 appeared to be the most active of the compounds in the cell culture glucose uptake assay, it was selected as the lead compound for the study. Overnight stimulation with the compound was chosen to represent long-term exposure to the drug to determine what were the most prominent proteins affected. In addition, it would ascertain if the drug was having a potential detrimental effect on cell homeostasis.

2D-electrophoresis was utilised in conjunction with mass spectrometry, as a method to identify changes in the proteome of cells treated with RTC-15. A number of protein changes were identified and subjected to secondary validation.

4.2 Method:

The mouse muscle cell line, C2C12, was cultured and differentiated into myotubes as described in section 2.1.2. Cells were treated with 10μM RTC-15 for 16 hours, with DMSO used as an appropriate control. Cells were harvested and the whole cell lysate was used for proteomic analysis (section 2.3.2 through to 2.3.7). 2D gels were first visualised using the phospho-protein stain Pro-Q Diamond to ascertain if the drug was having an effect on the phospho-proteome of the cell (section 2.4.1). Gels were subsequently visualised for whole protein levels using the sypro ruby fluorescent stain (section 2.4.2). Changes in the proteome of the cells were identified using the Progenesis SameSpots software. Only proteins showing a greater than 1 fold change with a statistical significance of <0.05 were chosen for identification by mass spectrometry (MS). A 2D gel was then selected as a reference gel and stained using silver stain (section 2.4.3). Protein spots showing alterations in expression level or phosphorylation were picked from the gel and proteins digested and extracted. MS analysis was subsequently conducted on digested protein spots (section 2.6). Once proteins were identified by peptide matching software a number of the most interesting proteins were selected for secondary validation using SDS-PAGE and Western blotting.

4.3 Results:

Several proteins were identified showing changes in either phosphorylation or expression levels in response to overnight treatment with 10μM RTC-15. Fig 4.3 depicts a representative gel of C2C12 whole cell lysate treated with RTC-15 overnight with proteins showing changes in phosphorylation or expression circled and numbered.

Selected protein spots were digested, peptides extracted and parent proteins identified by MS-Table 4.1. Peptides were identified using the NCBI protein database and only proteins matched with a score >54 were chosen as significant protein identifications. Fig. 4.4 represents individual phosphorylation changes observed in the proteins identified by MS. Fig. 4.5 represents individual expression changes observed in the proteins identified by MS.

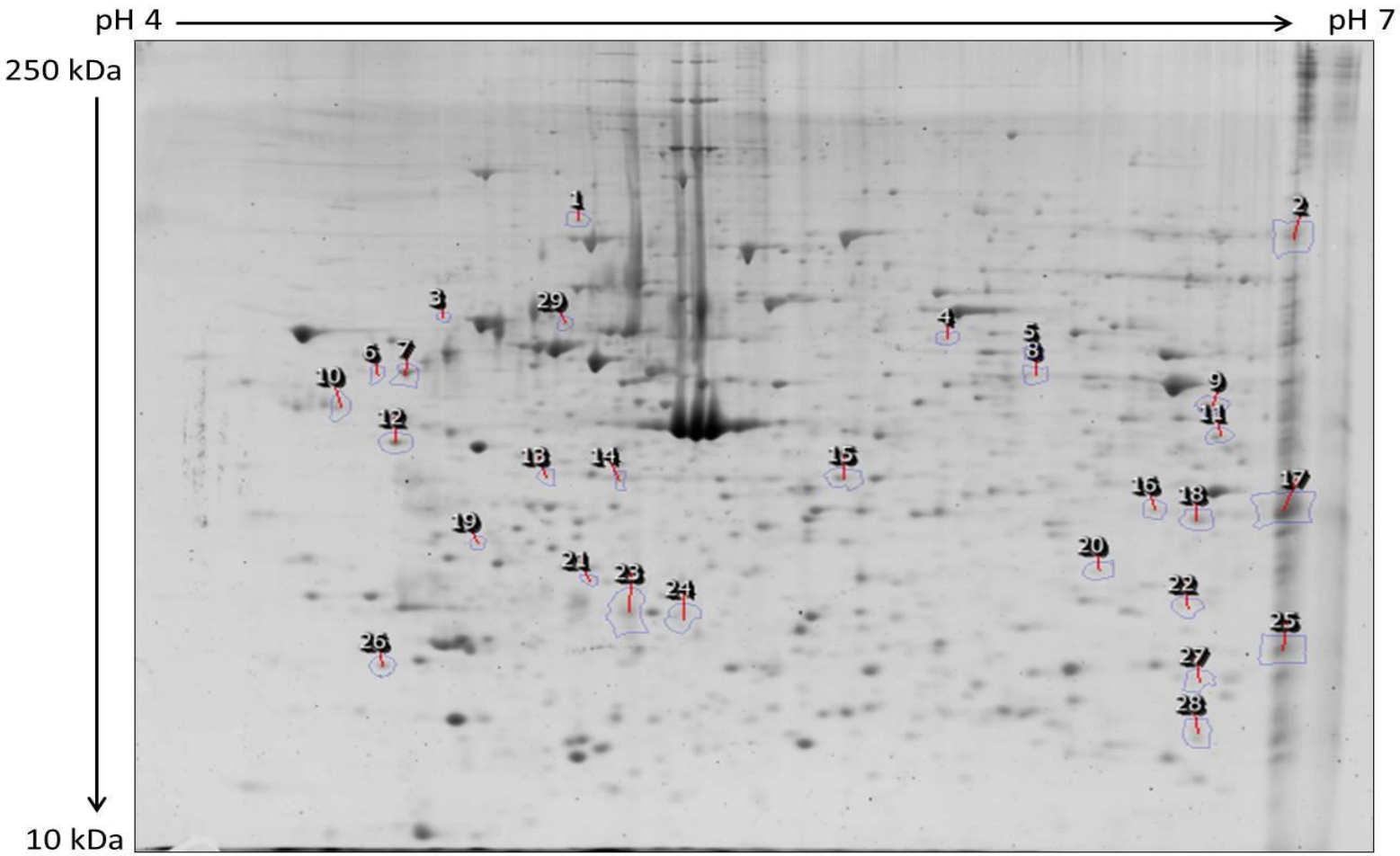

Fig 4.3 Identified protein changes from C2C12 cell lysate treated with 10µM RTC-15

Representative Sypro ruby image of C2C12 cell lysate treated with 10µM RTC-15, resolved by 2D electrophoresis. Spots circled and numbered represent proteins showing a statistically significant change in phosphorylation or expression.

Spot No.	Protein Identified	Accession No.	Fold Change	Change	Score	Peptides Matched	Cov (%)	MW	pI
1	*Alpha-Actinin	gi|28723	1.4	Down	251	7	11	68.7	5.10
2	Prelamin A/C	gi|162287370	1.6	Up	858	21	35	74.15	6.41
3	Zinc finger protein	gi|6756053	1.2	Up	353	6	13	50.68	4.71
4	Pyruvate dehydrogenase protein x	gi|28201978	1.2	Down	246	6	11	53.97	7.63
5	Heterogeneous Nuclear Ribonucleoprotein	gi|9845253	1.3	Up	83	3	11	49.25	5.89
6	MHR23A	gi|1044897	1.3	Up	185	4	21	39.75	4.59
7	Ribonuclease/angiogenesis inhibitor	gi|14577933	1.1	Up	263	7	19	49.60	4.64
8	PANDA_012419	gi|281341811	1.2	Up	353	6	16	39.32	4.84
9	Elongation factor Tu	gi|27370092	1.3	Up	578	14	28	49.48	7.23
10	Calumenin	gi|6680840	1.3	Up	296	10	33	37.04	4.49
11	Isovaleryl Co-A dehydrogenase	gi|9789985	1.3	Up	414	12	22	46.30	8.53
12	*Reticulocalbin-1	gi|6677691	1.3	Down	572	13	35	38.09	4.70
13	Ser/Thr Kinase Receptor associated protein	gi|4063383	1.3	Down	204	4	16	38.51	4.99
14	Ciapin 1	gi|18314528	1.4	Down	115	3	14	28.54	5.30
15	*Calponin 3	gi|21312564	1.3	Up	346	8	30	36.41	5.46
16	*Delta-aminolevulinic acid dehydratase	gi|188036156	1.4	Up	302	8	24	35.82	6.17
17	Annexin A2	gi|6996913	1.4	Up	485	10	34	38.65	7.55
18	PDZ and LIM domain protein 1	gi|158635992	1.4	Up	251	6	22	35.75	6.38

Table 4.1 Proteins Identified by mass spectrometry showing changes in phosphorylation or abundance in response to RTC-15 treatment.

All proteins were identified using the NCBI protein database and demonstrated a score >54 indicating significant protein identification. Proteins denoted with * represent proteins showing a change in phosphorylation.

Spot No.	Protein Identified	Accession No.	Fold Change	Change	Score	Peptides Matched	Cov (%)	MW	pI
19	Cathepsin Z	gi|291411144	1.2	Up	62	1	3	33.97	6.13
20	delta(3,5)-Delta(2,4)-dienoyl-CoA isomerase	gi|7949037	1.7	Up	303	8	28	36.10	7.60
21	EF-hand domain-containing protein D2	gi|31981086	1.2	Up	229	4	33	26.78	5.07
22	Elongation Factor Ts	gi|21313468	1.7	Up	103	4	13	35.31	6.62
23	Cathepsin B	gi|227293	1.1	Up	154	5	12	37.34	5.46
24	Cathepsin B	gi|227293	1.3	Up	133	3	12	37.34	5.46
25	Triosephosphate isomerase	gi|54855	1.6	Up	96	4	16	26.68	6.90
26	*Eukaryotic translation initiation factor 6	gi|27501448	1.2	Up	231	7	26	26.49	4.63
27	LSM12 homolog	gi|22748747	1.5	Up	136	2	18	21.69	7.63
28	ATP Synthase Subunit α	gi|57029	1.2	Up	199	4	6	59.72	9.22
29	Vimentin	gi|2078001	1.6	Down	241	6	16	53.66	5.06

Table 4.1 continued. Proteins Identified by mass spectrometry showing changes in phosphorylation or abundance in response to RTC-15 treatment.

All proteins were identified using the NCBI protein database and demonstrated a score >54 indicating significant protein identification. Proteins denoted with * represent proteins showing a change in phosphorylation.

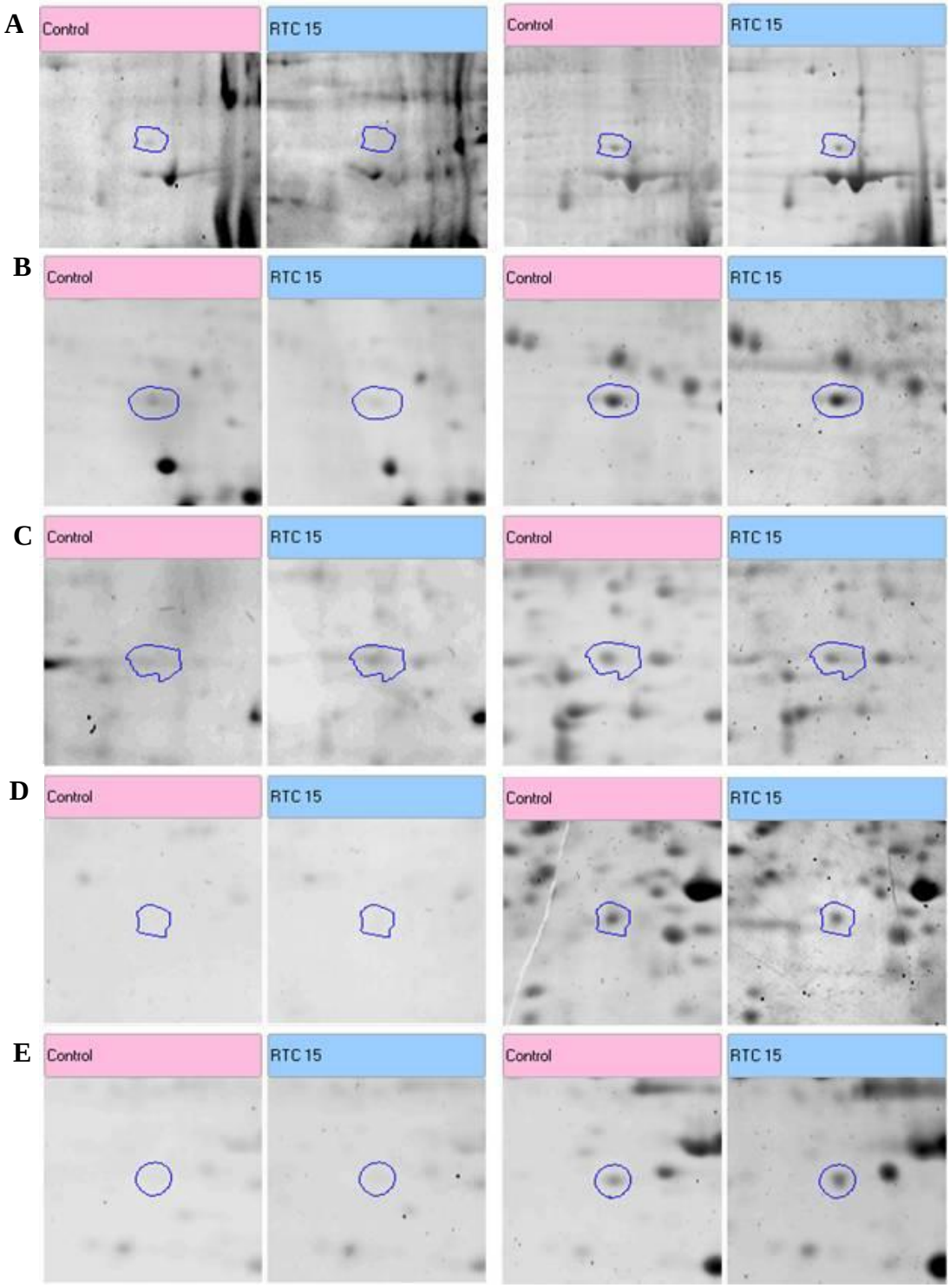

Fig 4.4. Phosphorylation changes observed in C2C12 muscle cells treated with 10µM RTC-15.

Single spot analysis of statistically significant phosphorylation changes in C2C12 cells treated with 10µM RTC-15 versus DMSO control. ProQ Diamond stained images are shown on the left and Sypro Ruby stained images are shown on the right. The following proteins are represented **A**. Alpha-actinin, **B**. Reticulocalbin-1, **C**. Calponin-3, **D**. Delta-aminolevulinic acid dehydratase, **E**. Eukaryotic translation initiation factor 6.

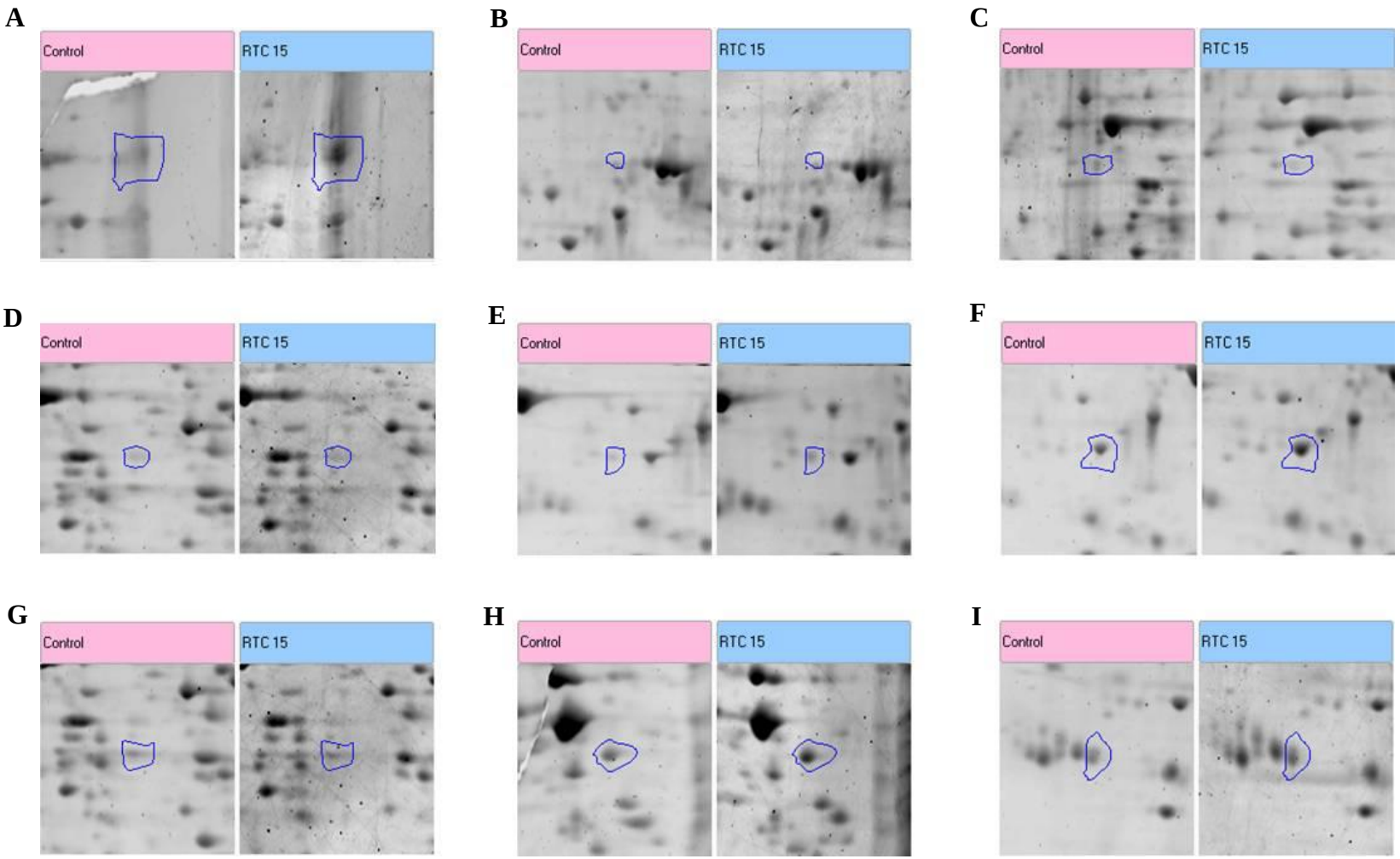

Fig 4.5 Changes in protein abundance observed in C2C12 muscle cells treated with 10µM RTC-15.

Single spot analysis of statistically significant changes in protein abundance in C2C12 cells treated with 10µM RTC-15 versus DMSO control. All images are Sypro ruby stained spots representing protein expression changes in **A**. Prelamin A/C, **B**. Zinc finger protein, **C**. Pyruvate Dehydrogenase, **D**. Heterogeneous Nuclear Ribonucleoprotein, **E**. MHR23A, **F**. Ribonuclease/angiogenesis inhibitor, **G**. PANDA_012419, **H**. Elongation factor Tu. **I**. Calumenin

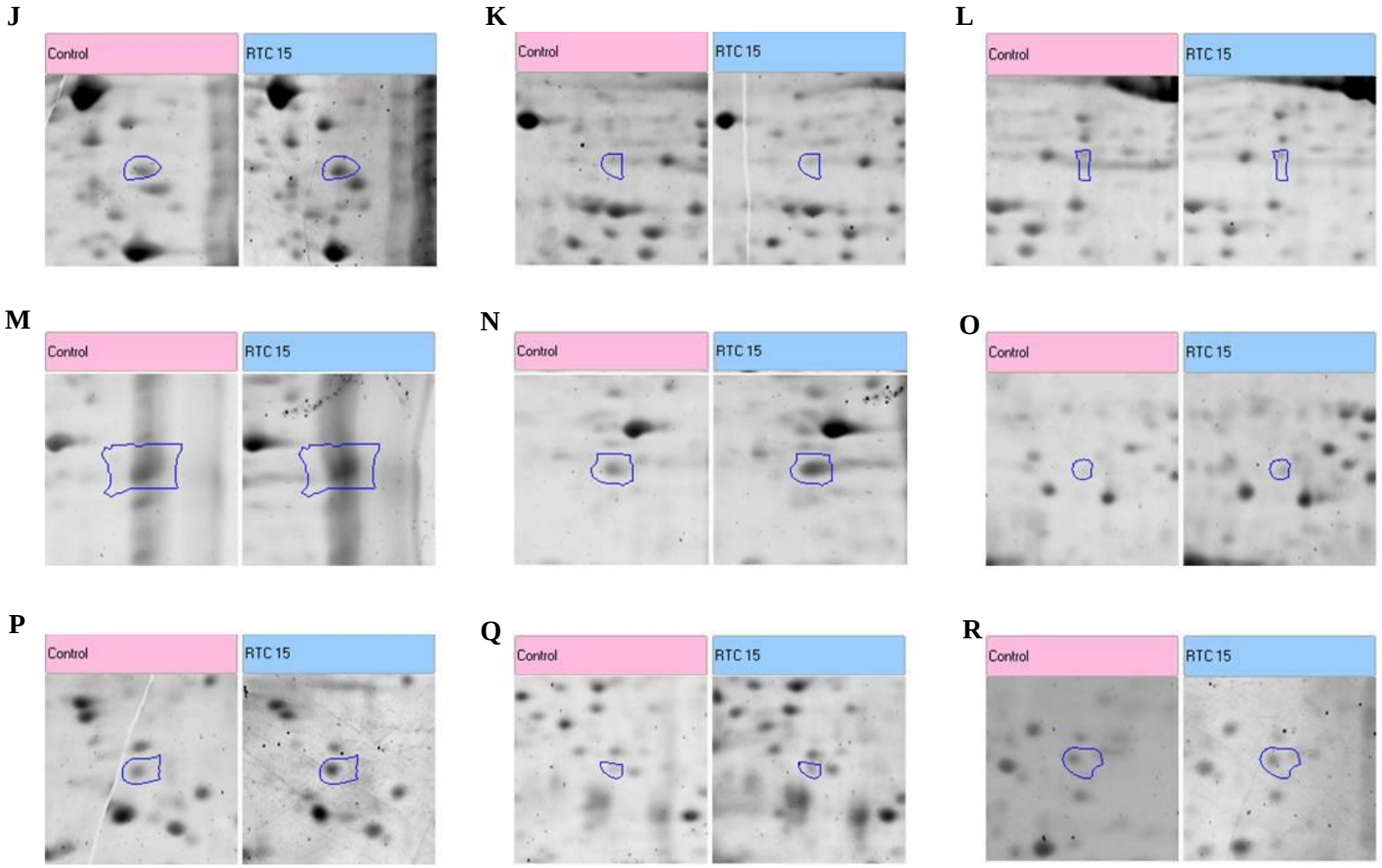

Fig 4.5 continued. Changes in protein abundance observed in C2C12 muscle cells treated with 10µM RTC-15.

Single spot analysis of statistically significant changes in protein abundance in C2C12 cells treated with 10µM RTC-15 versus DMSO control. All images are Sypro ruby stained spots representing protein expression changes in **J**. Isovaleryl Co-A dehydrogenase **K**. Ser/Thr Kinase Receptor associated protein **L**.Ciapin-1 **M**. Annexin A2 **N**. PDZ and LIM domain protein 1 **O**. Cathepsin Z **P**. delta(3,5)-Delta(2,4)-dienoyl-CoA isomerase **Q**. EF-hand domain-containing protein D2 **R**. Elongation Factor Ts

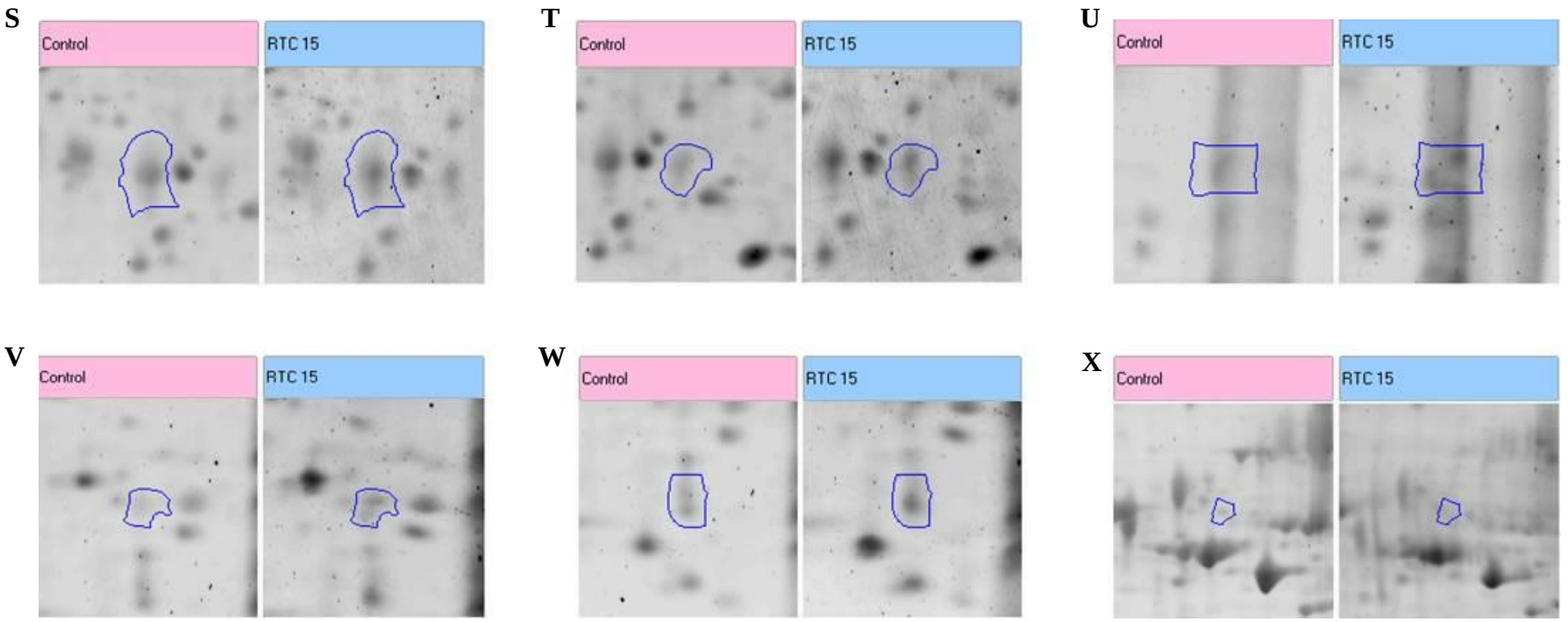

Fig 4.5 continued. Changes in protein abundance observed in C2C12 muscle cells treated with 10µM RTC-15.

Single spot analysis of statistically significant changes in protein abundance in C2C12 cells treated with 10µM RTC-15 versus DMSO control. All images are Sypro ruby stained spots representing protein expression changes in **S**. Cathepsin B **T**. Cathepsin B **U**. Triosephosphate isomerase **V**. LSM12 homolog **W**. ATP Synthase Subunit α **X**. Vimentin

Spot No.	Protein Identified	Function
1	*Alpha-Actinin	Alpha-actinin functions a cross-linking protein involved in anchoring actin to a variety of intracellular structures.
2	Prelamin A/C	Pre-Lamin A/C is a structural component of the nuclear lamina. It has been known to directly interact with chromatin and accelerate smooth muscle cell senescence.
3	Zinc finger protein-1 (ZPR1)	ZPR1 is involved in communicating mitogenic signals from the cytoplasm to the nucleus.
4	Pyruvate dehydrogenase protein x component	The x component of the pyruvate dehydrogenase (PDH) complex is essential for anchoring the E3 subunit to the E2 subunit. It is necessary for a functional PDH complex.
5	Heterogeneous Nuclear Ribonucleoprotein H2 (hnRNP H2)	hnRNP H2 is part of a complex that is required for the processing events that pre-mRNA undergoes before becoming functional mRNA in the cytoplasm.
6	MHR23A	MHR23A is a multiubiquitin chain receptor and is thought to be involved in proteasomal degradation and nucleotide excision repair.
7	Ribonuclease/angiogenesis inhibitor	It may inhibit RNAse1, RNAse2 and angiogenin. It could also play a role in redox homeostasis.
8	PANDA_012419	PANDA_012419 is an uncharacterised protein but it is homologous to the intermediate filament family of proteins.
9	Elongation factor Tu (EfTu)	EfTu promotes GTP-dependent binding of amino-acyl-tRNA to the A site of ribosomes during protein synthesis.
10	Calumenin	Calumenin is a calcium binding protein thought to be involved in regulation of the SERCA2 Ca^{2+} pump in the ER.
11	Isovaleryl Co-A dehydrogenase (IVD)	IVD is a member of the acyl coA dehydrogenase family and is responsible for the catabolism of branched chain amino acids for the production of acyl coA.
12	*Reticulocalbin-1 (RCN-1)	RCN-1 is a calcium binding protein thought to regulate calcium dependent activities in the endoplasmic reticulum.
13	Ser/Thr Kinase Receptor associated protein	Ser/Thr Kinase Receptor associated protein may play a role in the cellular distribution of the survival motor neuron complex.
14	Ciapin 1	Ciapin 1 inhibits apoptosis and may play a role in Fe/S protein assembly.
15	*Calponin 3	Calponin-3 is a thin filament associated protein that has been implicated in the regulation and modulation of smooth muscle contraction.

Table 4.2 Function of proteins identified by MS showing changes in response to RTC-15.

Proteins denoted with * represent proteins showing a change in phosphorylation. The function of each protein identified was compiled using the UniProt and NCBI protein databases.

16	*Delta-aminolevulinic acid dehydratase (ALAD)	ALAD catalyses an early step in the biosynthesis of tetrapyroles.
17	Annexin A2	Annexin A2 is a calcium regulated phospholipid binding protein involved in membrane organisation and trafficking.
18	PDZ and LIM domain protein 1	Also known as elfin, it is a cytoskeletal adaptor protein known to interact with alpha-actinin.
19	Cathepsin Z	Cathepsin Z is a cysteine protease in the papain family of proteins. It is a component of the lysosomal proteolytic system.
20	Delta(3,5)-delta(2,4)-dienoyl-CoA isomerase	Also known as ECH1, it is involved in the preparation of unsaturated fatty acids for fatty acid oxidation.
21	EF-hand domain-containing protein D2	As it contains an EF hand domain it is known to bind calcium. It is thought to bind to actin to modulate actin bundling.
22	Elongation Factor Ts (EfTs)	EfTs associates with the EfTu GDP complex and induces the exchange of GDP to GTP. It facilitates the binding of amino-acyl-tRNA to the ribosome.
23	Cathepsin B	Cathepsin B is a thiol protease thought to be involved in intracellular degradation of proteins.
24	Cathepsin B	Cathepsin B is a thiol protease thought to be involved in intracellular degradation of proteins.
25	Triosephosphate isomerase	Triosephosphate isomerase converts di-hydroxy acetone phosphate to D-glyceraldehyde 3-phosphate. Enzyme of the glycolytic pathway.
26	*Eukaryotic translation initiation factor 6 (eIF-6)	eIF-6 binds to the 60S ribosomal subunit and prevents its association with the 40S subunit to form the 80S initiation complex. Increased phosphorylation leads to release of the 60S subunit allowing the formation of the 80S complex.
27	LSM12 homolog	LSM12 homolog is a translation machinery associated protein.
28	ATP Synthase Subunit α	The α subunit forms the catalytic core of the ATP synthase complex or complex V in the electron transport chain.
29	Vimentin	Vimentin is an intermediate filament involved in cell migration and adhesion. It may also be involved in vesicle trafficking to the cell membrane.

Table 4.2 continued. Function of proteins identified by MS showing changes in response to RTC-15.

Proteins denoted with * represent proteins showing a change in phosphorylation. The function of each protein identified was compiled using the UniProt and NCBI protein databases.

4.3.1 Identification of common trends in proteome changes:

A number of intriguing changes in the proteome of the cell were observed in response to RTC-15 treatment overnight. Table 4.2 depicts the proteins identified and their predicted cellular functions. Interestingly, there were no striking changes in protein expression. The highest fold increase was 1.7. This demonstrates that the drug is eliciting a subtle effect on the proteome of the cell and not dramatic, potentially toxic events, even with direct stimulation at 10µM. Fig 4.6 demonstrates common processes in which some of the proteins identified are involved.

Proteins that showed changes in expression or phosphorylation can be categorised into the following groups; metabolic processes, integral structural proteins, protein biosynthesis, calcium binding, protein degradation and other functions.

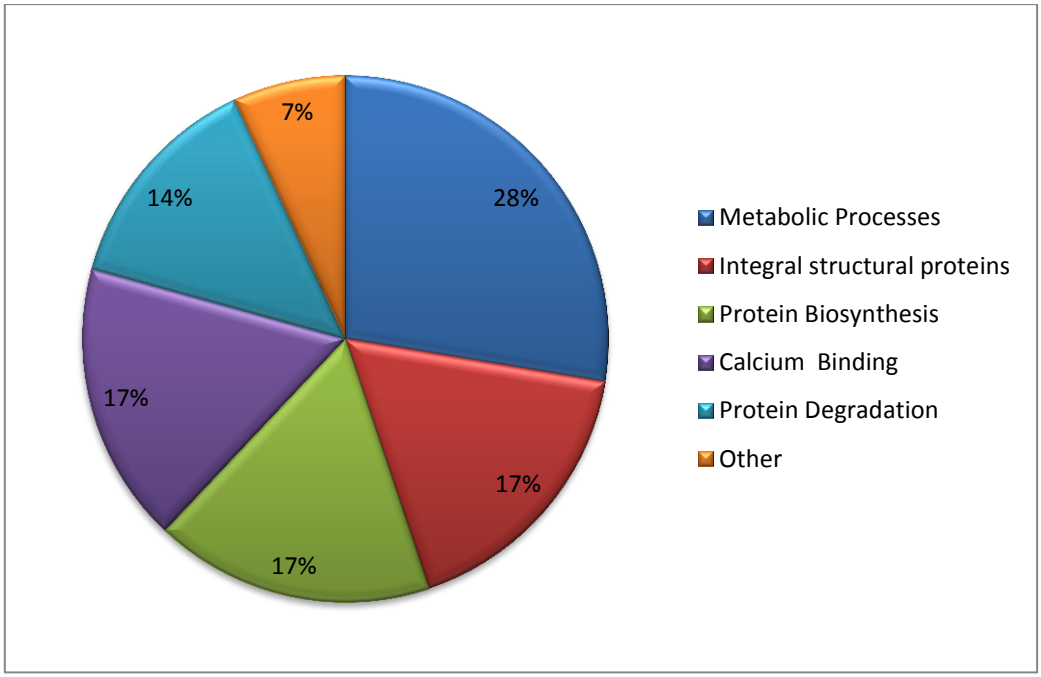

Fig 4.6 Distribution of common trends among proteins showing changes in response to RTC-15:

Several common cellular functions were identified in proteins affected by RTC-15 treatment. They fall under the categories, metabolic processes, integral structural proteins, protein biosynthesis, calcium binding, protein degradation and other functions.

4.3.2 Analysis of changes in the proteome affecting metabolism:

Several proteins demonstrated changes that are involved in metabolic processes in the cell, most notably fatty acid oxidation and oxidative phosphorylation. As discussed in section 4.1.2, mice treated with RTC-1 and a HFD demonstrated a decreased accumulation of fat mass compared to mice fed a HFD alone. This could suggest that the mice were more metabolically active and diverting energy away from storage as fat, towards energy consumption. The observation that the compounds were having an inhibitory action on complex I could also be impacting on how the cell generates ATP. Complex I is involved in the first step of oxidative phosphorylation and the production of NAD from NADH to generate a proton gradient (Fig 4.7). Dr. Breen found that the compounds inhibited oxygen consumption in a mitochondrial activity test. Malate was used as a substrate to increase NADH levels in isolated rat mitochondria. Addition of the compounds resulted in a drop in oxygen consumption, which was rescued with the addition of the complex II substrate, succinate. This suggests that the compounds directly inhibit complex I. Inhibition of complex I would result in oxidative phosphorylation beginning at succinate dehydrogenase or complex II. Complex II utilises FADH as the hydrogen donor. Inhibition of complex I would not have been detected in a proteomic approach as it is a direct inhibitory action of the drug on protein activity. However, several changes in proteins have been observed that could be occurring as a result of this inhibitory action. Complex I inhibition is a potentially toxic event, the complex I inhibitor, rotenone is moderately toxic to humans. However, RTC-15 does not seem to have a toxic effect on the cell i.e. other energy sources are being utilised to compensate for complex I inhibition and to maintain levels of ATP.

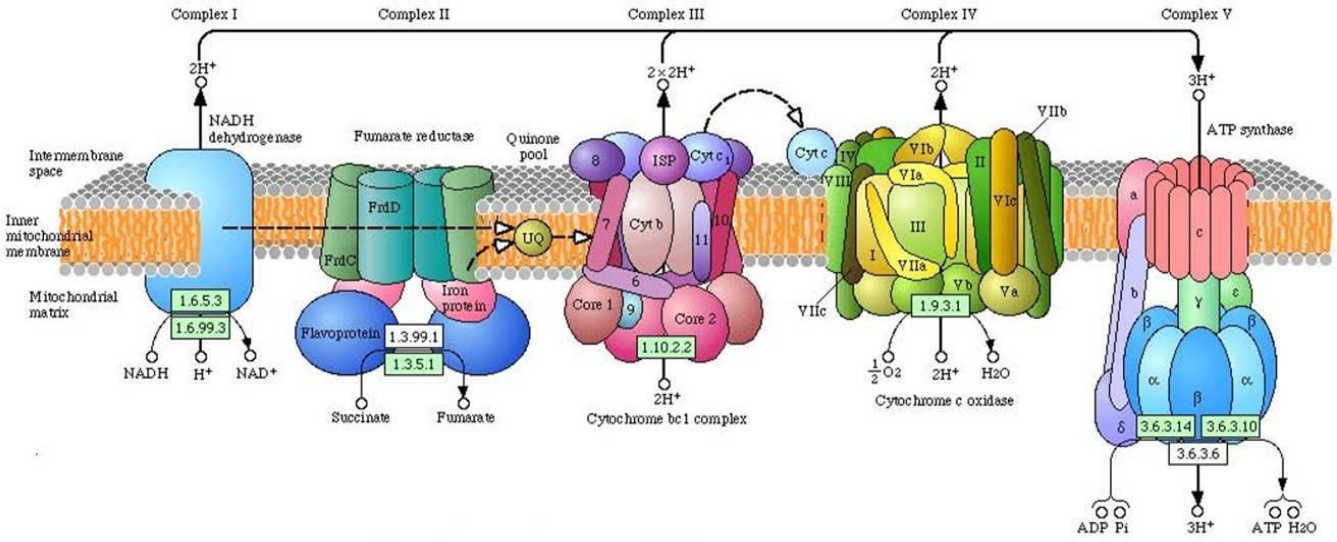

Fig 4.7 Representation of oxidative phosphorylation and the protein complexes involved.

Diagram depicting the electron transport chain of the inner mitochondrial membrane (Brockington et al., 2010).

4.3.2.1 Analysis of increased expression of isovaleryl co-A dehydrogenase:

A 1.3-fold increase was observed in isovaleryl co-A dehydrogenase (IVD) expression. IVD is involved in a dehydrogenation step in the catabolism of leucine to acetyl-co-A. Acetyl-co-A is the substrate utilised for the citric acid cycle (Fig 4.8). An increase in IVD expression could mean that the cell is using different energy sources, such as branched amino acids, to compensate for inhibition of complex I. Fig 4.9 shows the expression levels of IVD in response to DMSO vehicle or RTC-15. However, no significant change was observed in expression level when analysed directly by Western blotting.

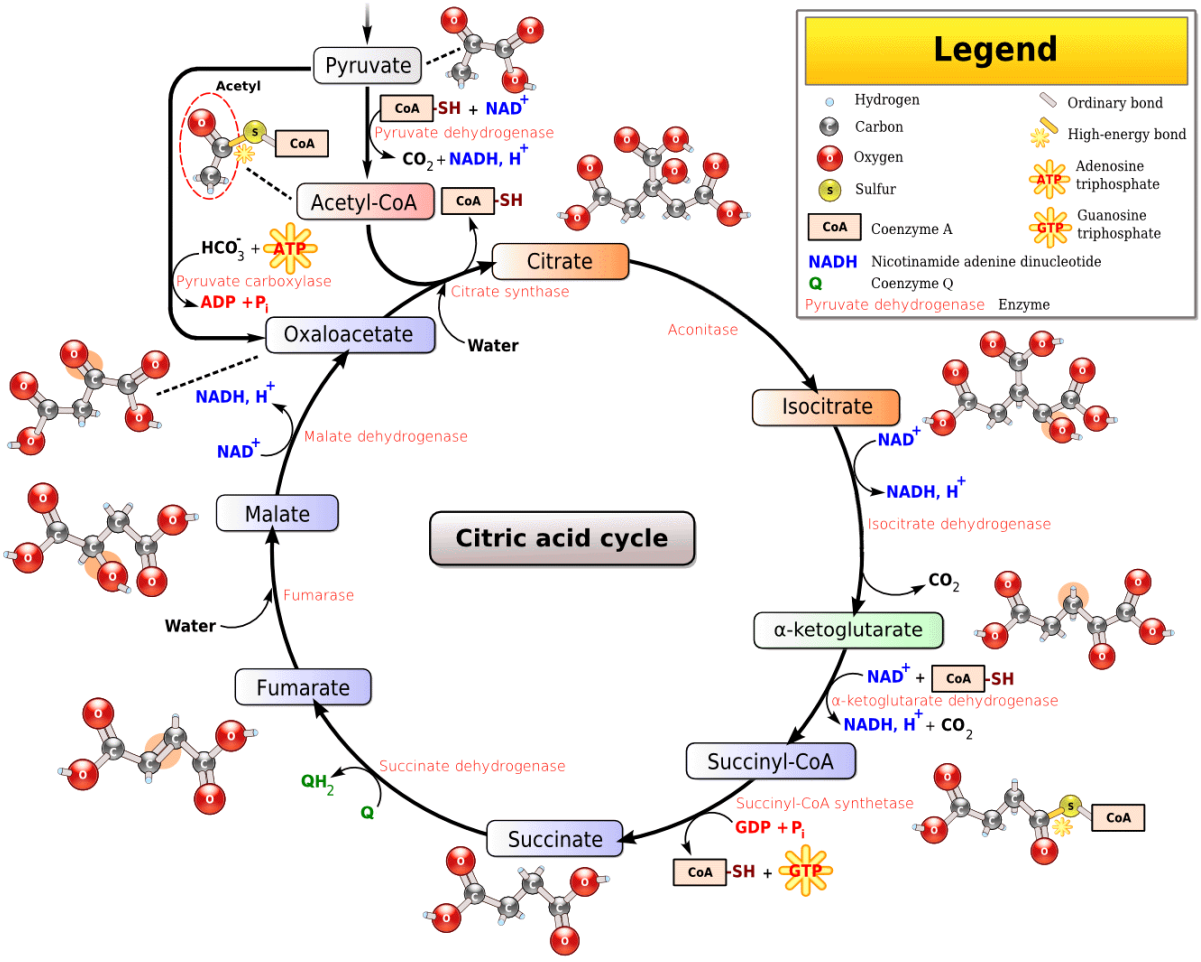

Fig 4.8 The citric acid cycle.

Representation of the citric acid cycle. Taken from www.biologycorner.com.

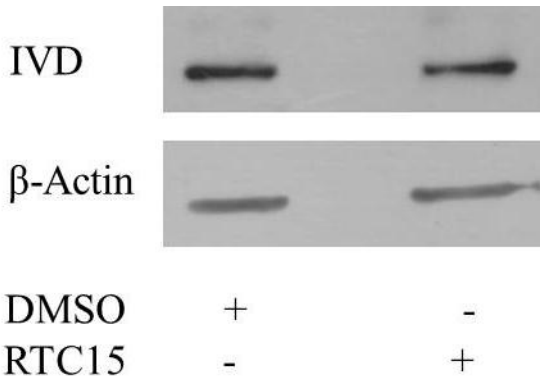

Fig 4.9 Analysis of expression levels of IVD.

Representative Western blot depicting expression levels of IVD in response to DMSO or 10µM RTC-15 overnight. C2C12 cells were treated with DMSO or 10µM RTC-15 overnight. Cells were harvested and lysed in RIPA buffer. Protein concentration was assessed using the PIERCE protein assay and 30µg/ml protein was used per sample. Cell lysate was electrophoresed using a 10% SDS-PAGE gel and protein was subsequently transferred to PVDF membrane. Western blotting analysis was conducted using anti-IVD specific antibody and β-Actin as a loading control. All analysis was conducted in triplicate.

4.3.2.2 Analysis of increased expression of delta(3,5)-delta(2,4)-dienoyl-CoA isomerase:

A 1.7-fold increase was observed in delta(3,5)-delta(2,4)-dienoyl-CoA isomerase (ECH1) expression. ECH1 is an auxiliary enzyme of β-oxidation. It is involved in preparing unsaturated fatty acids for fatty acid oxidation. One cycle through the β-oxidation pathway produces 1 molecule of FADH and 1 of NADH and also results in the production of acetyl-coA which can then enter the citric acid cycle (Kunau et al., 1995). Therefore, as a result of complex I inhibition the cell could be utilising fatty acids as an additional energy source. Fig 4.10 shows the expression levels of ECH1 in response to DMSO vehicle or 10µM RTC-15. As previously observed with 2D electrophoresis, ECH1 is indeed increased in expression in response to 10µM RTC-15.

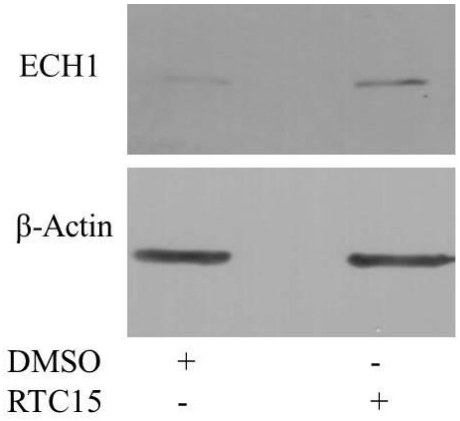

Fig 4.10 Analysis of expression levels of ECH1.

Representative Western blot depicting expression levels of ECH1 in response to DMSO or 10µM RTC-15 overnight.C2C12 cells were treated with DMSO or 10µM RTC-15 overnight. Cells were harvested and lysed in RIPA buffer. Protein concentration was assessed using the PIERCE protein assay and 30µg/ml protein was used per sample. Cell lysate was electrophoresed using a 10% SDS-PAGE gel and protein was subsequently transferred to PVDF membrane. Western blotting analysis was conducted using anti-ECH1 specific antibody and β-Actin as a loading control. All analysis was conducted in triplicate.

4.3.2.3 Analysis of decreased expression of PDH protein x component:

The PDH protein x component showed a 1.2-fold decrease in expression. PDH is involved in the catabolism of pyruvate to form acetyl-coA which then enters the citric acid cycle (Fig 4.8). The x component of the complex is necessary for anchoring the E3 catalytic subunit to the E2 catalytic subunit (Patel and Roche, 1990). The x component is also thought to transfer electrons to the E3 catalytic subunit. Removal of the lipoyl domain of the protein results in a dramatic reduction in activity of the complex (Gopalakrishnan et al., 1989). Increases in NADH and acetyl-coA levels leads to an inhibitory phosphorylation of the PDH complex resulting in decreased activity of the enzyme. This is particularly evident when fatty acid oxidation is the preferred energy source as increased amounts of NADH and acetyl-coA are produced (Patel and Roche, 1990). Expression of the protein may also be decreased by a negative feedback mechanism. When levels of NADH and acetyl-coA are abundant they may have an inhibitory effect on PDH component expression. Increased expression of ECH1 indicates that there could be increased utilisation of fatty acids as an energy source, leading to increased acetyl coA levels. Therefore, PDH protein x component expression may be reduced due to elevated levels of acetyl-coA, produced as a result of increased cellular demand for ATP.

4.3.2.4 Analysis of increased expression of ribonuclease/angiogenesis inhibitor-1:

A 1.1-fold increase in ribonuclease/angiogenesis inhibitor-1 (Rnh1) expression was observed. Rnh1 is thought to be involved in redox homeostasis and is found in the cytosol, nucleus and mitochondria. It was originally believed to bind to and inhibit ribonucleases to prevent cytotoxicity (Haigis et al., 2003). However, the protein contains a high number of cysteine residues which are prone to oxidation and it is now established that Rnh1 is a scavenging molecule, with the ability to mop up excess reactive oxygen species (ROS) (Cui et al., 2003). In a co-immunoprecipitation study, Furia et al demonstrated that Rnh1 can bind to several mitochondrial proteins, placing it in close proximity to areas of high ROS production (Furia et al., 2011). In particular, it was noted that Rnh1 can bind to ATP-synthase subunit alpha. Interestingly, ATP-synthase subunit alpha was another protein which demonstrated increased expression in response to RTC-15 treatment. The complex I inhibitor, Rotenone, causes an increase in ROS due to binding to the CoQ binding site in complex I (Cadenas et al., 1977). When the $NADH/NAD^+$ ratio is elevated in the mitochondria, ROS production increases, as a result of increased transfer of electrons to O_2 (Murphy, 2009). Complex I inhibition results in decreased utilisation of NADH, leading to a higher NADH to NAD^+ ratio. Therefore, RTC-15 may increase ROS production, stimulating the cell to activate compensatory mechanisms in the form of Rnh1 expression, to prevent oxidative stress in the cell.

4.3.2.5 Analysis of increased phosphorylation of δ-aminolevulinic acid dehydratase:

A 1.4-fold increase in δ-aminolevulinic acid dehydratase (ALAD) phosphorylation was observed. ALAD is involved in the condensation of two molecules of δ-aminolevulinic acid (ALA) to form porphobilinogen (Jaffe, 2004). Porphobilinogen is a precursor for the production of tetrapyrrole pigments such as haem. Haem is an essential co-factor in the ETC, acting as a mediator of electron transfer in several of the mitochondrial respiratory complexes (Kim et al., 2012). The precursors of haem synthesis are glycine and succinyl coA (Fig 4.11). Succinyl-coA is an intermediate substrate in the citric acid cycle. If increased levels of acetyl-coA were entering the citric acid cycle excess succinyl-coA would be produced. As a result, excess succinyl-coA may be stimulating an increase in

activity of tetrapyrrole synthetic enzymes such as ALAD. ALAD is not known to be phosphorylated but when the sequence was entered into the phosphorylation prediction server PhosphoSitePlus, a serine phosphorylation site was predicted at serine 215 (Fig 4.12) It is unknown how phosphorylation would affect the function of this enzyme.

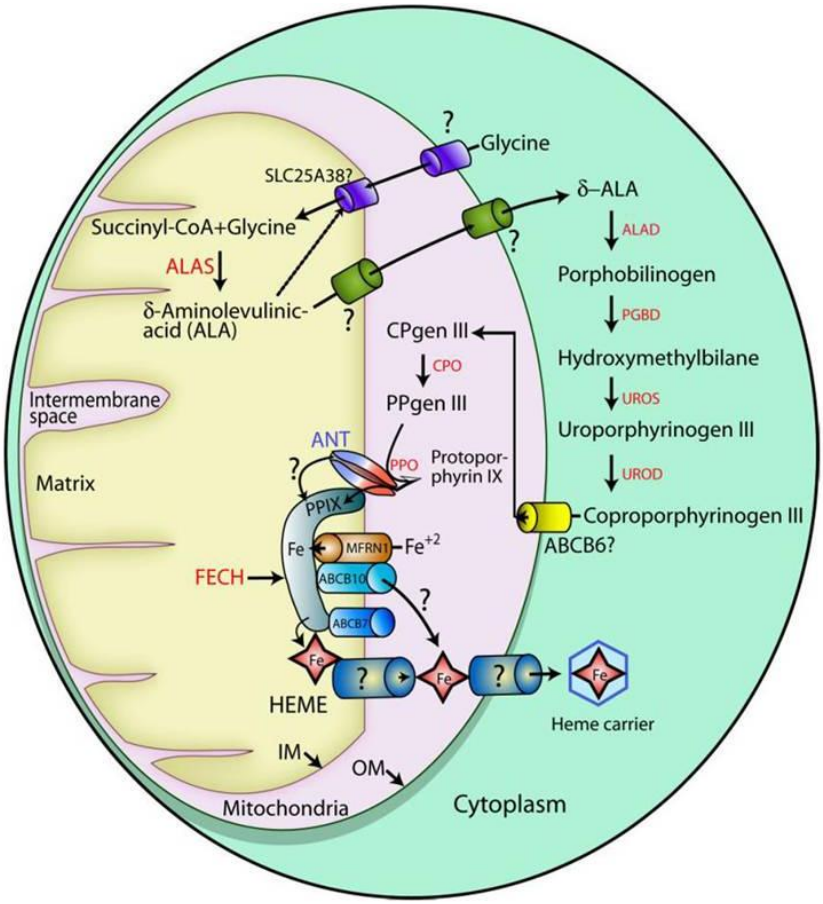

Fig 4.11 The haem biosynthetic pathway.

Diagram depicting the haem biosynthetic pathway. Haem synthesis is initiated by the production of ALA from glycine and succinyl-CoA. ALAD mediates the conversion of δ-aminolevulinic acid to porphobilinogen (Khan and Quigley, 2011).

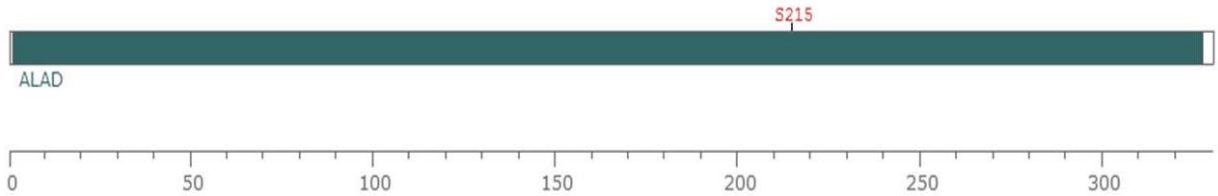

Fig 4.12 Prediction of potential phosphorylation sites in the sequence of ALAD.

Diagram depicting the predicted phosphorylation site of ALAD at Ser215. Image generated using the phosphorylation site prediction software, PhosphoSitePlus.

4.3.2.6 Analysis of increased expression of triosephosphate isomerase:

Triosephosphate isomerase (TPI) expression increased 1.6-fold in response to RTC-15 treatment and was verified by Western blotting analysis (Fig 4.13). This enzyme is involved in the glycolytic pathway. It converts dihydroxyacetone phosphate (DHAP) to D-glyceraldehyde-3-phosphate (D-GAP) (Wierenga et al., 2010). DHAP is produced as a by-product in glucose utilisation. TPI ensures that DHAP enters the glycolytic pathway for energy production and subsequently prevents toxicity that could occur as a result of increased levels of this metabolite. Increased expression of an enzyme involved in glycolysis is a strong indicator of increased metabolic rate.

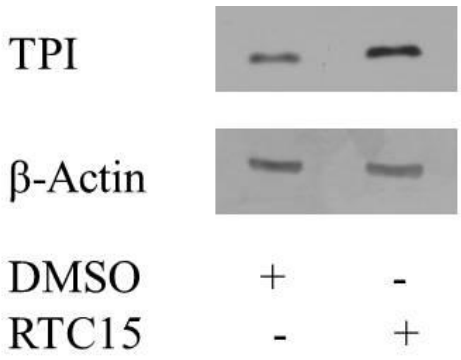

Fig 4.13 Analysis of expression levels of TPI.

Representative Western blot depicting expression levels of TPI in response to DMSO or 10μM RTC-15 overnight. C2C12 cells were treated with DMSO or 10μM RTC-15 overnight. Cells were harvested and lysed in RIPA buffer. Protein concentration was assessed using the PIERCE protein assay and 30μg/ml protein was used per sample. Cell lysate was electrophoresed using a 10% SDS-PAGE gel and protein was subsequently transferred to PVDF membrane. Western blotting analysis was conducted using anti-TPI specific antibody and β-Actin as a loading control. All analysis was conducted in triplicate.

4.3.2.7 Analysis of increased expression of ATP synthase subunit α:

ATP synthase is responsible for transporting the protons generated from the ETC across the membrane to generate new molecules of ATP for energy consumption. The α subunit of this complex showed a 1.2-fold increase in expression in response to RTC-15 treatment. This subunit is one of the core subunits of the F1 ATPase component of the complex (Fig 4.7). It forms part of the catalytic core of the enzyme along with the β and γ subunits, and is responsible for ATP hydrolysis. The α subunit does not directly catalyse ATP production but is thought to allosterically regulate the β subunit to

allow nucleotide binding (Yoshida et al., 2001). Increased expression of one of the subunits of ATP synthase could indicate an increased demand for ATP production, caused by complex I inhibition.

4.3.2.8 Analysis of decreased expression of ciapin-1:

Ciapin-1, which showed a 1.4-fold decrease in expression was originally identified as an anti-apoptotic protein (Shibayama et al., 2004). Expression of ciapin-1 is induced by cytokine activation of the Ras pathway. Ciapin-1 knockout is lethal in late gestation, possibly as a result of anaemia due to defects in the liver and spleen (Shibayama et al., 2004). Interestingly, no apparent abnormality was observed in the skeletal muscle of deceased ciapin-1 knockout mice, which suggests that a decrease in expression in muscle tissue may not have adverse effects. Other anti-apoptotic molecules may be compensating for lack of ciapin-1 expression.

Ciapin-1 is the human homolog of the yeast Dre2 protein which is involved in the assembly of Fe/S binding proteins in the mitochondria (Zhang et al., 2008). Expression of ciapin-1 in Dre2 knockout yeast prevented abnormalities associated with this deletion. Fe/S proteins are highly involved with complex I, complex II and complex III of the ETC. In vitro, ciapin-1 has been shown to bind Fe/S and associates with proteins involved in the formation of Fe/S cluster proteins (Banci et al., 2011).

A yeast two hybrid screen identified protein kinase C θ interacting cousin of thioredoxin (PICOT), as a binding partner of ciapin-1 (Saito et al., 2011b). PICOT can also bind Fe/S. Therefore, both proteins may be involved in Fe/S cluster assembly. PICOT was originally identified as an interacting protein of PKC θ, and has an inhibitory action on PKC activity (Witte et al., 2000). Interestingly, in ciapin-1 knockout cells, PKC was shown to be more active (Saito et al., 2011a). When ciapin-1 knockout cells were activated with a PKC agonist, the calcium independent protein kinases, PKC θ and δ, showed increased phosphorylation compared to WT cells. Therefore, ciapin-1 may be a negative regulator of PKC activity. RTC-15 appears to down-regulate ciapin-1 by an unknown mechanism, as a result PKC θ and δ could potentially be more active.

4.3.3 Analysis of changes in the proteome affecting integral structural proteins:

Treatment of C2C12 cells with RTC-15 overnight resulted in changes in several proteins which have structural roles in the cell. This set of proteins includes prelamin A/C, vimentin, PANDA_012419, calponin-3 and PDZ and LIM domain protein 1.

4.3.3.1 Analysis of increased expression of prelamin A/C:

Fig 4.14 depicts the expression level of lamin A/C and prelamin A/C in response to DMSO or RTC-15 treatment. 2D analysis predicted a 1.6-fold increase in prelamin A/C. Prelamin A/C is the precursor of lamin A/C. Cleavage of the last 18 C-terminal residues activates the protein. Lamin A/C is an intermediate filament protein of the inner nuclear lamina. It is thought to maintain the structure of the nucleus (Vergnes et al., 2004). Western blotting analysis was conducted using antibodies raised against lamin A/C, which should also react with prelamin A/C. Two bands were visible by Western blot analysis, the upper band corresponding to prelamin A/C and the lower band corresponding to lamin A/C. No significant change in expression level of either protein was subsequently observed in response to RTC-15 treatment.

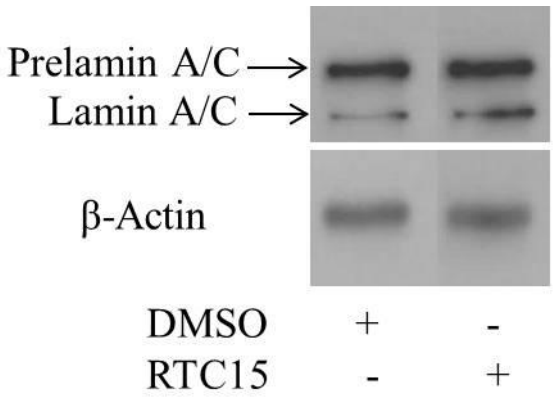

Fig 4.14 Analysis of expression levels of Prelamin A/C.

Representative Western blot depicting expression levels of Prelamin A/C and Lamin A/C in response to 10μM RTC-15 overnight. C2C12 cells were treated with DMSO or 10μM RTC-15 overnight. Cells were harvested and lysed in RIPA buffer. Protein concentration was assessed using the PIERCE protein assay and 30μg/ml protein was used per sample. Cell lysate was electrophoresed using a 10% SDS-PAGE gel and protein was subsequently transferred to PVDF membrane. Western blotting analysis was conducted using anti-Lamin A/C specific antibody and β-Actin as a loading control. All analysis was conducted in triplicate.

4.3.3.2 Analysis of decreased expression of vimentin:

Vimentin is a member of the intermediate filament family. It is thought to be involved in cell motility and has a scaffolding function in the cell (Ivaska et al., 2007). Fig 4.15 depicts the expression level of vimentin in response to DMSO or RTC-15 treatment. 2D analysis predicted a 1.6-fold decrease in expression. Secondary validation by Western blotting did not reveal a significant decrease in expression following RTC-15 treatment.

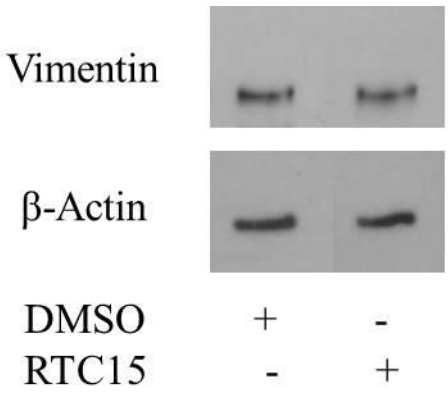

Fig 4.15 Analysis of expression levels of Vimentin.

Representative Western blot depicting expression levels of vimentin in response to DMSO or 10µM RTC-15 overnight. C2C12 cells were treated with DMSO or 10µM RTC-15 overnight. Cells were harvested and lysed in RIPA buffer. Protein concentration was assessed using the PIERCE protein assay and 30µg/ml protein was used per sample. Cell lysate was electrophoresed using a 10% SDS-PAGE gel and protein was subsequently transferred to PVDF membrane. Western blotting analysis was conducted using anti-vimentin specific antibody and β-Actin as a loading control. All analysis was conducted in triplicate.

4.3.3.3 Analysis of increased expression of PANDA_012419:

PANDA_012419 is an uncharacterised protein but it shares sequence similarity with the intermediate filament family. Lamin and vimentin are also part of this family. PANDA_012419 displayed a 1.2-fold increase in expression in response to RTC-15 treatment. The intermediate filament proteins are a family of cytoskeletal proteins which act as a scaffold for maintaining cell integrity.

4.3.3.4 Analysis of increased phosphorylation of calponin-3:

Calponin-3, which showed a 1.3-fold increase in phosphorylation, is involved in smooth muscle contraction. Calponin-3 interacts with actin and other cytoskeletal proteins. Phosphorylation of calponin-3 via protein kinase C (PKC) results in a diminished binding capacity of calponin-3 for other cytoskeletal proteins (Winder and Walsh, 1990). Loss of binding to actin results in the reversal of inhibition of the actomyosin MgATPase. Thus, calponin is a regulator of the actin myosin interaction and negatively regulates smooth muscle contraction. The phosphorylation site of calponin was determined by mutational analysis and appears to be located in the actin binding site, specifically Ser175 (Tang et al., 1996). Phosphorylation diminishes calponin's affinity for actin presumably by blocking the binding site. Therefore, elevated phosphorylation of claponin-3 with RTC-15 treatment would lead to decreased binding to actin and may result in increased contractility of actin fibres. The α and ε isoforms of PKC have been demonstrated to phosphorylate calponin *in vivo* and could be the kinase responsible for RTC-15 mediated calponin-3 phosphorylation (Patil et al., 2004) (Winder et al., 1998).

4.3.3.5 Analysis of increased expression of PDZ and LIM domain protein 1:

PDZ and LIM domain protein 1 (Pdlim1), also known as elfin, demonstrated a 1.4-fold increase in expression. As its name suggests, Pdlim1 contains an N-terminal PDZ domain and a C-terminal LIM domain. It is a member of the actinin-associated LIM protein (ALP) family and is known to bind to alpha-actinin. The PDZ domain of Pdlim1 binds to alpha-actinin at its EF hand domain and links it to the cytoskeletal protein, actin (Kotaka et al., 2000). It is thought to act as an adaptor protein as it can bind to two distinctly different regions via its PDZ and LIM domains. The function of the LIM domain is unknown at present but members of another PDZ/LIM containing subfamily, enigma, are known to bind PKC via the LIM domain (te Velthuis and Bagowski, 2007). This interaction has been postulated to enable PKC targeting to the sarcomere. Phosphorylation targets of PKC include vinculin and troponin which are known to regulate muscle contraction.

4.3.4 Analysis of changes in the proteome affecting protein biosynthesis:

Several proteins involved in protein biosynthesis also exhibited changes. This set of proteins includes Heterogeneous Nuclear Ribonucleoprotein H2 (hnRNP H2), elongation factor Tu (EfTu), elongation factor Ts (EfTs), eukaryotic translation initiation factor 6 (eIF-6), and Protein LSM12 homolog.

4.3.4.1 Analysis of increased expression of hnRNP H2, EfTu and EfTs:

hnRNP H2 which exhibited a 1.3-fold increase in expression, is an RNA binding protein and is thought to regulate alternative splicing and mRNA processing (Han et al., 2010). EfTu and EfTs both showed an increase in expression in response to RTC-15. These proteins are involved in transfer of amino-acyl tRNA molecules to the ribosomal complex for translation to occur. Interestingly, a proteomic study conducted by Wang et al, demonstrated that RA stimulation of a breast cancer cell line, MCF-7, caused an increase in hnRNP H2 and EfTu expression (Wang et al., 2007). Therefore, any increase in these proteins could be as a result of RTC-15 effects on the retinoid system and its influence on gene transcription.

4.3.4.2 Analysis of increased phosphorylation of eIF-6:

A 1.2-fold increase in eIF-6 phosphorylation was observed in response to RTC-15 treatment. *In vivo*, eIF-6 binds to the 60S ribosomal subunit, inhibiting its interaction with the 40S subunit. It is negatively regulated by phosphorylation which is conducted by PKC (Ceci et al., 2003). Phosphorylation of eIF-6 allows 60S release and subsequent binding to the 40S subunit and initiation of translation. As RTC-15 treatment lead to an increase in eIF-6 phosphorylation it could mean that PKC is more active.

4.3.4.3 Analysis of increased expression of protein LSM12 homolog:

A 1.5-fold increase was observed in protein LSM12 homolog expression. Very little is known about the function of this protein. LSM12 contains an RNA binding domain and is thought to be involved in RNA processing and is associated with the ribosomal complex (Fleischer et al., 2006).

4.3.5 Analysis of changes in the proteome affecting calcium binding proteins:

A common motif exists in several of the proteins showing changes in response to RTC-15 treatment. The EF hand domain is a highly conserved structural motif that allows a protein to bind calcium. The domain consists of two perpendicular alpha-helices and a connecting loop region, forming a binding site for a single calcium ion (Ikura, 1996). Calumenin, reticulocalbin-1 (RCN-1), EF hand domain containing protein D2 (also known as swiprosin-1) and alpha-actinin all have at least two EF hand domains. Annexin A2 has a high affinity binding site for EF hand domain containing proteins.

4.3.5.1 Analysis of increased expression of Annexin A2:

Fig 4.16 depicts the expression levels of annexin A2 in response to RTC-15 treatment (1.4-fold increase). Annexin proteins bind positively charged calcium via the annexin domain. This allows annexin proteins to bind to negatively charged phospholipid headgroups present in the plasma membrane (Gerke et al., 2005). Annexin A2 is involved in membrane organisation and trafficking. Vesicle transport to the plasma membrane is a known calcium dependent process. Annexin A2 is thought to be involved in the fusion of plasma secretory vesicles with the plasma membrane (Emans et al., 1993). Annexin A2 was found to be enriched at the plasma membrane, associated with GLUT4 vesicles which were recycled from the endosome (Aledo and Hundal, 1996). Huang et al demonstrated that the anti-diabetic drug troglitazone, a member of the thiazolidinedione family, was found to increase annexin A2 expression (Huang et al., 2004). Interestingly, insulin stimulated GLUT4 translocation was markedly inhibited when annexin A2 expression was down-regulated with siRNA. Conversely, cells over-expressing annexin A2 demonstrated increased insulin stimulated GLUT4 trafficking and increased glucose uptake (Huang et al., 2004). Thiazolidinedione anti-diabetic therapeutics may be having an insulin sensitizing effect by up-regulating proteins involved in insulin dependent GLUT4 incorporation into the plasma membrane. RTC-15-induced annexin A2 expression could potentiate GLUT4 translocation to the cell membrane.

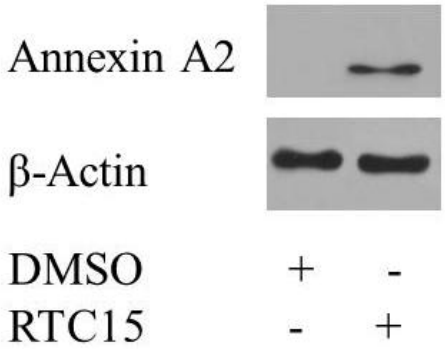

Fig 4.16 Analysis of expression levels of Annexin A2.

Representative Western blot depicting expression levels of annexin A2 in response to DMSO or 10μM RTC-15 overnight. C2C12 cells were treated with DMSO or 10μM RTC-15 overnight. Cells were harvested and lysed in RIPA buffer. Protein concentration was assessed using the PIERCE protein assay and 30μg/ml protein was used per sample. Cell lysate was electrophoresed using a 10% SDS-PAGE gel and protein was subsequently transferred to PVDF membrane. Western blotting analysis was conducted using anti-annexin A2 specific antibody and β-Actin as a loading control. All analysis was conducted in triplicate.

4.3.5.2 Analysis of increased expression of Calumenin:

Calumenin is a member of the CREC family which are calcium binding proteins with multiple EF hand domains. It is predominantly expressed in the ER and the sarcoplasmic reticulum (SR). It was observed to increase 1.3-fold in expression in response to RTC-15 treatment. Fig 4.17 shows the secondary validation of calumenin upregulation by Western blotting. Calcium release from the SR is mediated by the ryanodine receptor 1 (RyR1) and calcium uptake by the sarco/endoplasmic reticulum Ca^{2+} ATPase (SERCA). Calumenin is thought to regulate calcium release and uptake in the SR by direct interaction with both RyR1 and SERCA (Jung et al., 2006), (Sahoo and Kim, 2008). When calumenin was overexpressed in C2C12 myotubes, a net increase in calcium release from the SR was observed on caffeine treatment (Jung et al., 2006). However, a net decrease in calcium release was observed with depolarization (Jung et al., 2006). This could be due to direct interaction of calumenin with RyR1. Calumenin was also overexpressed in rat cardiomyocytes and shown to inhibit calcium uptake via its interaction with SERCA (Sahoo et al., 2009). This interaction is calcium-dependent and when calumenin binds to SERCA its affinity for calcium is diminished, thus reducing calcium influx. Calumenin may also play a role as a chaperone for protein folding in the ER. Calumenin was increased in expression in response to ER stress (Lee et al., 2013). Overexpression of this protein led to a decrease in stress mediated signalling events and had an anti-apoptotic effect.

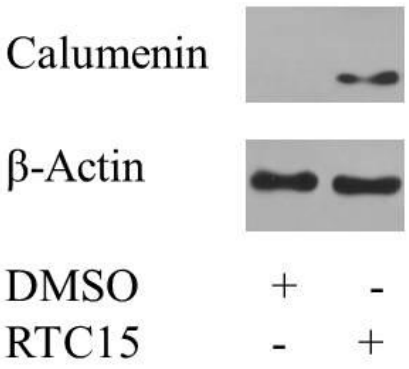

Fig 4.17 Analysis of expression levels of Calumenin.

Representative Western blot depicting expression levels of calumenin in response to DMSO or 10µM RTC-15 overnight. C2C12 cells were treated with DMSO or 10µM RTC-15 overnight. Cells were harvested and lysed in RIPA buffer. Protein concentration was assessed using the PIERCE protein assay and 30µg/ml protein was used per sample. Cell lysate was electrophoresed using a 10% SDS-PAGE gel and protein was subsequently transferred to PVDF membrane. Western blotting analysis was conducted using anti-calumenin specific antibody and β-Actin as a loading control. All analysis was conducted in triplicate.

4.3.5.3 Analysis of decreased phosphorylation of RCN-1:

Another member of the CREC family, RCN-1, showed a 1.3-fold decrease in phosphorylation in response to RTC-15 treatment. RCN-1 is primarily located in the ER and contains multiple EF hand domains. Therefore, it is thought to be involved in calcium handling in the ER (Ozawa and Muramatsu, 1993). Proteins expressed in the ER either contain an ER retention signal peptide or they are secreted from the ER. The Sec61 complex is a protein translocase responsible for the transport of proteins out of the ER. RCN-1 and calumenin were both found to associate with the Sec63p subunit of the Sec61 complex (Tyedmers et al., 2005). This association of RCN-1 and calumenin may prevent efflux of calcium ions as proteins are translocated across the ER membrane. As discussed in section 4.3.5.2, calumenin may have a chaperone like role in the ER. Association of RCN-1 and calumenin with Sec63p may also aid protein folding in the ER lumen.

As no phospho-specific RCN-1 antibodies were available for Western blotting, RCN-1 was first immunoprecipitated from mouse C2C12 cells treated with RTC-15 using a RCN-1 specific antibody. Purified protein was subsequently analysed by SDS-PAGE and Western blotting using general anti-

phospho amino acid antibodies. Fig 4.18 depicts the secondary validation of RCN-1 phosphorylation levels in response to RTC-15. Only the anti-phospho-serine antibody was reactive with RCN-1. Large scale proteomic analysis revealed human RCN-1 to be phosphorylated at threonine 76 (Olsen et al., 2010). Threonine 76 corresponds to serine 70 in the murine version of the protein (Fig 4.19). The human and the murine version of RCN-1 share extensive sequence similarity. Therefore, it is likely that the phosphorylation site is conserved across the two species. It is currently unknown which kinase is responsible for phosphorylation of RCN-1 and what impact a phosphate moiety has on the function of the protein.

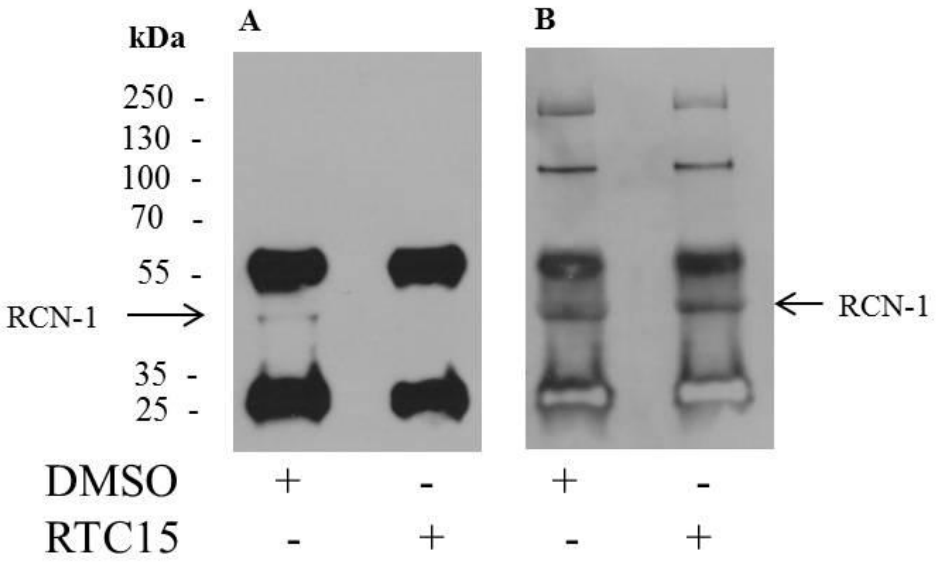

Fig 4.18 Analysis of phosphorylation levels of RCN-1.

Representative Western blot depicting phosphorylation levels of RCN-1 in response to DMSO or 10µM RTC-15 overnight. C2C12 cells were treated with DMSO or 10µM RTC-15 for 16 hours. Cells were harvested and lysed in RIPA buffer. Cell lysate was then incubated with anti-RCN-1 antibody overnight. Immunoprecipitated protein was purified using protein G agarose beads. Purified protein was then electrophoresed using a 10% SDS-PAGE gel and protein was subsequently transferred to PVDF membrane. **A**. Western blot representing total protein immunoblotted with anti-phospho-serine antibody. RCN-1 is a 38 kDa protein. The bands present at 55 kDa and 25 kDa, represent the heavy and light chain of the RCN-1 antibody respectively, which was used in the immunoprecipitation reaction. **B**.Western blot representing total levels of RCN-1 using anti-RCN-1antibody.

```
hRCN1           MARGGRGRRLGLALGLLLALVLAPRVLRAKPTVRKERVVRPDSELGERPPEDNQSFQYDH 60
mRCN1           MARGGR---LGLALGLLLALVLA---LRAKPTVRKERVVRPDSELGERPPEDNQSFQYDH 54
                ******   **************   **********************************

hRCN1           EAFLGKEDSKTFDQLTPDESKERLGKIVDRIDNDGDGFVTTEELKTWIKRVQKRYIFDNV 120
mRCN1           EAFLGKEDSKTFDQLSPDESKERLGKIVDRIDSDGDGLVTTEELKLWIKRVQKRYIYDNV 114
                ***************:****************.****:******* **********:***

hRCN1           AKVWKDYDRDKDDKISWEEYKQATYGYYLGNPAEFHDSSDHHTFKKMLPRDERRFKAADL 180
mRCN1           AKVWKDYDRDKDEKISWEEYKQATYGYYLGNPAEFHDSSDHHTFKKMLPRDERRFKASDL 174
                ************:*******************************************:**

hRCN1           NGDLTATREEFTAFLHPEEFEHMKEIVVLETLEDIDKNGDGFVDQDEYIADMFSHEENGP 240
mRCN1           DGDLTATREEFTAFLHPEEFEHMKEIVVLETLEDIDKNGDGFVDQDEYIADMFSHEDNGP 234
                :*********************************************************:***

hRCN1           EPDWVLSEREQFNEFRDLNKDGKLDKDEIRHWILPQDYDHAQAEARHLVYESDKNKDEKL 300
mRCN1           EPDWVLSEREQFNDFRDLNKDGKLDKDEIRHWILPQDYDHAQAEARHLVYESDKNKDEML 294
                ************:******************************************** *

hRCN1           TKEEILENWNMFVGSQATNYGEDLTKNHDEL 331
mRCN1           TKEEILDNWNMFVGSQATNYGEDLTKNHDEL 325
                ******:************************
```

Fig 4.19 Sequence alignment of human and mouse RCN-1

Comparison of the sequence of human RCN-1 (hRCN1) and mouse RCN-1 (mRCN1) reveals 95% sequence identity. The putative phosphorylation site, highlighted in red, is a very well conserved region with serine 70 of the murine version replacing threonine 76 in the human version. Alignment was performed using ClustalW2.

4.3.5.4 Analysis of decreased phosphorylation of alpha-actinin:

Alpha-actinin, which displayed a 1.4-fold decrease in phosphorylation, is involved in linking cytoskeletal proteins to signalling pathways. It can bind to actin and is responsible for actin bundling (Blanchard et al., 1989). Alpha-actinin is known to be phosphorylated by tyrosine kinases and this phosphorylation event decreases its ability to bind to actin (Otey and Carpen, 2004). Thus, stimulation of cells with RTC-15 leads to a reduction in alpha-actinin phosphorylation rendering the protein more active. This event is necessary for cell motility and muscle contraction. Interestingly, alpha-actinin also contains the EF hand calcium binding motif and increased calcium binding also reduces its binding capacity for actin. As discussed in section 4.3.3.5 alpha-actinin can bind to PDZ and LIM domain containing proteins such as Pdlim1 (Kotaka et al., 2000). Therefore, upon RTC-15 stimulation there appears to be a shift towards increased actin remodelling and structural adaptation.

4.3.5.5 Analysis of increased expression of swiprosin-1:

Swiprosin-1 displayed a 1.2-fold increase in expression in response to RTC-15 treatment. It contains two EF hand domains. The protein was originally identified in lymphocytes and shown to regulate mast cell activation via actin remodelling (Kwon et al., 2013). Swiprosin-1 is found in the cell associated with actin and may also have an actin bundling function (Kwon et al., 2013). It can bind actin in the absence of calcium but its bundling activity is diminished. Therefore, calcium binding increases swiprosin-1 mediated actin bundling. Swiprosin-1 expression is increased in response to PKC activation (Kim et al., 2013b). Targeted down-regulation of PKC isoform expression by siRNA revealed that PKC θ is specifically responsible for regulating swiprosin-1 expression. Therefore, increased PKC activity, induced by RTC-15, could result in elevated expression levels of swiprosin-1.

4.3.6 Analysis of changes in the proteome affecting protein degradation:

Several proteins involved in protein degradation demonstrated changes in response to RTC-15 treatment. This set of proteins includes MHR23A, cathepsin Z and cathepsin B.

4.3.6.1 Analysis of increased expression of MHR23A:

A 1.3-fold increase in MHR23A expression was observed with RTC-15 treatment. MHR23A, also known as Rad23a, is primarily involved in binding poly-ubiquinated proteins and directing them to the proteasome for degradation. It forms part of the Rad4/Rad23 sensor complex involved in DNA damage repair (Dantuma et al., 2009). As a result of inhibition of complex I, excess ROS may be present in the cell. MHR23A increased expression may be acting as a protective mechanism to prevent oxidative injury to the cell and also to direct damaged proteins to the proteasome.

4.3.6.2 Analysis of increased expression of cathepsin Z and cathepsin B:

Both cathepsin Z and cathepsin B belong to the papain family of cysteine proteases located in the lysosome and comprise one of the groups of enzymes responsible for protein degradation (Turk et al., 2012). This family of enzymes are optimally active in the acidic environment of the lysosome. Cathepsins are expressed as inactive pre-proenzymes. The pre-peptide is removed in the ER and only when the pH drops slightly, as occurs in the lysosome, will the pro-enzyme be converted to the active enzyme (Turk et al., 2000). A drop in pH appears to weaken the interaction between the pro-peptide sequence and the catalytic domain of the enzyme. The pro-peptide sequence is then removed by cleavage and degraded. Interestingly, upon RTC-15 treatment overnight the cell culture media is often yellowish compared to the DMSO control, indicative of a slightly acidic pH. Increased levels of the cathepsin proteins as a result of RTC-15 treatment may not be a direct effect on protein expression but rather an increase in proteolytic processing of the enzymes due to a more acidic environment.

4.3.7 Analysis of changes in the proteome affecting other cellular processes:

Expression changes were also noted in several proteins that could not be categorised into the other functional groups. These proteins include ZPR1 and Ser/Thr kinase receptor associated protein (STRAP).

4.3.7.1 Analysis of increased expression of ZPR1:

The zinc finger domain containing-protein, ZPR1 demonstrated a 1.2-fold increase in expression. Co-immunoprecipitation experiments revealed that ZPR1 binds to the cytoplasmic domain of receptor tyrosine kinases, such as the epidermal growth factor (EGF) receptor (Galcheva-Gargova et al., 1998). When the receptor is activated by its ligand, EGF, ZPR1 is dislodged and subsequently translocates to the nucleus. As a result of this process, ZPR1 is thought to convey mitogenic signals from the cytoplasm to the nucleus. Not much is known about the exact function of ZPR1 but it is thought to be involved in normal nucleolar function, as selective knockdown of the gene resulted in decreased pre-rRNA processing (Galcheva-Gargova et al., 1996). Another study demonstrated that selective knockdown of ZPR1 resulted in a total decrease in gene transcription in response to mitogenic signals (Gangwani, 2006). The two processes may be linked. ZPR1 is known to interact with eukaryotic translation elongation factor-1α (eEF-1α) resulting in the translocation of this complex to the nucleus (Gangwani et al., 1998). It is unknown as yet what exact function this protein complex has in the nucleus, though prevention of complex formation resulted in cell cycle arrest. Thus, ZPR1 and eEF-1α may be required for normal cell proliferation in response to mitogenic signals such EGF. Secondary validation by Western blotting confirmed that ZPR1 expression is increased in response to RTC-15 treatment (Fig 4.20).

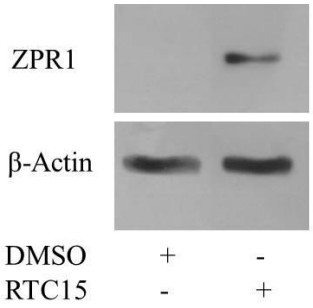

Fig 4.20 Analysis of expression levels of ZPR1.

Representative Western blot depicting expression levels of ZPR1 in response to DMSO or 10μM RTC-15 overnight. C2C12 cells were treated with DMSO or 10μM RTC-15 overnight. Cells were harvested and lysed in RIPA buffer. Protein concentration was assessed using the PIERCE protein assay and 30μg/ml protein was used per sample. Cell lysate was electrophoresed using a 10% SDS-PAGE gel and protein was subsequently transferred to PVDF membrane. Western blotting analysis was conducted using anti-ZPR1 specific antibody and β-Actin as a loading control. All analysis was conducted in triplicate.

4.3.7.2 Analysis of decreased expression of STRAP:

STRAP also known as UNR-interacting protein (Unrip) demonstrated a 1.3-fold decrease in expression. This protein has been shown to bind to the smooth muscle neuron complex (SMN) which is a large oligomeric assembly thought to take part in cellular RNA metabolism. Small nuclear ribonucleoproteins (snRNP) are necessary for the processing of pre-mRNA to mature mRNA and are composed of a small nuclear ribonucleic acid (snRNA) and a core of seven proteins known as sm proteins (Yong et al., 2004). The SMN complex is involved in the assembly of these seven proteins to form the core of the snRNP molecule. In a co-immunoprecipitaton experiment, STRAP was found to associate with the complex (Grimmler et al., 2005). Specific knockdown of STRAP resulted in a decrease in the cytosolic SMN complex and an increase in nuclear localisation. Thus, STRAP may modulate SMN complex compartmentalisation. As a reduction of STRAP expression was observed with RTC-15 treatment, this may reflect an increase in nuclear SMN complex localisation. Interestingly, ZPR1 is required for nuclear translocation of SMN (Ahmad et al., 2012). As described earlier, ZPR1 knockdown results in a decrease in pre-mRNA processing, this could be as a result of decreased SMN complex in the nucleus. An increase in ZPR1 was observed with RTC-15 treatment. Thus, the cellular response to RTC-15 treatment involves an increase in ZPR1, a protein responsible for SMN complex nuclear localisation and a decrease in STRAP, a protein responsible for cytoplasmic retention.

4.4 Conclusions of proteomic profiling of the effect of RTC-15 on C2C12 cells:

Several changes in protein expression and phosphorylation are observed when muscle cells are exposed to the anti-diabetic compound, RTC-15. Secondary validation by Western blotting confirmed some of these changes. In some cases, expression changes observed by Western blotting analysis such as with annexin A2, calumenin and ZPR1, appeared much greater than indicated via 2D electrophoresis. This could be due to differences in sensitivity of the two techniques. 2D electrophoresis and subsequent staining and image analysis is highly reliant on statistical evaluation. Direct assessment of expression level by Western blotting analysis is a much more sensitive method and this could account for the discrepancy between the two techniques. Changes observed in the proteomic profile of the cell may not be a direct effect of RTC-15 but as a result of complex I inhibition and the consequent re-orientation of cellular activity to maintain ATP levels. Complex I inhibition results in inhibition of the ETC in the mitochondrial membrane, an increase in the AMP to ATP ratio and subsequent activation of the AMP sensing molecule, AMPK. In a separate study, this RTC-15 related AMPK activation was demonstrated together with an increase in downstream AS160 phosphorylation, GLUT4 translocation to the plasma membrane and elevated glucose uptake.

The most widely used treatment for type II diabetes is Metformin. The precise mechanism of action of the drug is still under debate, but it is established that Metformin also increases AMPK phosphorylation, thus activating the AMPK signalling cascade, though the activation is weak (Zhou et al., 2001). Exercise mediated glucose uptake also occurs as a result of activation of the AMPK signalling cascade (Cohen, 1978). In addition, activation of AMPK can lead to increased fatty acid oxidation as an alternate energy source (Winder and Hardie, 1996). The exact mechanism of Metformin-induced activation of AMPK is as yet unknown-one potential mechanism of action is complex I inhibition (Owen et al., 2000). Owen et al found that Metformin treatment resulted in complex I inhibition which reduced liver gluconeogenesis while increasing glucose utilisation in other tissues such as muscle. Metformin-induced glucose uptake in peripheral tissues occurs as a result of increased GLUT4 translocation to the plasma membrane (Hundal et al., 1992). The insecticide, rotenone, a known complex I inhibitor also induces GLUT4 translocation to the cell membrane

(Wheeler et al., 1994). Therefore, complex I inhibition stimulates the cell to acquire increased sources of ATP, in an insulin-independent manner.

A large proportion of the proteins identified in this study are associated with metabolic processes. Inhibition of complex I could be initiating a shift towards compensatory mechanisms inside the cell, so that net energy levels are maintained. As this occurs in an insulin-independent fashion, there is great potential for the treatment of insulin resistance and indeed type I diabetes, in a whole animal model. Increases in ECH1 and TPI expression illustrate that the cell is increasing the use of energy sources such as unsaturated fatty acids and glucose. One of the main proteins involved in ATP production, ATP synthase, appears to be increased in expression and this potentially means that ATP synthesis is increased. Increased metabolic activity could result in reduced glucose conversion to fat which could account for the observed decrease in accumulation of fat mass in mice fed a HFD and RTC-15, opposed to mice fed a HFD diet alone. As discussed in section 4.3.6.2, the colour of the cell media was altered with RTC-15 treatment, compared to vehicle control. It suggests that the media is more acidic. A decrease in media pH is indicative of increased metabolic rate. Cathepsin processing is reliant on a decrease in pH. Therefore, this may be the reason for an increase in cathepsin B and Z levels compared to control cells.

Several proteins associated with calcium binding were found to be altered in response to RTC-15. An increase in expression of proteins associated with calcium binding is consistent with an increase in intracellular calcium levels. Upregulated calumenin expression is associated with increased release of calcium from the SR (Jung et al., 2006; Sahoo et al., 2009). Elevated calcium levels are closely associated with the transport of secretory vesicles to the cell membrane (Koenig et al., 1993). In order for increased glucose uptake to occur, increased numbers of the GLUT4 glucose transporter must be present at the plasma membrane. Complex I inhibition appears to initiate GLUT4 translocation to the membrane, but other auxiliary proteins aid this process. As discussed in section 4.3.5.1, troglitazone was shown to increase annexin A2 expression and this was associated with the insulin sensitizing effect of thiazolidinediones (Huang et al., 2004). RTC-15 may act in the same manner; increasing annexin A2 expression would contribute to a higher level of GLUT4 in the plasma membrane.

Globally, RTC-15-induced expression of proteins involved in calcium handling will contribute to increased secretory vesicle fusion with the plasma membrane.

In conjunction with calcium handling proteins, several cytoskeletal proteins were observed to be affected by RTC-15. The two events may be intrinsically linked. Cytoskeletal proteins play an integral role in the fusion of secretory vesicles to the plasma membrane and many are regulated by calcium. Actin re-modelling is a necessary event to allow membrane fusion of secretory vesicles. Actin rearrangement before vesicle translocation has been demonstrated in several cell types (Koffer et al., 1990; Lang et al., 2000). With RTC-15 treatment, there was an increase in inhibitory phosphorylation of calponin, which would allow actin contraction. There was also a decrease in alpha-actinin phosphorylation, rendering the protein more active and leading to increased actin bundling. Increased calcium binding to swiprosin can also lead to increased actin bundling. Foster et al demonstrated that several cytoskeletal proteins were co-purified with GLUT4 upon insulin stimulation (Foster et al., 2006), most notably alpha-actinin 1 and 4. Thus, cytoskeletal proteins are crucial to enable increased GLUT4 translocation to the plasma membrane. Thus, upon RTC-15 stimulation, there is an alteration in proteins involved in actin remodelling, facilitating the translocation of secretory vesicles to the cell membrane.

The increase observed in proteins associated with protein biosynthesis and protein degradation could simply be as a result of increased metabolic rate in the cell. However, some proteins may be increased in expression as a result of activation of RA responsive genes. A proteomic study conducted by Wang et al showed that hnRNP H2 and EfTu expression was increased with RA treatment (Wang et al., 2007). These proteins are involved in transcription regulation. An increase in such regulatory proteins could be as a result of RTC-15 mediated effects on the retinoid system and its influence on gene transcription.

RTC-15 treatment resulted in increased ZPR1 expression and decreased STRAP expression. There appears to be a shift in proteins involved in cytosolic localisation of SMN complex to proteins involved in nuclear localisation of the complex. As several proteins involved in protein biosynthesis

were altered in response to RTC-15, this shift could be as a result of a requirement for increased mRNA processing in the nucleus. The SMN complex is responsible for the assembly of snRNPs which are essential for the processing of pre-mRNA to mature mRNA (Yong et al., 2004).

Ciapin-1 expression was decreased in response to RTC-15 treatment. Interestingly, PKC δ and θ activity was increased in ciapin-1 knockout cells (Saito et al., 2011a). Several known phosphorylation targets of PKC were found to have increased phosphorylation levels in response to RTC-15. Inhibition of ciapin-1 expression could be causing an increase in PKC activity which is reflected in the observed increase in phosphorylation of calponin-3 and eIF-6. In two separate studies, calponin was found to be phosphorylated by the calcium dependent PKC kinases, PKC α and ε, respectively (Patil et al., 2004) (Winder and Walsh, 1990). eIF-6 is phosphorylated by PKCβII (Ceci et al., 2003). Swiprosin-1 expression was also found to be increased in the cell which is directly linked to increased PKC θ activity (Kim et al., 2013b).

If PKC activity is increased in the cell in response to RTC-15 treatment, the exact pathways affected would be highly reliant on which isoform of the enzyme is activated. The downstream targets of several isoforms of PKC (α, βII, δ, ε and θ) appear altered in response to RTC-15. A rise in intracellular calcium is a well-established mediator of PKC activation and this kinase is highly involved in cytoskeletal remodelling (Larsson, 2006). The isoforms of PKC which show evidence of activation in this study are known to phosphorylate substrates which are involved in cytoskeletal rearrangement. Therefore, if RTC-15 is activating PKC, this kinase may contribute to vesicle trafficking to the cell membrane. PKC βII facilitates GLUT4 trafficking to the membrane via activation of myristoylated, alanine-rich C kinase substrate (MARCKS) (Chappell et al., 2009). In addition, Park et al demonstrated that PKC ε is necessary for depolarisation-induced translocation of vesicles to the cell membrane (Park et al., 2006). PKC θ may have a direct effect on the actin cytoskeleton by increasing swiprosin-1 expression (Kim et al., 2013b). Thus, increased PKC activity may be the cause of several changes in the cytoskeleton, potentiating the movement of vesicles to the cell membrane. Further study of the activation state of PKC in response to RTC-15 is necessary.

Chapter 5

Structural and functional characterisation of the C-Terminus of STRA6

5.1 Introduction:

The recombinant expression of membrane proteins is integral to our studies on how these proteins are organised in the membrane and how they function. Membrane proteins contain large stretches of hydrophobic residues to allow them to fold into the lipid bi-layer of the cell membrane. The distribution of distinct stretches of hydrophobic amino acids poses a significant problem for the expression, purification and subsequent structural analysis of membrane proteins. In order to avoid this problem, one strategy has evolved to look at isolated hydrophilic domains of a membrane protein. These hydrophilic regions lie either in the intracellular region or exposed to the extracellular environment. This makes them attractive domains to study in relation to protein-protein interactions.

5.1.1 STRA6 topology:

As discussed in section 1.2.5 there has been much debate over the exact topology of STRA6. Topology modelling experiments have yielded varying results. An experimental analysis indicated a 9 transmembrane structure (Kawaguchi et al., 2008b). By insertion of a Myc epitope tag into putative extra and intracellular regions, the localisation of distinct regions of the receptor was assessed. 9 transmembrane regions were observed along with an extracellular N-terminus and an intracellular C-terminus. The study predicted the C-terminal region of STRA6 to be a large intracellular domain of approximately 170 amino acids.

5.1.2 Inter-species conservation of the C-Terminal region:

STRA6 is not homologous to any known protein and only exists in vertebrate species. It is highly conserved across species, with several regions in the C-terminus particularly so. The putative phosphorylation site located in the C-terminus, discussed in section 1.2.8, is very well conserved across species (Fig 5.1) and through deleterious mutations appears to be vital for activity. This would suggest that this region is integral to the structure and function of the whole protein.

```
478  LTVALAVILQNIAANWIFLRTHHGYPELTNRRMLCVATFLLFPINMLVGAIMAVWRVLIS  537  O70491   STRA6_MOUSE
478  LTLALAVTLQNAAAHWAFLDTHHGRPGLTNRRALYAATFLLFPVNVLVGTMVAAWRVLLS  537  Q0V8E7   STRA6_BOVIN
478  LTLVLAVILQNIAANWVFLESHHGYPELTNRRMLCVATFLLFPINMLVGAIMAIWRVLLS  537  Q4QR83   STRA6_RAT
477  LTLALAVILQNMAAHWVFLETHDGHPQLTNRRVLYAATFLLFPLNVLVGAMVATWRVLLS  536  Q9BX79   STRA6_HUMAN
     **:.*** *** **.* ** :*.* * ***** * .*******:*:***:::* ****:*

538  SLYNTVHLGQMDLSLLPQRAASLDPGYHTYQNFLRIEASQSHPGVIAFCALLLHAPSPQP  597  O70491   STRA6_MOUSE
538  ALYNAVHLGRMDLSLLPLRAATLDPGYHTYCNFLRMEASQSHPAATAFCALLLRTQRP--  595  Q0V8E7   STRA6_BOVIN
538  SLYNTVHLGQMDLSLLPQRAASLDPGYHTYRNFLRIEASQSHPGVIAFCALLLHVPSPQP  597  Q4QR83   STRA6_RAT
537  ALYNAIHLGQMDLSLLPPRAATLDPGYYTYRNFLKIEVSQSHPAMTAFCSLLLQAQSLLP  596  Q9BX79   STRA6_HUMAN
     :***::***:******* ***:*****:** ***::*.*****.  ***:***:.

598  RPPLAPQDSLRPAEEEEGMQLLQTKDLMAKGAGHKGSQSRARWGLAYTLLHNPSLQAFRK  657  O70491   STRA6_MOUSE
596  KPRATPQDGLRLGEEEEGIQLLQTKDLVAKGAGPRARQGRARWGLAYTLLHNPALQAFRK  655  Q0V8E7   STRA6_BOVIN
598  QPPLAPQDSLRPAAEEEGMQLLQTKDLMAKGAGPKGSRSRARWGLAYTLLHNPSLQAFRK  657  Q4QR83   STRA6_RAT
597  RTMAAPQDSLRPGEEDEGMQLLQTKDSMAKGARPGASRGRARWGLAYTLLHNPTLQVFRK  656  Q9BX79   STRA6_HUMAN
     :   :***.** . *:**:******* :****   . :.*************:**.***

658  AALTSAKANGTQP  670  O70491   STRA6_MOUSE
656  TALPGARPNGAQP  668  Q0V8E7   STRA6_BOVIN
658  AALTSAKANGTQP  670  Q4QR83   STRA6_RAT
657  TALLGAN--GAQP  667  Q9BX79   STRA6_HUMAN
     :** .*.  *:**
```

Fig 5.1 Sequence alignment of the C-terminal region of STRA6 across *Mus musculus, Bos taurus, Rattus norvegicus* and *Homo sapiens* species.

The amino acid sequence of human STRA6 shares >71% sequence identity with all of the species listed above. Areas of extensive conserved residues exist in the C-terminal region. The putative SH2 domain sequence, highlighted in red, is a very well conserved region. Alignment performed using Blast/Uniprot.

5.1.3 The function of the C-terminus:

As the C-terminus is a large intracellular domain, it is an attractive region to study protein-protein docking. Berry et al have demonstrated that the C-terminus is phosphorylated at T644 and is a potential SH2 domain containing the sequence YTLL (Berry et al., 2011). Experimentally, they have shown that STRA6 interacts with JAK2 at the SH2 domain. In addition, mutational analysis of this region diminished the ability of STRA6 to bind to CRBP (Berry and Noy, 2012). This residue may be a direct interaction site for CRBP or have some structural influence on a neighbouring docking site. Increasingly, it is becoming established that membrane proteins form oligomeric structures in the cell membrane. Preliminary experimental data conducted in our lab also suggests that STRA6 occurs as an oligomer. The C-terminus could be a potential interaction site for the formation of an ordered quaternary structure.

5.1.4 Fusion tags to aid protein expression and purification:

As domains of a membrane protein are usually part of a large, complex structure, often it is necessary to tether these regions to a fusion protein to aid solubility of the protein. Fusion tags have been used for decades as a strategy to allow proteins to both fold properly and remain soluble. Originally fusion proteins were utilised to facilitate the detection and purification of the partner protein. It was soon realised that some fusions can vastly improve yields of the desired protein. The most commonly used ones are green fluorescent protein (GFP), glutathione s-transferase (GST), maltose binding protein (MBP), and thioredoxin (Trx). For this study, the MBP tag was utilised. MBP is natively expressed in *E. coli* making it an ideal fusion protein for soluble expression. It has outperformed many other tags in relation to yields of soluble protein (Kapust and Waugh, 1999). The tag also allows for the affinity purification of the fusion protein using amylose resin.

Aims and Objectives:

Analysis of the structure of a membrane protein is critical to gain insights as to how the protein functions. Expression and purification of a full length membrane protein can be a very high risk approach to gain structural information. A more cautious approach is to analyse the structure of particular domains of interest. The C-terminal domain of STRA6 is a large intracellular region and has a size and predicted structure to suggest it could represent an independently folding domain. It is a prime candidate for a protein-protein interaction site, due to its large size and intracellular location. It is a highly conserved region across species highlighting its evolutionary importance. This domain of STRA6 is a known phosphorylation site, which may be a prime target for interacting proteins.

The C-terminus of STRA6 was expressed in *E. coli* for the purpose of structural and functional analysis. This chapter describes the optimisation of expression, purification and structural characteristics of soluble C-terminus generated as a fusion protein with MBP.

Potential protein-protein interactions of the C-terminal domain were also explored by use of co-purification strategies and chemical crosslinking.

5.2 Materials and Methods:

There is some disagreement as to whether the C-terminus begins at threonine 497 or leucine 535. Incorporation of residues 497 through to 535 as part of the C-terminal domain places a significantly hydrophobic region at the N-terminus of this sequence (Kawaguchi et al., 2008a). Previous experimental analysis of expression of the C-terminus of STRA6 consisting of residues 497-667 revealed that the protein was largely insoluble (unpublished data). By truncating this region to consist of residues 535 to 667, a more soluble version of the protein was generated. This could mean that residues 497-535 are part of the last transmembrane sequence. Indeed, the topology modelling software PredictProtein predicts that residues 517 through to 536 form a transmembrane region (Fig 5.2).

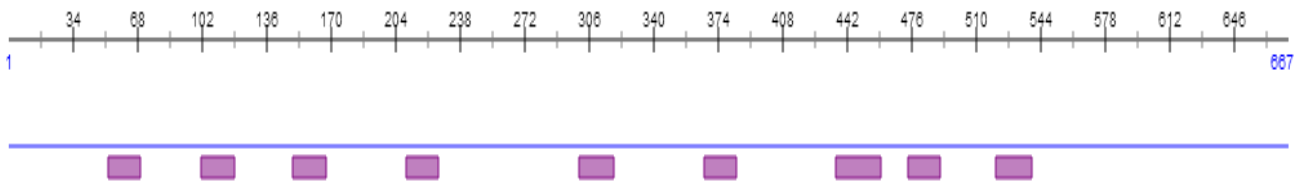

Fig 5.2 Topology model of human STRA6 generated using PredictProtein.

PredictProtein generated a 9 transmembrane topology model of STRA6. Predicted transmembrane regions are highlighted in purple corresponding to the residue numbers above. A transmembrane region was predicted for residues 517 to 536 in accordance with previous experimental findings that inclusion of this sequence generated an insoluble version of the C-terminus of STRA6.

5.2.1 Molecular cloning:

All experimental analysis in this study was conducted using the C-terminal sequence consisting of residues 535 through to 667. From the previous experimental study the C-terminus of STRA6, consisting of these residues, was cloned into a pGEX-4T-3 plasmid, conjugated to a GST tag. As GST can form homodimers *in vivo* (Edwards et al., 2000) a different epitope tag was utilised. To improve expression and purification of the C-terminus of STRA6 a new construct was designed to include an N-terminal MBP fusion tag. The plasmid used for the entire study was pET-30a (Fig 5.3).

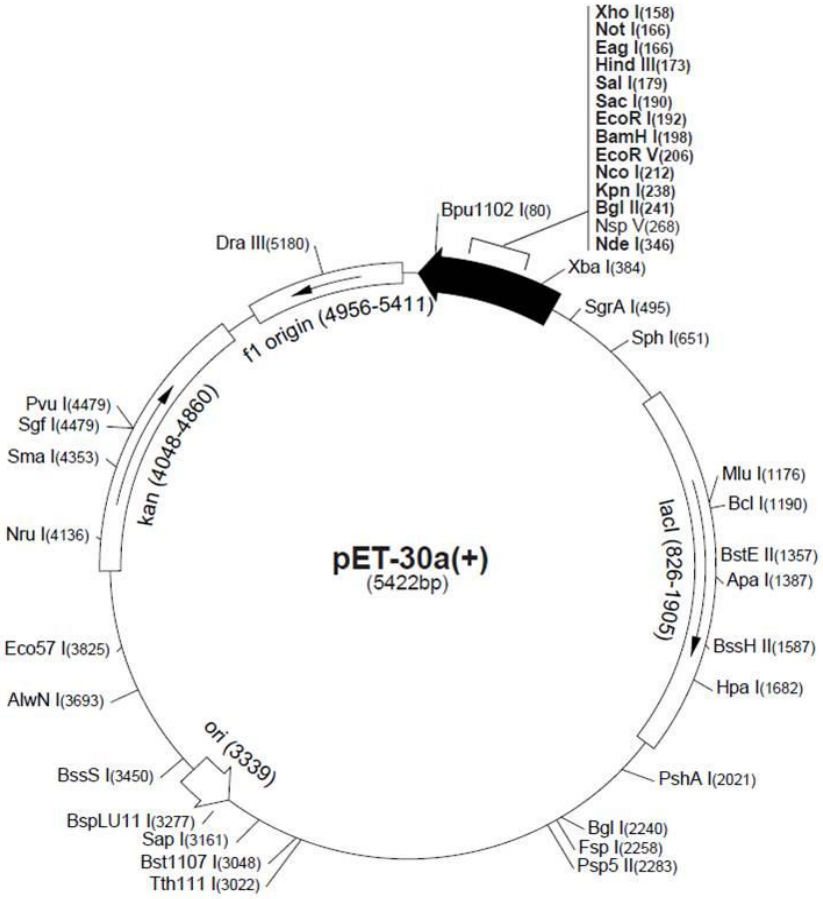

Fig 5.3 Expression plasmid pET-30a.

Vector map of the bacterial expression plasmid pET-30a. The plasmid contains a kanamycin resistance marker. Gene expression is under control of a T7 lac promoter, inducible by addition of IPTG into the culture media. Taken from the pET system manual, Novagen.

5.2.2 Insertion of MBP into pET-30a:

The pMAL-c5E plasmid from New England Biolabs (N8110) was used as the DNA template for MBP. This plasmid lacks the signal sequence that directs MBP to the periplasmic space, i.e. MBP would be expressed in the cytosol. MBP was cloned first into the pET-30a plasmid using the NdeI and KpnI restriction enzymes. A FLAG tag was incorporated at the 3'end of MBP.

The primers used were:

5'-AAA TCG AGC ATA TGA AAA TCG AAG AAG GTA AAC TGG TAA TCT GGA TTA ACG GCG ATA AAG GCT-3' which incorporates a NdeI restriction site and start codon (underlined) and bases 1 through 49 of the MBP DNA sequence. An 8 residue overhang was included at the 5' end of the sequence to aid restriction digestion of the PCR product by NdeI.

3'-TCG TAC GGT ACC CTT ATC GTC GTC ATC CTT GTA ATC ATT AGT CTG CGC GTC TTT CA-5' which incorporates a KpnI restriction site (underlined) a FLAG tag and the final 20 residues of the MBP DNA sequence. A 6 residue overhang was included at the 3' end of the sequence to aid restriction digestion of the PCR product by KpnI.

The unique 1,151 base pair PCR product was subsequently purified from an agarose gel as described in section 2.8.2, digested using the NdeI and KpnI restriction enzymes and purified once again. The digested, purified insert was then ligated into the similarly digested pET-30a destination plasmid. Successful ligation of the PCR product into the plasmid was confirmed by digestion and verified by sequencing (Eurofins). This plasmid was subsequently used as a control MBP-FLAG expression plasmid.

5.2.3 Sequence verification of MBP in pET30a:

Sequences were aligned using ClustalW2 (Fig 5.4). The sequence was verified using the T7 promoter primer and the T7 terminator primer.

T7 Promoter sequence verification

```
MBP-pET30a      MKIEEGKLVIWINGDKGYNGLAEVGKKFEKDTGIKVTVEHPDKLEEKFPQVAATGDGPDI 60
T7Promoter      MKIEEGKLVIWINGDKGYNGLAEVGKKFEKDTGIKVTVEHPDKLEEKFPQVAATGDGPDI 60
                ************************************************************

MBP-pET30a      IFWAHDRFGGYAQSGLLAEITPDKAFQDKLYPFTWDAVRYNGKLIAYPIAVEALSLIYNK 120
T7Promoter      IFWAHDRFGGYAQSGLLAEITPDKAFQDKLYPFTWDAVRYNGKLIAYPIAVEALSLIYNK 120
                ************************************************************

MBP-pET30a      DLLPNPPKTWEEIPALDKELKAKGKSALMFNLQEPYFTWPLIAADGGYAFKYENGKYDIK 180
T7Promoter      DLLPNPPKTWEEIPALDKELKAKGKSALMFNLQEPYFTWPLIAADGGYAFKYENGKYDIK 180
                ************************************************************

MBP-pET30a      DVGVDNAGAKAGLTFLVDLIKNKHMNADTDYSIAEAAFNKGETAMTINGPWAWSNIDTSK 240
T7Promoter      DVGVDNAGAKAGLTFLVDLIKNKHMNADTDYSIAEAAFNKGETAMTINGPWAWSNIDTSK 240
                ************************************************************
```

T7 Terminator sequence verification

```
MBP-pET30a      MKIEEGKLVIWINGDKGYNGLAEVGKKFEKDTGIKVTVEHPDKLEEKFPQVAATGDGPDI 60
T7reverse       ------------------------------------------------------------


MBP-pET30a      IFWAHDRFGGYAQSGLLAEITPDKAFQDKLYPFTWDAVRYNGKLIAYPIAVEALSLIYNK 120
T7reverse       -----------------------------LYPFTWDAVRYNGKLIAYPIAVEALSLIYNK 31
                                              ******************************

MBP-pET30a      DLLPNPPKTWEEIPALDKELKAKGKSALMFNLQEPYFTWPLIAADGGYAFKYENGKYDIK 180
T7reverse       DLLPNPPKTWEEIPALDKELKAKGKSALMFNLQEPYFTWPLIAADGGYAFKYENGKYDIK 91
                ************************************************************

MBP-pET30a      DVGVDNAGAKAGLTFLVDLIKNKHMNADTDYSIAEAAFNKGETAMTINGPWAWSNIDTSK 240
T7reverse       DVGVDNAGAKAGLTFLVDLIKNKHMNADTDYSIAEAAFNKGETAMTINGPWAWSNIDTSK 151
                ************************************************************

MBP-pET30a      VNYGVTVLPTFKGQPSKPFVGVLSAGINAASPNKELAKEFLENYLLTDEGLEAVNKDKPL 300
T7reverse       VNYGVTVLPTFKGQPSKPFVGVLSAGINAASPNKELAKEFLENYLLTDEGLEAVNKDKPL 211
                ************************************************************

MBP-pET30a      GAVALKSYEEELVKDPRIAATMENAQKGEIMPNIPQMSAFWYAVRTAVINAASGRQTVDE 360
T7reverse       GAVALKSYEEELVKDPRIAATMENAQKGEIMPNIPQMSAFWYAVRTAVINAASGRQTVDE 271
                ************************************************************

MBP-pET30a      ALKDAQTNDYKDDDDK---------------------------------------- 376
T7reverse       ALKDAQTNDYKDDDDKGTDDDDKAMADIGSEFELRRQACGRTRAPPPPPLRSGCQSP 328
                ***************
```

Fig 5.4 Validation of the MBP sequence in the pET30a expression plasmid.

Verification of the presence of the sequence for MBP in the correct position in the pET30a expression plasmid. Sequence alignment conducted using ClustalW2 and the T7 promoter and T7 reverse promoter primers.

5.2.4 Completion of the MBP-C-Term expression plasmid:

Once MBP was successfully inserted into the plasmid, the DNA sequence encoding the C-terminal region of STRA6 (residues 535-667) was obtained from the previous pGEX-4T-3 C-term expression plasmid using the BamHI and EcoRI restriction enzymes. The insert taken from the pGEX-4T-3 plasmid also contained a 3' 6XHistidine sequence tag and a stop codon. Using the combination of BamHI and EcoRI restriction enzymes, the enterokinase cleavage site between the MBP fusion tag and the C-term remained intact (see fig 5.5), to allow for removal of the MBP tag. The unique 430 base pair digestion product was subsequently purified from an agarose gel as described in section 2.8.2. The digested, purified insert was then ligated into the similarly digested pET-30a destination plasmid already containing the MBP DNA sequence. Successful ligation of the insert into the plasmid was confirmed by digestion and verified by sequencing (Eurofins).

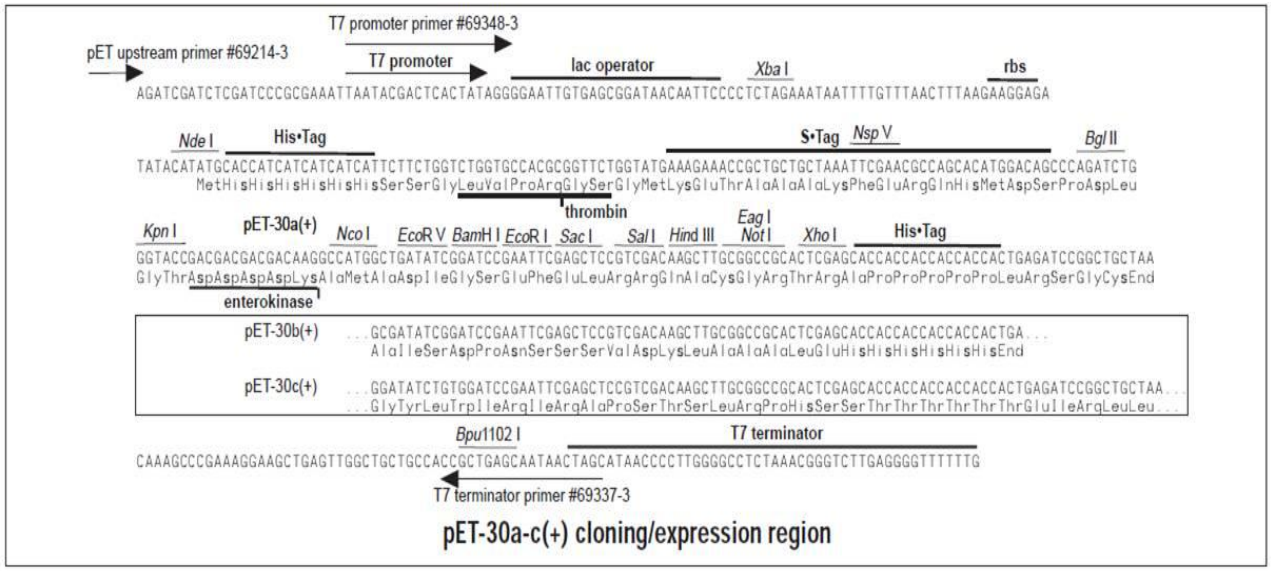

Fig 5.5 Cloning region of the pET-30a plasmid.

Map of the cloning region of the bacterial expression plasmid pET-30a. Insertion of the coding sequence for MBP using the NdeI and KpnI restriction sites removed the sequence of the His and Strep epitope tags. Insertion of the DNA sequence for the C-terminus of STRA6 using the BamHI and EcoRI restriction sites, allowed for the preservation of the enterokinase cleavage site between the MBP fusion tag and the C-term. Taken from the pET system manual, Novagen.

5.2.5 Sequence verification of the C-Terminus of STRA6 in pET30a:

Sequences were aligned using ClustalW2 (Fig 5.6). The sequence was verified using the T7 terminator primer. Following sequence verification of the plasmid construct, BL21 cells supplied by Invitrogen (44-0048) were transformed with the pET30a-MBP-C-term fusion plasmid as described in section 2.8.5.

```
C-Term-pET30a      LSALYNAIHLGQMDLSLLPPRAATLDPGYYTYRNFLKIEVSQSHPAMTAFCSLLLQAQSL 60
T7Term             LSALYNAIHLGQMDLSLLPPRAATLDPGYYTYRNFLKIEVSQSHPAMTAFCSLLLQAQSL 60
                   ************************************************************

C-Term-pET30a      LPRTMAAPQDSLRPGEEDEGMQLLQTKDSMAKGARPGASRGRARWGLAYTLLHNPTLQVF 120
T7Term             LPRTMAAPQDSLRPGEEDEGMQLLQTKDSMAKGARPGASRGRARWGLAYTLLHNPTLQVF 120
                   ************************************************************

C-Term-pET30a      RKTALLGANGAQPHHHHHH---------------------------- 139
T7Term             RKTALLGANGAQPHHHHHHEFELRRQACGRTRAPPPPPLRSGCQSPK 167
                   ******************
```

Fig 5.6 Validation of the presence of the sequence of the C-terminal domain of STRA6 in the pET30a expression plasmid.

Verification of the presence of the sequence for the C-terminal domain of STRA6 in the correct position in the pET30a expression plasmid. Sequence alignment conducted using ClustalW2 and the T7 reverse promoter primer.

5.2.6 TEV MBP-C-Term plasmid:

Due to problems with enterokinase cleavage efficiency of the MBP-C-term fusion protein, a new plasmid was designed containing a TEV protease cleavage site. The TEV cleavage site amino acid sequence is ENLYFQG. The previously generated plasmid was used as a template for PCR and a new reverse primer was designed to incorporate the TEV sequence between the MBP and C-term sequences respectively.

The primers used were:

5’-AAA TCG AGC ATA TGA AAA TCG AAG AAG GTA AAC TGG TAA TCT GGA TTA ACG GCG ATA AAG GCT-3’ which incorporates a NdeI restriction site and start codon (underlined) and bases 1 through 49 of the MBP DNA sequence. An 8 residue overhang was included at the 5’ end of the sequence to aid restriction digestion of the PCR product by NdeI.

3'-GGC TTA GGT ACC GCC CTG AAA ATA CAG GTT TTC CTT ATC GTC GTC ATC C -5' which incorporates a KpnI restriction site (underlined) a TEV cleavage site (highlighted) and a FLAG tag. A 6 residue overhang was included at the 3' end of the sequence to aid restriction digestion of the PCR product by KpnI.

The unique 1,172 base pair PCR product was subsequently purified from an agarose gel as described in section 2.8.2, digested using the NdeI and KpnI restriction enzymes and purified once again. The digested, purified insert was then ligated into the similarly digested pET-30a destination plasmid which already contained the C-terminus. Successful ligation of the PCR product into the plasmid was confirmed by digestion and verified by sequencing (Eurofins) using the T7 terminator primer.

Sequencing results were compared using ClustalW2 (Fig 5.7). After verification BL21 cells were transformed with the pET30a-MBP-TEV-C-Term plasmid as described in section 2.8.5 and subsequently used for all expression experiments.

```
pET30a-MBP-TEV-C-Term      FKGQPSKPFVGVLSAGINAASPNKELAKEFLENYLLTDEGLEAVNKDKPL 300
T7Term                     -----------------NAASPNKELAKEFLENYLLTDEGLEAVNKDKPL 33
                                            ********************************

pET30a-MBP-TEV-C-Term      GAVALKSYEEELVKDPRIAATMENAQKGEIMPNIPQMSAFWYAVRTAVIN 350
T7Term                     GAVALKSYEEELVKDPRIAATMENAQKGEIMPNIPQMSAFWYAVRTAVIN 83
                           **************************************************

pET30a-MBP-TEV-C-Term      AASGRQTVDEALKDAQTNDYKDDDDKENLYFQGGTDDDDKAMADIGSLSA 400
T7Term                     AASGRQTVDEALKDAQTNDYKDDDDKENLYFQGGTDDDDKAMADIGSLSA 133
                           **************************************************

pET30a-MBP-TEV-C-Term      LYNAIHLGQMDLSLLPPRAATLDPGYYTYRNFLKIEVSQSHPAMTAFCSL 450
T7Term                     LYNAIHLGQMDLSLLPPRAATLDPGYYTYRNFLKIEVSQSHPAMTAFCSL 183
                           **************************************************

pET30a-MBP-TEV-C-Term      LLQAQSLLPRTMAAPQDSLRPGEEDEGMQLLQTKDSMAKGARPGASRGRA 500
T7Term                     LLQAQSLLPRTMAAPQDSLRPGEEDEGMQLLQTKDSMAKGARPGASRGRA 233
                           **************************************************

pET30a-MBP-TEV-C-Term      RWGLAYTLLHNPTLQVFRKTALLGANGAQPHHHHHH 536
T7Term                     RWGLAYTLLHNPTLQVFRKTALLGANGAQPHHHHHH 269
                           ************************************
```

Fig 5.7 Validation of the insertion of the TEV protease cleavage sequence in the pET30a expression plasmid.

Verification of the presence of the cleavage sequence for TEV protease in the correct position in the pET30a expression plasmid. The TEV protease cleavage site is highlighted in yellow. Sequence alignment conducted using ClustalW2 and the T7 reverse promoter primer.

5.2.7 Expression of the MBP C-Term fusion protein:

Following a small expression trial to ascertain optimal expression parameters, the MBP-C-term fusion protein was routinely expressed as described in section 2.9.4. Briefly, single colonies of BL21 *E. coli* cells containing the pET-30a MBP-C-term expression plasmid were suspended in 10mL TB media for overnight culture at 37^{o}C, with shaking (225-250 rpm). Following overnight incubation, cultures were diluted 1:100 into fresh TB media and grown to an optical density (OD600nm) of 0.6. Protein expression was induced by the addition of 0.1mM IPTG and incubated at room temperature overnight.

Collected cell pellets were lysed as described in section 2.9.4. The soluble fraction was retained for subsequent purification of the protein of interest. Samples from each stage of the initial protein expression and purification of MBP-C-term were retained and stored at -20^{o}C for subsequent analysis by SDS-PAGE and Western blotting as described in section 2.7.1 and 2.7.5 respectively.

5.2.8 Protein purification:

The MBP-C-Term fusion protein was purified using affinity chromatography. All purification experiments were conducted at 4^{o}C with protease inhibitors to prevent protein degradation and or aggregation. Following purification, protein concentrations were determined using absorbance at 280nm.

<u>Amylose Resin Affinity Chromatography:</u>

Due to the high affinity of MBP for amylose, purification using this resin was the method of choice during early phases of this study. Subsequent analysis of contaminants revealed that a large proportion of native MBP was purified along with the C-term fusion protein. In later phases of this study, to eliminate this problem, Ni-NTA affinity chromatography was conducted prior to amylose affinity chromatography. In each case the method used to purify the protein was the same.

Briefly, 2mL of packed amylose resin per 400mL of original bacterial culture was washed with 5 bed volumes of PBS. The resin was then incubated with the soluble portion of the bacterial cell lysate or Ni-NTA eluate, for 90 minutes at 4^{o}C with constant rotation. Resin was then collected by gravity flow using 5mL disposable columns. Collected resin was washed with ten bed volumes of ice-cold wash buffer as described in section 2.9.4. Protein was eluted with 3 bed volumes of ice-cold wash buffer supplemented with 20% glycerol (v/v) and 10mM maltose. Eluate was assessed for protein concentration using absorbance at 280nm and either concentrated for size exclusion chromatography or stored as aliquots at -20^{o}C.

Ni-NTA Affinity Chromatography:

The MBP-C-term fusion protein was designed to incorporate a C-terminal 6XHistidine tag. This would allow for a double purification strategy and for purification of cleaved protein from the MBP fusion tag. Briefly, 2mL of packed amylose resin per 400mL of original bacterial culture was washed with 5 bed volumes of PBS. The resin was then incubated with the soluble portion of the bacterial cell lysate for 90 minutes at 4^{o}C with constant rotation. Resin was then collected by gravity flow using 5mL disposable columns. Collected resin was washed with ten bed volumes of ice-cold wash buffer as described in section 2.9.4. Protein was eluted with 3 bed volumes of ice-cold wash buffer supplemented with 20% glycerol (v/v) and 250mM imidazole. Eluate was then purified once more using amylose affinity chromatography, as described above.

5.2.9 TEV cleavage of the MBP-C-Term fusion protein:

Following a brief optimisation trial, TEV cleavage of the MBP-C-term fusion protein was routinely conducted as follows. 1µl of halo-TEV protease supplied by Promega (G6601) was used per 100µg of purified MBP-C-term. The cleavage reaction was then incubated with rotation at room temperature for 16 hours. An aliquot of the cleavage reaction was retained to assess cleavage efficiency by SDS-PAGE and Western blotting. Cleaved C-terminus was then purified away from the cleavage reaction by Ni-NTA affinity chromatography as described in section 5.2.8. Eluted protein was concentrated and analysed using size exclusion chromatography.

5.2.10 Detection of protein expression:

Protein expression was analysed by SDS-PAGE, gel-staining and Western blotting as described previously. Western blots were probed with either anti-FLAG or anti-His antibodies. Routinely, anti-FLAG antibody was used at a 1:1,000 dilution in PBS with 0.05% (v/v) Tween-20 overnight at 4^{o}C. Anti-His-HRP antibody was used at a 1:10,000 dilution in PBS with 0.05% (v/v) Tween-20 and 2% (w/v) non-fat dried milk, either overnight at 4^{o}C or for 2 hours at room temperature.

For the purpose of protein interaction studies the following antibodies were also used:

Anti-Ha antibody at a 1:1,000 dilution in PBS with 0.05% (v/v) Tween-20 and 2% (w/v) non-fat dried milk, overnight at 4^{o}C.

Anti-CRBP antibody at a 1:500 dilution in PBS with 0.05% (v/v) Tween-20 overnight at 4^{o}C.

5.3 Results:

5.3.1 Expression of MBP-C-Term in BL21 *E. coli* cells:

E. coli BL21 cells are an ideal expression host to produce large amounts of protein in an inexpensive manner. Unfortunately, some proteins may form insoluble aggregates, otherwise known as inclusion bodies within the *E. coli* cell. One of the first tasks of bacterial protein expression is to assess whether the protein is in the insoluble fraction of the cell lysate or in the soluble fraction. Following a brief expression optimisation trial, the insoluble and soluble fractions were assessed for the presence of MBP-C-term. Fortunately, the majority of expressed MBP-C-term was present in the soluble fraction and purified away from *E. coli* contaminants (Fig 5.8).

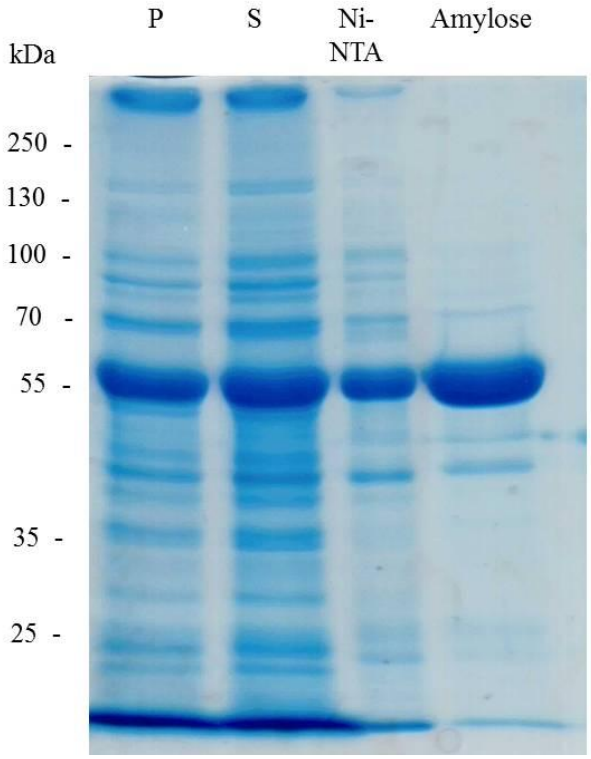

Fig 5.8 Expression and purification of MBP-C-term.

Coomassie brilliant blue stained SDS-PAGE gel depicting the purification of 59kDa MBP-C-term from *E. coli* lysate. The first lane represents insoluble protein (P) retained in a high speed centrifugation pellet. The second lane represents the soluble protein (S) present in the supernatant of a high speed centrifugation. The third lane represents all purified protein following incubation of cell lysate with Ni-NTA affinity chromatography resin. The last lane represents all purified protein following incubation of Ni-NTA eluate with amylose affinity chromatography resin.

5.3.2 Size Exclusion Chromatography:

Once soluble protein was expressed and purified structural characteristics of the protein were assessed. Size exclusion chromatography (SEC) is an ideal method to determine the molecular weight of a protein in its native conformation. It may reveal valuable insights as to the quaternary structure of the protein i.e. whether it forms a higher molecular weight species such as a dimer, trimer or tetramer. For the present study, two size exclusion columns were used, the Superose 6 10/300 column (17-5172-01) and the Superdex 200 10/300 GL column (17-5175-01) supplied by GE coupled to an AKTA purifier system supplied by Amhersham Biosciences. The Superose 6 column is composed of crosslinked agarose. The Superdex 200 column is composed of crosslinked agarose and dextran. Molecular weight standards were run on both columns to obtain an elution profile to compare the protein of interest against (Fig 5.9 and 5.10). Purified proteins were concentrated and passed through the size exclusion column to assess the native molecular weight. Absorbance at 280nm was utilised as a method to detect eluted protein. After 7mL of the mobile phase had passed through the column samples were taken every 0.5mL eluted from the column. Every second sample was assessed by Western blot for the presence of the desired protein.

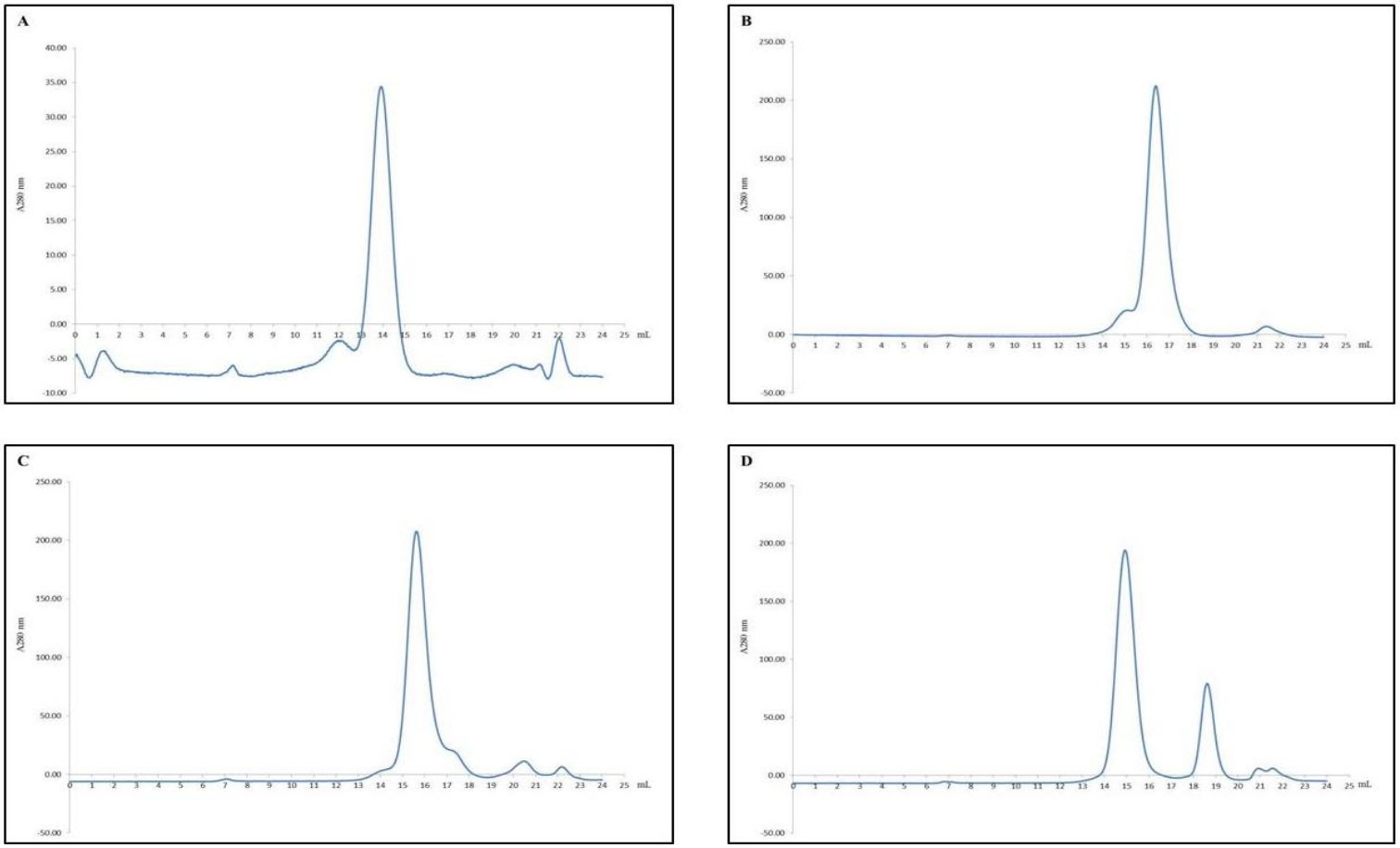

Fig 5.9 Molecular weight standards utilised to calibrate the Superose 6 column.

Absorbance at 280nm was used to analyse protein eluting from the column per mL of mobile phase eluted from the column. **A**. The 440kDa molecular weight standard, ferritin eluting at approximately 14mL. **B**. The 66kDa molecular weight standard, BSA, eluting at approximately 16mL. **C**. The 150kDa molecular weight standard, alcohol dehydrogenase, eluting at approximately 15.5mL. **D**. The 200kDa and 13.8kDa molecular weight standards, β-amylase and cytochrome c, eluting at approximately 15mL and 18.5mL respectively.

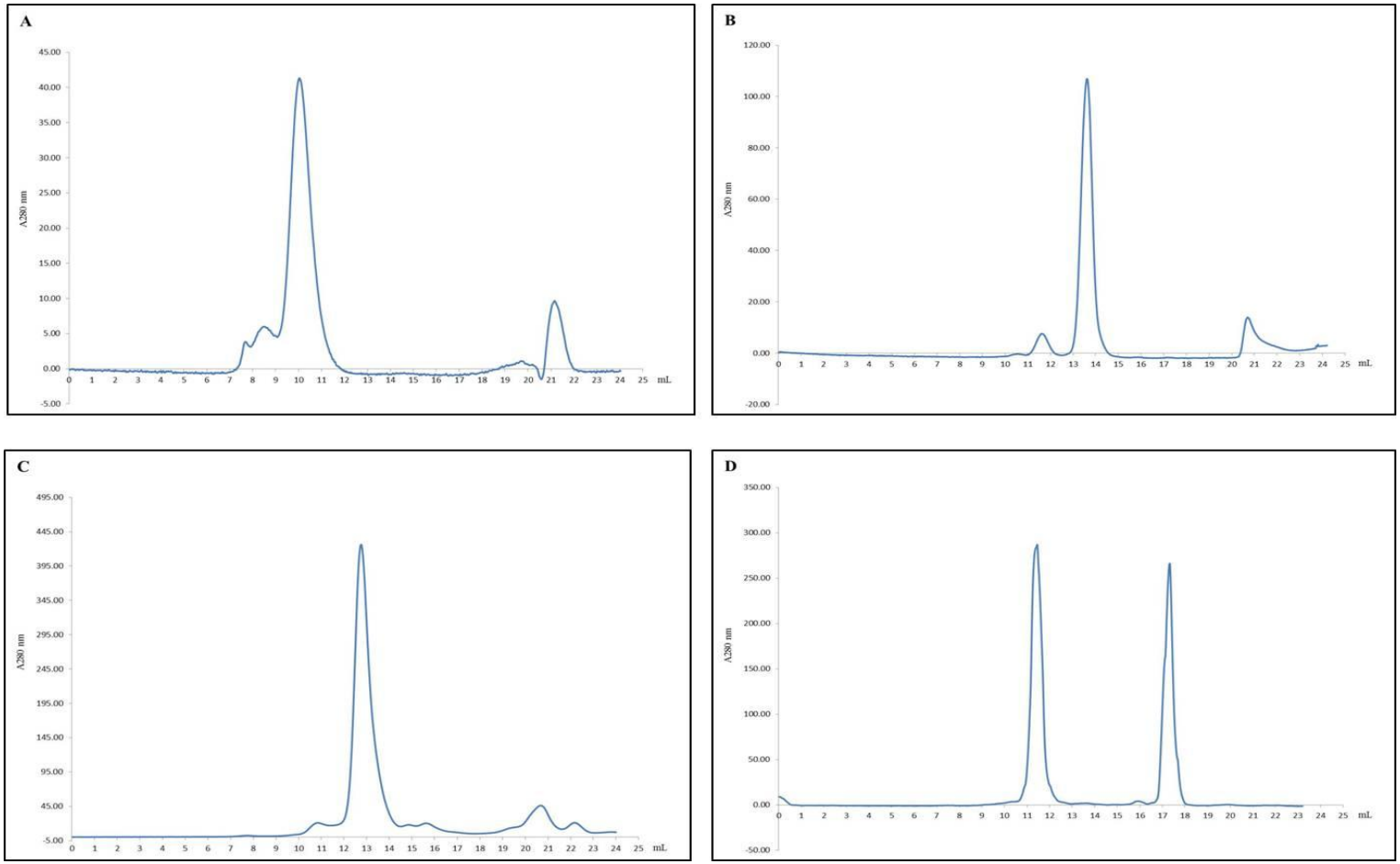

Fig 5.10 Molecular weight standards utilised to calibrate the Superdex 200 column.

Absorbance at 280nm was used to analyse protein eluting from the column per mL of mobile phase eluted from the column. **A**. The 440kDa molecular weight standard, ferritin eluting at approximately 10mL. **B**. The 66kDa molecular weight standard, BSA, eluting at approximately 13.5mL. **C**. The 150kDa molecular weight standard, alcohol dehydrogenase, eluting at approximately 13mL. **D**. The 200kDa and 13.8kDa molecular weight standards, β-amylase and cytochrome c, eluting at approximately 11.5mL and 17.5mL respectively.

5.3.3 SEC of MBP-C-term:

Purified and concentrated MBP-C-term was analysed by SEC using the Superose 6 column (Fig 5.11). As the protein has a molecular weight of 59kDa, the protein should elute from the column at roughly the same position as BSA, which is 16mL (Fig 5.9). However, MBP-C-term eluted from the column at a position which represents a molecular weight >600kDa. Therefore, the protein was forming a large aggregated species.

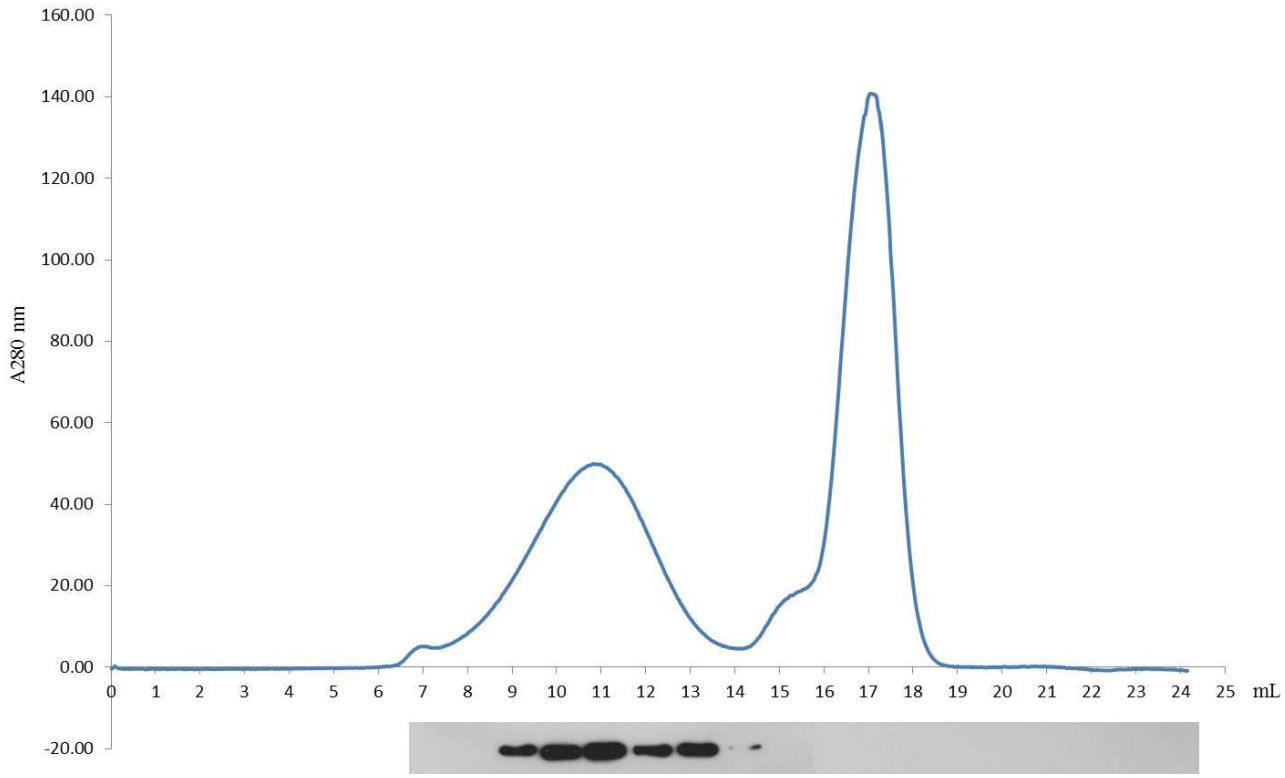

Fig 5.11 Elution profile of MBP-C-term.

MBP-C-term was purified as described in section 5.2.8. Purified and concentrated protein was analysed by SEC using the Superose 6 column. Absorbance at 280nm was used to analyse protein eluting from the column per mL of mobile phase eluted from the column. After the void volume of 7mL had eluted from the column every 0.5mL fraction was collected. Every second fraction from 7mL onwards was assessed for the presence of MBP-C-term by Western blotting. Anti-His-HRP antibody was used to detect MBP-C-term. The large peak present at 17mL represents native MBP purified as a contaminant from *E. coli* cells.

5.3.4 SEC of MBP-FLAG:

As a control, the fusion partner for the C-term of STRA6, MBP, was purified as described for MBP-C-term in section 5.2.8 and analysed by SEC (Fig 5.12). As the protein has a molecular weight of 45kDa, the protein should elute from the column after BSA at approximately 16.5mL. However, it was observed that MBP was eluting from the column at two positions. The first peak representing a molecular weight >600kDa and the second peak eluting at the same position as BSA, representing monomeric protein.

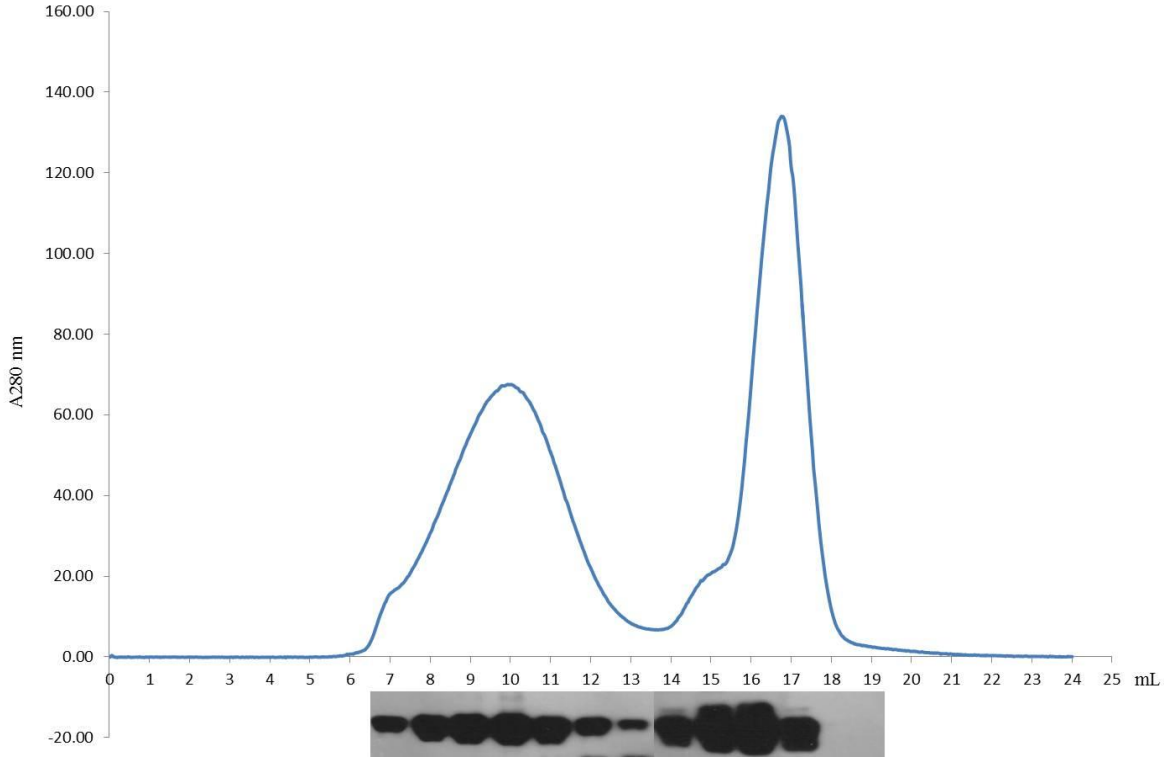

Fig 5.12 Elution profile of MBP-FLAG.

MBP-FLAG was purified as described in section 5.2.8. Purified and concentrated protein was analysed by SEC using the Superose 6 column. Absorbance at 280nm was used to analyse protein eluting from the column per mL of mobile phase eluted from the column. After the void volume of 7mL had eluted from the column every 0.5mL fraction was collected. Every second fraction from 7mL onwards was assessed for the presence of MBP-FLAG by Western blotting. Anti-FLAG antibody was used to detect the protein of interest.

5.3.5 Optimisation of MBP-FLAG SEC:

Following analysis of the MBP tag alone via SEC, it was observed that the tag itself was running as a separate higher molecular weight species. As MBP is a monomer *in vivo*, this was unexpected. According to the findings of Garcia et al MBP may associate to form an aggregate species due to ionic interactions (Garcia et al., 2006). An optimisation trial then ensued to remove the higher molecular weight species caused by association of MBP. Ionic interactions can be prevented by increasing salt concentration. KCl was added to the lysis buffer at 100mM and maintained at this concentration throughout the purification process. Purified protein was subsequently analysed by SEC (Fig 5.13, Panel B).

The MBP-FLAG protein also contains an additional cysteine residue that the MBP-C-term protein does not. In order to rule out formation of disulphide bridges, the sulphydryl alkylating agent, n-ethylmaleamide (NEM) was utilised at 20mM in the lysis buffer and maintained at this concentration throughout the purification process. Purified protein was subsequently analysed by SEC (Fig 5.13, Panel C).

Increasing salt concentration is often an advantageous method to prevent formation of aggregated protein. As the MBP-FLAG protein was forming a higher molecular weight species at 0.3M NaCl, the salt concentration was increased to 0.8M NaCl in the lysis buffer and maintained at this concentration throughout the purification process. Purified protein was subsequently analysed by SEC (Fig 5.13, Panel D).

All three conditions removed the higher molecular weight complex observed to elute at approximately 10mL, which had been observed previously (Fig 5.12). Therefore, ionic interactions could have been responsible for the aggregated species observed, as this was removed by increasing salt concentration. The addition of NEM also removed the higher molecular weight species. The MBP-FLAG protein could form aggregate species due to disulphide bonds, as this was inhibited by modifying the cysteine residues.

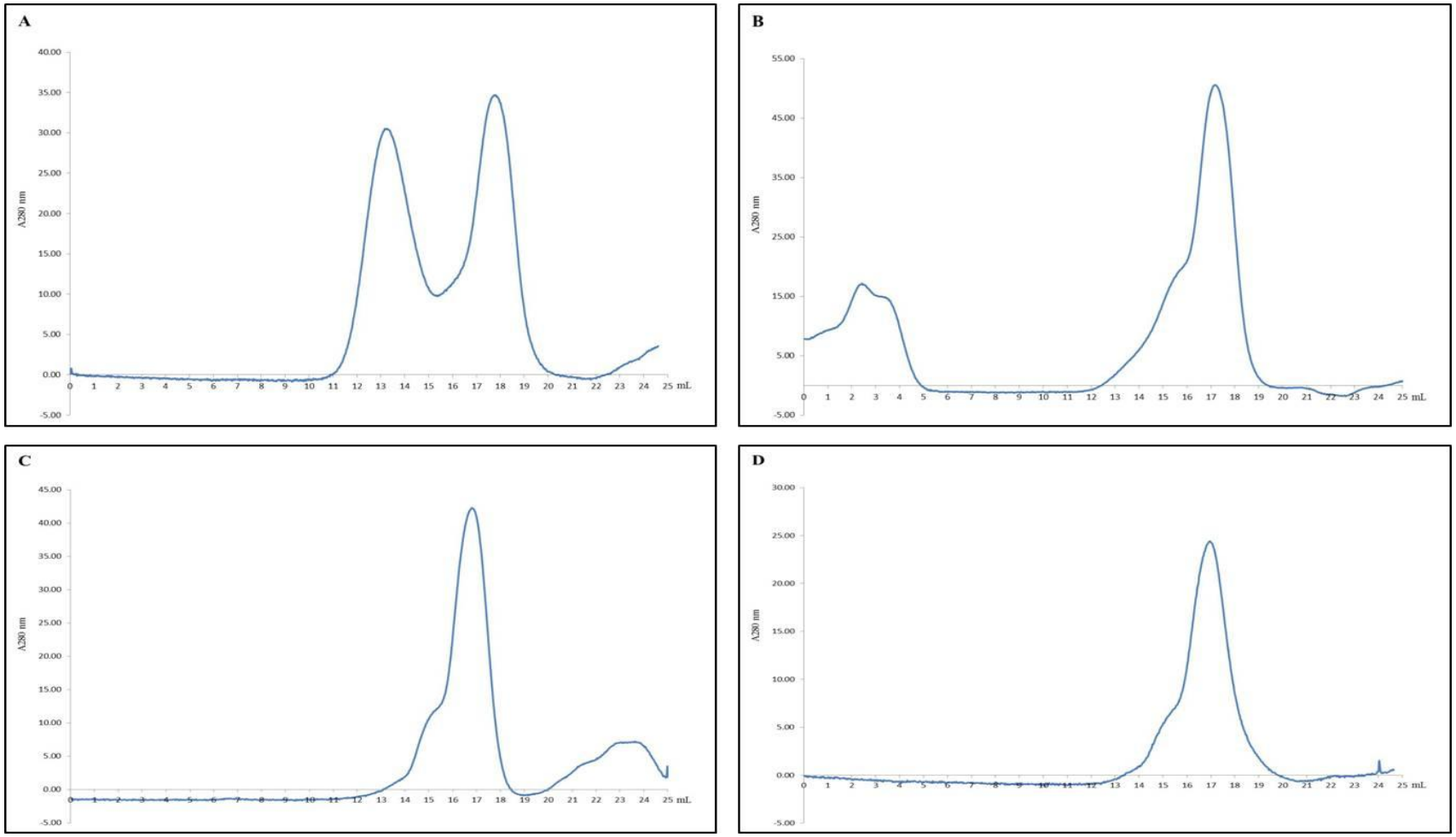

Fig 5.13 Optimisation of the MBP-FLAG elution profile.

Absorbance at 280nm was used to analyse protein eluting from the column per mL of mobile phase eluted from the column. **A**. Elution profile of MBP-FLAG purified in the presence of 0.3M NaCl. **B**. Elution profile of MBP-FLAG purified in the presence of 0.3M NaCl and 0.1M KCL **C**. Elution profile of MBP-FLAG purified in the presence of 0.3M NaCl and 20mM NEM **D**. Elution profile of MBP-FLAG purified in the presence of 0.8M NaCl.

5.3.6 Optimisation of MBP-C-term SEC:

Following successful optimisation of SEC using the MBP-FLAG fusion protein alone, the same strategy was adopted for the MBP-C-term protein. Lysis buffer supplemented with 100mM KCl was chosen as the optimal buffer for purification of the protein. NEM would cause non-native modifications to the protein and high salt concentration may cause the protein to precipitate out of solution. MBP-C-term was purified as described previously with 100mM KCl present throughout the purification process. Purified protein was then subjected to SEC using the Superdex 200 column (Fig 5.14). BSA with a molecular weight of 66kDa elutes at 13.5mL using this column (Fig 5.10), as MBP-C-term is 59kDa, it would be expected to elute at a similar position. However, it eluted near the void volume of the column. Therefore, the addition of KCl did not prevent the formation of aggregated protein.

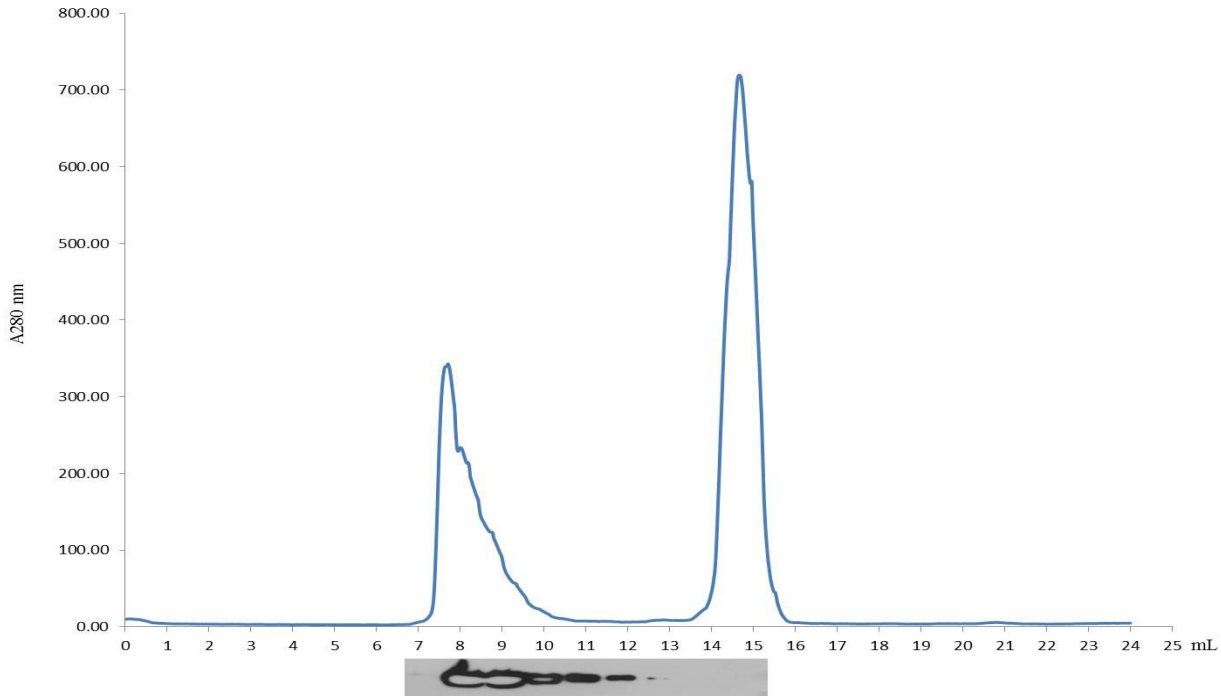

Fig 5.14 Elution profile of MBP-C-term in the presence of 100mM KCl.

MBP-C-term was purified as described previously with 100mM KCl supplemented in all buffers. Purified protein was analysed by SEC using the Superdex 200 column. Absorbance at 280nm was used to analyse protein eluting from the column per mL of mobile phase eluted from the column. After the void volume of 7mL had eluted from the column every 0.5mL fraction was collected. Every second fraction from 7mL was assessed for the presence of MBP-C-term by Western blotting. Anti-His-HRP antibody was used to detect the protein of interest. The peak present at 14.5mL represents native MBP purified as a contaminant from *E. coli*.

5.3.7 Further optimisation of MBP-C-term SEC:

As demonstrated in Fig 5.14, 100mM KCl did not prevent the formation of a higher molecular weight aggregate species of MBP-C-term. Several attempts then ensued to dis-aggregate the MBP-C-term fusion protein. The strong chaotropic reagents, urea and guanidine hydrochloride (G-HCl) have successfully been used to aid solubilisation of aggregated proteins (Hatefi and Hanstein, 1969). 2M urea and 2.5M G-HCl were used in an attempt to solubilise the high molecular weight aggregated protein (Fig 5.15, Panel A and B). However, this did not result in soluble protein.

In extreme cases, complete denaturation of aggregated protein using urea and re-folding by dialysis can yield soluble, functional protein. MBP-C-term denatured with 8M urea eluted at a position representing a molecular weight of 440kDa. MBP-C-term previously denatured with 8M urea was dialysed into a buffer without urea and theoretically re-folded. Subsequent analysis by SEC revealed that the protein eluted at the same position as when denatured (Fig 5.15, Panel C and D). One explanation for this result would be that the protein did not re-fold on dialysis. If this were the case the MBP portion of the fusion protein would not bind to amylose resin, as it would not be properly folded. To test this theory, a small portion of the original, dialysed sample used for the SEC analysis was purified using amylose resin (Fig 5.16). As Fig 5.16 demonstrates all of the protein was found in the elution fraction. This showed that the protein had re-folded. Therefore, attempts to disaggregate the protein using denaturing conditions did not yield soluble protein.

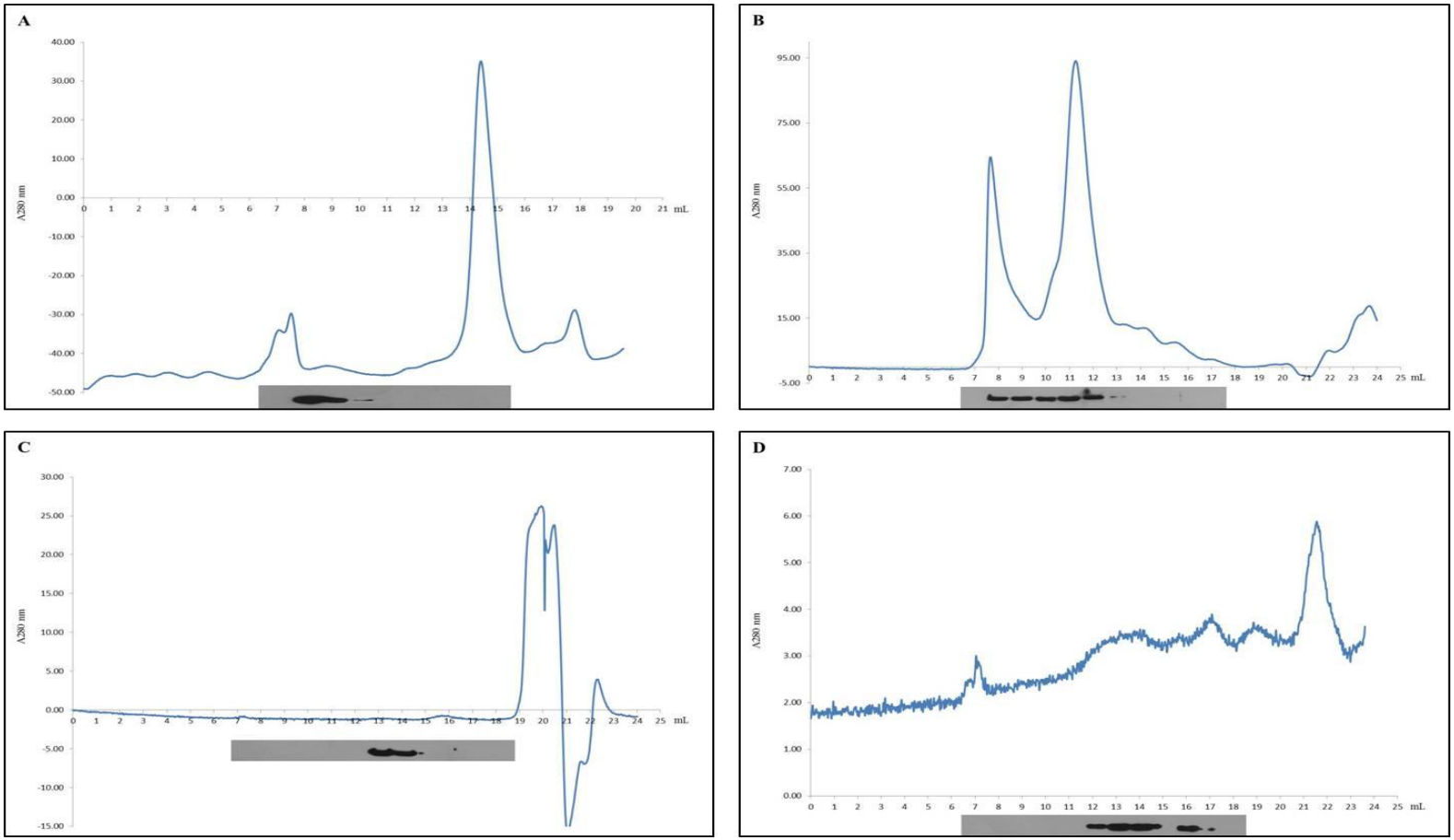

Fig 5.15 Optimisation of the MBP-C-term elution profile via the use of chaotropic agents.

MBP-C-term was purified as described previously with either **A**. 2M urea supplemented in all buffers, **B**. 2.5M G-HCl supplemented in all buffers **C**. 8M urea supplemented in all buffers **D**. 8M urea supplemented in all buffers and subsequently dialysed to remove urea. Purified protein was analysed by SEC using the Superdex 200 column (**A** and **B**) or the Superose 6 column (**C** and **D**). Absorbance at 280nm was used to analyse protein eluting from the column per mL of mobile phase eluted from the column. After the void volume of 7mL had eluted from the column every 0.5mL fraction was collected. Every second fraction from 7mL was assessed for the presence of MBP-C-term by Western blotting. Anti-His-HRP antibody was used to detect the protein of interest.

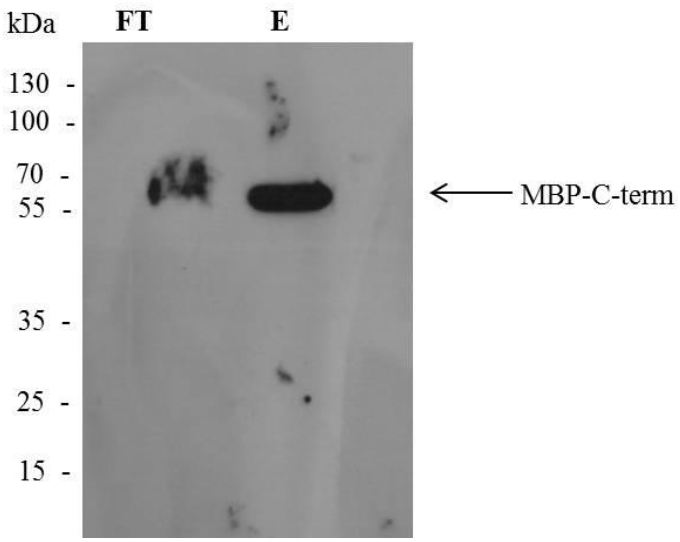

Fig 5.16 Amylose affinity chromatography of MBP-C-Term previously denatured with 8M urea and re-folded by dialysis.

MBP-C-term was purified as described previously in the presence of 8M urea. The urea was subsequently removed by dialysis to allow re-folding of the protein. Dialysed protein was then incubated with amylose affinity chromatography resin, to assess the re-folding of the MBP tag. The resin was centrifuged and supernatant retained (FT), containing any un-bound protein. The resin was washed and any bound protein eluted with the addition of 10mM maltose (E). Protein content from the FT and E fractions was analysed by Western blotting and MBP-C-Term detected using anti-His-HRP antibody.

5.3.8 Detergent solubilisation of MBP-C-term:

Solubilisation using urea and G-HCl did not result in a successful yield of soluble protein. Another method used to solubilise aggregated protein is the addition of detergents. N,N-dimethyldodecylamine N-oxide (LDAO) was used in an effort to solubilise the MBP-C-term fusion protein. 1% Triton X-100 (v/v) present in the cell lysis buffer was substituted with 1% LDAO (w/v) and LDAO was maintained at a concentration of 0.5% throughout the purification process, following cell lysis. Purified protein was analysed by SEC using the Superdex 200 column, with 2mM LDAO supplemented in the mobile phase (Fig 5.17, Panel B). Utilisation of LDAO as a solubilisation agent resulted in a shift of molecular weight of a large proportion of purified protein to the expected elution position of approximately 13 ml. However, yields of purified protein were not as high as previously observed. The detergent used was substituted to n-Dodecyl β-D-maltopyranoside (DDM). Yields of protein vastly improved and protein analysed by SEC eluted at a position consistent with the predicted molecular weight of the protein (59kDa), at 13 to 14mL (Fig 5.17, Panel C).

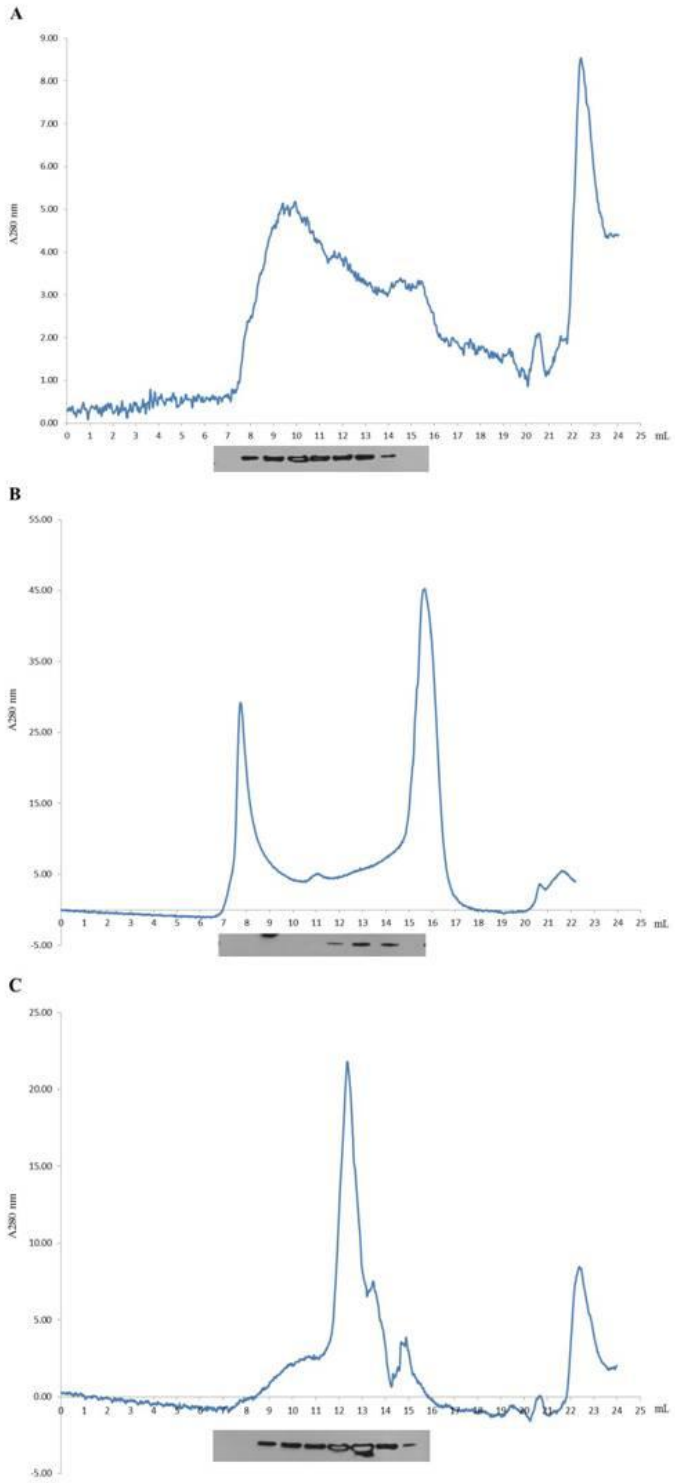

Fig 5.17 Elution profile of MBP-C-term in the presence of detergent.

MBP-C-term was purified as described previously with either **A**. No detergent present **B**. 0.5% LDAO present in all buffers **C**. 0.5% DDM present in all buffers. Purified protein was analysed by SEC using the Superdex 200 column. Absorbance at 280nm was used to analyse protein eluting from the column per mL of mobile phase. After the void volume of 7mL had eluted from the column every 0.5mL fraction was collected. Every second fraction from 7mL was assessed for the presence of MBP-C-term by Western blotting. Anti-His-HRP antibody was used to detect the protein of interest. The molecular weight of the protein is 59kDa. BSA with a molecular weight of 66kDa elutes at 13.5mL.

5.3.9 Characterisation of cleaved C-term:

Following successful expression and purification of soluble mono-disperse fusion protein as analysed by SEC, characterisation of the cleaved version of the protein was conducted. Fusion tags can vastly improve expression yields and solubility of a protein, but they may have adverse effects on protein function and more detailed structural analysis. A TEV protease cleavage site was incorporated into the expression plasmid to allow for the removal of the MBP and FLAG epitope tags. Cleavage was conducted as described in section 5.2.9. Cleavage of the full length protein results in a 16.8kDa product with a C-terminal His tag. A trial was conducted to determine the optimal conditions for TEV cleavage (Fig 5.18, A). The cleavage reaction was subsequently conducted at room temperature for 16 hours. The effect of DDM on the cleavage reaction was also assessed (Fig 5.18, B). Cleavage of the C-term fusion protein does not appear to be altered with the presence of DDM.

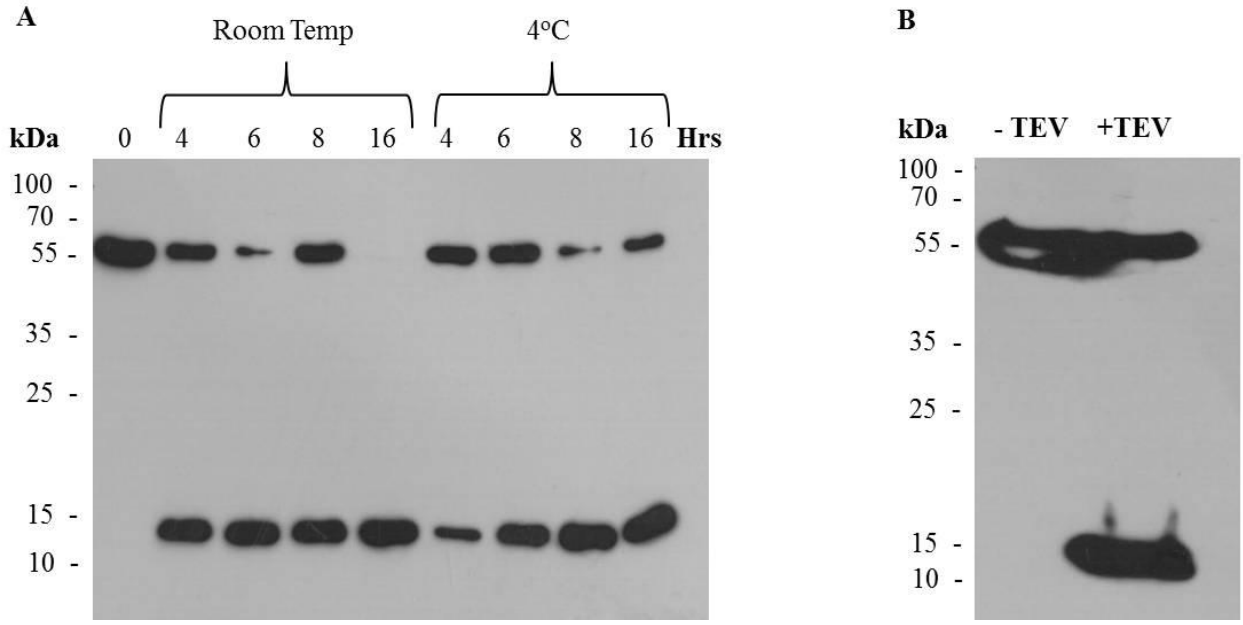

Fig 5.18 Optimisation of the removal of the MBP-FLAG tag by the addition of TEV protease.

A. MBP-C-term was purified as described previously. 100µg of purified protein was incubated with 1µl TEV protease for 0,4,6,8 and 16 hours at room temperature or 4°C. Cleavage products were then analysed by SDS-PAGE and Western blotting. Anti-His-HRP antibody was used to detect protein of interest. Full length protein is observed at 59kDa and the C-term-His cleavage product is observed at approximately 16kDa. **B.** Overnight TEV cleavage of purified MBP-C-term in the presence of 0.5% DDM at room temperature. Cleavage products were then analysed by SDS-PAGE and Western blotting. Anti-His-HRP antibody was used to detect protein of interest. Full length protein is observed at 59kDa and the C-term-His cleavage product is observed at approximately 16kDa.

5.3.10 SEC of purified and cleaved C-term:

Following successful optimisation of MBP-C-term cleavage, the cleaved version of the C-term was analysed by SEC using the Superose 6 column, in the presence of 2mM DDM (Fig 5.19).

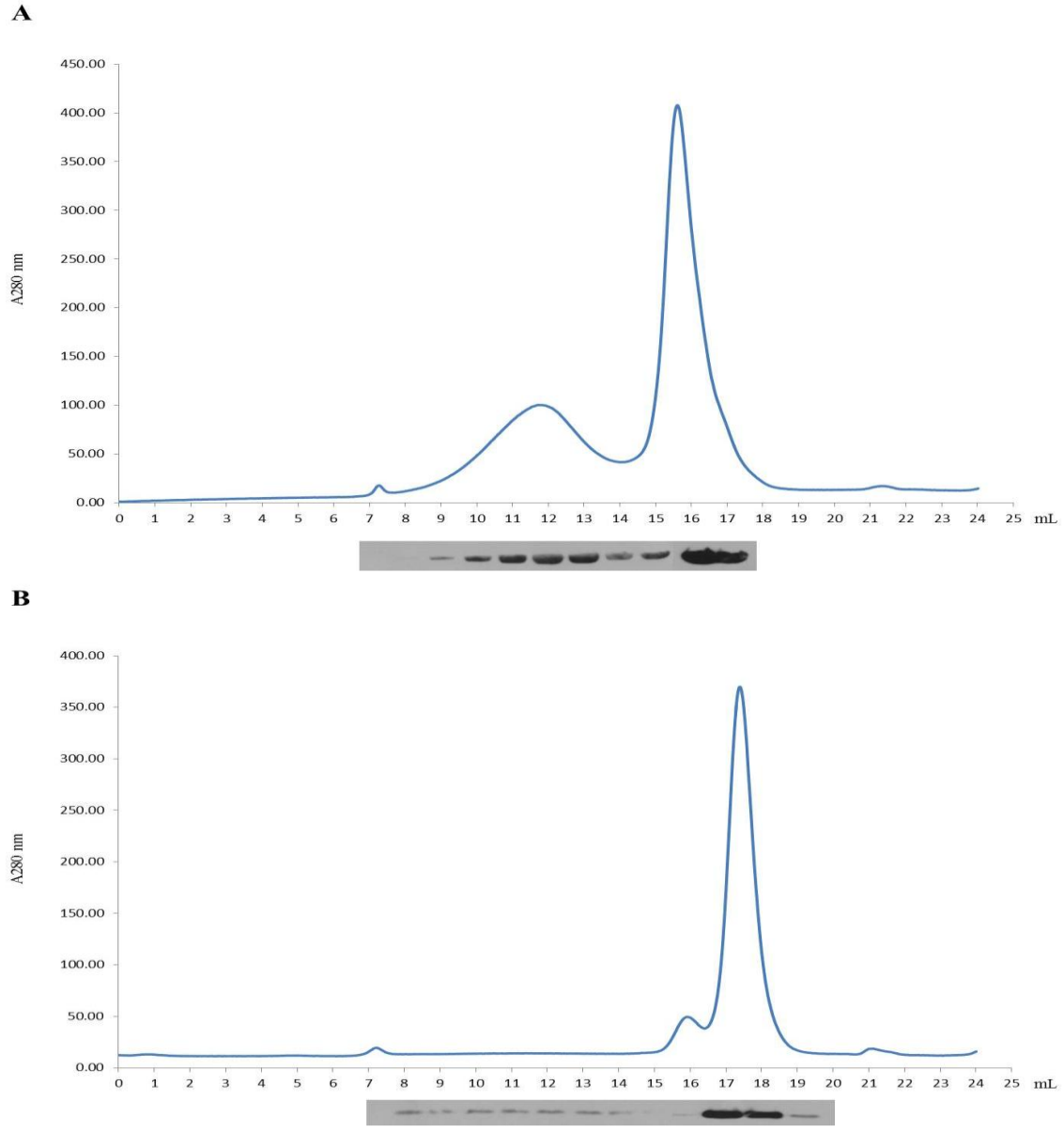

Fig 5.19 Elution profile of MBP-C-term and Cleaved C-term in the presence of 2mM DDM.

MBP-C-term was purified and cleaved as described previously. Both the full length fusion protein (59kDa) (**A**) and the cleaved protein (16kDa) (**B**) were analysed by SEC using the Superose 6 column with 2mM DDM present in the mobile phase. Absorbance at 280nm was used to analyse protein eluting from the column per mL of mobile phase eluted from the column. After the void volume of 7mL had eluted from the column every 0.5mL fraction was collected. Every second fraction from 7mL was assessed for the presence of desired protein by Western blotting. Anti-His-HRP antibody was used to detect the protein of interest. BSA with a molecular weight of 66kDa elutes at 16mL and cytochrome c with a molecular weight of 13.8kDa elutes at 18.5mL

5.3.11 Long term stability of mono-disperse protein:

A critical aspect in the structural analysis of recombinant proteins is their stability at room temperature. For protein crystallisation it is necessary that the protein does not precipitate at room temperature or form aggregate species. In order to assess the stability of the recombinant proteins generated in this study, the peak fractions from the previous SEC analysis were incubated at room temperature for 5 days and analysed once more by SEC using the same column. The 16mL fraction from the MBP-C-term SEC analysis (Fig 5.19) was retained and incubated at room temperature for 5 days. The same sample was then analysed by SEC (Fig.5.20, A). The 17mL fraction from the cleaved C-term SEC analysis (Fig 5.19) was retained and incubated at room temperature for 5 days. The same sample was then analysed by SEC (Fig.5.20, B). The majority of the full length protein retained its solubility when incubated at room temperature. However, the cleaved C-term formed an aggregate species, observed at the void volume of the column.

5.3.12 Optimisation of C-term stability at room temperature:

Analysis of the stability of the cleaved C-term protein at room temperature revealed that it formed a high molecular weight aggregate with room temperature storage (Fig 5.20). One strategy to stabilise a protein is to lower the pH below the predicted pI of the protein. The pI of the cleaved C-term was predicted to be 7.3 using the ProtParam software tool provided by ExPASy. Previously purified and cleaved C-term protein was dialysed into two different buffers differing in one and two pH units below the predicted pI respectively, 6.3 and 5.3. Dialysed protein was subsequently incubated at room temperature for 5 days. The molecular weight of the protein was then analysed by SEC (Fig 5.21). A reduction in pH allowed for the retention of soluble protein, when incubated at room temperature for long periods.

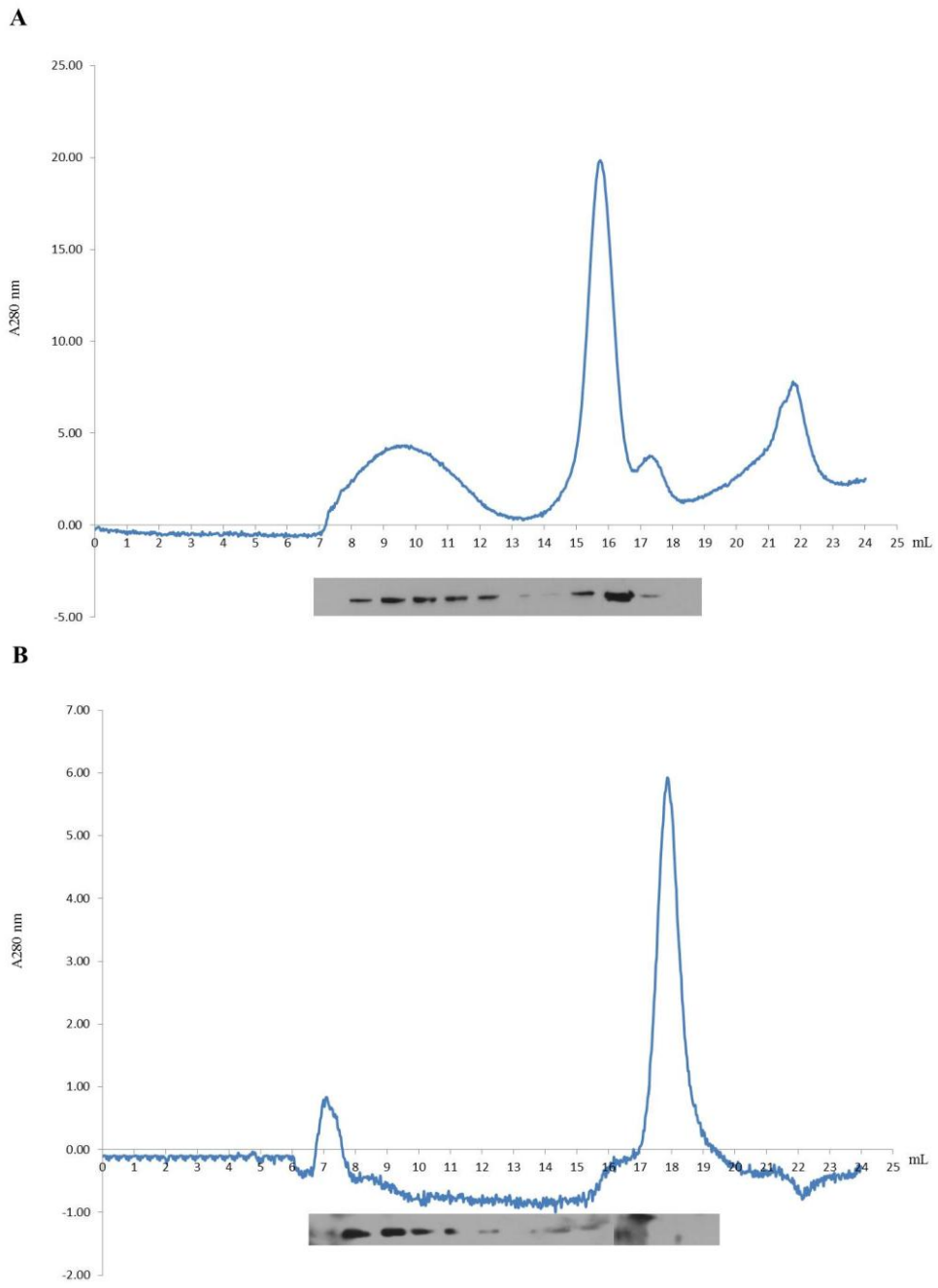

Fig 5.20 Long term stability of MBP-C-term and cleaved C-term when incubated at room temperature.

Soluble protein previously analysed by SEC using the Superose 6 column was retained and incubated at room temperature for 5 days. Protein was analysed once again by SEC using the Superose 6 column Absorbance at 280nm was used to analyse protein eluting from the column per mL of mobile phase eluted from the column. After the void volume of 7mL had eluted from the column every 0.5mL fraction was collected. Every odd fraction from 7mL was assessed for the presence of desired protein by Western blotting. Anti-His-HRP antibody was used to detect the protein of interest. **A**. Elution profile of MBP-C-term incubated at room temperature for 5 days, with corresponding Western blot. **B**. Elution profile of cleaved C-term incubated at room temperature for 5 days, with corresponding Western blot. The peak present at 18mL represents the contaminant MBP.

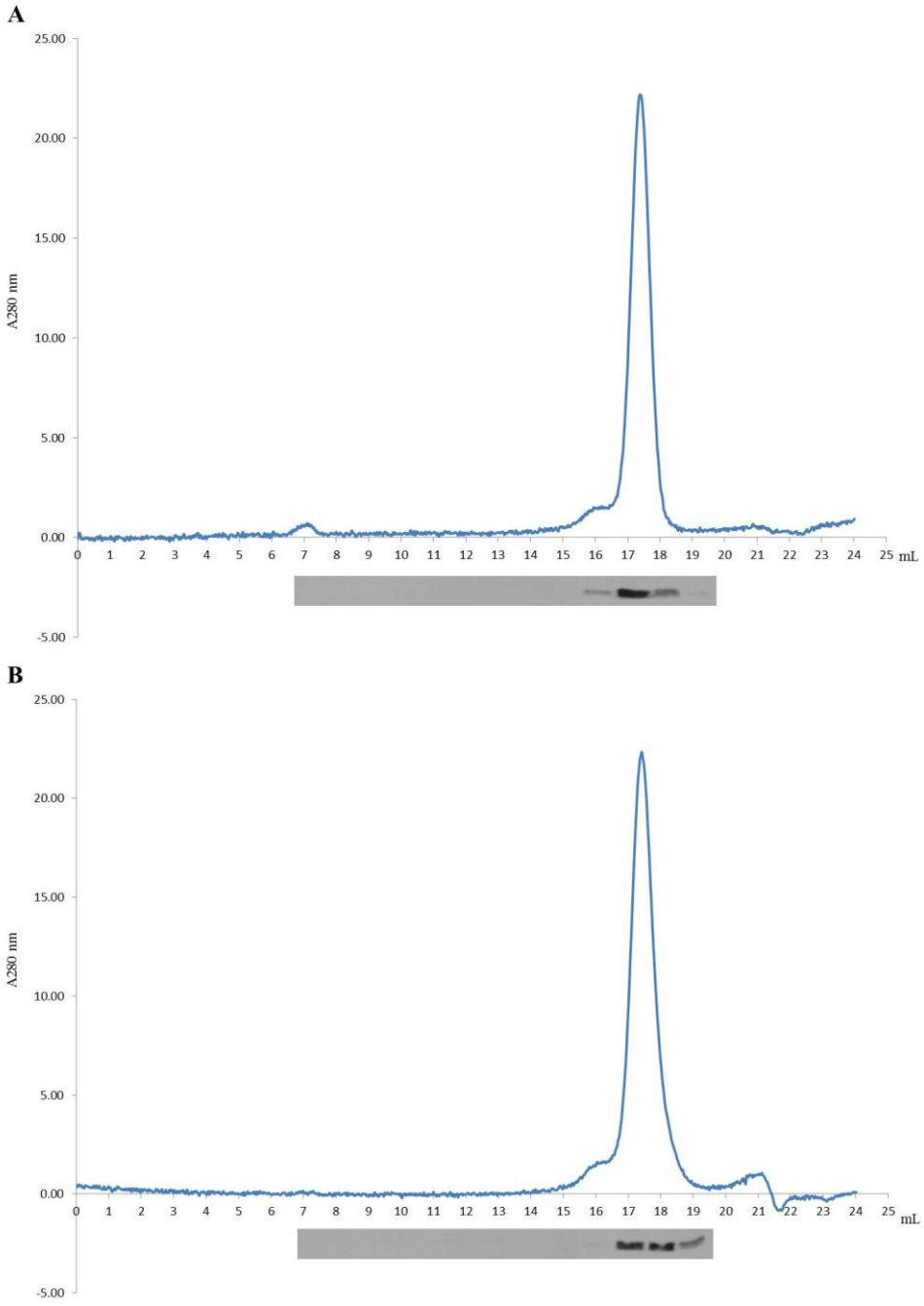

Fig 5.21 Optimisation of room temperature stability of cleaved C-term, using varying pH.

Soluble, cleaved C-term protein previously analysed by SEC using the Superose 6 column was retained and dialysed into a buffer composed of the same components with varying pH of either 6.3 or 5.3. Dialysed protein was then incubated at room temperature for 5 days. Protein was analysed once again by SEC using the Superose 6 column. Absorbance at 280nm was used to analyse protein eluting from the column per mL of mobile phase eluted from the column. After the void volume of 7mL had eluted from the column every 0.5mL fraction was collected. Every second fraction from 7mL was assessed for the presence of desired protein by Western blotting. Anti-His-HRP antibody was used to detect the protein of interest. **A**. Elution profile of cleaved C-term at pH 6.3, incubated at room temperature for 5 days, with corresponding Western blot. **B**. Elution profile of cleaved C-term at pH 5.3, incubated at room temperature for 5 days, with corresponding Western blot.

5.3.13 Secondary structure analysis of purified mono-disperse C-term:

Circular dichroisim (CD) is an accurate, non-destructive technique to assess the secondary structure of a recombinant protein. It utilises the path of plane polarised light as it travels through a protein to determine structural motifs. Defined secondary structure motifs display characteristic CD spectra as summarised in Fig 5.22.

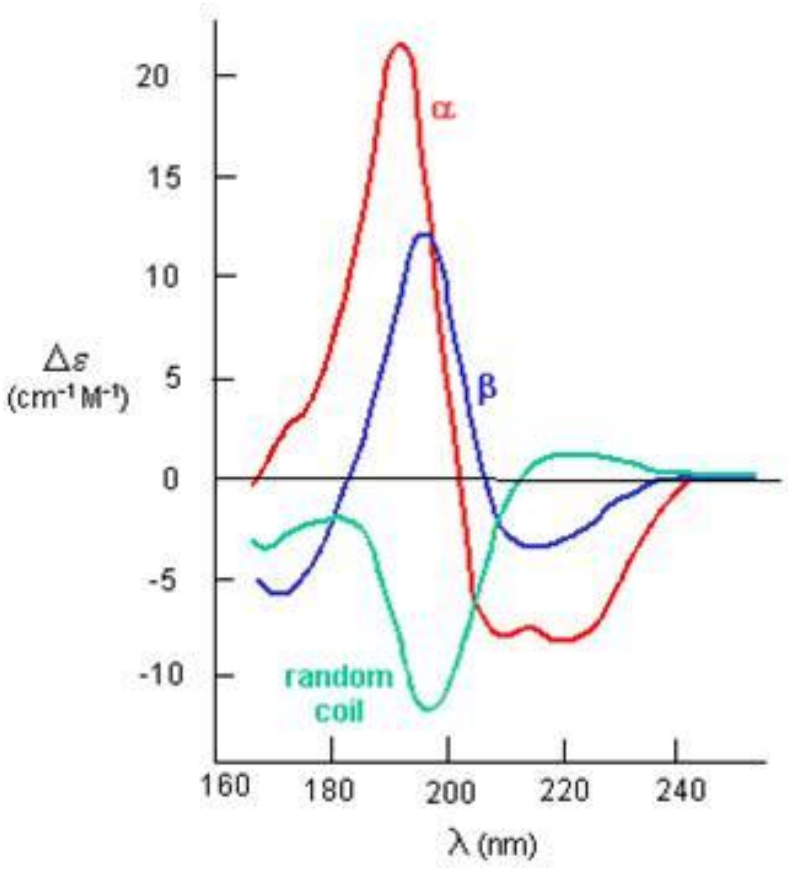

Fig 5.22 Representative plot of structural motifs depicted by CD.

CD-Spectra of defined structural motifs. Red line depicts alpha helix, blue line depicts beta sheet, green line depicts random coil. Taken from http://biochem-vivek.tripod.com/id19.html

MBP-FLAG, MBP-C-term and cleaved C-term were purified as described previously and subjected to SEC. The mono-disperse elution peak for each respective protein was concentrated to 0.2mg/mL. 3µg of each respective protein was analysed by SDS-PAGE and Coomassie staining to assess purity (Fig 5.23). Purified protein was then analysed using a Chiroscan CD spectropolarimeter (AppliedPhotophysics), courtesy of the Astbury Centre for Structural Molecular Biology, University of Leeds. The high tension of the carrier buffer was analysed to assess the absorption properties of the buffer alone (Fig 5.24). A high tension reading of above 500 at 200nm would imply that the detector is saturated and the buffer alone is causing a high amount of absorbance. Following verification that the buffer was compatible with CD analysis, purified protein was analysed at 0.2mg/ml in a thermostated 1mm quartz cuvette. Absorption was recorded from bandwidth 280nm to 180nm at 20^{o}C at 1nm per second with a wavelength step of 1nm. 2 scans were acquired and an average calculated for accuracy. Data were recorded in millidegrees (mθ) and subsequently converted to mean residue ellipticity, in order to directly compare all 3 proteins, using a formula as described in Greenfield (Greenfield, 2006) (Fig 5.25).

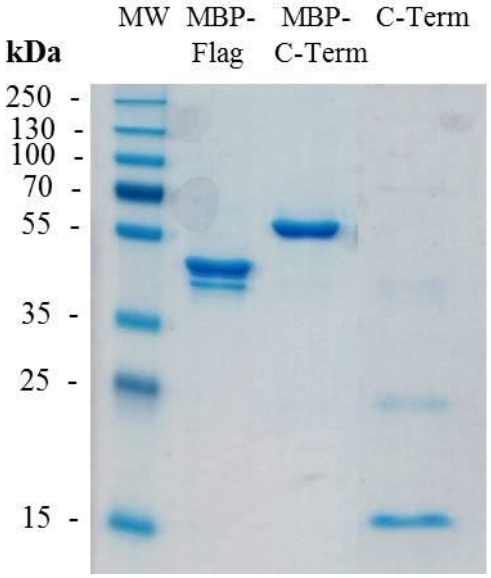

Fig 5.23 Purity of protein samples utilised for CD analysis.

MBP-FLAG, MBP-C-term and cleaved C-term were purified and analysed by SEC. Peak elution fractions were concentrated to 0.2mg/ml and 3µg analysed by SDS-PAGE. Coomassie brilliant blue was utilised to visualise the purity of the recombinant proteins.

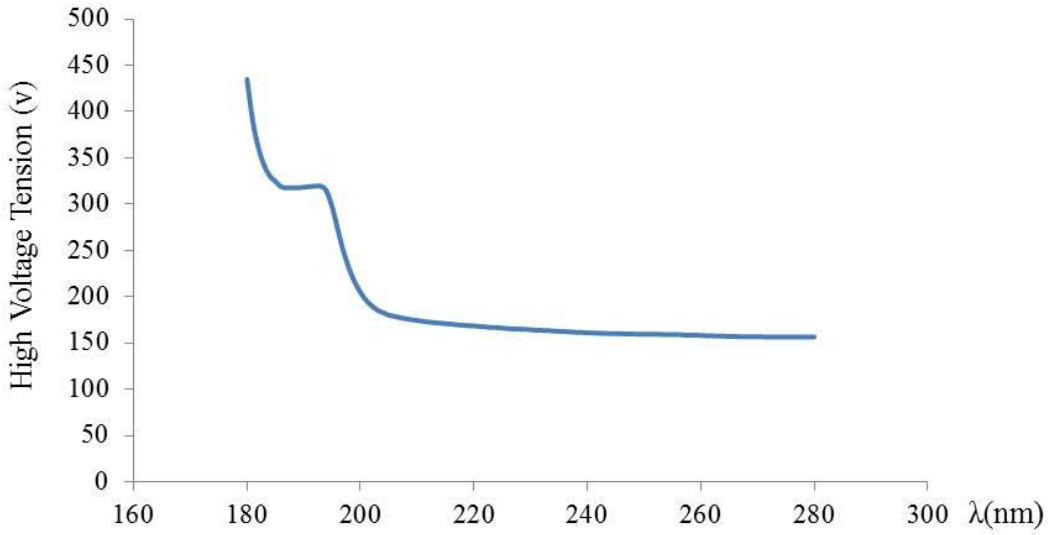

Fig 5.24 High voltage tension spectra of buffer used with recombinant proteins analysed by CD.

High voltage tension graph depicting the spectra obtained for buffer alone without protein present. A high reading at 200nm would indicate that the buffer alone has a high background absorbance. A reading below 400 at 200nm is acceptable to conduct CD spectra analysis in a particular buffer.

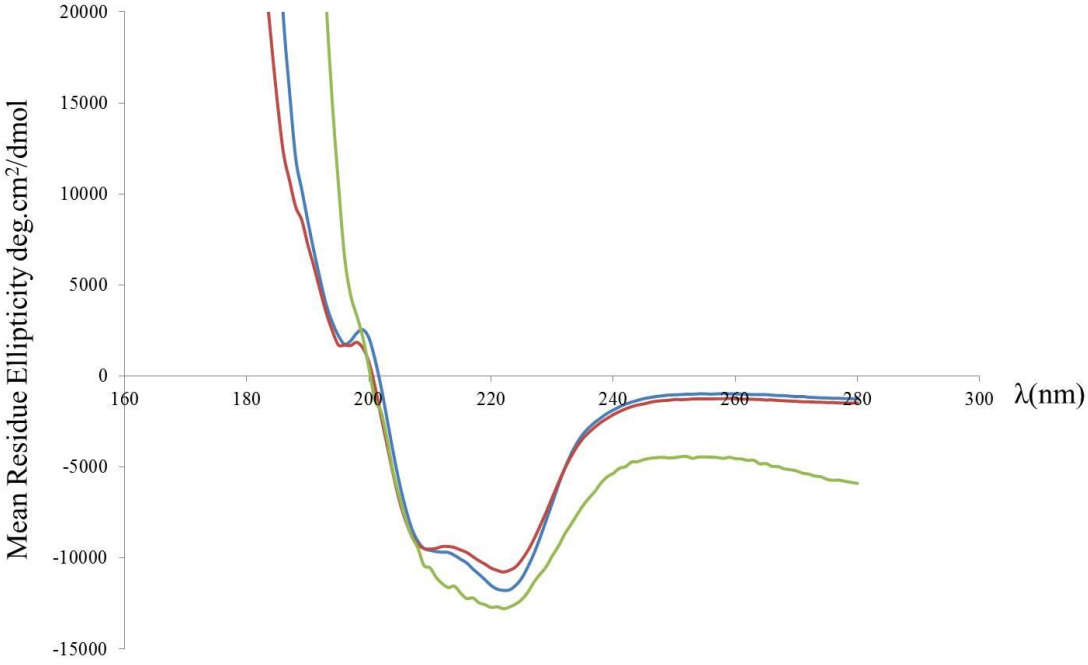

Fig 5.25 CD spectra of MBP, MBP-C-term and cleaved C-term.

Representation of the CD spectra obtained for MBP (blue line), MBP-C-term (red line) and cleaved C-term (green line). All proteins display a typical alpha helical CD spectra.

5.3.14 Calculation of structural content of recombinant proteins:

CD spectra data previously converted to mean residue ellipticity, as described in section 5.3.13 was subsequently used to determine the distribution of structural motifs in the recombinant proteins analysed. The online sever DichroWeb was utilised to calculate the structural composition of each protein based on spectra obtained (Whitmore and Wallace, 2004, 2008). The analysis was conducted using the CONTIN algorithm with the structural reference database SMP180 (Abdul-Gader et al., 2011). The reference database is composed of the CD spectra of proteins which have had their structure solved by x-ray crystallography and thus can be used to accurately predict the composition of an unknown protein. MBP has a known alpha helical content of 40% and beta sheet content of 20%, based on the solved crystal structure of the protein (Spurlino et al., 1991). The algorithm and dataset used in this study to determine structural composition were chosen based on the accuracy of prediction of MBP structural content, compared to the solved crystal structure. Table 5.1 describes the structural content calculated for MBP alone, the MBP-C-term fusion protein and cleaved C-term.

Protein	Helix1	Helix2	Strand1	Strand2	Turns	Unordered	Total
MBP	0.350	0.000	0.132	0.039	0.184	0.294	0.999
MBP-CT	0.288	0.050	0.114	0.055	0.167	0.327	1.001
CT	0.650	0.000	0.000	0.000	0.350	0.000	1

Table 5.1 Fractional structural content of purified and analysed recombinant proteins.

Calculated structural content of MBP (MBP), MBP-C-term (MBP-CT) and cleaved C-term (CT) respectively, using the online server DichroWeb. The algorithm CONTIN was used to calculate predicted structural characteristics of the proteins by comparison with the SMP180 reference dataset of known structures.

5.3.15 Modelling the predicted structure of the C-terminus of STRA6:

Helical content of the cleaved C-term of STRA6 was determined to be 65% based on CD spectra analysis with the remaining residues formulating 35% turns between the helices (Table 5.1). The 3D structure of the C-term was predicted using the web server iTasser, in collaboration with Dr. Gemma Kinsella (NUI Maynooth). iTasser uses the threading technique to match the amino acid sequence of a protein of interest to a dataset of proteins which have had their crystal structure solved. The protein's secondary structure is first predicted from the amino acid sequence and then both the amino acid sequence and the predicted secondary structure are used to predict the overall tertiary structure of the protein by comparison with known protein structures in the PDB database (Zhang, 2008).

Fig. 5.26 shows the predicted secondary structure content of the C-term based on the amino acid sequence. The structural content of the top three predicted 3D models are shown below. The best match or model 1 depicts a structure with helical content of 75% and the rest 25% coil or turn. This closely resembles the predicted structure based on CD analysis. Fig 5.27 shows the predicted 3D model based on the best match or model 1 for the C-terminus of STRA6. The confidence score or C-score estimates the quality of the predicted structure and can range from -5 to 2. The higher the C-score the more confidence the user has in the predicted structure. The C-score for the most accurate model of the C-term was -2.43. The Tm score of a model is a standard to assess the structural similarity between the predicted structure and known structures. A score of >0.5 indicates a model with a correct topology and a score of <0.17 indicates a model with random similarity. The Tm score of model 1 was 0.43 indicating that the model is a high quality model prediction. There should be a strong correlation between the C-score and the Tm score. The discrepancy between these scores may be as a result of the unique characteristics of STRA6. The C-score is generated from comparison of the predicted secondary structure of the protein and known structures. The moderate C-score may be a result of the uniqueness of STRA6 in the human system. It is unlike any known protein. Therefore, the ability of the software to predict the structure compared to other structures in the database may not be a true reflection on the accuracy of the model. From 3D modelling we can gain valuable insight as to how the structure is ordered and where potential interaction sites might be located.

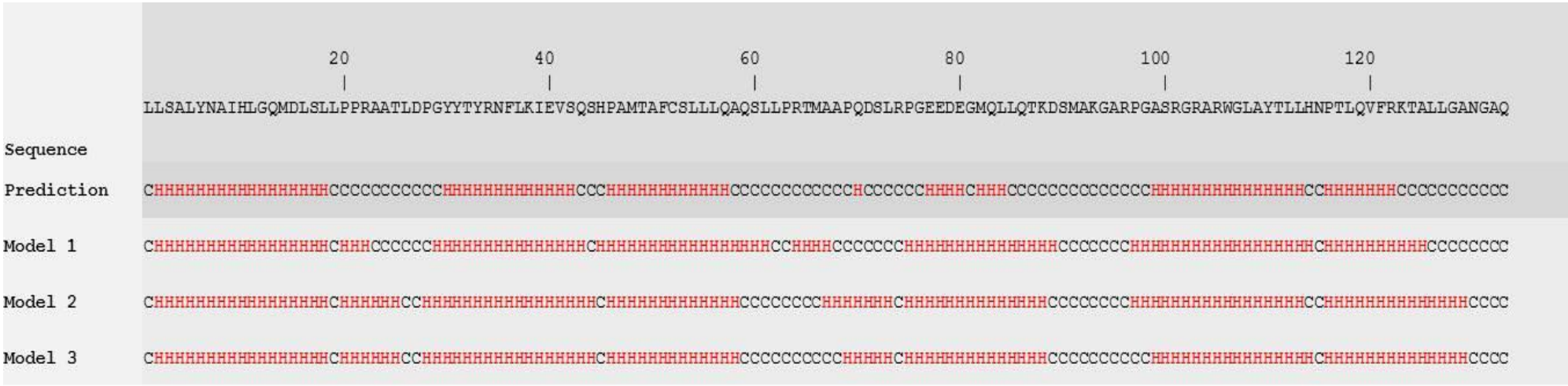

Fig 5.26 iTasser structural homology comparison.

Structural homology comparison of the C-terminus of STRA6 (residues 535-667). The sequence prediction represents the predicted secondary structure of the C-term as generated by the iTasser web server. Model 1, 2 and 3 depicts the structural content of the best fit 3D structures generated by iTasser based on the amino acid sequence and predicted secondary structure. The amino acid sequence of the C-term is shown above. C shown in black text denotes coil and H shown in red text denotes alpha helix.

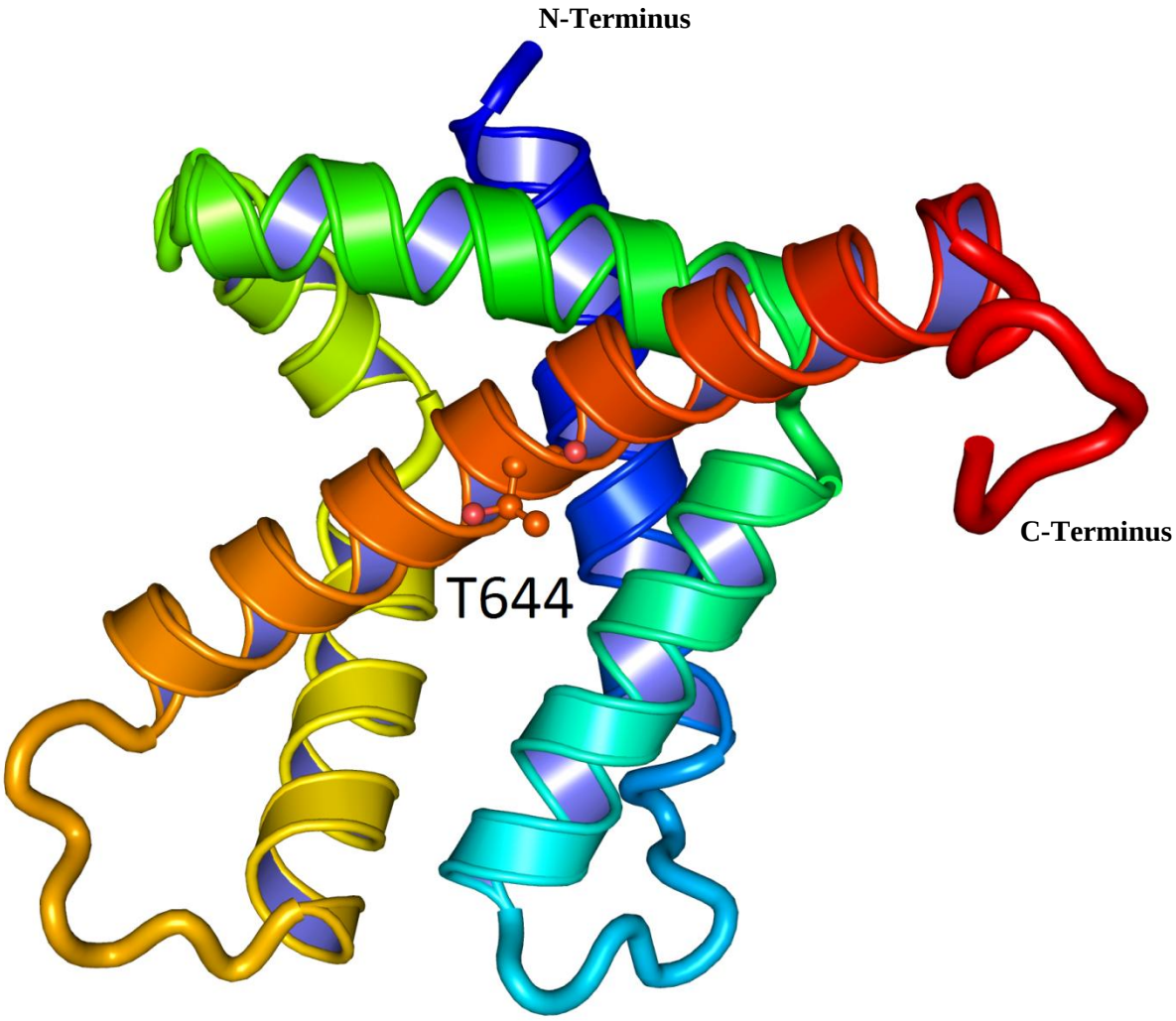

Fig 5.27 3D model of the C-terminus of STRA6.

Representation of the predicted structure of the C-terminus of STRA6 generated using the online server iTasser. Alpha helix is represented by the coiled structures. The N-terminal region begins at the dark blue helix and the C-terminal region is represented by the red helix. The genetic mutation site and known phosphorylation site, T644, is highlighted. Image kindly provided by Dr. Gemma Kinsella (NUI Maynooth).

5.3.16 Functional analysis of purified, soluble C-term:

The cellular uptake and transport of ROH is mediated by the RBP receptor, STRA6 (Kawaguchi et al., 2007). Several studies have shown that once ROH enters the cell it is coupled with CRBP (Sundaram et al., 1998), (Kawaguchi et al., 2012). As the C-terminus of STRA6 is a large intracellular domain it may interact directly with CRBP. Following extensive optimisation of the purification of the C-terminus of STRA6, the functional characteristics of the domain were assessed. 10µg of purified MBP-C-term was coupled to amylose affinity chromatography resin and allowed to interact with 10µg CRBP at room temperature for 30 minutes, with MBP-FLAG as a negative control. The resin was pelleted by centrifugation and the supernatant containing any un-bound protein retained for subsequent analysis. The resin was washed and any bound protein eluted in Laemmli sample buffer. Protein content of each fraction was then assessed by SDS-PAGE and Western blotting (Fig 5.28). CRBP was not found associated with MBP-C-term in the protein fraction bound to the amylose resin.

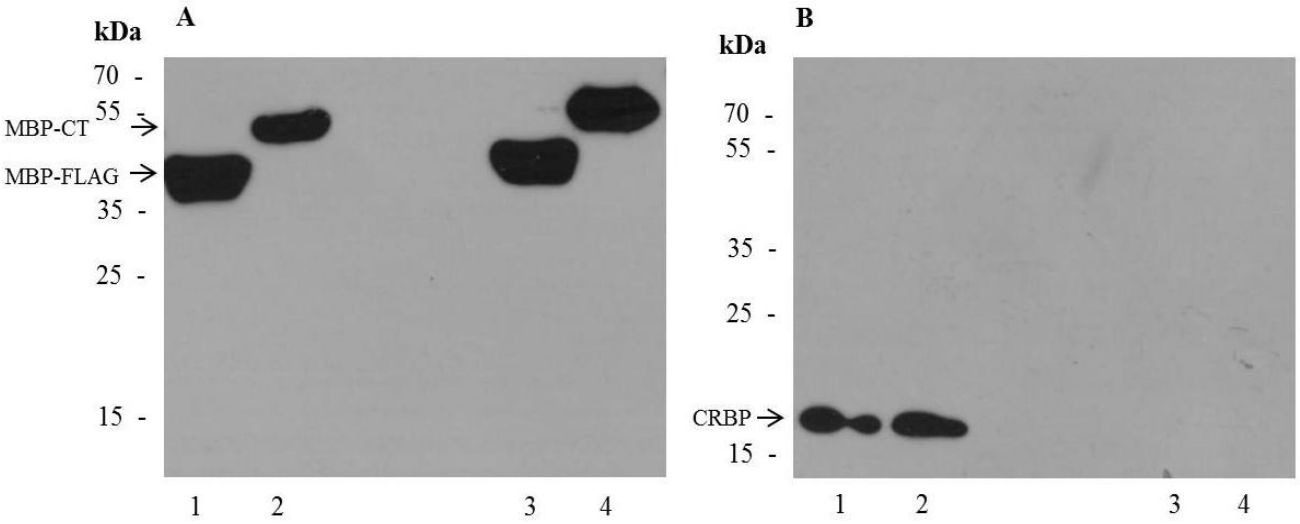

Fig 5.28 Binding assay to determine the interaction of MBP-C-Term with CRBP.

MBP-C-Term was purified as described previously in the presence of DDM. 10µg of MBP-C-term was coupled to amylose affinity chromatography resin and allowed to interact with 10µg CRBP for 30 minutes at room temperature. MBP-FLAG was used as a negative control. Protein bound to the resin was separated by centrifugation and any un-bound protein present in the supernatant retained. The resin was washed and any bound protein eluted by incubation with Laemmli sample buffer. The un-bound and bound fractions were analysed by SDS-PAGE and Western blotting. **A**. Representative Western blot using anti-FLAG antibody. **B**. Representative Western blot using anti-CRBP antibody. For both panels track 1 represents the un-bound fraction from the MBP-FLAG and CRBP interaction assay. Track 2 represents the un-bound fraction from the MBP-C-term and CRBP interaction assay. Track 3 represents the bound fraction from the MBP-FLAG and CRBP interaction assay. Track 4 represents the bound fraction from the MBP-C-term and CRBP interaction assay.

5.3.17 Chemical crosslinking of potential protein interactions:

When STRA6 was originally identified as the elusive receptor for RBP, it was isolated as a result of chemical crosslinking to RBP (Kawaguchi et al., 2007). The interaction is transient in nature, allowing for a high turnover of holo-RBP to bind to the receptor. The use of chemical crosslinking agents allows for the identification of protein interactions which may not be stable. In this investigation the photo-activated crosslinker, sulpho-NHS-SS-diazirine (SDAD) was utilised as a chemical linker between two potentially interacting proteins. SDAD has a spacer arm of 13.5 Å, with an internal disulphide bond, allowing for the cleavable association of two closely interacting proteins. Chemical crosslinking was conducted as described in section 2.9.3. Crosslinking was performed following incubation of purified, soluble, cleaved C-term with either CRBP or full length STRA6, purified as described in sections 2.8.2 and 2.8.5 respectively, at room temperature for 30 minutes. Once the theoretical interaction was allowed to take place the chemical crosslinker, SDAD was incubated with the reaction. Following quenching of the amine reactive site of the crosslinker using 100mM Tris-HCl, the photo-reactive site of the crosslinker was allowed to bind to any nearby proteins by incubation under a UV source. Samples were then treated with Laemmli sample buffer for resolution by SDS-PAGE, with or without β-mercaptoethanol (β-ME). If the C-term interacted with CRBP or STRA6 one would observe a shift in position on a Western blot to a position consistent with the combined molecular weight of the two proteins. On treatment with β-ME the disulphide bond located in the spacer arm of SDAD would be reduced and both proteins would theoretically dissociate. The proteins would then appear at their predicted molecular weight position on a Western blot. No interaction was observed when C-term was incubated with CRBP or STRA6, Fig 5.29 and 5.30.

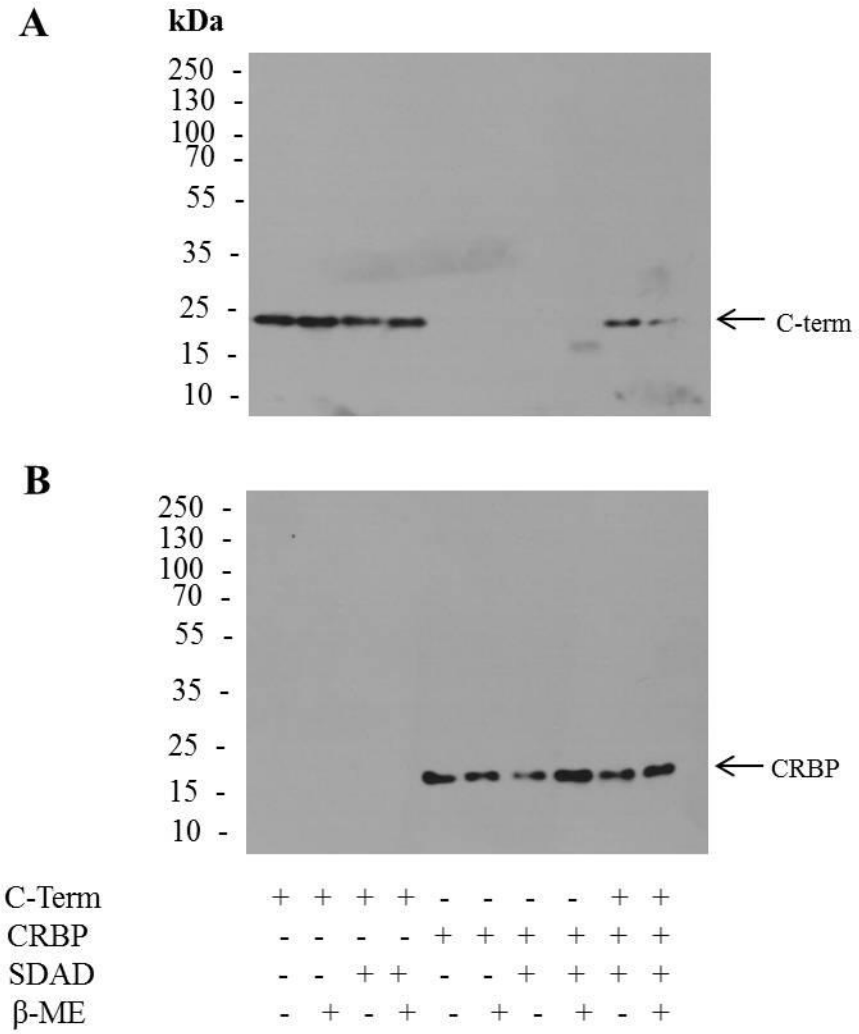

Fig 5.29 Chemical crosslinking of C-term with CRBP.

10µg of purified and cleaved C-term was incubated with 10µg CRBP at room temperature for 30 minutes, along with appropriate controls. The photo-activated crosslinker SDAD was then added to appropriate samples and incubated on ice for 2 hours. The crosslinking reaction was terminated with the addition of 100mM Tris-HCl. The reaction was then photo-activated on ice using a UV source. Samples were subsequently incubated with Laemmli sample buffer with or without β-ME at 75^{o}C for 5 minutes and analysed by SDS-PAGE and Western blotting. **A**. Representative anti-His Western blot showing the molecular weight of C-Term (16.8 kDa) following incubation with the crosslinking agent, SDAD and CRBP. **B**. Representative anti-CRBP Western blot showing the molecular weight of CRBP (15 kDa) following incubation with the crosslinking agent, SDAD and C-term.

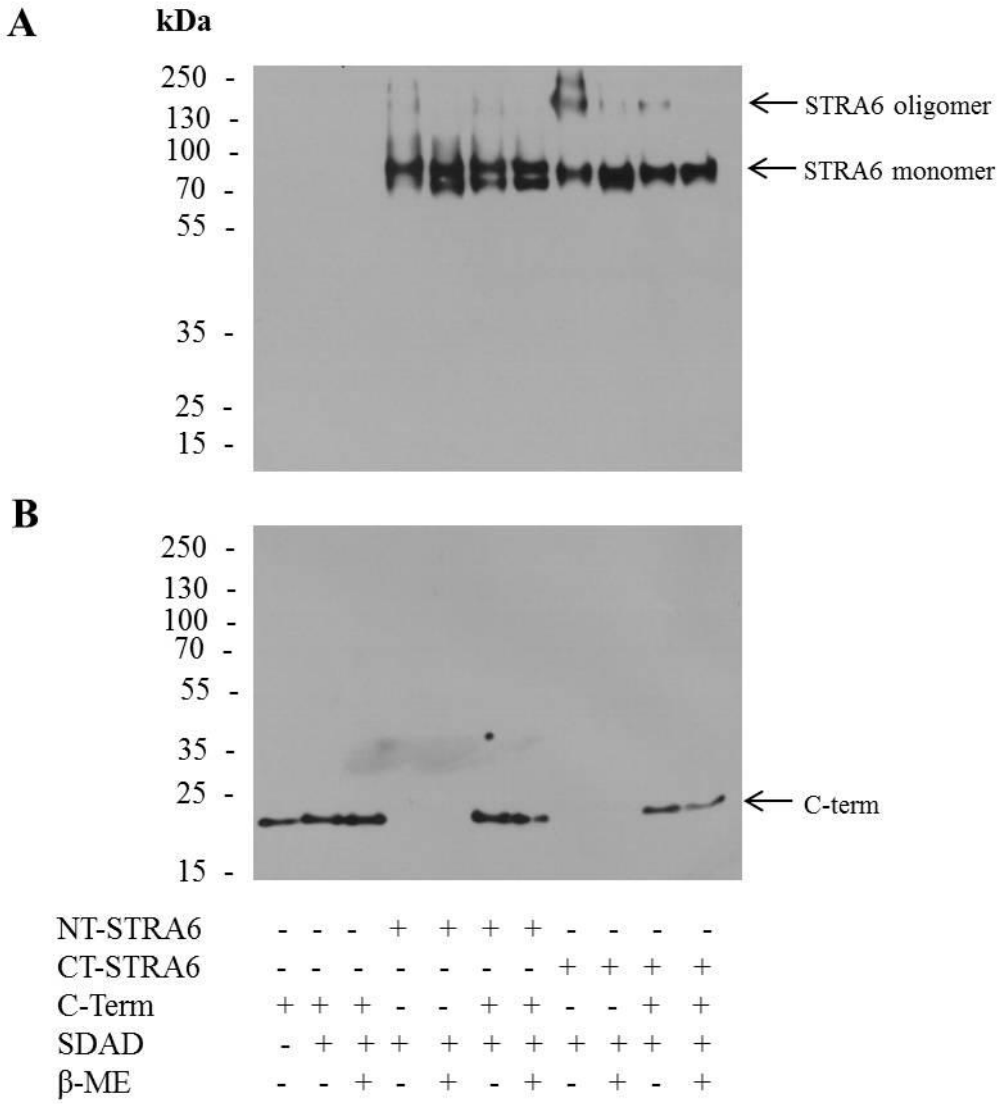

Fig 5.30 Chemical crosslinking of C-term with full length STRA6.

10µg of purified and cleaved C-term was incubated with 10µg of either N-terminal (NT-STRA6) or C-terminal (CT-STRA6) HA tagged STRA6 at room temperature for 30 minutes, along with appropriate controls. The photo-activated crosslinker SDAD was then added to appropriate samples and incubated on ice for 2 hours. The crosslinking reaction was terminated with the addition of 100mM Tris-HCl. The reaction was subsequently photo-activated on ice using a UV source. Samples were incubated with Laemmli sample buffer with or without β-ME at 75^{o}C for 5 minutes and analysed using a 4-20% gradient SDS-PAGE gel and Western blotting. **A**. Representative anti-HA Western blot showing the monomeric molecular weight of STRA6 (72 kDa) following incubation with the crosslinking agent, SDAD and C-term. **B**. Representative anti-His Western blot showing the molecular weight of C-term (16.8 kDa) following incubation with the crosslinking agent, SDAD and STRA6.

5.4 Summary of the structural and functional analysis of the C-terminus of STRA6:

The C-terminal region of STRA6 is a large intracellular domain with a putative phosphorylation site and SH2 motif. Efforts to produce a pure and soluble recombinant version of the C-terminus were largely successful. Topology prediction suggested the C-terminal region to consist of residues 497-667. Initial expression studies indicated that inclusion of residues 497-535, resulted in insoluble protein. Therefore, residues 535-667 were utilised in this study to represent this intracellular, C-terminal domain. As this stretch of amino acids only became soluble with the addition of detergent, there may still be a proportion of the structure partially inserted into the cell membrane.

With the addition of DDM, the MBP-tagged C-terminal domain eluted as a mono-disperse peak, at a position representing approximately 60 kDa, its predicted molecular weight. Upon removal of the MBP tag via TEV protease the resultant molecular weight of the domain would be 16.8 kDa. The cleaved domain eluted at 17-18 ml on gel filtration. Cytochrome c elutes at 18.5 ml which is 13.8 kDa. As both the tagged and cleaved versions of the C-terminus elute as a single mono-disperse peak at approximately the predicted molecular weight, one can assume the quaternary structure of the protein is monomeric.

As seen in Fig 5.30, STRA6 forms a higher molecular weight species with the addition of a chemical crosslinking agent, which is reversible with the addition of the reducing agent β-ME. This suggests that the receptor forms an oligomer. In order to determine if the C-terminal domain is a potential oligomerisation site, co-purification experiments were conducted with the protein and full length STRA6. The domain did not bind to STRA6, even in the presence of a crosslinking agent suggesting that it is not associated with the rest of the receptor and may be freely accessible to the intracellular milieu.

The C-terminal domain of STRA6 contains the highly conserved sequence, YTLL, which is a potential SH2 domain. In addition, it is a large intracellular domain which may be a potential interaction site for cytosolic proteins. Co-purification experiments with the intracellular acceptor for ROH, CRBP, did not reveal any interaction of the two proteins. Should they interact *in vivo*, the

contact may be transient in nature. Therefore, the crosslinking agent SDAD was utilised to stabilise any bond formed between the two proteins. Crosslinking studies did not reveal an interaction between them. Berry et al demonstrated that CRBP can bind to another intracellular region, IC3 (Berry et al., 2012). In addition, they indicated that the SH2 domain present in the C-terminus was necessary for the interaction of STRA6 with CRBP. They suggest this is due to the binding of JAK2 to the C-terminal region and subsequent phosphorylation of STRA6. The C-term may stabilise the interaction of CRBP with the IC3 region of STRA6, but not participate directly with the interaction.

Analysis of the secondary structure of the C-terminus revealed that it is primarily composed of alpha helix and connecting turns. As it has a defined structure, this suggests that this domain is independently folded. A predicted structure based on the "threading" algorithm is indicated. Thus, the C-terminal domain expressed in *E. coli* and purified in the presence of detergent appears to have a recognised, folded structure, the precise function of which has yet to be determined.

Chapter 6

Discussion

6.1 Summary of glycogen enzyme alterations in response to holo-RBP:

Several proteins were altered in the proteome of C2C12 muscle cells treated with holo-RBP overnight. Some of these changes can be attributed to the influx of ROH into the cell. However, other changes may be more complex. Most notably this exposure to holo-RBP resulted in the alteration of some of the enzymes involved in the regulation of glycogen storage and consumption. The abundance of the phosphatase, PP1β was reduced following 12 hours stimulation with holo-RBP. PP1β is an important phosphatase, responsible for the regulation of the rate limiting enzymes involved in glycogen metabolism. A decrease in PP1β levels would be anticipated to result in elevated levels of phosphorylation of its downstream targets, glycogen synthase and glycogen phosphorylase. Interestingly, glycogen phosphorylase expression was decreased in response to holo-RBP treatment. This event was unexpected and warrants further investigation. As expected, glycogen synthase phosphorylation levels were increased with holo-RBP treatment, but this event may occur before a downregulation of PP1β is evident. Therefore, there may be other factors contributing to increased glycogen synthase phosphorylation. This could be due to increased activity of the kinase responsible for this phosphorylation event, GSK3β.

Holo-RBP was demonstrated to cause a decrease in phosphorylation of the A subunit of PP2A. This may result in increased activity of the phosphatase. Interestingly, PP2A is the phosphatase responsible for activating GSK3β and may provide the link between holo-RBP treatment and increased glycogen synthase phosphorylation. Clearly holo-RBP has a negative impact on the enzymes involved in glycogen processing. The long-term consequences of this may contribute to RBP induced insulin resistance.

6.1.1 The potential long-term consequences of PP1β downregulation:

A decrease in PP1β abundance was observed. Sustained inhibition of this phosphatase could result in a decrease in glycogen synthase activity and potentially inefficient glycogen synthesis. It is unknown how expression of PP1β is regulated. However, the phosphatase's activity is controlled by subunits which direct it to glycogen granules. Alterations in the subunits of PP1β which target the enzyme to glycogen granules have uncovered some interesting results.

The G_m subunit is responsible for targeting PP1β to glycogen granules, and is the most abundant glycogen targeting subunit in skeletal muscle (Cohen, 2002). Mice in which the gene encoding G_m was disrupted, demonstrated a decreased ability to clear a bolus of glucose (Delibegovic et al., 2003). With age, mice developed overt insulin resistance. G_m knockout also resulted in decreased expression of total PP1β levels in skeletal muscle, which could also have contributed to insulin resistance (Delibegovic et al., 2003). G_m knockout mice displayed decreased PP1β activity and correspondingly lower levels of muscle glycogen compared to WT. Interestingly, G_m knockout mice also displayed excessive weight gain. This is thought to be due to the inability to direct glucose towards storage as glycogen, and subsequent storage of glucose as fat (Delibegovic et al., 2003). Therefore, long term downregulation of PP1β in muscle tissue may have a detrimental effect on glycogen storage and this could result in impaired glucose clearance and insulin resistance.

6.1.2 The physiological impact of decreased abundance of glycogen phosphorylase:

Unexpectedly, glycogen phosphorylase abundance was also decreased following holo-RBP treatment. One would expect phosphorylation levels to increase as a result of PP1β downregulation, but not expression levels. This may be due to lowered levels of glycogen present in the cell. Total levels of glycogen would need to be assessed in order to determine if this may be having a negative impact on glycogen phosphorylase expression. Glycogen phosphorylase is an important enzyme for the utilisation of energy stores in times of high energy consumption, such as during exercise. Prolonged downregulation of this enzyme may have detrimental effects on energy generation in the cell.

The predominant storage sites of glycogen are the liver and muscle. Interestingly, inhibition of liver glycogen phosphorylase is a novel strategy for the treatment of type II diabetes. When the liver becomes insulin resistant excess glucose release into the bloodstream can occur, elevating already higher than normal levels of plasma glucose (Moller, 2001). Excess hepatic glucose production occurs due to a reduction in insulin signalling, leading to uncontrolled glycogen phosphorylase activity and glycogenolysis. Specific inhibition of glycogen phosphorylase is one strategy used to prevent mobilisation of excess glucose into the bloodstream. In ob/ob diabetic mice, a selective glycogen phosphorylase inhibitor reduced fasting plasma glucose to near normal levels (Martin et al., 1998). In the present study hepatic HEPG2 cells treated with holo-RBP did not display a decrease in glycogen phosphorylase expression. This may be due to the lack of STRA6 expression in this cell type. Therefore, the effect of holo-RBP on glycogen phosphorylase may be muscle specific. In the whole animal system, holo-RBP may not affect the liver isoform.

McArdle's disease is a unique glycogen storage disorder. Mutations in the muscle glycogen phosphorylase gene result in loss of expression of the enzyme specifically in muscle tissue (Lubran, 1975). Patients with the disease display chronic elevated muscle glycogen levels and fatigue very quickly during exercise as a result of inefficient use of this important energy store. A study conducted by Nielson and colleagues observed that patients with McArdle's disease display insulin resistance (Nielsen et al., 2002). A small cohort of patients was assessed for their responsiveness to insulin treatment. Four out of six patients demonstrated impaired insulin stimulated glucose clearance. Decreased glycogen synthase activity was observed and this was concomitant with elevated phosphorylation levels of this enzyme. Elevated glycogen levels may be the reason for decreased insulin signalling in patients with the disorder (Nielsen et al., 2002).

Overnight stimulation of muscle cells with holo-RBP resulted in a dramatic decrease in glycogen phosphorylase expression. More study is needed to determine if this effect persists with time and if glycogen levels are affected. It would be very interesting to assess the effect of long-term holo-RBP treatment in mice on glycogen levels in muscle and abundance and phosphorylation state of the

enzymes involved in its regulation. Cleary disorders affecting glycogen utilisation and production can be a contributing factor to insulin resistance.

6.1.3 Elevated glycogen synthase phosphorylation and its impact on glycogen storage:

Elevated levels of glycogen synthase phosphorylation were observed after 8 hours treatment with holo-RBP. Phosphorylation peaked at 12 hours which is the timepoint at which PP1β downregulation became apparent. Decreased levels of the phosphatase, PP1β, may be the underlying cause of an increase in glycogen synthase phosphorylation. It is not known how expression of PP1β is regulated but its activity is controlled by targeting subunits. Delibegovic and colleagues observed that when cells were deficient in the glycogen targeting subunit G_m there was a decrease in PP1β abundance (Delibegovic et al., 2003). They attribute this event to increased degradation of the phosphatase, although this has not been substantiated. Events may be occurring prior to a downregulation of PP1β to prevent its localisation with glycogen granules where glycogen synthase is located. This may explain why an increase in glycogen synthase phosphorylation was apparent before a decrease in PP1β expression became significant. Further work is required to assess the localisation of PP1β in response to holo-RBP treatment.

The phospho-specific glycogen synthase antibody utilised in this study was selective for serine 640. This residue is the predominant phosphorylation site and a known target of GSK3β (Roach et al., 2012). Another explanation for elevated glycogen synthase phosphorylation levels would therefore be increased GSK3β activity. The activity of this kinase may be elevated due to increased PP2A-B56δ phosphatase activity. As described in section 3.3.6, PP2A in complex with the B56δ subunit removes the inhibitory phosphate located at serine 9 of GSK3β. No definitive decrease in phosphorylation of this residue was observed in response to holo-RBP treatment. However, GSK3β activity is also controlled by phosphorylation at tyrosine 216 (Hughes et al., 1993; Rayasam et al., 2009). Phosphorylation of this site results in increased activity of the kinase. The kinase responsible for phosphorylating GSK3β at tyrosine 216 has not been formally identified but a study conducted by Pijet et al suggests that mitogen-activated protein kinase kinase (MEK) may be involved (Pijet et al.,

2013). A specific inhibitor of the enzyme prevented leptin induced phosphorylation at tyrosine 216. It would be interesting to determine if holo-RBP treatment results in elevated phosphorylation of this residue.

Elevated glycogen synthase phosphorylation may have a physiological impact on glycogen storage in muscle cells. Glycogen synthase is rendered inactive when phosphorylated. Prolonged inhibition of activity could result in the inability to convert glucose into glycogen stores. Glycogen synthase phosphorylation is reversed in response to insulin stimulation. It would be interesting to observe whether holo-RBP inhibits insulin stimulated glycogen synthase activation. Glycogen synthesis is impaired in patients with type II diabetes, most likely due to a reduction in glucose uptake as a result of insulin resistance (Roach et al., 2012). A disruption in the muscle glycogen synthase gene (GYS1) results in decreased glycogen content in muscle (Groop and Orho-Melander, 2008). A study conducted by Groop et al observed a disruption in the GYS1 gene in 30% of type II diabetic patients that they studied (Groop et al., 1993). Patients in which the mutation was observed also had a stronger familial pre-disposition to the disease.

Collectively holo-RBP appears to negatively regulate several enzymes involved in glycogen storage and utilisation. The long term physiological effect of elevated serum RBP levels may have a considerable impact on total muscle glycogen levels. Both the inability to store glucose as glycogen and the inability to utilise glycogen stores appear to be contributing factors to insulin resistance. Whole animal studies may be necessary to reveal the glycogen content of muscle tissue in response to holo-RBP. Should interruption of glycogen metabolism occur in muscle tissue before the onset of overt insulin resistance it may reveal the underlying mechanism of RBP induced insulin resistance.

6.2 Summary of the proteomic analysis of the effect of RTC-15 on C2C12 cells:

Proteomic analysis of C2C12 cells treated with RTC-15 overnight revealed changes in several proteins involved in diverse regulatory pathways of the cell. The underlying mechanism of action of the compound was not revealed by proteomics but by alternative means. Inhibition of NADH dehydrogenase appears to be the root cause of RTC-15 stimulated glucose uptake in muscle cells. Alterations in the proteome substantiate this inhibitory action, as several proteins involved in metabolic activity were affected. The proteomic study did demonstrate that the effect of RTC-15 on the cell was not toxic, as compensatory mechanisms are activated to combat decreased energy production. ECH1 expression is elevated which suggests that fatty acid consumption is increased. This may also explain why animals administered the RTC compounds along with a high fat diet appear not to gain weight when compared to animals on a high fat diet alone. In addition, TPI expression was increased, which strongly suggests elevated levels of glycolysis.

Interestingly, several changes were observed in cytoskeletal proteins and calcium binding proteins. Increased glucose influx into the cell can only occur via elevated GLUT4 translocation to the cell membrane. Increased intracellular calcium is known to stimulate vesicle trafficking to the membrane and this event is dependent on cytoskeletal proteins to navigate the vesicle to the correct location. It would be interesting to assess intracellular calcium levels in response to RTC-15 treatment to determine if this may be stimulating GLUT4 translocation to the cell surface.

Several downstream targets of PKC were altered in response to RTC-15, such as swiprosin-1, calponin-3 and eIF-6. This is a strong indicator that some isoforms of PKC are activated with RTC-15 treatment. PKC is a known regulator of the cytoskeleton in muscle cells. Therefore, PKC activation via RTC-15 may also contribute to vesicle trafficking to the cell membrane.

6.3 Characterisation of the C-terminal domain of STRA6:

Structural analysis of the C-terminal region of STRA6 has revealed that this stretch of amino acids is a highly ordered and potentially an independently folded domain. CD analysis and 3D modelling revealed that the C-terminus is primarily composed of alpha helix with other residues ordered as turns between the helices. Removal of the MBP tag appears not to alter the structure of the C-terminus and it remains a structured domain. This bodes well for further structural analysis. In addition, with the alteration of pH, the cleaved C-terminal region is stable for long periods at room temperature. Quaternary structure of the C-terminus can be definitively assigned as monomeric. The domain did not co-purify with full length STRA6 and did not crosslink with either itself or the full length receptor.

Functional analysis did not reveal an interaction of the domain with CRBP, the intracellular acceptor for ROH. It may, however, form a docking site for other cytosolic proteins. Further study is required to determine if the recombinant domain produced in *E. coli*, is functional. One caveat with bacterial protein expression is the lack of eukaryotic post translational modifications. According to Berry et al the C-terminus contains a highly conserved phosphorylation site which forms a putative SH2 domain (Berry et al., 2011). In addition, phosphorylation of the C-terminus was only observed upon stimulation of the full length receptor with holo-RBP. The independently expressed C-terminal region may not possess the capability for phosphorylation, which could be necessary to initiate binding of interacting proteins. Perhaps the introduction of a phosphomimetic residue such as glutamic acid could aid in the search for proteins that interact with this important domain.

6.4 Future Work:

During the course of this study several of the original aims were achieved. However, most aspects of the research covered in this body of work warrant further study. Continuation of this investigation can be divided into the respective studies conducted.

6.4.1 Investigation of the effect of holo-RBP on the proteome of muscle cells:

Several unanswered questions exist regarding work carried out to determine the effect of holo-RBP on muscle cells. PP2A phosphorylation levels were elevated in response to RBP treatment overnight. Phosphorylation may increase the activity of the phosphatase, resulting in a downstream effect on glycogen synthase. The phosphatase inhibitor okadaic acid can be used to selectively inhibit PP2A activity. It would be interesting to observe if the administration of okadaic acid prevented the downstream effects of holo-RBP on glycogen regulating enzymes.

B56δ expression appeared to decrease in a time-dependent manner in response to holo-RBP treatment. This may be due to activation of a negative feedback mechanism involving c-Myc. Analysis of c-Myc abundance may reveal whether PP2A complexed with B56δ results in increased degradation of c-Myc. This may shed light on whether the PP2A holo-enzyme is more active with RBP treatment.

The assessment of glycogen levels in muscle cells treated with holo-RBP may reveal if this protein is having a detrimental effect on glucose storage. If glycogen levels are decreased in response to holo-RBP it may explain why an affiliated decrease in glycogen phosphorylase expression is observed. It may also partially explain why insulin resistance occurs in muscle tissue of mice treated with elevated levels of holo-RBP.

6.4.2 Investigation of the effect of RTC-15 on the proteome of muscle cells:

Several proteins appeared altered in response to RTC-15 treatment. The implications of the observed changes in the proteome need to be addressed. It appears that due to NADH dehydrogenase inhibition the cell is utilising alternate energy sources. The enzyme ECH1 was elevated in expression, and this protein is involved in fatty acid oxidation. It would be interesting to assess the total levels of fatty acid in control cells versus cells treated with RTC-15. As discussed previously, mice fed a high fat diet and RTC-15 showed reduced weight gain. Consumption of fatty acid as an energy source may explain why this occurs.

Variations in several proteins involved in calcium handling were observed. This may be as a result of elevated intracellular calcium levels. Therefore, assessment of calcium levels is necessary to determine the nature of expression of this cohort of proteins. As discussed in section 4.4 increased cytosolic calcium levels are associated with vesicle trafficking to the cell membrane. RTC-15 may cause an influx of calcium to the cytosol and subsequent translocation of GLUT4 vesicles to the plasma membrane. The abundance of GLUT4 in the membrane in response to RTC-15 should also be assessed to identify by what means glucose is entering the cell.

Numerous downstream targets of PKC appeared altered with RTC-15 administration. This suggests an increase in activity of this kinase. Therefore, the effect of RTC-15 on PKC should be assessed to determine if this kinase is altered by the compound. A specific inhibitor of PKC such as calphostin C could be used to address this issue. PKC-induced alterations in expression of downstream targets such as swiprosin-1 and phosphorylation targets such as calponin-3 could be monitored to reveal if RTC-15 is activating the kinase.

6.4.3 Characterisation of the C-terminus of STRA6:

Large amounts of a recombinant version of the C-terminus of STRA6 can be generated in a soluble and stable form. Preliminary structural analysis of the protein has revealed that it is folded into an ordered domain. The ultimate goal for production of soluble and stable recombinant protein is determination of the 3-D structure. The cleaved version of the C-terminus will be subjected to crystallisation trials in the hope of generating this structural information.

Further work is necessary to determine the exact function of this independently folded domain. As the C-terminal region is intracellular it may interact with cytosolic proteins involved in ROH handling. Over-expression of LRAT alone has been shown to cause an increase ROH influx (Kawaguchi et al., 2011). This suggests a direct interaction with STRA6. Therefore, the C-terminal region may be a potential binding site for LRAT. Berry et al also suggest that it is a docking site for JAK2 (Berry et al., 2011). This specific interaction should be verified with the recombinant protein generated in this study. Work is on-going in our laboratory to uncover novel interacting proteins for STRA6. The C-terminal domain will be assessed as a putative binding site for some of the novel interactions. As discussed in section 6.3, the C-terminus is also a potential phosphorylation site. Thus, it may be necessary to express the domain in mammalian cells to determine novel protein interactions.

The transport and utilisation of retinoids is a tightly regulated process, an intensive operation for such a small, seemingly insignificant molecule. The study of retinoid biology has revealed many interesting aspects of the importance of this simple vitamin for cellular homeostasis. However, there are many aspects of the system which have yet to be discovered.

.

Chapter 7

Bibliography

Abdul-Gader, A., A. J. Miles, and B. A. Wallace, 2011, A reference dataset for the analyses of membrane protein secondary structures and transmembrane residues using circular dichroism spectroscopy: Bioinformatics, v. 27, p. 1630-6.

Agrawal, G. K., and J. J. Thelen, 2005, Development of a simplified, economical polyacrylamide gel staining protocol for phosphoproteins: Proteomics, v. 5, p. 4684-8.

Aguirre, V., T. Uchida, L. Yenush, R. Davis, and M. F. White, 2000, The c-Jun NH(2)-terminal kinase promotes insulin resistance during association with insulin receptor substrate-1 and phosphorylation of Ser(307): J Biol Chem, v. 275, p. 9047-54.

Ahmad, S., Y. Wang, G. M. Shaik, A. H. Burghes, and L. Gangwani, 2012, The zinc finger protein ZPR1 is a potential modifier of spinal muscular atrophy: Hum Mol Genet, v. 21, p. 2745-58.

Aledo, J. C., and H. S. Hundal, 1996, Isolation and characterization of two intracellular GLUT4 glucose transporter pools in rat skeletal muscle: Biochem Soc Trans, v. 24, p. 190S.

Banci, L., I. Bertini, S. Ciofi-Baffoni, F. Boscaro, A. Chatzi, M. Mikolajczyk, K. Tokatlidis, and J. Winkelmann, 2011, Anamorsin is a [2Fe-2S] cluster-containing substrate of the Mia40-dependent mitochondrial protein trapping machinery: Chem Biol, v. 18, p. 794-804.

Baron, J. M., R. Heise, W. S. Blaner, M. Neis, S. Joussen, A. Dreuw, Y. Marquardt, J. H. Saurat, H. F. Merk, D. R. Bickers, and F. K. Jugert, 2005, Retinoic acid and its 4-oxo metabolites are functionally active in human skin cells in vitro: J Invest Dermatol, v. 125, p. 143-53.

Berry, D. C., H. Jin, A. Majumdar, and N. Noy, 2011, Signaling by vitamin A and retinol-binding protein regulates gene expression to inhibit insulin responses: Proc Natl Acad Sci U S A, v. 108, p. 4340-5.

Berry, D. C., and N. Noy, 2012, Signaling by vitamin A and retinol-binding protein in regulation of insulin responses and lipid homeostasis: Biochim Biophys Acta, v. 1821, p. 168-76.

Berry, D. C., S. M. O'Byrne, A. C. Vreeland, W. S. Blaner, and N. Noy, 2012, Cross Talk between Signaling and Vitamin A Transport by the Retinol-Binding Protein Receptor STRA6: Mol Cell Biol, v. 32, p. 3164-75.

Blanchard, A., V. Ohanian, and D. Critchley, 1989, The structure and function of alpha-actinin: J Muscle Res Cell Motil, v. 10, p. 280-9.

Bouillet, P., V. Sapin, C. Chazaud, N. Messaddeq, D. Décimo, P. Dollé, and P. Chambon, 1997, Developmental expression pattern of Stra6, a retinoic acid-responsive gene encoding a new type of membrane protein: Mech Dev, v. 63, p. 173-86.

Brady, M. J., and A. R. Saltiel, 2001, The role of protein phosphatase-1 in insulin action: Recent Prog Horm Res, v. 56, p. 157-73.

Brautigan, D. L., 1995, Flicking the switches: phosphorylation of serine/threonine protein phosphatases: Semin Cancer Biol, v. 6, p. 211-7.

Brockington, A., P. R. Heath, H. Holden, P. Kasher, F. L. Bender, F. Claes, D. Lambrechts, M. Sendtner, P. Carmeliet, and P. J. Shaw, 2010, Downregulation of genes with a function in axon outgrowth and synapse formation in motor neurones of the VEGFdelta/delta mouse model of amyotrophic lateral sclerosis: BMC Genomics, v. 11, p. 203.

Cadenas, E., A. Boveris, C. I. Ragan, and A. O. Stoppani, 1977, Production of superoxide radicals and hydrogen peroxide by NADH-ubiquinone reductase and ubiquinol-cytochrome c reductase from beef-heart mitochondria: Arch Biochem Biophys, v. 180, p. 248-57.

Campos-Sandoval, J. A., C. Redondo, G. K. Kinsella, A. Pal, G. Jones, G. S. Eyre, S. C. Hirst, and J. B. Findlay, 2011, Fenretinide derivatives act as disrupters of interactions of serum retinol binding protein (sRBP) with transthyretin and the sRBP receptor: J Med Chem, v. 54, p. 4378-87.

Carling, D., 2007, The role of the AMP-activated protein kinase in the regulation of energy homeostasis: Novartis Found Symp, v. 286, p. 72-81; discussion 81-5, 162-3, 196-203.

Casey, J., R. Kawaguchi, M. Morrissey, H. Sun, P. McGettigan, J. E. Nielsen, J. Conroy, R. Regan, E. Kenny, P. Cormican, D. W. Morris, P. Tormey, M. N. Chróinín, B. N. Kennedy, S. Lynch, A. Green, and S. Ennis, 2011, First implication of STRA6 mutations in isolated anophthalmia, microphthalmia, and coloboma: a new dimension to the STRA6 phenotype: Hum Mutat, v. 32, p. 1417-26.

Ceci, M., C. Gaviraghi, C. Gorrini, L. A. Sala, N. Offenhäuser, P. C. Marchisio, and S. Biffo, 2003, Release of eIF6 (p27BBP) from the 60S subunit allows 80S ribosome assembly: Nature, v. 426, p. 579-84.

Ceulemans, H., and M. Bollen, 2004, Functional diversity of protein phosphatase-1, a cellular economizer and reset button: Physiol Rev, v. 84, p. 1-39.

Chambon, P., 1996, A decade of molecular biology of retinoic acid receptors: FASEB J, v. 10, p. 940-54.

Chappell, D. S., N. A. Patel, K. Jiang, P. Li, J. E. Watson, D. M. Byers, and D. R. Cooper, 2009, Functional involvement of protein kinase C-betaII and its substrate, myristoylated alanine-rich C-kinase substrate (MARCKS), in insulin-stimulated glucose transport in L6 rat skeletal muscle cells: Diabetologia, v. 52, p. 901-11.

Chassaing, N., N. Ragge, A. Kariminejad, A. Buffet, S. Ghaderi-Sohi, J. Martinovic, and P. Calvas, 2012, Mutation analysis of the STRA6 gene in isolated and non-isolated anophthalmia/microphthalmia: Clin Genet, v. 9999.

Chazaud, C., P. Bouillet, M. Oulad-Abdelghani, and P. Dollé, 1996, Restricted expression of a novel retinoic acid responsive gene during limb bud dorsoventral patterning and endochondral ossification: Dev Genet, v. 19, p. 66-73.

Chen, L., D. J. Magliano, and P. Z. Zimmet, 2012, The worldwide epidemiology of type 2 diabetes mellitus--present and future perspectives: Nat Rev Endocrinol, v. 8, p. 228-36.

Chipman, D. M., and N. Sharon, 1969, Mechanism of lysozyme action: Science, v. 165, p. 454-65.

Christou, G. A., A. D. Tselepis, and D. N. Kiortsis, 2012, The metabolic role of retinol binding protein 4: an update: Horm Metab Res, v. 44, p. 6-14.

Clagett-Dame, M., and D. Knutson, 2011, Vitamin A in reproduction and development: Nutrients, v. 3, p. 385-428.

Cohen, P., 1978, The role of cyclic-AMP-dependent protein kinase in the regulation of glycogen metabolism in mammalian skeletal muscle: Curr Top Cell Regul, v. 14, p. 117-96.

Cohen, P. T., 2002, Protein phosphatase 1--targeted in many directions: J Cell Sci, v. 115, p. 241-56.

Copps, K. D., and M. F. White, 2012, Regulation of insulin sensitivity by serine/threonine phosphorylation of insulin receptor substrate proteins IRS1 and IRS2: Diabetologia, v. 55, p. 2565-82.

Cui, X. Y., P. F. Fu, D. N. Pan, Y. Zhao, J. Zhao, and B. C. Zhao, 2003, The antioxidant effects of ribonuclease inhibitor: Free Radic Res, v. 37, p. 1079-85.

Dantuma, N. P., C. Heinen, and D. Hoogstraten, 2009, The ubiquitin receptor Rad23: at the crossroads of nucleotide excision repair and proteasomal degradation: DNA Repair (Amst), v. 8, p. 449-60.

Dawson, M. I., and Z. Xia, 2012, The retinoid X receptors and their ligands: Biochim Biophys Acta, v. 1821, p. 21-56.

Dekaney, C. M., G. Wu, Y. L. Yin, and L. A. Jaeger, 2008, Regulation of ornithine aminotransferase gene expression and activity by all-transretinoic acid in Caco-2 intestinal epithelial cells: J Nutr Biochem, v. 19, p. 674-81.

Dekaney, C. M., Wu, G., & Jaeger, L. A, 2000, Regulation and function of ornithine aminotransferase in animals.: *Trends Comp Biochem Physiol*, v. 6, p. 175-83.

del Arco, A., and J. Satrústegui, 2004, Identification of a novel human subfamily of mitochondrial carriers with calcium-binding domains: J Biol Chem, v. 279, p. 24701-13.

Delibegovic, M., C. G. Armstrong, L. Dobbie, P. W. Watt, A. J. Smith, and P. T. Cohen, 2003, Disruption of the striated muscle glycogen targeting subunit PPP1R3A of protein phosphatase 1 leads to increased weight gain, fat deposition, and development of insulin resistance: Diabetes, v. 52, p. 596-604.

Donovan, M., B. Olofsson, A. L. Gustafson, L. Dencker, and U. Eriksson, 1995, The cellular retinoic acid binding proteins: J Steroid Biochem Mol Biol, v. 53, p. 459-65.

Dukes, A. A., V. S. Van Laar, M. Cascio, and T. G. Hastings, 2008, Changes in endoplasmic reticulum stress proteins and aldolase A in cells exposed to dopamine: J Neurochem, v. 106, p. 333-46.

Edwards, R., D. P. Dixon, and V. Walbot, 2000, Plant glutathione S-transferases: enzymes with multiple functions in sickness and in health: Trends Plant Sci, v. 5, p. 193-8.

Emans, N., J. P. Gorvel, C. Walter, V. Gerke, R. Kellner, G. Griffiths, and J. Gruenberg, 1993, Annexin II is a major component of fusogenic endosomal vesicles: J Cell Biol, v. 120, p. 1357-69.

Fleischer, T. C., C. M. Weaver, K. J. McAfee, J. L. Jennings, and A. J. Link, 2006, Systematic identification and functional screens of uncharacterized proteins associated with eukaryotic ribosomal complexes: Genes Dev, v. 20, p. 1294-307.

Fontana, J. A., and A. K. Rishi, 2002, Classical and novel retinoids: their targets in cancer therapy: Leukemia, v. 16, p. 463-72.

Foster, L. J., A. Rudich, I. Talior, N. Patel, X. Huang, L. M. Furtado, P. J. Bilan, M. Mann, and A. Klip, 2006, Insulin-dependent interactions of proteins with GLUT4 revealed through stable isotope labeling by amino acids in cell culture (SILAC): J Proteome Res, v. 5, p. 64-75.

Franzoni, L., C. Lücke, C. Pérez, D. Cavazzini, M. Rademacher, C. Ludwig, A. Spisni, G. L. Rossi, and H. Rüterjans, 2002, Structure and backbone dynamics of Apo- and holo-cellular retinol-binding protein in solution: J Biol Chem, v. 277, p. 21983-97.

Furia, A., M. Moscato, G. Calì, E. Pizzo, E. Confalone, M. R. Amoroso, F. Esposito, L. Nitsch, and G. D'Alessio, 2011, The ribonuclease/angiogenin inhibitor is also present in mitochondria and nuclei: FEBS Lett, v. 585, p. 613-7.

Galcheva-Gargova, Z., L. Gangwani, K. N. Konstantinov, M. Mikrut, S. J. Theroux, T. Enoch, and R. J. Davis, 1998, The cytoplasmic zinc finger protein ZPR1 accumulates in the nucleolus of proliferating cells: Mol Biol Cell, v. 9, p. 2963-71.

Galcheva-Gargova, Z., K. N. Konstantinov, I. H. Wu, F. G. Klier, T. Barrett, and R. J. Davis, 1996, Binding of zinc finger protein ZPR1 to the epidermal growth factor receptor: Science, v. 272, p. 1797-802.

Gangwani, L., 2006, Deficiency of the zinc finger protein ZPR1 causes defects in transcription and cell cycle progression: J Biol Chem, v. 281, p. 40330-40.

Gangwani, L., M. Mikrut, Z. Galcheva-Gargova, and R. J. Davis, 1998, Interaction of ZPR1 with translation elongation factor-1alpha in proliferating cells: J Cell Biol, v. 143, p. 1471-84.

Garcia, A. D., J. Otero, J. Lebowitz, P. Schuck, and B. Moss, 2006, Quaternary structure and cleavage specificity of a poxvirus holliday junction resolvase: J Biol Chem, v. 281, p. 11618-26.

Gerke, V., C. E. Creutz, and S. E. Moss, 2005, Annexins: linking Ca2+ signalling to membrane dynamics: Nat Rev Mol Cell Biol, v. 6, p. 449-61.

Ghyselinck, N. B., C. Båvik, V. Sapin, M. Mark, D. Bonnier, C. Hindelang, A. Dierich, C. B. Nilsson, H. Håkansson, P. Sauvant, V. Azaïs-Braesco, M. Frasson, S. Picaud, and P. Chambon, 1999, Cellular retinol-binding protein I is essential for vitamin A homeostasis: EMBO J, v. 18, p. 4903-14.

Golzio, C., J. Martinovic-Bouriel, S. Thomas, S. Mougou-Zrelli, B. Grattagliano-Bessieres, M. Bonniere, S. Delahaye, A. Munnich, F. Encha-Razavi, S. Lyonnet, M. Vekemans, T. Attie-Bitach, and H. C. Etchevers, 2007, Matthew-Wood syndrome is caused by truncating mutations in the retinol-binding protein receptor gene STRA6: Am J Hum Genet, v. 80, p. 1179-87.

Goodman, D. S., 1984, Overview of current knowledge of metabolism of vitamin A and carotenoids: J Natl Cancer Inst, v. 73, p. 1375-9.

Gopalakrishnan, S., M. Rahmatullah, G. A. Radke, S. Powers-Greenwood, and T. E. Roche, 1989, Role of protein X in the function of the mammalian pyruvate dehydrogenase complex: Biochem Biophys Res Commun, v. 160, p. 715-21.

Graham, T. E., C. J. Wason, M. Blüher, and B. B. Kahn, 2007, Shortcomings in methodology complicate measurements of serum retinol binding protein (RBP4) in insulin-resistant human subjects: Diabetologia, v. 50, p. 814-23.

Graham, T. E., Q. Yang, M. Blüher, A. Hammarstedt, T. P. Ciaraldi, R. R. Henry, C. J. Wason, A. Oberbach, P. A. Jansson, U. Smith, and B. B. Kahn, 2006, Retinol-binding protein 4 and insulin resistance in lean, obese, and diabetic subjects: N Engl J Med, v. 354, p. 2552-63.

Greenfield, N. J., 2006, Using circular dichroism spectra to estimate protein secondary structure: Nat Protoc, v. 1, p. 2876-90.

Grimmler, M., S. Otter, C. Peter, F. Müller, A. Chari, and U. Fischer, 2005, Unrip, a factor implicated in cap-independent translation, associates with the cytosolic SMN complex and influences its intracellular localization: Hum Mol Genet, v. 14, p. 3099-111.

Groop, L., and M. Orho-Melander, 2008, New insights into impaired muscle glycogen synthesis: PLoS Med, v. 5, p. e25.

Groop, L. C., M. Kankuri, C. Schalin-Jäntti, A. Ekstrand, P. Nikula-Ijäs, E. Widén, E. Kuismanen, J. Eriksson, A. Franssila-Kallunki, and C. Saloranta, 1993, Association between polymorphism of the glycogen synthase gene and non-insulin-dependent diabetes mellitus: N Engl J Med, v. 328, p. 10-4.

Guo, H., and Z. Damuni, 1993, Autophosphorylation-activated protein kinase phosphorylates and inactivates protein phosphatase 2A: Proc Natl Acad Sci U S A, v. 90, p. 2500-4.

Haigis, M. C., E. L. Kurten, and R. T. Raines, 2003, Ribonuclease inhibitor as an intracellular sentry: Nucleic Acids Res, v. 31, p. 1024-32.

Han, S. P., Y. H. Tang, and R. Smith, 2010, Functional diversity of the hnRNPs: past, present and perspectives: Biochem J, v. 430, p. 379-92.

Hatefi, Y., and W. G. Hanstein, 1969, Solubilization of particulate proteins and nonelectrolytes by chaotropic agents: Proc Natl Acad Sci U S A, v. 62, p. 1129-36.

Heller, J., 1975, Interactions of plasma retinol-binding protein with its receptor. Specific binding of bovine and human retinol-binding protein to pigment epithelium cells from bovine eyes: J Biol Chem, v. 250, p. 3613-9.

Heller, J., and J. Horwitz, 1973, Conformational changes following interaction between retinol isomers and human retinol-binding protein and between the retinol-binding protein and prealbumin: J Biol Chem, v. 248, p. 6308-16.

Huang, J., S. H. Hsia, T. Imamura, I. Usui, and J. M. Olefsky, 2004, Annexin II is a thiazolidinedione-responsive gene involved in insulin-induced glucose transporter isoform 4 translocation in 3T3-L1 adipocytes: Endocrinology, v. 145, p. 1579-86.

Hughes, K., E. Nikolakaki, S. E. Plyte, N. F. Totty, and J. R. Woodgett, 1993, Modulation of the glycogen synthase kinase-3 family by tyrosine phosphorylation: EMBO J, v. 12, p. 803-8.

Hundal, H. S., T. Ramlal, R. Reyes, L. A. Leiter, and A. Klip, 1992, Cellular mechanism of metformin action involves glucose transporter translocation from an intracellular pool to the plasma membrane in L6 muscle cells: Endocrinology, v. 131, p. 1165-73.

Hyung, S. J., S. Deroo, and C. V. Robinson, 2010, Retinol and retinol-binding protein stabilize transthyretin via formation of retinol transport complex: ACS Chem Biol, v. 5, p. 1137-46.

Idres, N., J. Marill, M. A. Flexor, and G. G. Chabot, 2002, Activation of retinoic acid receptor-dependent transcription by all-trans-retinoic acid metabolites and isomers: J Biol Chem, v. 277, p. 31491-8.

Ikura, M., 1996, Calcium binding and conformational response in EF-hand proteins: Trends Biochem Sci, v. 21, p. 14-7.

Isken, A., M. Golczak, V. Oberhauser, S. Hunzelmann, W. Driever, Y. Imanishi, K. Palczewski, and J. von Lintig, 2008, RBP4 disrupts vitamin A uptake homeostasis in a STRA6-deficient animal model for Matthew-Wood syndrome: Cell Metab, v. 7, p. 258-68.

Ivaska, J., H. M. Pallari, J. Nevo, and J. E. Eriksson, 2007, Novel functions of vimentin in cell adhesion, migration, and signaling: Exp Cell Res, v. 313, p. 2050-62.

Jaffe, E. K., 2004, The porphobilinogen synthase catalyzed reaction mechanism: Bioorg Chem, v. 32, p. 316-25.

Jensen, J., E. Jebens, E. O. Brennesvik, J. Ruzzin, M. A. Soos, E. M. Engebretsen, S. O'Rahilly, and J. P. Whitehead, 2006, Muscle glycogen inharmoniously regulates glycogen synthase activity, glucose uptake, and proximal insulin signaling: Am J Physiol Endocrinol Metab, v. 290, p. E154-E162.

Jin, J., E. E. Arias, J. Chen, J. W. Harper, and J. C. Walter, 2006, A family of diverse Cul4-Ddb1-interacting proteins includes Cdt2, which is required for S phase destruction of the replication factor Cdt1: Mol Cell, v. 23, p. 709-21.

Jung, D. H., S. H. Mo, and D. H. Kim, 2006, Calumenin, a multiple EF-hands Ca2+-binding protein, interacts with ryanodine receptor-1 in rabbit skeletal sarcoplasmic reticulum: Biochem Biophys Res Commun, v. 343, p. 34-42.

Kahn, S. E., R. L. Hull, and K. M. Utzschneider, 2006, Mechanisms linking obesity to insulin resistance and type 2 diabetes: Nature, v. 444, p. 840-6.

Kamei, Y., T. Kawada, J. Mizukami, and E. Sugimoto, 1994, The prevention of adipose differentiation of 3T3-L1 cells caused by retinoic acid is elicited through retinoic acid receptor alpha: Life Sci, v. 55, p. PL307-12.

Kapust, R. B., and D. S. Waugh, 1999, Escherichia coli maltose-binding protein is uncommonly effective at promoting the solubility of polypeptides to which it is fused: Protein Sci, v. 8, p. 1668-74.

Kawaguchi, R., J. Yu, J. Honda, J. Hu, J. Whitelegge, P. Ping, P. Wiita, D. Bok, and H. Sun, 2007, A membrane receptor for retinol binding protein mediates cellular uptake of vitamin A: Science, v. 315, p. 820-5.

Kawaguchi, R., J. Yu, M. Ter-Stepanian, M. Zhong, G. Cheng, Q. Yuan, M. Jin, G. H. Travis, D. Ong, and H. Sun, 2011, Receptor-mediated cellular uptake mechanism that couples to intracellular storage: ACS Chem Biol, v. 6, p. 1041-51.

Kawaguchi, R., J. Yu, P. Wiita, J. Honda, and H. Sun, 2008a, An essential ligand-binding domain in the membrane receptor for retinol-binding protein revealed by large-scale mutagenesis and a human polymorphism: J Biol Chem, v. 283, p. 15160-8.

Kawaguchi, R., J. Yu, P. Wiita, M. Ter-Stepanian, and H. Sun, 2008b, Mapping the membrane topology and extracellular ligand binding domains of the retinol binding protein receptor: Biochemistry, v. 47, p. 5387-95.

Kawaguchi, R., M. Zhong, M. Kassai, M. Ter-Stepanian, and H. Sun, 2012, STRA6-Catalyzed Vitamin A Influx, Efflux, and Exchange: J Membr Biol.

Kawaguchi, R., M. Zhong, M. Kassai, M. Ter-Stepanian, and H. Sun, 2013, Differential and Isomer-Specific Modulation of Vitamin A Transport and the Catalytic Activities of the RBP Receptor by Retinoids: J Membr Biol, v. 246, p. 647-60.

Khan, A. A., and J. G. Quigley, 2011, Control of intracellular heme levels: heme transporters and heme oxygenases: Biochim Biophys Acta, v. 1813, p. 668-82.

Kim, H. J., O. Khalimonchuk, P. M. Smith, and D. R. Winge, 2012, Structure, function, and assembly of heme centers in mitochondrial respiratory complexes: Biochim Biophys Acta, v. 1823, p. 1604-16.

Kim, W., M. Kim, and E. H. Jho, 2013a, Wnt/β-catenin signalling: from plasma membrane to nucleus: Biochem J, v. 450, p. 9-21.

Kim, Y. D., M. S. Kwon, B. R. Na, H. R. Kim, H. S. Lee, and C. D. Jun, 2013b, Swiprosin-1 Expression Is Up-Regulated through Protein Kinase C-θ and NF-κB Pathway in T Cells: Immune Netw, v. 13, p. 55-62.

Koenig, J. H., K. Yamaoka, and K. Ikeda, 1993, Calcium-induced translocation of synaptic vesicles to the active site: J Neurosci, v. 13, p. 2313-22.

Koffer, A., P. E. Tatham, and B. D. Gomperts, 1990, Changes in the state of actin during the exocytotic reaction of permeabilized rat mast cells: J Cell Biol, v. 111, p. 919-27.

Kotaka, M., S. Kostin, S. Ngai, K. Chan, Y. Lau, S. M. Lee, H. Li, E. K. Ng, J. Schaper, S. K. Tsui, K. Fung, C. Lee, and M. M. Waye, 2000, Interaction of hCLIM1, an enigma family protein, with alpha-actinin 2: J Cell Biochem, v. 78, p. 558-65.

Kunau, W. H., V. Dommes, and H. Schulz, 1995, beta-oxidation of fatty acids in mitochondria, peroxisomes, and bacteria: a century of continued progress: Prog Lipid Res, v. 34, p. 267-342.

Kwon, M. S., K. R. Park, Y. D. Kim, B. R. Na, H. R. Kim, H. J. Choi, I. Piragyte, H. Jeon, K. H. Chung, W. K. Song, S. H. Eom, and C. D. Jun, 2013, Swiprosin-1 is a novel actin bundling protein that regulates cell spreading and migration: PLoS One, v. 8, p. e71626.

Lang, T., I. Wacker, I. Wunderlich, A. Rohrbach, G. Giese, T. Soldati, and W. Almers, 2000, Role of actin cortex in the subplasmalemmal transport of secretory granules in PC-12 cells: Biophys J, v. 78, p. 2863-77.

Larsson, C., 2006, Protein kinase C and the regulation of the actin cytoskeleton: Cell Signal, v. 18, p. 276-84.

Lazzeroni, M., S. Gandini, M. Puntoni, B. Bonanni, A. Gennari, and A. DeCensi, 2011, The science behind vitamins and natural compounds for breast cancer prevention. Getting the most prevention out of it: Breast, v. 20 Suppl 3, p. S36-41.

Lechward, K., O. S. Awotunde, W. Swiatek, and G. Muszyńska, 2001, Protein phosphatase 2A: variety of forms and diversity of functions: Acta Biochim Pol, v. 48, p. 921-33.

Lee, A., 1987, Coordinated regulation of a set of genes by glucose and calcium ionophores in mammalian cells.: Trends Biochem Sci, v. 12, p. 20-23.

Lee, J. H., E. J. Kwon, and D. H. Kim, 2013, Calumenin has a role in the alleviation of ER stress in neonatal rat cardiomyocytes: Biochem Biophys Res Commun.

Li, E., and A. W. Norris, 1996, Structure/function of cytoplasmic vitamin A-binding proteins: Annu Rev Nutr, v. 16, p. 205-34.

Liu, L., and R. N. Eisenman, 2012, Regulation of c-Myc Protein Abundance by a Protein Phosphatase 2A-Glycogen Synthase Kinase 3β-Negative Feedback Pathway: Genes Cancer, v. 3, p. 23-36.

Lubran, M. M., 1975, McArdle's disease: a review: Ann Clin Lab Sci, v. 5, p. 115-22.

Malpeli, G., C. Folli, and R. Berni, 1996, Retinoid binding to retinol-binding protein and the interference with the interaction with transthyretin: Biochim Biophys Acta, v. 1294, p. 48-54.

Manchester, J., A. V. Skurat, P. Roach, S. D. Hauschka, and J. C. Lawrence, 1996, Increased glycogen accumulation in transgenic mice overexpressing glycogen synthase in skeletal muscle: Proc Natl Acad Sci U S A, v. 93, p. 10707-11.

Mark, M., N. B. Ghyselinck, and P. Chambon, 2006, Function of retinoid nuclear receptors: lessons from genetic and pharmacological dissections of the retinoic acid signaling pathway during mouse embryogenesis: Annu Rev Pharmacol Toxicol, v. 46, p. 451-80.

Martin, W. H., D. J. Hoover, S. J. Armento, I. A. Stock, R. K. McPherson, D. E. Danley, R. W. Stevenson, E. J. Barrett, and J. L. Treadway, 1998, Discovery of a human liver glycogen phosphorylase inhibitor that lowers blood glucose in vivo: Proc Natl Acad Sci U S A, v. 95, p. 1776-81.

Matarese, V., and H. F. Lodish, 1993, Specific uptake of retinol-binding protein by variant F9 cell lines: J Biol Chem, v. 268, p. 18859-65.

Mazzarella, R. A., N. Marcus, S. M. Haugejorden, J. M. Balcarek, J. J. Baldassare, B. Roy, L. J. Li, A. S. Lee, and M. Green, 1994, Erp61 is GRP58, a stress-inducible luminal endoplasmic reticulum protein, but is devoid of phosphatidylinositide-specific phospholipase C activity: Arch Biochem Biophys, v. 308, p. 454-60.

McCright, B., A. M. Rivers, S. Audlin, and D. M. Virshup, 1996, The B56 family of protein phosphatase 2A (PP2A) regulatory subunits encodes differentiation-induced phosphoproteins that target PP2A to both nucleus and cytoplasm: J Biol Chem, v. 271, p. 22081-9.

Mcilroy, G. D., M. Delibegovic, C. Owen, P. N. Stoney, K. D. Shearer, P. J. McCaffery, and N. Mody, 2013, Fenretinide treatment prevents diet-induced obesity in association with major alterations in retinoid homeostatic gene expression in adipose, liver, and hypothalamus: Diabetes, v. 62, p. 825-36.

Mills, J. P., H. C. Furr, and S. A. Tanumihardjo, 2008, Retinol to retinol-binding protein (RBP) is low in obese adults due to elevated apo-RBP: Exp Biol Med (Maywood), v. 233, p. 1255-61.

Moller, D. E., 2001, New drug targets for type 2 diabetes and the metabolic syndrome: Nature, v. 414, p. 821-7.

Muenzner, M., N. Tuvia, C. Deutschmann, N. Witte, A. Tolkachov, A. Valai, A. Henze, L. E. Sander, J. Raila, and M. Schupp, 2013, RBP4 and its Membrane Receptor STRA6 Control Adipogenesis by Regulating Cellular Retinoid Homeostasis and RARα Activity: Mol Cell Biol.

Murphy, M. P., 2009, How mitochondria produce reactive oxygen species: Biochem J, v. 417, p. 1-13.

Napoli, J. L., 1999, Retinoic acid: its biosynthesis and metabolism: Prog Nucleic Acid Res Mol Biol, v. 63, p. 139-88.

Napoli, J. L., 2000, A gene knockout corroborates the integral function of cellular retinol-binding protein in retinoid metabolism: Nutr Rev, v. 58, p. 230-6.

Naylor, H. M., and M. E. Newcomer, 1999, The structure of human retinol-binding protein (RBP) with its carrier protein transthyretin reveals an interaction with the carboxy terminus of RBP: Biochemistry, v. 38, p. 2647-53.

Newcomer, M. E., T. A. Jones, J. Aqvist, J. Sundelin, U. Eriksson, L. Rask, and P. A. Peterson, 1984, The three-dimensional structure of retinol-binding protein: EMBO J, v. 3, p. 1451-4.

Ng, W. Y., F. Pasutto, T. M. Bardakjian, M. J. Wilson, G. Watson, A. Schneider, D. A. Mackey, J. R. Grigg, M. Zenker, and R. V. Jamieson, 2013, A puzzle over several decades: eye anomalies with FRAS1 and STRA6 mutations in the same family: Clin Genet, v. 83, p. 162-8.

Nielsen, J. N., J. Vissing, J. F. Wojtaszewski, R. G. Haller, N. Begum, and E. A. Richter, 2002, Decreased insulin action in skeletal muscle from patients with McArdle's disease: Am J Physiol Endocrinol Metab, v. 282, p. E1267-75.

Norseen, J., T. Hosooka, A. Hammarstedt, M. M. Yore, S. Kant, P. Aryal, U. A. Kiernan, D. A. Phillips, H. Maruyama, B. J. Kraus, A. Usheva, R. J. Davis, U. Smith, and B. B. Kahn, 2012, Retinol-binding protein 4 inhibits insulin signaling in adipocytes by inducing proinflammatory cytokines in macrophages through a c-Jun N-terminal kinase- and toll-like receptor 4-dependent and retinol-independent mechanism: Mol Cell Biol, v. 32, p. 2010-9.

Noy, N., and Z. J. Xu, 1990, Interactions of retinol with binding proteins: implications for the mechanism of uptake by cells: Biochemistry, v. 29, p. 3878-83.

Olsen, J. V., M. Vermeulen, A. Santamaria, C. Kumar, M. L. Miller, L. J. Jensen, F. Gnad, J. Cox, T. S. Jensen, E. A. Nigg, S. Brunak, and M. Mann, 2010, Quantitative phosphoproteomics reveals widespread full phosphorylation site occupancy during mitosis: Sci Signal, v. 3, p. ra3.

Otey, C. A., and O. Carpen, 2004, Alpha-actinin revisited: a fresh look at an old player: Cell Motil Cytoskeleton, v. 58, p. 104-11.

Owen, M. R., E. Doran, and A. P. Halestrap, 2000, Evidence that metformin exerts its anti-diabetic effects through inhibition of complex 1 of the mitochondrial respiratory chain: Biochem J, v. 348 Pt 3, p. 607-14.

Ozawa, M., and T. Muramatsu, 1993, Reticulocalbin, a novel endoplasmic reticulum resident Ca(2+)-binding protein with multiple EF-hand motifs and a carboxyl-terminal HDEL sequence: J Biol Chem, v. 268, p. 699-705.

Palczewski, K., 2012, Chemistry and biology of vision: J Biol Chem, v. 287, p. 1612-9.

Park, J. H., H. Y. Sung, J. Y. Lee, H. J. Kim, J. H. Ahn, and I. Jo, 2013, B56α subunit of protein phosphatase 2A mediates retinoic acid-induced decreases in phosphorylation of endothelial nitric oxide synthase at serine 1179 and nitric oxide production in bovine aortic endothelial cells: Biochem Biophys Res Commun, v. 430, p. 476-81.

Park, Y. S., E. M. Hur, B. H. Choi, E. Kwak, D. J. Jun, S. J. Park, and K. T. Kim, 2006, Involvement of protein kinase C-epsilon in activity-dependent potentiation of large dense-core vesicle exocytosis in chromaffin cells: J Neurosci, v. 26, p. 8999-9005.

Pasutto, F., H. Sticht, G. Hammersen, G. Gillessen-Kaesbach, D. R. Fitzpatrick, G. Nürnberg, F. Brasch, H. Schirmer-Zimmermann, J. L. Tolmie, D. Chitayat, G. Houge, L. Fernández-Martínez, S. Keating, G. Mortier, R. C. Hennekam, A. von der Wense, A. Slavotinek, P. Meinecke, P. Bitoun, C. Becker, P. Nürnberg, A. Reis, and A. Rauch, 2007, Mutations in STRA6 cause a broad spectrum of malformations including anophthalmia, congenital heart defects, diaphragmatic hernia, alveolar capillary dysplasia, lung hypoplasia, and mental retardation: Am J Hum Genet, v. 80, p. 550-60.

Patel, M. S., and T. E. Roche, 1990, Molecular biology and biochemistry of pyruvate dehydrogenase complexes: FASEB J, v. 4, p. 3224-33.

Patel, P. S., E. D. Buras, and A. Balasubramanyam, 2013, The role of the immune system in obesity and insulin resistance: J Obes, v. 2013, p. 616193.

Patil, S. B., M. D. Pawar, and K. N. Bitar, 2004, Direct association and translocation of PKC-alpha with calponin: Am J Physiol Gastrointest Liver Physiol, v. 286, p. G954-63.

Pijet, M., B. Pijet, A. Litwiniuk, B. Pajak, B. Gajkowska, and A. Orzechowski, 2013, Leptin impairs myogenesis in C2C12 cells through JAK/STAT and MEK signaling pathways: Cytokine, v. 61, p. 445-54.

Pitt, G. A., 1965, Chemical structure and vitamin A activity: Proc Nutr Soc, v. 24, p. 153-9.

Preitner, F., N. Mody, T. E. Graham, O. D. Peroni, and B. B. Kahn, 2009, Long-term Fenretinide treatment prevents high-fat diet-induced obesity, insulin resistance, and hepatic steatosis: Am J Physiol Endocrinol Metab, v. 297, p. E1420-9.

Quadro, L., W. S. Blaner, L. Hamberger, P. M. Novikoff, S. Vogel, R. Piantedosi, M. E. Gottesman, and V. Colantuoni, 2004, The role of extrahepatic retinol binding protein in the mobilization of retinoid stores: J Lipid Res, v. 45, p. 1975-82.

Quadro, L., W. S. Blaner, L. Hamberger, R. N. Van Gelder, S. Vogel, R. Piantedosi, P. Gouras, V. Colantuoni, and M. E. Gottesman, 2002, Muscle expression of human retinol-binding protein (RBP). Suppression of the visual defect of RBP knockout mice: J Biol Chem, v. 277, p. 30191-7.

Rask, L., H. Anundi, J. Böhme, U. Eriksson, A. Fredriksson, S. F. Nilsson, H. Ronne, A. Vahlquist, and P. A. Peterson, 1980, The retinol-binding protein: Scand J Clin Lab Invest Suppl, v. 154, p. 45-61.

Rayasam, G. V., V. K. Tulasi, R. Sodhi, J. A. Davis, and A. Ray, 2009, Glycogen synthase kinase 3: more than a namesake: Br J Pharmacol, v. 156, p. 885-98.

Redondo, C., M. Vouropoulou, J. Evans, and J. B. Findlay, 2008, Identification of the retinol-binding protein (RBP) interaction site and functional state of RBPs for the membrane receptor: FASEB J, v. 22, p. 1043-54.

Reynolds, J. G., S. A. McCalmon, T. Tomczyk, and F. J. Naya, 2007, Identification and mapping of protein kinase A binding sites in the costameric protein myospryn: Biochim Biophys Acta, v. 1773, p. 891-902.

Roach, P. J., A. A. Depaoli-Roach, T. D. Hurley, and V. S. Tagliabracci, 2012, Glycogen and its metabolism: some new developments and old themes: Biochem J, v. 441, p. 763-87.

Rochette-Egly, C., and P. Germain, 2009, Dynamic and combinatorial control of gene expression by nuclear retinoic acid receptors (RARs): Nucl Recept Signal, v. 7, p. e005.

Ruiz, A., M. Mark, H. Jacobs, M. Klopfenstein, J. Hu, M. Lloyd, S. Habib, C. Tosha, R. A. Radu, N. B. Ghyselinck, S. Nusinowitz, and D. Bok, 2012, Retinoid content, visual responses, and ocular morphology are compromised in the retinas of mice lacking the retinol-binding protein receptor, STRA6: Invest Ophthalmol Vis Sci, v. 53, p. 3027-39.

Sahoo, S. K., and d. H. Kim, 2008, Calumenin interacts with SERCA2 in rat cardiac sarcoplasmic reticulum: Mol Cells, v. 26, p. 265-9.

Sahoo, S. K., T. Kim, G. B. Kang, J. G. Lee, S. H. Eom, and d. H. Kim, 2009, Characterization of calumenin-SERCA2 interaction in mouse cardiac sarcoplasmic reticulum: J Biol Chem, v. 284, p. 31109-21.

Saito, Y., H. Shibayama, H. Tanaka, A. Tanimura, and Y. Kanakura, 2011a, A cell-death-defying factor, anamorsin mediates cell growth through inactivation of PKC and p38MAPK: Biochem Biophys Res Commun, v. 405, p. 303-7.

Saito, Y., H. Shibayama, H. Tanaka, A. Tanimura, I. Matsumura, and Y. Kanakura, 2011b, PICOT is a molecule which binds to anamorsin: Biochem Biophys Res Commun, v. 408, p. 329-33.

Saltiel, A. R., and C. R. Kahn, 2001, Insulin signalling and the regulation of glucose and lipid metabolism: Nature, v. 414, p. 799-806.

Seeling, J. M., J. R. Miller, R. Gil, R. T. Moon, R. White, and D. M. Virshup, 1999, Regulation of beta-catenin signaling by the B56 subunit of protein phosphatase 2A: Science, v. 283, p. 2089-91.

Seshacharyulu, P., P. Pandey, K. Datta, and S. K. Batra, 2013, Phosphatase: PP2A structural importance, regulation and its aberrant expression in cancer: Cancer Lett, v. 335, p. 9-18.

Shevchenko, A., H. Tomas, J. Havlis, J. V. Olsen, and M. Mann, 2006, In-gel digestion for mass spectrometric characterization of proteins and proteomes: Nat Protoc, v. 1, p. 2856-60.

Shibayama, H., E. Takai, I. Matsumura, M. Kouno, E. Morii, Y. Kitamura, J. Takeda, and Y. Kanakura, 2004, Identification of a cytokine-induced antiapoptotic molecule anamorsin essential for definitive hematopoiesis: J Exp Med, v. 199, p. 581-92.

Shull, J. D., K. L. Pennington, J. A. Gurr, and A. C. Ross, 1995, Cell-type specific interactions between retinoic acid and thyroid hormone in the regulation of expression of the gene encoding ornithine aminotransferase: Endocrinology, v. 136, p. 2120-6.

Sivaprasadarao, A., and J. B. Findlay, 1988a, The interaction of retinol-binding protein with its plasma-membrane receptor: Biochem J, v. 255, p. 561-9.

Sivaprasadarao, A., and J. B. Findlay, 1988b, The mechanism of uptake of retinol by plasma-membrane vesicles: Biochem J, v. 255, p. 571-9.

Sivaprasadarao, A., and J. B. Findlay, 1994, Structure-function studies on human retinol-binding protein using site-directed mutagenesis: Biochem J, v. 300 (Pt 2), p. 437-42.

Song, M. J., K. H. Kim, J. M. Yoon, and J. B. Kim, 2006, Activation of Toll-like receptor 4 is associated with insulin resistance in adipocytes: Biochem Biophys Res Commun, v. 346, p. 739-45.

Spurlino, J. C., G. Y. Lu, and F. A. Quiocho, 1991, The 2.3-A resolution structure of the maltose- or maltodextrin-binding protein, a primary receptor of bacterial active transport and chemotaxis: J Biol Chem, v. 266, p. 5202-19.

Streb, J. W., X. Long, T. H. Lee, Q. Sun, C. M. Kitchen, M. A. Georger, O. J. Slivano, W. S. Blaner, D. W. Carr, I. H. Gelman, and J. M. Miano, 2011, Retinoid-induced expression and activity of an immediate early tumor suppressor gene in vascular smooth muscle cells: PLoS One, v. 6, p. e18538.

Summerbell, D., 1983, The effect of local application of retinoic acid to the anterior margin of the developing chick limb: J Embryol Exp Morphol, v. 78, p. 269-89.

Sun, H., 2012, Membrane receptors and transporters involved in the function and transport of vitamin A and its derivatives: Biochim Biophys Acta, v. 1821, p. 99-112.

Sundaram, M., A. Sivaprasadarao, M. M. DeSousa, and J. B. Findlay, 1998, The transfer of retinol from serum retinol-binding protein to cellular retinol-binding protein is mediated by a membrane receptor: J Biol Chem, v. 273, p. 3336-42.

Szanto, A., V. Narkar, Q. Shen, I. P. Uray, P. J. Davies, and L. Nagy, 2004, Retinoid X receptors: X-ploring their (patho)physiological functions: Cell Death Differ, v. 11 Suppl 2, p. S126-43.

Szeto, W., W. Jiang, D. A. Tice, B. Rubinfeld, P. G. Hollingshead, S. E. Fong, D. L. Dugger, T. Pham, D. G. Yansura, T. A. Wong, J. C. Grimaldi, R. T. Corpuz, J. S. Singh, G. D. Frantz, B. Devaux, C. W. Crowley, R. H. Schwall, D. A. Eberhard, L. Rastelli, P. Polakis, and D. Pennica, 2001, Overexpression of the retinoic acid-responsive gene Stra6 in human cancers and its synergistic induction by Wnt-1 and retinoic acid: Cancer Res, v. 61, p. 4197-205.

Tang, D. C., H. M. Kang, J. P. Jin, E. D. Fraser, and M. P. Walsh, 1996, Structure-function relations of smooth muscle calponin. The critical role of serine 175: J Biol Chem, v. 271, p. 8605-11.

te Velthuis, A. J., and C. P. Bagowski, 2007, PDZ and LIM domain-encoding genes: molecular interactions and their role in development: ScientificWorldJournal, v. 7, p. 1470-92.

Theodosiou, M., V. Laudet, and M. Schubert, 2010, From carrot to clinic: an overview of the retinoic acid signaling pathway: Cell Mol Life Sci, v. 67, p. 1423-45.

Torchia, J., C. Glass, and M. G. Rosenfeld, 1998, Co-activators and co-repressors in the integration of transcriptional responses: Curr Opin Cell Biol, v. 10, p. 373-83.

Tsutsumi, C., M. Okuno, L. Tannous, R. Piantedosi, M. Allan, D. S. Goodman, and W. S. Blaner, 1992, Retinoids and retinoid-binding protein expression in rat adipocytes: J Biol Chem, v. 267, p. 1805-10.

Turk, B., D. Turk, and V. Turk, 2000, Lysosomal cysteine proteases: more than scavengers: Biochim Biophys Acta, v. 1477, p. 98-111.

Turk, V., V. Stoka, O. Vasiljeva, M. Renko, T. Sun, B. Turk, and D. Turk, 2012, Cysteine cathepsins: from structure, function and regulation to new frontiers: Biochim Biophys Acta, v. 1824, p. 68-88.

Tyedmers, J., M. Lerner, W. Nastainczyk, and R. Zimmermann, 2005, Calumenin and reticulocalbin are associated with the protein translocase of the mammalian endoplasmic reticulum: Journal of Biological Sciences, v. 5, p. 70-75.

Ueki, K., T. Kondo, and C. R. Kahn, 2004, Suppressor of cytokine signaling 1 (SOCS-1) and SOCS-3 cause insulin resistance through inhibition of tyrosine phosphorylation of insulin receptor substrate proteins by discrete mechanisms: Mol Cell Biol, v. 24, p. 5434-46.

Vergnes, L., M. Péterfy, M. O. Bergo, S. G. Young, and K. Reue, 2004, Lamin B1 is required for mouse development and nuclear integrity: Proc Natl Acad Sci U S A, v. 101, p. 10428-33.

Wang, R., H. Gao, W. Xu, H. Li, Y. Mao, Y. Wang, T. Guo, X. Wang, R. Song, Z. Li, D. M. Irwin, G. Niu, and H. Tan, 2013, Differential expression of genes and changes in glucose metabolism in the liver of liver-specific glucokinase gene knockout mice: Gene, v. 516, p. 248-54.

Wang, Y., Q. Y. He, H. Chen, and J. F. Chiu, 2007, Synergistic effects of retinoic acid and tamoxifen on human breast cancer cells: proteomic characterization: Exp Cell Res, v. 313, p. 357-68.

Weisberg, S. P., D. McCann, M. Desai, M. Rosenbaum, R. L. Leibel, and A. W. Ferrante, 2003, Obesity is associated with macrophage accumulation in adipose tissue: J Clin Invest, v. 112, p. 1796-808.

Wheeler, T. J., R. D. Fell, and M. A. Hauck, 1994, Translocation of two glucose transporters in heart: effects of rotenone, uncouplers, workload, palmitate, insulin and anoxia: Biochim Biophys Acta, v. 1196, p. 191-200.

White, T., T. Lu, R. Metlapally, J. Katowitz, F. Kherani, T. Y. Wang, K. N. Tran-Viet, and T. L. Young, 2008, Identification of STRA6 and SKI sequence variants in patients with anophthalmia/microphthalmia: Mol Vis, v. 14, p. 2458-65.

Whitmore, L., and B. A. Wallace, 2004, DICHROWEB, an online server for protein secondary structure analyses from circular dichroism spectroscopic data: Nucleic Acids Res, v. 32, p. W668-73.

Whitmore, L., and B. A. Wallace, 2008, Protein secondary structure analyses from circular dichroism spectroscopy: methods and reference databases: Biopolymers, v. 89, p. 392-400.

Wierenga, R. K., E. G. Kapetaniou, and R. Venkatesan, 2010, Triosephosphate isomerase: a highly evolved biocatalyst: Cell Mol Life Sci, v. 67, p. 3961-82.

Winder, S. J., B. G. Allen, O. Clément-Chomienne, and M. P. Walsh, 1998, Regulation of smooth muscle actin-myosin interaction and force by calponin: Acta Physiol Scand, v. 164, p. 415-26.

Winder, S. J., and M. P. Walsh, 1990, Smooth muscle calponin. Inhibition of actomyosin MgATPase and regulation by phosphorylation: J Biol Chem, v. 265, p. 10148-55.

Winder, W. W., and D. G. Hardie, 1996, Inactivation of acetyl-CoA carboxylase and activation of AMP-activated protein kinase in muscle during exercise: Am J Physiol, v. 270, p. E299-304.

Witte, S., M. Villalba, K. Bi, Y. Liu, N. Isakov, and A. Altman, 2000, Inhibition of the c-Jun N-terminal kinase/AP-1 and NF-kappaB pathways by PICOT, a novel protein kinase C-interacting protein with a thioredoxin homology domain: J Biol Chem, v. 275, p. 1902-9.

Wysocka-Kapcinska, M., J. A. Campos-Sandoval, A. Pal, and J. B. Findlay, 2010, Expression and characterization of recombinant human retinol-binding protein in Pichia pastoris: Protein Expr Purif, v. 71, p. 28-32.

Yang, Q., T. E. Graham, N. Mody, F. Preitner, O. D. Peroni, J. M. Zabolotny, K. Kotani, L. Quadro, and B. B. Kahn, 2005, Serum retinol binding protein 4 contributes to insulin resistance in obesity and type 2 diabetes: Nature, v. 436, p. 356-62.

Yong, J., L. Wan, and G. Dreyfuss, 2004, Why do cells need an assembly machine for RNA-protein complexes?: Trends Cell Biol, v. 14, p. 226-32.

Yoon, J. H., J. S. Koo, D. Norford, K. Guzman, T. Gray, and P. Nettesheim, 1999, Lysozyme expression during metaplastic squamous differentiation of retinoic acid-deficient human tracheobronchial epithelial cells: Am J Respir Cell Mol Biol, v. 20, p. 573-81.

Yoshida, M., E. Muneyuki, and T. Hisabori, 2001, ATP synthase--a marvellous rotary engine of the cell: Nat Rev Mol Cell Biol, v. 2, p. 669-77.

Zanotti, G., S. Ottonello, R. Berni, and H. L. Monaco, 1993, Crystal structure of the trigonal form of human plasma retinol-binding protein at 2.5 A resolution: J Mol Biol, v. 230, p. 613-24.

Zerbes, R. M., M. Bohnert, D. A. Stroud, K. von der Malsburg, A. Kram, S. Oeljeklaus, B. Warscheid, T. Becker, N. Wiedemann, M. Veenhuis, I. J. van der Klei, N. Pfanner, and M. van der Laan, 2012a, Role of MINOS in mitochondrial membrane architecture: cristae morphology and outer membrane interactions differentially depend on mitofilin domains: J Mol Biol, v. 422, p. 183-91.

Zerbes, R. M., I. J. van der Klei, M. Veenhuis, N. Pfanner, M. van der Laan, and M. Bohnert, 2012b, Mitofilin complexes: conserved organizers of mitochondrial membrane architecture: Biol Chem, v. 393, p. 1247-61.

Zhang, Y., 2008, I-TASSER server for protein 3D structure prediction: BMC Bioinformatics, v. 9, p. 40.

Zhang, Y., E. R. Lyver, E. Nakamaru-Ogiso, H. Yoon, B. Amutha, D. W. Lee, E. Bi, T. Ohnishi, F. Daldal, D. Pain, and A. Dancis, 2008, Dre2, a conserved eukaryotic Fe/S cluster protein, functions in cytosolic Fe/S protein biogenesis: Mol Cell Biol, v. 28, p. 5569-82.

Zhang, Y. R., Y. Q. Zhao, and J. F. Huang, 2012, Retinoid-binding proteins: similar protein architectures bind similar ligands via completely different ways: PLoS One, v. 7, p. e36772.

Zhou, G., R. Myers, Y. Li, Y. Chen, X. Shen, J. Fenyk-Melody, M. Wu, J. Ventre, T. Doebber, N. Fujii, N. Musi, M. F. Hirshman, L. J. Goodyear, and D. E. Moller, 2001, Role of AMP-activated protein kinase in mechanism of metformin action: J Clin Invest, v. 108, p. 1167-74.